The Effects of Aberrant Wnt Signalling on the Murine Intestinal Stem Cell Compartment

Madeleine A Young

Cardiff University

Ph.D.

2009-2013

Declarations

This work has not been submitted in substance for any other degree or award at this or any other university or place of learning, nor is being submitted concurrently in candidature for any degree or other award.

This thesis is being submitted in partial fulfilment of the requirements for the degree of PhD.

This thesis is the result of my own independent work/investigation, except where otherwise stated. Other sources are acknowledged by explicit references. The views expressed are my own.

I hereby give consent for my thesis, if accepted, to be available for photocopying and for inter-library loan, and for the title and summary to be made available to outside organisations.

Signed …….. (Candidate) Date ……..

Acknowledgements

I dedicate this thesis to my Dad, whose short battle with cancer inspired my career choice.

Firstly I would like to thank Prof Alan Clarke, for enabling me to pursue such an interesting and exciting PhD project, and giving me guidance and independence in equal measure. I would also like to thank the whole ARC group, especially Dr Karen Reed for her time, patience, enthusiasm and general loveliness, Dr Valerie Méniel for her encouragement, kindness and support and my work wife, Lili Ordonez, for her friendship and humour. Everyone within the group has been amazingly supportive throughout my PhD and have helped me to start believing in my own abilities as a researcher.

Balancing my social life with the demands of a PhD has been challenging and so I would like to thank my amazing friends, especially the P.P.s, who have been there for me whenever I needed to eat cake and talk rubbish. I am always amazed at the ability of these wonderful people to make me forget about work stresses and concentrate on the important things in life such as fizzy booze and being silly.

My family have been wonderful throughout my studies, and my Mum's love, support and proof-reading services have been second to none. Just knowing that I can come back to Brixham whenever I want to and be looked after has made this whole process a lot easier! My brother Roly and sister Poppy have also encouraged me in their own way, usually displayed through a constant willingness to drink with me.

Finally I'd like to thank my partner Mark, for his love, patience and pasta making skills throughout my PhD, all of which have meant that the last four years have not only been manageable, they've been awesome.

Table of Contents

List of Figures

List of Tables

Abbreviations and Definitions

Symbols

°C= Degrees Celsius

µg= Micrograms

µm= Micrometre

µM= Micromolar

A

ABC= Avidin Biotin Complex

APC= Adenamatous Polyposis Coli

APL= Acute Promyelocytic leukaemia

APS= Ammonium Persulphate

$Ascl_2$= Achaete Scutelike 2

AXIN2= Axis Inhibitor Protein 2

B

Bmi1= polycomb ring finger oncogene

BMP= Bone Morphogenic Protein

BNF= β-napthoflavone

bp= Base Pair

BrDU= 5'-bromo-2-deoxyuridine

BSA= Bovine Serum Albumin

C

CBC cells= Crypt-Base-Columnar cells

Col1A2CreER^T= Collagen Type 1, Alpha 2 Cre recombinase Estrogen Receptor transgene

Cox-1= Cyclooxygnease 3

CRC= Colorectal Cancer

CreER^T= Cre recombinase-Estrogen receptor fusion transgene

CSL= A transcription factor important within the Notch signalling pathway

C_T = Cycle threshold

D

DAB= Diaminobenzidine

Dckl1= Doublecortin And CaM Kinase-Like 1

DEPC= H_2O Diethylpyrocarbonate treated water

dH_2O= Deionised H_2O

ddH_2O= Double Distilled H_2O

Dhh= Desert Hedgehog

Dkk1= Dickkopf1, a Wnt inhibitor

Dll4= Delta-Like Ligand 4, a notch ligand

DMEM/F12= Dulbecco's Modified Eagle Medium, nutrient mixture F12

DNA= Deoxyribonucleic Acid

DNase= Deoxyribonuclease

dNTP= deoxynucleotide triphosphate

Dsh= Dishevelled

DTT= Dithiothreitol

E

ECL= Electochemiluminescence

EDTA= Ethylenediaminetetraacetic acid

EGTA= Ethyleneglycoltetraacetic acid

EMT= Epithelial-to-mesenchyme transition

EpCAM= Epithelial Cell Adhesion Molecule

ER= Estrogen Receptor

EtOH= Ethanol

F

FACs= Fluorescence Activated Cell Sorting

FAP= Familial Adenamatous Polyposis

FLP= Flippase

FOX1=Forkhead Box L1

Fz= Frizzled

G

gDNA= Genomic Deoxyribonucleic Acid

Gli= Glioma Associated Oncogene

Groucho= A Wnt inhibitor

GSK-3= Glycogen Synthase Kinase-3

H

HBSS= Hanks Balanced Salt Solution

H&E= Haematoxylin and Eosin

HNPCC= Hereditary Nonpolyposis Colorectal Cancer

HopX= Homeodomain-only protein X

hr= Hour

HRP= Horse Radish Peroxidase

I

IGF-1= Insulin-Like Growth Factor-1

IHC= Immunohistochemistry

Ihh= Indian Hedgehog

IL17= Interleukin 17

I.P.= Intraperitoneal

ISC= Intestinal Stem Cell

K

KRAS= Kirsten Rat Sarcoma viral oncogene homolog

kV= Kilovolts

L

L= Litre

LEF= Lymphoid Enhancer-Binding Factor 1

LOH= Loss of heterozygosity

LoxP= Locus of crossover of Bacteriophage P1

Lgr5= Leucine-rich repeat containing G-protein coupled receptor 5

Lrig1= Leucine-Rich Repeats and Immunoglobulin-Like Domains

Lrp= low density lipoprotein receptor-related protein complex

M

mg= milligram

MIN= Multiple Intestinal Neoplasia

mins= minutes

ml= millilitre

mM= millimolar

MRU= Mammary Repopulating Unit

Msi1= Musashi RNA-Binding Protein

mTERT= Mouse telomerase reverse transcriptase

mTOR= mammalian target of rapamycin

N

NGS= Normal Goat Serum

NICD= Notch Intracellular Domain

NRS= Normal Rabbit Serum

O

Olfm4= Olfactomedin 4

O/N= Overnight

Opn= Osteopontin

P

pAkt= Phosphorylated Akt

PBS= Phosphate Buffered Saline

PCR= Polymerase Chain Reaction

PI3K= Phosphatidylinositol-3-Kinase

PIP_2= Phosphatidylinositol 4,5-biphosphate

PIP_3= Phosphatidylinositol 3,4,5-biphosphate

PipC= Polyinosinic-polycytidylic acid

PKA= Protein Kinase A

PJS= Peutz-Jeghers Syndrome

PLL= Poly-L-Lysine coated slides

PML= Promyelocytic leukemia protein

PML-NB= PML Nuclear Body

pmTOR= Phosphorylated mTOR

PTEN= Phosphatase and tensin homolog deleted on chromosome ten

Q

qRT PCR= Quantitative Reverse Transcription Polymerase Chain Reaction

R

RA= Retinoic Acid

RARα= Retinoic Acid Receptor alpha

RNA= Ribonucleic Acid

RNase= Ribonuclease

rpm= Revolutions per minute

Rspo1= R-spondin 1

RT= Room Temperature

S

SDS= Sodium Dodecyl Sulphate

SDS-PAGE= Sodium Dodecyl Sulphate-Polyacrylamide Gel Electrophoresis

secs= Seconds

Shh= Sonic Hedgehog

SMADs= intracellular proteins important within BMP signalling

STAT3= Signal Transducer And Activator Of Transcription 3

T

T3= Thyroid Hormone 3

TA= Transit-amplifying

TACE= Tumour Necrosis Factor-α-Converting Enzyme

Taq= DNA polymerase derived from Thermus aquaticus

TBS/T= Tris Buffered Saline with 0.1% Tween

Tcf= T cell-specific transcription factor

TEMED= Tetramethylethylenediamine

TGF-α= Transforming Growth Factor-α

TGF-β= Transforming Growth Factor-β

TNFα= Tumour Necrosis Factor Alpha

U

UV= Ultra Violet

V

V= Volts

VillinCreER^{T}= Villin Cre recombinase Estrogen Receptor Transgene

W

Wnt= Wingless-type murine mammary tumour virus Integration site family

WT= Wild Type

123

+4= Crypt cell located 4 cells from the top of the Paneth cells.

Abstract

Colorectal cancer is the 2nd most common cause of death by cancer in the UK, but it is treatable if diagnosed early. In order to increase the likelihood of early diagnosis, more must be understood about the early stages of colorectal tumourigenesis. It is known that intestinal stem cells (ISCs) are the cells of origin of colorectal tumourigenesis, and that an expansion of undifferentiated cell types, akin to ISCs, is one of the earliest events in mouse models of tumourigenesis. This indicates the importance of the relationship between the ISC compartment and tumourigenesis.

In order to understand how changes in the ISC compartment may be contributing to tumourigenesis, the ability to accurately quantify this compartment is essential. Currently, analysis of the ISC compartment relies on the analysis of gene expression levels of ISC markers. However, there is a great deal of controversy surrounding the majority of these markers and there is no evidence that alterations in expression levels of these markers results in a functional change in the ISC compartment.

Here I present a novel method for assessing the ISC compartment based on a functional capacity of ISCs; the ability to form intestinal organoids in culture. This new method uses organoid formation efficiency as a readout of changes in the ISC compartment, and can be used in conjunction with traditional methods of ISC marker expression to understand the relationship between expression of ISC markers and ISC functionality. I have used this method to further analyse the intestinal phenotype of a range of mouse models of colorectal cancer based on gene deletion of *Apc*, *Cited1*, *Apc2*, *Pten* and *Pml*. These experiments have shown that organoid formation efficiency can be a useful method for assessing the ISC compartment, although changes within this compartment may not be accurately predictive of tumourigenesis.

1 General Introduction

1.1 Intestinal anatomy and function

The intestine is a tube which runs from the stomach to the anus, which ingested food passes through for the absorption of nutrients and water. The small intestine can be divided into three parts; the duodenum, the jejunum and the ileum. The luminal surface of the small intestine consists of a sheet of epithelial cells which are organized into invaginations called the crypts of Lieberkuhn and finger-like projections called villi (see Figure 1.1) which maximize surface area for increased absorption efficiency. These epithelial cells are polarized, with microvilli on the luminal side which further increase surface area. Beneath the single-cell epithelial sheet are stromal fibroblasts which surround the crypts and extend into the villi (the stromal component of which is referred to as the lamina propria) encasing a blood supply to these cells. Beneath both the epithelial and stromal compartments is the smooth muscle layer, which is responsible for the peristaltic action essential for the movement of food along the intestine.

1.1.1 Intestinal histology

Structurally, the intestinal epithelium is a highly regulated tissue, with up to nine crypts feeding cells into each villus. The proliferative zone of the intestinal epithelium is located within the crypt. Transit amplifying cells within the crypt divide 4-5 times, with each cycle taking about 12 hours whilst migrating up the crypt-villus axis towards the crypt-villus junction where they terminally differentiate (Marshman *et al.* 2002). There are four main types of differentiated cells found within the intestine; the absorptive enterocytes and the secretory lineages of goblet cells, enteroendocrine cells and Paneth cells, Figure 1.1. Differentiated cells (apart from Paneth cells) continue to migrate up the villus eventually being sloughed off into the lumen at the villus apex and replaced by the continual stream of new cells migrating upwards from the crypt. This rapid turnover of cells is maintained by an intestinal stem cell (ISC) population at the base of the crypt, the daughter cells of which are capable of becoming any of the epithelial lineages within the intestine.

The majority of differentiated cells found in the villi are enterocytes, which are the absorptive cells responsible for nutrient uptake. Cells from this differentiated cell lineage are tightly packed together, with close cell-to-cell adhesions forming an epithelial barrier which helps to prevent microbes from entering the bloodstream. Enterocytes can be identified by their expression of the enzyme alkaline phosphatase.

Goblet cells are responsible for the secretion of mucins which aid the lubrication of the epithelium and protect it from the high level of mechanical stress which occurs as a result of food movement through the intestine. Goblet cells also secrete trefoil proteins which facilitate tissue repair (Mashimo *et al.* 1996). Goblet cells are found throughout the villus, often at the crypt-villus junction. The mucins secreted by the goblet cells can be stained using Alcian Blue, and this staining technique is used to identify the number and position of intestinal goblet cells.

Enteroendocrine cells are scarce in comparison to the other differentiated cell types but are found throughout the whole of the crypt-villus axis. These function to secrete hormones which control many gut functions such as regulating glucose levels and signalling to empty food from the stomach. They can be identified by their ability to reduce silver ions, marking them with black deposits when stained with Grimelius silver stain.

Finally, Paneth cells are long-lived cells (6-8 weeks), found exclusively at the base of the intestinal crypt. In contrast to the other cell types, they migrate back down the crypt-villus axis as they differentiate (Bjerknes and Cheng 1981, 2006). The Paneth cells secrete a variety of anti-microbials and as such they are responsible for immunity and protection within the intestinal crypt. The Paneth cells also secrete a range of other factors which have a less well understood role in tissue maintenance, such as TGF-α, Wnt3 and the Notch ligand Dll4 (Bevins and Salzman 2011; Sato *et al.* 2010). These factors are thought to be important in maintaining the ISC population by regulating the ISC niche, see section 1.3.3.

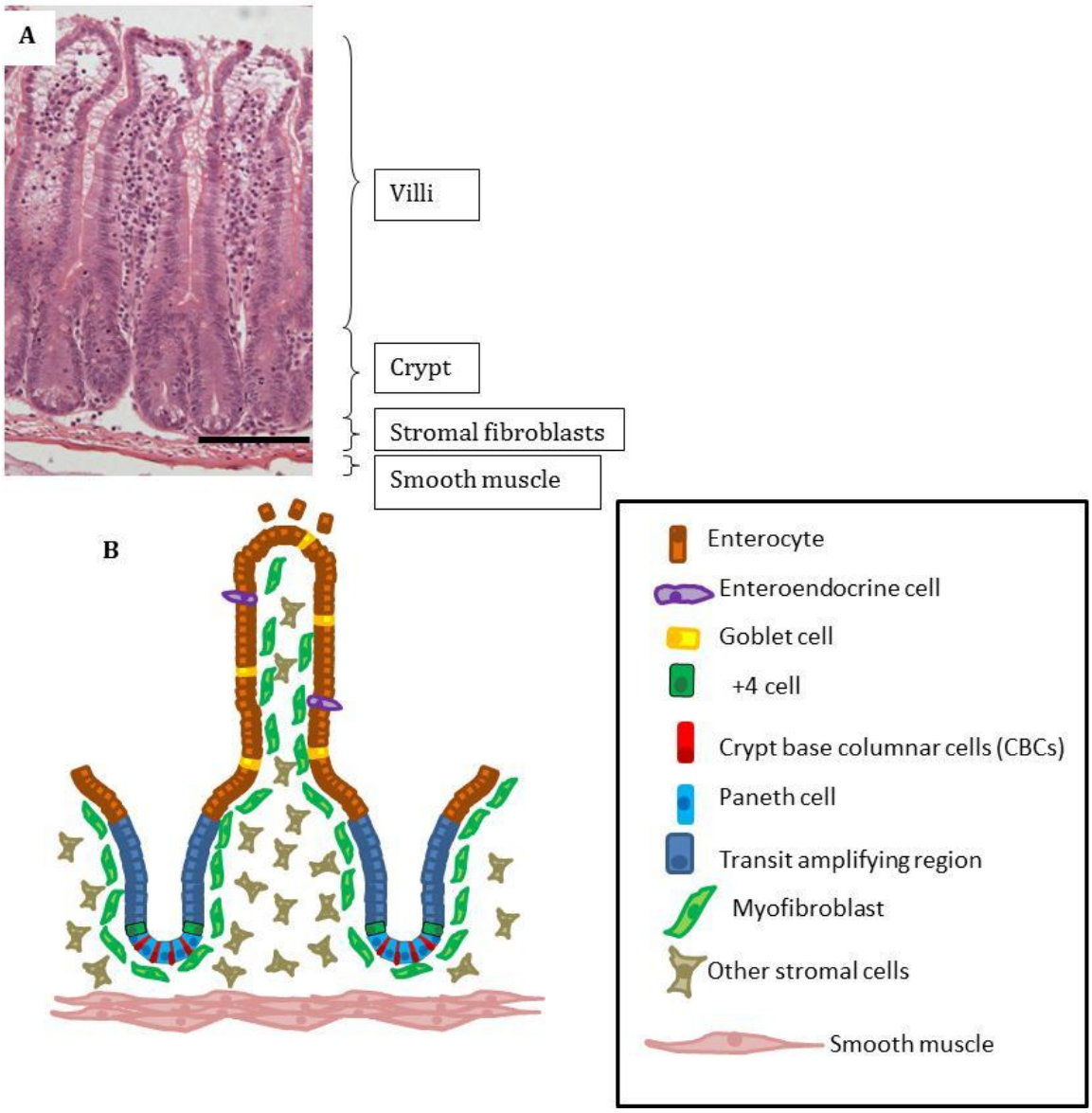

Figure 1.1 **A**; Haemotoxylin and Eosin stain of a normal mouse small intestine. Black bar indicates 100μm. **B**; Cartoon representation of a normal intestinal crypt and villus showing the differentiated cell types.

1.2 Signalling pathways involved in intestinal homeostasis

The delicate balance of cell proliferation, migration and apoptosis within the intestine must be carefully regulated in order to maintain intestinal structure and function. This is achieved by controlling gene expression through a number of important signalling pathways, the most important of which are discussed here.

1.2.1 Canonical Wnt signalling Pathway

Canonical Wnt signalling is a signalling pathway which is essential during embryonic development due to its role in establishing the basic body pattern. This signalling pathway relies on the binding of a secreted ligand to a receptor, and the Wnt signalling molecules are highly conserved throughout the animal kingdom.

In the absence of a Wnt signal, the intracellular proteins adenomatous polyposis coli (APC) and axin are phosphorylated by glycogen synthase kinase-3ß (GSK3) which increases their ability to bind to ß-catenin. When ß-catenin binds to these proteins it is also phosphorylated by GSK3, a process which results in the breakdown of ß-catenin, Figure 1.2.

When a Wnt ligand binds to a Wnt receptor (a Frizzled (Fz)/low density lipoprotein (LDL) receptor-related protein (LRP) complex), a signal is transduced to the intracellular proteins stimulating interaction between Dishevelled (Dsh) and Axin, making it unavailable for binding to ß-catenin and initiating its breakdown (Logan and Nusse 2004). This results in an accumulation of ß-catenin in the cytoplasm and the nucleus, where it interacts with any member of the lymphoid enhancer-binding factor 1 or T cell-specific transcription factor (LEF/TCF) to enhance transcription of a number of Wnt target genes (Behrens *et al.* 1996; Clevers and Van de Wetering 1997).

Many Wnt target genes are associated with cell proliferation, migration and adhesion, processes which are all essential for the maintenance of the intestine. Indeed, the appropriate regulation of Wnt signalling is vital for the maintenance of the intestinal stem cell (ISC) population. The ISC population is found at the base of the intestinal crypt, and throughout the crypt-villus axis there is a gradient of Wnt agonists, with higher levels found near the ISC population (Gregorieff *et al.* 2005).

The importance of Wnt signalling within intestinal homeostasis has been demonstrated using a range of experimental formats. Ireland *et al.* showed that conditional homozygous deletion of β-catenin in the mouse resulted in catastrophic disruption of normal intestinal homeostasis, with crypt ablation, reduced numbers of goblet cells, increased apoptosis and detachment of sheets of enterocytes (Ireland *et al.* 2004). Likewise, transgenic ectopic expression of the Wnt inhibitor *Dickkopf1* (Dkk1) resulted in reduced numbers of secretary cells, reduced proliferation and loss of crypts (Pinto *et al.* 2003), while deletion of the important Wnt-target gene *C-myc* was lethal to intestinal cells, resulting in a complete loss of all *C-myc*$^{-/-}$ crypts (Muncan *et al.* 2006).

1.2.2 Notch Signalling pathway

Notch signalling is a cell-to-cell signalling pathway, meaning that signalling can only occur via direct cell-to-cell contact of adjacent cells. Notch ligands (such as Jagged or Delta) interact with the Notch receptor and this causes two proteolytic cleavage events. The first, mediated by the tumour necrosis factor-α-converting enzyme (TACE), involves the cleavage of the extracellular domain from the Notch receptor. Once this has occurred, the second cleavage event takes place, releasing the Notch intracellular domain (NICD) which can then enter the nucleus and activate the transcription factor CSL, resulting in expression of Notch target genes, Figure 1.2. Like Wnt target genes, Notch target genes have a variety of functions which influence tissue homeostasis via roles in controlling apoptosis, proliferation, spatial patterning and cell fate determination (Artavanis-Tsakonas *et al.* 1999).

Conditional inactivation of CSL within the mouse intestine (which effectively prevents Notch signalling), results in the conversion of proliferative cells within the intestine into post-mitotic goblet cells (Van Es *et al.* 2005). Not only does this demonstrate the importance of the Notch signalling pathway in homeostasis, but crucially it highlights that the maintenance of the undifferentiated cells, the ISCs, within the crypt is essential for intestinal homeostasis. Therefore the importance of Notch signalling is due to its role as a regulator of the ISC compartment, supported by the high levels of Notch ligands found at the base of the crypt in comparison to the rest of the crypt-villus axis.

1.2.3 TGFβ, BMP signalling pathway

Both the TGF-β pathway and the BMP signalling pathway are activated by the binding of a ligand to the membrane-bound type II receptor which enables the type II receptor to dimerise with type I receptors, and phosphorylate its cytoplasmic domain. Once phosphorylated, the type I receptor can then recruit and phosphorylate either the SMAD2/3 proteins (TGF-β), or the SMAD1/5/8 proteins (BMP) which, once phosphorylated are collectively known as receptor regulated SMADS (R-SMADS). The R-SMADS can then disassociate from the receptor and form a complex with SMAD4, thereby enabling its translocation into the nucleus. Once in the nucleus, SMAD4 can interact with regulatory proteins and regulate a range of gene transcription events (Figure 1.2). Target genes of the TGF-β/BMP signalling pathway have a range of functions, but are most commonly associated with inhibition of cellular growth and proliferation.

Within the intestine, expression of TGF-β ligands is highest at the villus tip, concomitant with absence of cellular growth and proliferation, in accordance with its role within intestinal homeostasis (Barnard *et al.* 1993).

1.2.4 The Hedgehog Pathway

The Hedgehog signalling pathway is controlled by two cell membrane spanning proteins called Patched and Smoothened. When no ligand is bound, Patched inhibits Smoothened, which enables protein kinase A (PKA) to phosphorylate the transcription factors Gli2/3 resulting in the targeting of Gli2 for degradation. This leaves the truncated Gli3 protein free to enter the nucleus and act as a transcriptional repressor of Hedgehog target genes.

When a Hedgehog ligand (either Sonic Hedgehog, Shh, Indian Hedgehog, Ihh or Desert Hedgehog, Dhh in vertebrates) binds to Patched, the inhibition of Smoothened is prevented, and active Smoothened prevents the phosphorylation and degradation of Gli2/3. This enables Gli2/3 to enter the nucleus and act as a transcription factor for a number of Hedgehog target genes. One of these target genes is FoxL1 (Madison *et al.* 2009), which has been shown by Kaestner *et al*. to be a regulator of BMP and Wnt signalling (Kaestner *et al.* 1997). Loss of the Hedgehog target FoxL1 results in increased proliferation in the intestinal epithelium and a distorted crypt-villus architecture

(Kaestner *et al*. 1997). A similar effect is caused by the loss of the Hedgehog ligand (and therefore activator) Ihh in the intestinal epithelium, which results in increased proliferation, crypt fission, and expanded ISC compartment (Kosinski *et al.* 2010). Most importantly, as Hedgehog is a paracrine signalling pathway with ligands being expressed in the epithelium and secreted, the pathway is activated in the stromal cells and so loss of Ihh in the epithelium resulted in disruption of the mesenchymal architecture and deterioration of the extracellular matrix. This highlights the importance of the interactions between the epithelium and the mesenchymal in tissue homeostasis.

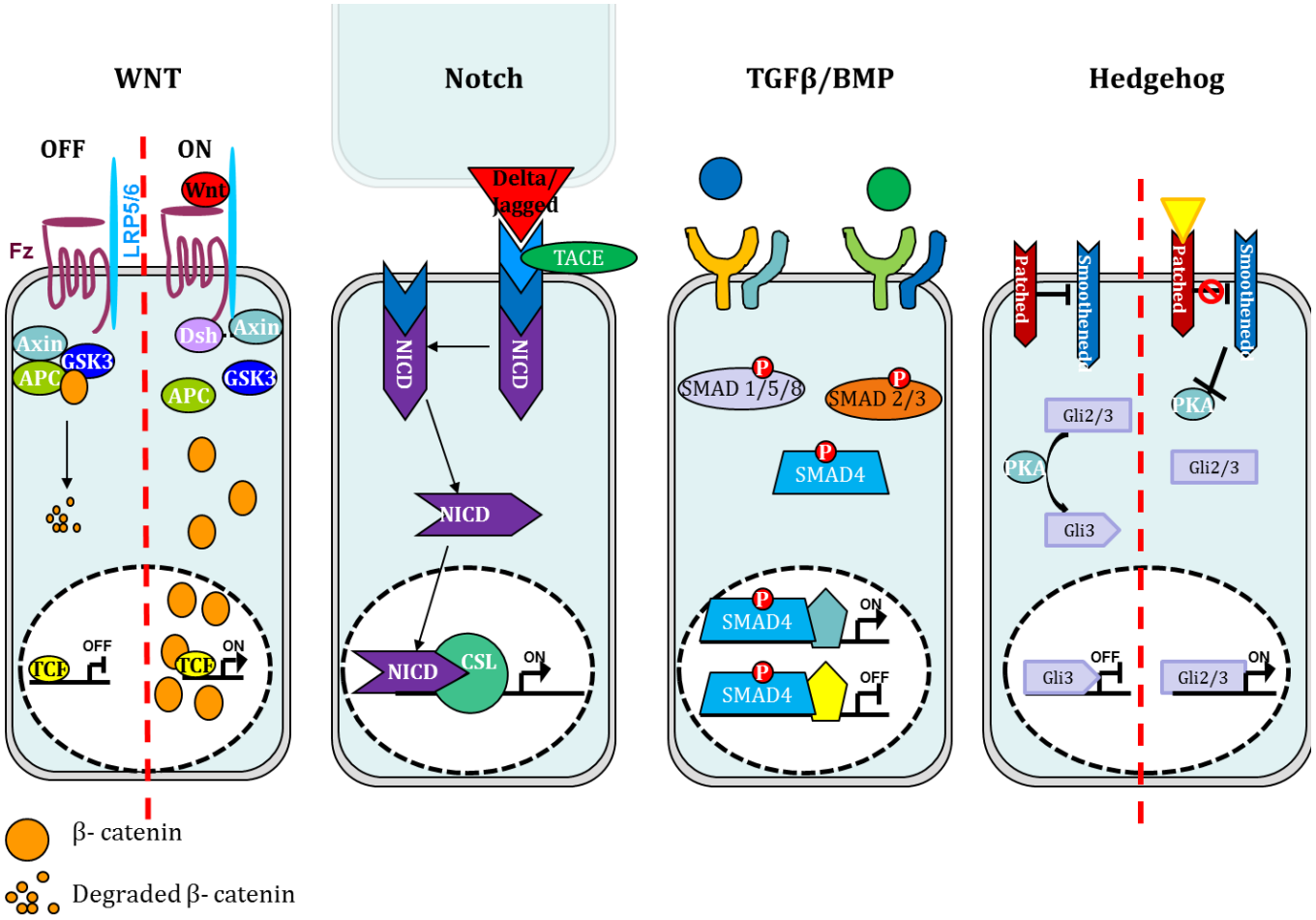

Figure 1.2 The four main signalling pathways involved in intestinal homeostasis; WNT, Notch,TGF/BMP and Hegdgehog signalling, which all control the expression of genes associated with homeostatic processes such as proliferation, apoptosis, differentiation, growth and migration.

1.3 Adult intestinal stem cells

The least well understood cells within the intestine are the undifferentiated cells found at the base of the crypt, referred to as intestinal stem cells (ISCs). These stem cells persist throughout the lifetime of an individual, and their progeny are capable of differentiating into any of the intestinal epithelial cell lineages. Both the location and the gene expression patterns seen within the ISC population are controversial. It has previously been reported that ISCs can be subcategorized into two distinct populations; the crypt base columnar cells (CBC cells) which are responsible for intestinal homeostasis and a quiescent population found at the +4 position within the intestinal epithelia which is only active after intestinal trauma (Tian *et al.* 2011; Yan *et al.* 2012). However, the data produced from extensive studies on the matter has been interpreted in a number of different ways.

1.3.1 Identifying the ISC: location and markers

Traditionally, an adult stem cell is described as a long-lived, slowly dividing cell, multi-potent and asymmetrically dividing. This does not appear to be the case for ISCs which despite being long-lived and multi-potent, are relatively very rapidly dividing cells, dividing every 24 hours (Barker *et al.* 2007) and appear to divide symmetrically (see section 1.3.2) (Escobar *et al.* 2011). However, this is relatively new knowledge and the quest to find ISC markers that match this dogma has hindered the identification of ISCs to date. However, this has not been the only problem encountered when studying ISCs. Due to the small number of ISCs (predicted to be 4-6 per intestinal crypt) (Booth and Potten 2000) expression levels of any markers are low, thereby making immunohistochemistry difficult. As a result, most ISC identification methods rely on FAC sorting or *in situ* hybridisation, both of which make it difficult to determine the exact location of cells expressing the markers (Gregorieff et al. 2005). Thus a number of stem cell markers have been proposed and later refuted making this is a very dynamic and evolving area of research.

For many years, DNA label retaining experiments were used to identify the "label retaining cell", assumed to be the ISC. Cells at the +4 position within the intestinal crypt were shown to retain thymidine DNA labels long term despite continued cell division (Potten *et al.* 1974). Later, studies reported that the +4 cells specifically express the

marker *Bmi1*, and that these cells were proliferative and capable of self-renewal, and so *Bmi1* expression has been widely used as a marker of ISCs (Sangiorgi and Capecchi 2008).

CBC cells are rapidly dividing (rapid in terms of stem cells) elongated cells at the base of the crypt which are interspersed with Paneth cells. In 2007, it was reported that CBC cells are specifically positive for the expression of *Lgr5*. Lgr5 was at the time classified as an orphan receptor, but it is now known to interact with R-spondins, Wnt activators found at the base of the crypt (Zhao *et al.* 2007). Despite their rapid cell division, $Lgr5^{+}$ cells were shown, using lineage tracing experiments, to be capable of generating all the cell lineages of the intestinal epithelium (Barker *et al*. 2007; Zhu *et al.* 2008). More recently, the $Lgr5^{+}$ cells were shown to be specifically capable of forming intestinal organoids in culture (Sato *et al.* 2009), see section 1.3.4. By analysing the differential gene expression profiles of $Lgr5^{hi}$ and $Lgr5^{low}$ intestinal epithelial cells, it has been possible to identify other proteins which are specifically expressed in CBCs, and it was through this method that expression *Olfm4* and *Ascl2* was identified as a potential marker of the ISC compartment (van der Flier *et al.* 2009a; van der Flier *et al.* 2009b). *Olfm4* encodes an anti-apoptotic factor that promotes tumour growth and facilitates cell adhesion, whereas *Ascl2* is an imprinted gene that encodes a basic helix loop helix transcription factor. Interestingly, of these three markers of CBC cells, only *Olfm4* is not a Wnt target gene, and so can be used to differentiate between changes in Wnt signalling and changes in the ISC population (Barker *et al*. 2007; Jubb *et al.* 2006; van der Flier *et al*. 2009a).

Other ISC markers have been proposed over the last decade, including *Hes1* and *Msi1* (Kayahara *et al.* 2003; Potten *et al.* 2003) due to the localisation of expression within normal and post-irradiated intestinal crypts, as well as increased expression in tumours derived from mouse models of intestinal tumourigenesis. The authors of these papers are careful that they only tentatively propose these genes as potential markers of the ISC population as a result of their localisation of expression, but much research has since been conducted which does not take this into account. This misunderstanding has resulted in new ISC markers being proposed as a result of their co-localisation with these genes. For example, Dckl1 was proposed as an ISC marker due to its co-

localisation with Msi1 (May *et al.* 2007), but was later reported to be in fact a marker of a rare intestinal epithelium secretory lineage called "tuft" cells (Saqui-Salces *et al.* 2011).

The ISC markers which seem to have been most successfully used, are those which were determined by comparing the gene expression pattern of $Lgr5^{+}$ cells to $Lgr5^{-}$ intestinal cells such as *Prominin1/Cd133*, *Ascl2* and *Olfm4* (Snippert *et al.* 2009; van der Flier *et al*. 2009a; van der Flier *et al*. 2009b) all of which specifically mark the CBC cells.

Over recent years it has been proposed that ISCs should be sub-categorised into rapidly dividing CBC cells which are responsible for intestinal homeostasis (identified by expression of *Lgr5*), and the more slowly dividing, label retaining +4 cells, which are thought of as "quiescent" stem cells and are activated in response to injury or cell death (identified by expression of *Bmi1*) (Tian *et al*. 2011; Yan *et al*. 2012). However, a recent paper from Hans Clever's laboratory has disputed this, by using both single transcript *in situ* hybridisation and transcriptional profiling of sorted $Lgr5^{hi}$ expressing cells to show that all of the current ISC markers overlap in their expression, although there appears to be a gradient of expression of many of the markers between the CBCs and the +4 cells (Muñoz *et al.* 2012). Other proposed markers for the +4 population of stem cells are HopX, mTERT and Lrig1 (Montgomery *et al.* 2011; Powell *et al.* 2012; Takeda *et al.* 2011), however, evidence contradicting the ability of each of these proteins to act as a marker for the +4 cell has been published by Barker *et al*., and so the controversy continues (Barker *et al.* 2012).

The controversy surrounding the idea of two distinct ISC populations has been more recently explored by Buczacki *et al*, who showed that the quiescent label retaining stem cells are in fact committed to the secretory lineage and will invariably mature into Paneth and enteroendocrine cells. This seems to be the case during homeostasis, however, after injury these previously quiescent cells can undergo rapid proliferation and produce all of the main epithelial lineages, indicating that they can be pulled back from committed quiescent cells into active stem cells (Buczacki *et al.* 2013). This was achieved through pulse-chase experiments showing that the label retaining cells can only form clonally populated crypts after injury by radiation, hydroxyurea or

doxorubicin. This seminal work shows not only the complexity and fluidity of the system, but the utility of lineage tracing experiments in dissecting this complex system.

All of the contradictory information published makes it very difficult to produce a definitive list of ISC markers. Much of the current literature is anchored around genes specifically expressed at the base of the crypt, although there is a growing consensus that *Lgr5*, *Ascl2* and *Olfm4* are key markers of an ISC population, but potentially not the only ISC population.

1.3.2 ISC division

The +4 stem cell is often referred to as the "quiescent" stem cell, due to its ability to retain a thymidine DNA label despite division (Potten *et al.* 1997). This assumed quiescence however, is not the conclusion arrived at by the research group who conducted the label-retaining experiment. This group presented a hypothesis known as the immortal strand hypothesis (Potten *et al.* 1978; Potten *et al.* 2002; Smith 2005). It was thought that the only way in which ISCs were able to protect their genome from a lifetime's build-up of mutations was by some form of strand selection, whereby the original DNA template strand is retained within the daughter stem-cell. This argument has since been refuted by studying DNA segregation within the CBCs as opposed to the +4 ISCs and clearly demonstrates unbiased segregation of the DNA strands at division (Escobar *et al*. 2011).

The retention of DNA labels lead to the assumption for many years that the intestinal stem cells divide asymmetrically to produce one intestinal stem cell, and one transit amplifying cell. (Potten *et al*. 2002; Smith 2005). This form of division is referred to as "invariant asymmetry". However, it was observed that intestinal crypts tend to drive towards monoclonality whereby, after a given period of time, the entire crypt is descended from one ISC (Loeffler *et al.* 1993). This does not correspond with the idea of invariant asymmetry which fails to provide an adequate explanation for crypt monoclonality.

Recently, another explanation has been proposed, whereby ISCs divide symmetrically either to produce two transit amplifying (TA) or two stem cells (SC) in an entirely stochastic manner (Figure 1.3), meaning that any of the ISCs within the crypt have an

equal likelihood of becoming the dominant clone. This hypothesis, termed "neutral drift" has been supported by mathematical modelling as well as some beautiful lineage tracing experiments from Hans Clever's laboratory whereby each ISC is individually labelled and the development of clonality can be seen (Fletcher *et al.* 2012; Lopez-Garcia *et al.* 2010; Snippert *et al.* 2010).

Interestingly, as ISCs provide both homeostatic and regenerative functions, it should be considered that there may be some kind of "choice" as to whether an ISC divides asymmetrically, or symmetrically to produce 2 stem cells or 2 transit amplifying cells. It could be argued that stochastic symmetrical or asymmetrical division is required for homeostasis, and during times when the stem cell is required for regeneration, the rate of stem cell division is increased in order to replace lost cells. However, there is also a case for the idea that gross intestinal cell damage drives a regenerative stem cell division pathway, with more cells dividing symmetrically to produce 2 TA cells. This would enable the regeneration of the intestine without exposing the stem cell to the damage which results from an increased number of divisions, however a mechanism which could drive this division choice remains unclear.

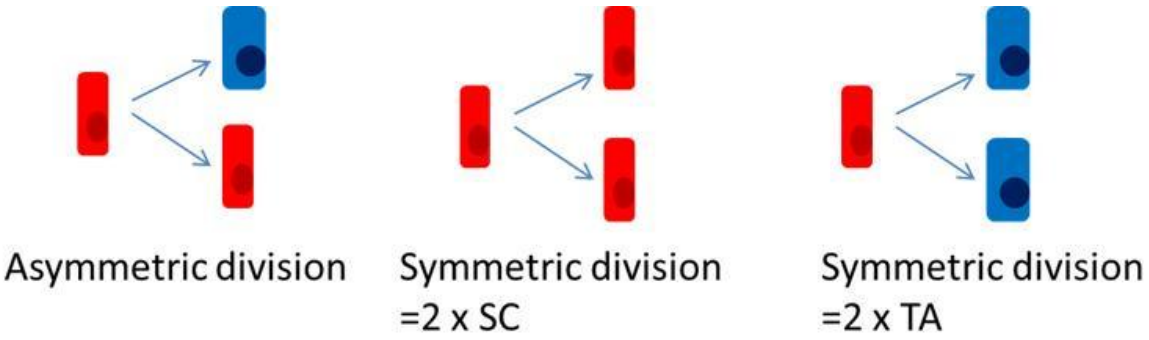

Figure 1.3 Diagrammatic representation of the three division "choices" which stem cells face. SC= Stem cell, TA= transit amplifying cell.

1.3.3 Stem cell niche

The ISC niche is described as the microenvironment in which the ISCs reside. It is thought that the niche may help establish or maintain stem cells by providing them with a range of signals. Paneth cells have long been thought of as the main constituent of the ISC niche due to their expression of TGF-α, Wnt3, the Notch ligand Dll4 as well as a range of antimicrobial factors, which are necessary in both the establishment and

maintenance of *in vitro* culture of ISCs (Bevins and Salzman 2011; Sato *et al*. 2010). This was supported by a study which showed that organoid growth efficiency (see section 1.3.4) was increased by the co-culture of $Lgr5^{+}$ cells with Paneth cells (Sato *et al*. 2010). Due to the importance of Notch signalling in the maintenance of the ISC population, coupled with the fact that Notch receptors and delta ligands are membrane bound requiring cell contact with the $Lgr5^{+}$ in order to activate Notch in the ICS, it is thought that the main role of Paneth cells within the ISC niche is the ability to activate the Notch signalling pathway (Fre *et al.* 2005).

If the Paneth cells are essential for the maintenance of the ISC niche then it would be assumed that loss of Paneth cells would result in complete crypt ablation. This experiment was attempted in two ways; by expressing the diphtheria toxin gene within Paneth cells (Garabedian *et al.* 1997) and by conditional knockout of *Sox9* (Bastide *et al.* 2007), both of which resulted in some crypt dysplasia, but failed to result in complete breakdown in crypt villus structure which would be expected from a loss of the ISC population. This was explained as being the result of incomplete loss of Paneth cells, and the ability of the intestine to repair itself after even major damage. Furthermore, at the time of the experiment there were few ISC markers available resulting in an incomplete analysis of the effects on the ISC compartment.

More recently, complete ablation of Paneth cells from the mouse intestine was achieved through the use of the $Math1^{-/-}$ mouse with the surprising result that Lgr5-expressing cells are in fact capable of survival, renewal and performance of all normal functions in the absence of Paneth cells (Kim *et al.* 2012). *Math1* is described as a Notch-repressed target gene since inhibition of the Notch pathway activates its expression. It is a driver of differentiation by pushing cells into the secretory lineage and inhibiting proliferation. An explanation for the surprising result from the study by Kim *et al.* is offered by the proposition that loss of the important differentiation factor *Math1*, may render ISCs independent of Notch signalling, thereby removing their dependency on neighbouring Paneth cells (Schuijers and Clevers 2012; Van Es *et al.* 2010).

A newly acquired self-sufficiency of Lgr5 stem cells due to the loss of *Math1* could explain why no change in intestinal homeostasis was seen in the absence of Paneth cells and could be tested by culturing $Lgr5^{+}$ cells from $Math1^{-/-}$ mice to assess if they are

capable of forming organoids in the absence of the Notch ligand Jagged which is required for the growth of organoids from single wildtype Lgr5$^+$ cells (section 1.3.4). However, it does not explain the observation by Kim *et al.* that Lgr5$^+$ cells are present at an earlier stage of intestinal development than the Paneth cells in normal mice (Kim *et al*. 2012), which would require the culturing of Lgr5$^+$ cells from an early developmental stage to assess if Notch dependency increases throughout development.

Despite the evidence discussed indicating that ISCs do not rely on the presence of Paneth cells for capacity to maintain intestinal homeostasis, recently we showed that Paneth cells are required for the ability of ISCs to repair the gut after trauma. By inducing loss of expression of *β*-catenin within the intestinal epithelium using either Villin-Cre (which recombines within the ISC and the Paneth cell as well as the other epithelial lineages) or AH-Cre (which recombines in the ISC and epithelia but not the Paneth cell) we were able to show that surviving ISCs were able to repopulate the intestine and retain function when the Paneth cell was unharmed, but were unable to in the absence of Paneth cells, thereby resulting in loss of crypt-villus architecture (Parry *et al.* 2013). This indicates that if there are indeed two distinct populations of ISCs, with one population responsible for homeostasis and the other responsible for damage repair, Paneth cells are an essential niche component only for the +4 cells, or they are required for interconversion between the two subsets of stem cells.

Despite the contradictory evidence, it is clear from these studies that Paneth cells play an important role in the maintenance of the Lgr5$^+$ ISCs, but their exact role is still far from clear, and the contribution of extraepithelial factors should not be underestimated. For example, it has been shown that the loss of Wnt3 from the intestinal epithelium *in vivo* causes no effect on intestinal morphology and function. However, the loss of Wnt3 in organoid cultures (where the extraepithelia compartment of the intestine is absent) results in organoid death, an effect rescued when the organoids are in co-culture with mesenchymal cells (Farin *et al.* 2012). This indicates that Wnt3 from sources other than the Paneth cell and the epithelial compartment plays an essential role in the maintenance of the ISC niche.

As previously mentioned, the importance of components contributing to the ISC niche can be assessed by their presence/absence during the time of development of the ISC

compartment. The establishment of the crypt-villus architecture with an ISC population occurs during perinatal development. Interestingly, during this stage of development thyroid hormone (T3) levels are particularly high. It is also known that loss of functional thyroid hormone receptor α results in deregulated intestinal morphology (Plateroti *et al.* 2001). This knowledge led to the recent study by Hasebe *et al*, in which T3 levels were manipulated during intestinal remodelling in amphibian metamorphosis to show that T3 is required by both the intestinal epithelium and the non-epithelial intestine (stroma and myofibroblasts) for the formation of ISCs (Hasebe *et al.* 2013). It has been shown that T3 regulates Hedgehog and BMP signalling (both important pathways involved in homeostasis of the ISC compartment) within the intestinal connective tissue, but not the epithelium, indicating the important role of cell-cell interactions and extra-epithelial factors in the maintenance of the ISC niche.

The complexity of the stem cell niche lies in its self-regulation. Potentially, the ISCs may be regulating their own niche by manipulating their microenvironment to suit their own requirements. The Kim *et al.* study in which Paneth cells were totally ablated from the intestinal epithelium without affecting homeostasis highlighted quite how fluid the system could be, with signals feeding both ways. This fluidity of the ISC niche is perhaps unsurprising, due to the importance of protecting the intestinal stem cell, and a highly regulated system has undoubtedly evolved to meet this requirement (Kim *et al*. 2012) .

1.3.4 In vitro culture of ISCs

In 2009 Sato *et al.* published a method which enabled the growth of intestinal organoids in culture. These organoids were grown from single mouse intestinal crypts and consisted of multiple crypt-like structures formed by crypt fission (Figure 1.4). Organoids can also be grown from single $Lgr5^{+}$ cells, thereby cementing the use of *Lgr5* expression as a marker of the ISC population (Sato *et al*. 2009). The culture conditions artificially mimic those found within the intestine; they are seeded in Matrigel, which not only enables 3-dimensional growth, but is laminin-rich, as laminin has been found to prevent cell anoikis when in culture (Sato et al. 2009). Epidermal Growth factor (EGF) is also used in intestinal organoid culture as it is associated with intestinal proliferation. Inhibition of the BMP signalling pathway is achieved by the addition of Noggin in order to prevent the inhibition of intestinal self-renewal caused by BMP

signalling (Haramis *et al.* 2004; He *et al.* 2004). Importantly, the growth factor R-spondin1 (Rspo1) is also required for intestinal organoid culture. R-spondins are only capable of enhancing the Wnt-signal within cells in the presence of canonical Wnt ligands, indicating that Rspo1 only enhances the Wnt-signal in cells which are already Wnt-activated, and within cells expressing an Rspo1 receptor, such as Lgr5 (Kim *et al.* 2008).

When growing these organoids from single cells sorted for their expression of Lgr5, there are additional growth factor requirements, as the "stem cell niche" is no longer present. These growth factors are Jagged, a Notch ligand which activates the Notch signalling pathway within the $Lgr5^{+}$ cells (a function normally carried out by Paneth cells) and the Rho kinase inhibitor Y27632. Rho kinase normally stimulates the activity of the tumour suppressor protein PTEN, and so it can be assumed that the addition of a Rho kinase inhibitor will result in higher levels of the oncogenic factor phosphorylated Akt (pAkt) (see Figure 1.6) which promotes cell survival (Li *et al.* 2005).

The organoid structures produced contained all the differentiated epithelial cell types found within the intestine and are structurally very similar to intestinal tissue.

This method represents not only a highly useful tool by which to test drugs, but also a way in which to understand the ISC niche. By altering the growth factor which enables single $Lgr5^{+}$ cells to form organoids, it could greatly help the understanding of what is required for an ISC to function as an ISC.

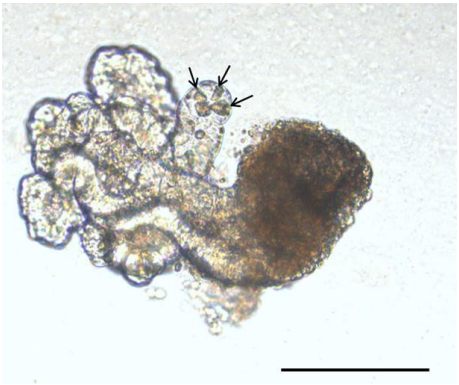

Figure 1.4 Organoid grown from a single intestinal crypt. Black bar represents 100μm. Black arrows indicate visible Paneth cells.

1.4 Colorectal cancer

Colorectal cancer (CRC) is the third most common cancer in the UK, with 37,500 people being diagnosed every year. Although CRC survival rates have doubled in the last 30 years, over half of all sufferers do not survive for longer than 5 years after diagnosis, despite it being curable if diagnosed early.

There are a number of reasons why the incidence of CRC is so high. The high rate of cell division required to maintain the rapid turnover of cells within the intestinal epithelia, results in a high incidence of DNA replication errors and so a build-up of DNA mutations in these cells makes oncogenic mutations likely. Also, the direct exposure of intestinal cells to potential carcinogens via ingested food further increases the mutation rate.

The development of sporadic CRC is a multistep process in which an accumulation of genetic mutations leads to the progression from normal intestinal epithelium to dysplastic tissue to benign adenoma through to metastatic carcinoma. Based on studies of the frequency of gene mutations at various stages of progression in human tumours, Fearon and Vogelstein proposed a model whereby loss of function of *Adenomatous polyposis coli (*APC) initiates the formation of a benign lesion, followed by an activating mutation in KRAS, allelic loss of the 18q locus and mutation of p53, which all contribute to the progression to malignant disease (Fearon and Vogelstein 1990), (Figure 1.5).

The reason that the levels of mortality associated with this disease are so high is mainly due to late detection, as a patient usually only presents with symptoms once the disease has reached late stages and metastasised. It has been shown that one round of faecal occult blood screening (which examines a patients stool for non-visible traces of blood) reduces the relative risk of mortality associated with CRC by 25% as a consequence of earlier detection (Hewitson *et al.* 2007; Mandel *et al.* 1993). In order to develop more screens for early detection of CRC it is essential that the early stages of colorectal tumourigenesis are well understood.

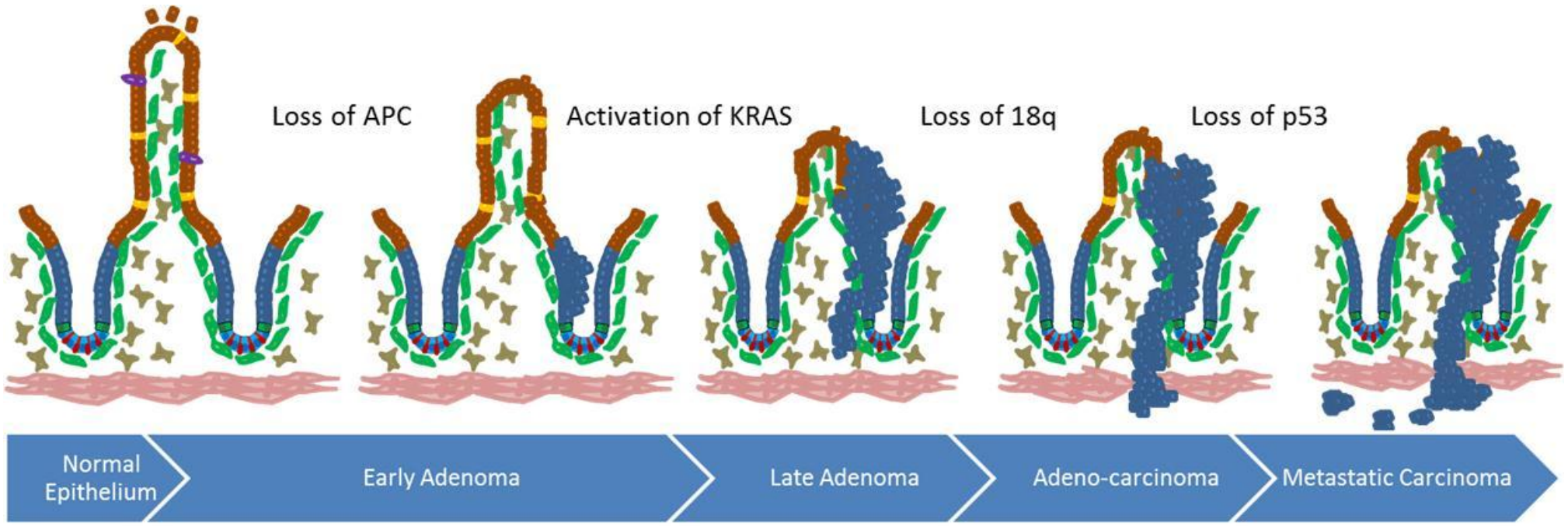

Figure 1.5 Model of tumour intitiation and progression as proposed by Fearon and Vogelstein

1.4.1 Signalling Pathways associated with CRC

As cancer is simply unregulated cell division it is unsurprising that most of the signalling pathways which are implicated as playing a role in CRC are pathways which play an important role in intestinal homeostasis.

1.4.1.1 PI3K pathway

Mutations which cause the constitutive activation of the phosphoinositide-3-kinase pathway (PI3K pathway) are found in 40% of all CRC tumours (Parsons *et al.* 2005). Activation of this pathway is normally the result of upstream receptor tyrosine kinases (RTKs) which cause phosphorylation of phosphatidylinositol-4-5-biphosphate (PIP_2) which generates phosphatidylinositol-3-4-5-biphosphate (PIP_3). PIP_3 recruits AKT to the cell membrane where it is phosphorylated by phosphoinositide dependent kinases, converting it into its active form (pAKT) which can initiate translation, transcription, cell cycle progression as well as inhibit apoptosis through its kinase activity, see Figure 1.6. PTEN (phosphatase homolog of tensin) is a lipid phosphatase and an important negative regulator of the PI3K pathway. It is therefore a tumour suppressor, which acts by converting PIP_3 into PIP_2. Reduction of PIP_3 via PTEN results in the prevention of Akt recruitment to the membrane and its subsequent activation. Mutations which result in constitutive activation of this pathway can be either activating mutations of RTKs or inactivating mutations of downstream negative regulators of the pathway, such as PTEN. Interestingly, pAKT is responsible for the activation of GSK3 (Voskas *et al.* 2010), an important negative regulator of the Wnt pathway, and so there is a great deal of cross talk between the two pathways.

Knowledge of the PI3K pathway has led to the development of a number of targeted therapies such as Trastuzumab, an antibody which targets human epidermal growth factor receptor 2 (HER2), a potent activator of the PI3K pathway. This therapy has been shown in phase III trials to significantly increase survival in patients with gastric tumours which express HER2 when used in conjunction with chemotherapy (Roukos 2010). However, this treatment only increases survival for a couple of months as tumours become resistant via downstream activation of the pathway. Because of this, more targeted therapies are being sought from the range of proteins downstream in the pathway and many inhibitors of the PI3K pathway are currently in clinical development.

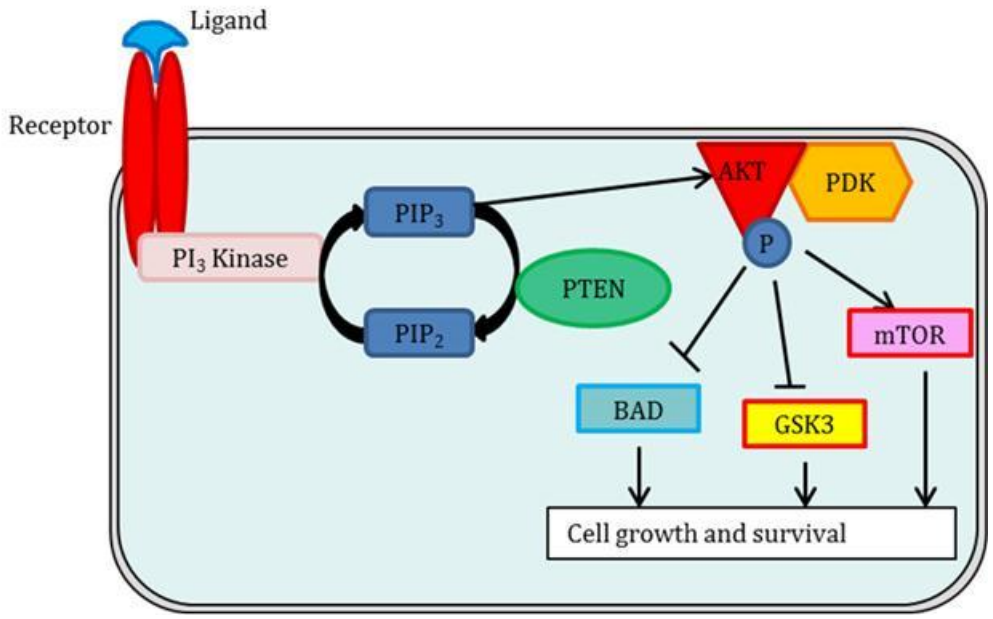

Figure 1.6 The PI3Kinase pathway. Activation of the pathway by receptor binding results in the conversion of PIP_2 to PIP_3 which translocates AKT to the plasma membrane where it is phosphorylated by phosphoinositide dependent kinases (PDKs) into its active form, pAKT.

1.4.1.2 Wnt and cancer

As Wnt-target genes have been shown to control a number of regulatory processes associated with tumourigenesis, such as cell proliferation and adhesion (Staal *et al.* 2004), it is unsurprising that abnormalities within this pathway are closely associated with cancer, particularly CRC (Bienz and Clevers 2000; Polakis 2000).

Wnt signalling has also been linked to cell migration within the colon, and so may also be involved in the ability of early tumourigenic cells to metastasise. There seems to be a great deal of potential to target the Wnt pathway therapeutically to control tumourigenesis and metastasis and much work is ongoing to develop Wnt inhibitors as a potential therapeutic treatment to colorectal cancer (Dihlmann and von Knebel Doeberitz 2005). In order to do this effectively the Wnt signalling pathway needs to be fully elucidated with gene interactions and their effect on the tumourigenic properties of the cells and organism understood.

Mutations in the important negative regulator of the Wnt signalling pathway, *APC,* are an early initiating step in the formation of spontaneous CRC, with loss of heterozygosity (LOH) of the *APC* gene occuring at an early stage of colorectal tumour progression. It has also been shown that *APC* mutations which result in activated Wnt-signalling are

present in over 80% of human colorectal tumours (Powell *et al.* 1992). Loss of functional APC leads to an increase in nuclear β-catenin, where it can act, along with TCF as a transcription factor to drive expression of a range of Wnt target genes.

1.5 Modelling CRC in the mouse

The importance of the Wnt signalling pathway, particularly during development, means that many of the molecular interactions and signalling strategies used within the Wnt pathway are highly conserved between species. As such, the pathways are extremely comparable between humans and mice. Mouse models are useful not only because genetically engineered mice can be generated in a relatively short space of time, but because they also enable the long term study of tumourigenesis, as well as investigating the roles that diet and environment play in tumourigenesis, which is not possible when using cancer cell lines.

1.5.1 Mouse models of FAP

APC was originally identified as the gene that is mutated in cases of familial adenomatous polyposis (FAP). FAP is an inherited autosomal disorder, sufferers of which develop multiple colonic polyps at a young age. Although the polyps are benign, there is a high risk that some will progress into malignant adenocarcinomas if left untreated (Groden *et al.* 1991).

In 1990 a mouse which modelled FAP was identified within a colony of mice following random mutagenesis. Termed the Multiple Intestinal Neoplasia mouse (MIN), it carries a truncation mutation at codon 850 in one allele of the mouse homologue of *APC* and was reported to develop multiple adenomas throughout the entire intestinal tract from an early age (Moser *et al.* 1990). The development of the Apc^{min} model was a turning point in the study of CRC, and it was soon followed by a variety of different $Apc^{+/-}$ mutants, which shared the same phenotype of development of multiple adenomas, but interestingly differed in the number, size and location of the adenomas depending on the type of *Apc* mutation (Fodde *et al.* 1994; Su *et al.* 1992).

$Apc^{+/-}$ mutants proved exceptionally useful in the study of modulators of Wnt-dependent tumourigenesis. Using these model mice, it was possible to perform microarrays at various stages of tumour development, and establish a list of genes

which are expressed abnormally from the earliest stages of tumourigenesis, as these genes potentially play an important role in tumour initiation (Young *et al.* 2013). It was through such a study that the importance of the *COX-2* (*PTGS2*) gene was determined. Cox-2 was shown to be expressed from a very early stage of polyp formation, and so *Cox-2* knockout mice were crossed with $Apc^{+/-}$ mice and it was shown that COX-2 deficiency drastically reduced adenoma formation in these mice, and that chemical inhibitors of COX-2 could achieve the same effect (Oshima *et al.* 1996). Drug trials showed that the effect seen in *Apc*-deficient mouse models was also true for humans and although prescription must be carefully regulated due to cardiovascular side effects, the COX-2 inhibitor can significantly lower the number of colorectal polyps formed in FAP patients (Steinbach *et al.* 2000).

1.5.2 Cre-lox technology

Despite the utility of the Apc^{min} mouse in studying intestinal tumourigenesis, it has limited use when trying to study the earliest stages of disease. One of the earliest stages of disease onset is the inactivation of both alleles of *APC* (Gryfe *et al.* 1997) and in the min mouse the time of LOH is unknown, so a model whereby both *Apc* alleles could be deleted at a known time point was essential. Use of the Cre-loxP recombination system (Figure 1.7) has enabled the initial stages of intestinal tumourigenesis to be studied in detail. By inducing conditional loss of both alleles of *Apc* within the intestinal epithelium it has been shown that functional Apc is essential to maintain normal intestinal homeostasis, and loss of *Apc* immediately deregulates the tissue morphology by affecting migration, differentiation, proliferation and apoptosis (Sansom *et al.* 2004). Interestingly, this paper observed that the intestinal cells took on the appearance of "crypt progenitor cells", supporting the evidence that Wnt signalling controls the intestinal stem cell population.

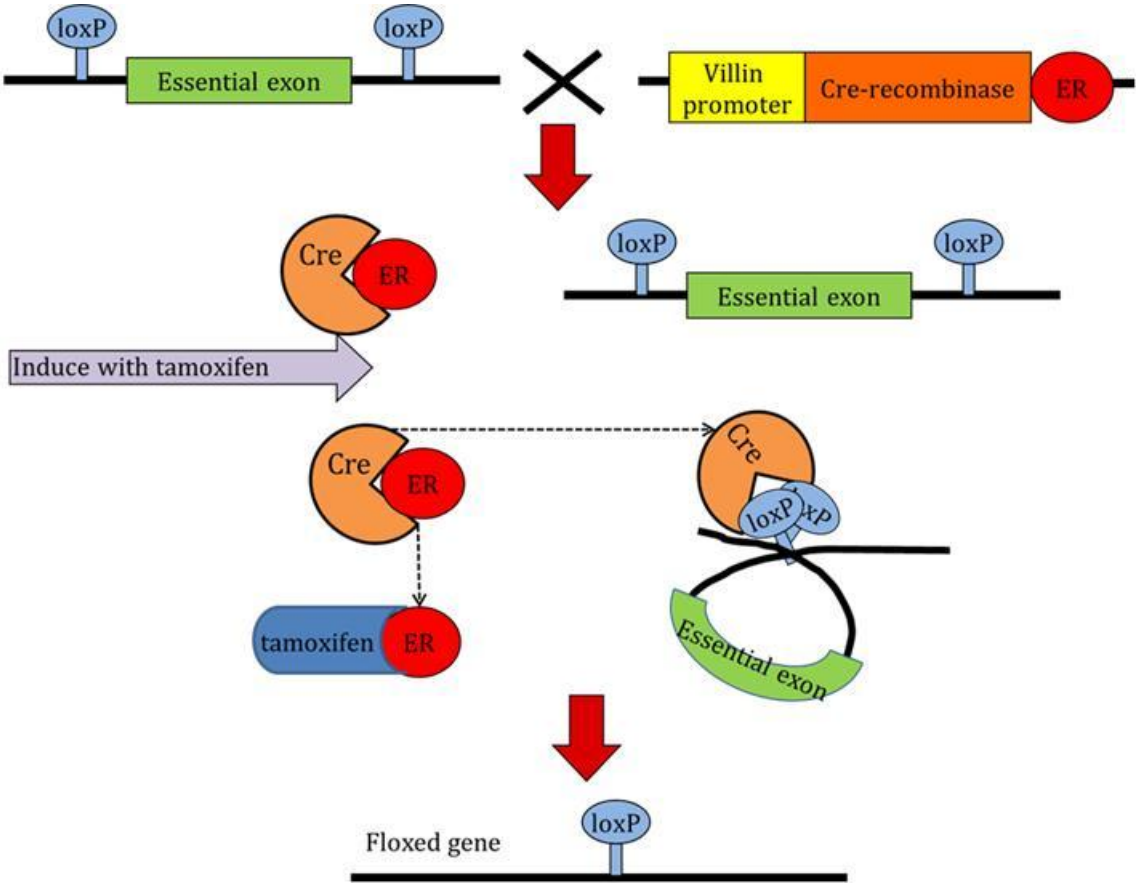

Figure 1.7 Cre-Lox Technology. When tamoxifen is administrated to mice which possess both the essential exon of the gene of interest flanked by LoxP sites and an oestrogen bound Cre-recombinase, the tamoxifen frees the Cre-recombinase and enables recombination between LoxP sites resulting in the excision of the essential exon. This method is used to temporally control gene loss.

When expressed, Cre-recombinase will recombine DNA between any two loxP sites in the same orientation. In this example, Cre-expression is linked to the tissue-specific promoter villin, which will express in the intestinal epithelia, including the ISCs. The transgene encodes a Cre-recombinase estrogen-receptor (ER) linked protein, which is inactive until an injection of tamoxifen binds the ER, freeing the Cre-Recombinase. This results in a tissue specific conditional knock out, induced by tamoxifen injection. One of the main advantages of this model is the ability to use different promoters to drive expression of the Cre-recombinase, and thereby drive recombination of the floxed gene in any number of specific cell compartments, for example using a Cre-recombinase linked to expression of the ISC marker Lgr5 results in recombination specifically within the ISC compartment. The utility of this extends beyond providing the ability to

determine the importance of mutation location on tumourigenesis, but also enables cell lineage tracing experiments using a lacZ reporter gene which once recombined expresses β-galactosidase which can easily be stained blue by performing an X-gal stain. Daughter cells of the recombined cells will also stain blue, as can be seen from Figure 1.8 where recombination within ISC compartment enables visualisation of all daughter cells of single ISCs as they migrate up the crypt-villus.

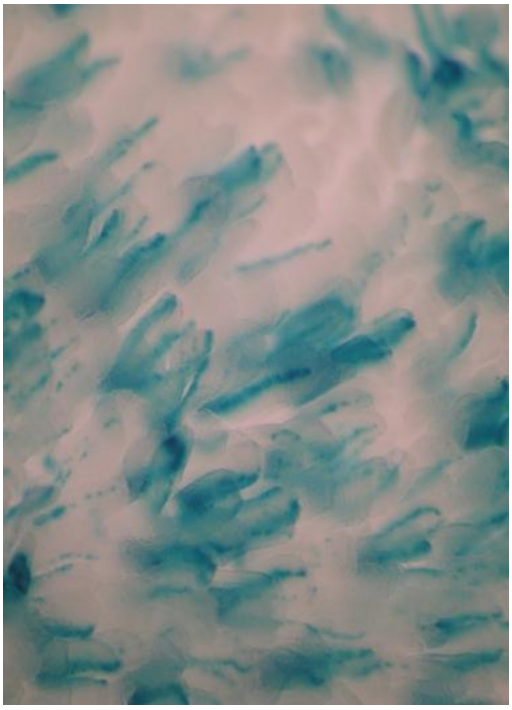

Figure 1.8 LacZ stain of mouse small intestinal villi. Each stripe of blue represents all of the progeny of a single recombined ISC using Cre-recombinase linked to Lgr5 expression.

Cre-lox technology not only enables the study of the early stages of tumourigenesis via *Apc* deletion, but also enables the study of loss of genes which are embryonic lethal. For example, Cre-Lox technology has been used to study the effects of the loss of expression of the important tumour suppressor *Pten*, which is embryonic lethal. Loss of *Pten* results in increased levels of PiP_3 which recruits Akt to the membrane, thereby increasing the levels of activated Akt. This effectively models the effects of constitutive PI3K pathway activation which is seen in many human CRC tumours. This method was used by Marsh *et al.*, and showed that *Pten* loss in the adult mouse has no effect on the

homeostasis of normal intestine, but does cause accelerated tumourigenesis when coupled with defiency of *Apc* (Marsh *et al.* 2008).

1.5.3 β-catenin mutant mouse models

Another method of modelling Wnt-dependent CRC is via the expression of a mutant form of β-catenin which is far more stable in the cell and therefore resistant to proteasomal degradation. Mutations which result in a stabilised form of β-catenin are found in a subset of human colon tumours which do not carry the *APC* mutation. When modelled in the mouse, conditional stabilisation of β-catenin results in the formation of multiple tumours. Interestingly, the work was originally performed with expression of Cre-recombinase being driven by the calbindin promoter (which is not expressed in the proliferative zone of the intestine) and resulted in few tumours (Romagnolo *et al.* 1999). Subsequently Cre-expression driven by a fatty acid binding protein gene promoter (which is expressed in the proliferative zone) was shown to result in many thousands of adenoma (Harada *et al.* 1999). These mouse models of CRC lead to the idea that oncogenic mutations in cells at the base of the crypt play a more important role in CRC than mutations in the differentiated cells along the crypt-villus axis.

1.6 Intestinal stem cells as the cells of origin of CRC

A study in 2008 used an Lgr5-promoter driven Cre to show that when *Apc* is deleted specifically within the $Lgr5^{+}$ cell population, microadenomas form within the intestine within 3-5 weeks and develop rapidly to adenomas, whereas when *Apc* is deleted specifically from the transit-amplifying region, microadenomas are rare (Barker *et al.* 2008). The loss of *Apc* in differentiating cells is thought to have so little effect because the cells are so rapidly lost from the villi. However, *Apc* mutations in $Lgr5^{+}$ cells, as the ISCs, results in the population the whole crypt and villus with $Apc^{-/-}$ cells, thereby causing tumourigenesis. This result shows the importance of the relationship between the ISCs and tumourigenesis, and that expansions in the ISC compartment would provide the intestine with a higher number of cells of potential cancer origin.

Despite the ISC being described as the cell of origin of intestinal cancer, other epithelial cells are capable of driving tumourigenesis, but it has been presented that ISC derived tumours are more aggressive (Barker *et al*. 2008).

1.7 Cancer stem cells

Cells within a tumour often maintain a high degree of similarity to the cells of the tissue from which they originated, with similar interactions with the environment, and responses to molecular control mechanisms. This similarity with normal tissue could be taken forward to suggest that, like their tissue of origin, tumour cells are also organised into a hierarchy, with less and more potent cells present. The cancer stem cell hypothesis maintains that only a sub-population of cancer cells are capable of populating and maintaining the tumour, and it is only these cells which are capable of metastasising to form new tumours. As such it is essential that these cells are targeted by treatment.

This idea is now supported with a great deal of data, which show that in both Leukaemia (Bonnet and Dick 1997; Lapidot *et al.* 1994) and a variety of solid tumours such as breast (Al-Hajj *et al.* 2003), brain (Singh *et al.* 2004) and colon (O'Brien *et al.* 2006) there is a sub-population of cells which can form a new tumour when transplanted into an immune deficient mouse, but that the bulk of tumour cells are incapable of this. This insight has led to the cancer stem cell hypothesis.

In the field of CRC, analysing the heterogeneity of tumour cells taken from solid primary tumours of CRC patients enabled the sorting of tumour cells according to the expression of various cell surface makers. It was found that of all the different expression patterns of these tumour cells, a small subpopulation of epithelial cells which expressed a high level of epithelial cell adhesion molecule (EpCAM) as well as CD44 (which is a reported breast cancer stem cell marker) were the only population of tumour cells capable of engraftment into immune-deficient mice (Dalerba *et al.* 2007). Interestingly, the tumours that they formed in these xenograft experiments re-acquired the same heterogeneity of expression patterns and phenotype seen in the parental tumour. This indicates that the $EpCAM^{high}/CD44^{+}$ tumour cells represent a subpopulation of CRC cells capable of populating and expanding a tumour, therefore potentially represent the cancer stem cell population.

The ability of tumour cells to form tumours upon transplantation and serial transplantation into immune deficient animal models is seen as the gold standard for identification of cancer stem cells, however many argue that xenotransplantation is an

inappropriate method for identification of such cells. This controversy is based on the idea that xenotransplantation does not model a physiologically relevant environment of tumour growth, and that these assays are simply isolating a subpopulation of cells that have an increased fitness for survival in abnormal conditions. Interestingly, it was shown by Quintana *et al.* that the frequency of melanoma cells with tumourigenic ability is dramatically altered by the level of immune deficiency of the host animal into which they are transplanted (Quintana *et al.* 2008). This work indicates that the xenotransplantation assay may not be the most appropriate method for identifying CSCs.

The recent drive to expand the knowledge base surrounding the cancer stem cell hypothesis has resulted in new, convincing supporting evidence using lineage tracing in models of sporadic tumourigenesis. Schepers *et al*. used the confetti mouse (previously used to elucidate monoclonality within the crypt) in order to demonstrate that intestinal adenoma growth is fuelled by a subpopulation of adenoma cells which express the ISC marker Lgr5 (Schepers *et al.* 2012). This important study also showed that the $Lgr5^{+}$ adenoma cells are intermingled with Paneth cells, indicating that they may require a similar sort of niche environment to normal ISCs. It should be noted that sorted $Lgr5^{+}$ intestinal tumour cells have not yet been able to form tumours when transplanted into immune deficient mice and so despite being multipotent, they have not yet been shown to possess self-renewal capacity.

This work highlights the importance of choice of approach when attempting to identify CSC markers, and hints that despite the attractiveness of the CSC hypothesis, many of the markers which have already been published do not necessarily represent a true CSC population.

1.7.1 Cancer stem cells and chemotherapy

Most currently used chemotherapeutics target rapidly dividing cells which make up the bulk of the tumour, however it is thought that they are not as effective against the slowly dividing cancer stem cells. This results in the relapse of disease as cancer stem cells can repopulate the tumour after treatment (Figure 1.9). This knowledge has led to an increase in the number of studies aimed at understanding the drug sensitivity of CSCs to compounds used to treat the cancer, and it has been found in a number of

studies that less differentiated cell types within a tumour are often less sensitive to drugs (Ho *et al.* 2007; Levina *et al.* 2008).

Interestingly, it has recently been shown that a number of ABC transporter proteins (which have been associated with drug efflux) are associated with stem cells, and if this is the case in CSCs then potentially this sub-population of tumour cells may be markedly more resistant to chemotherapeutics than the bulk of the tumour (Al-Hajj *et al.* 2004).

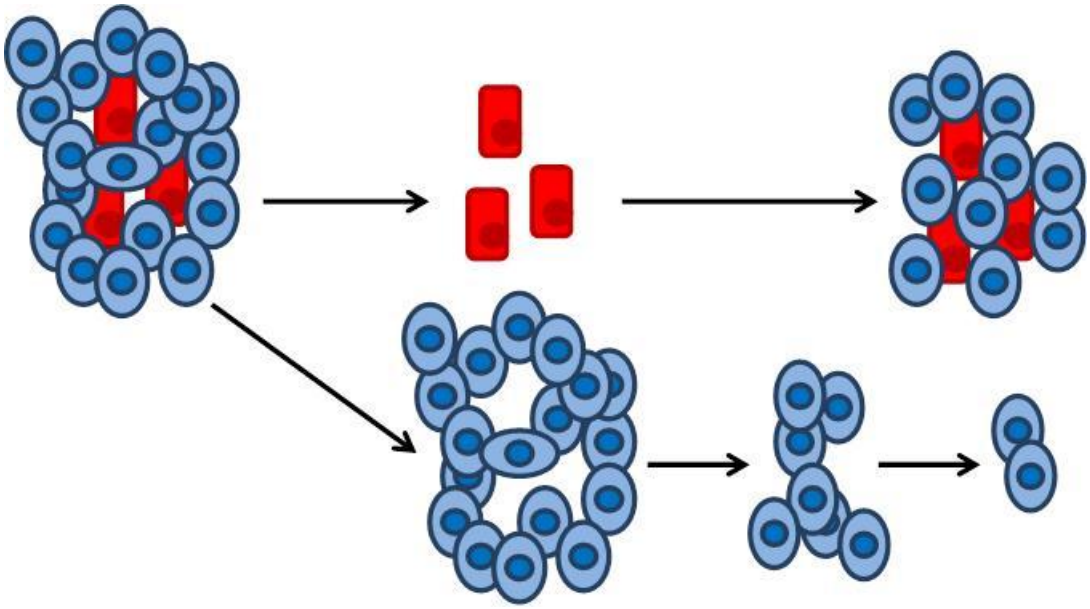

Figure 1.9 Cancer stem cells and chemotherapeutics. Current chemotherapeutics target rapidly dividing cells, thereby reducing tumour size (tumour bulk shown as blue cells) but can leave the less rapidly dividing cancer stem cells (represented in red) unaffected, enabling them to re-establish the tumour and cause relapse. By targeting the cancer stem cells, it may be possible to cause tumour regression as well as prevent metastasis.

It is evident that some method of targeting cancer stem cells is necessary in order to permanently treat the disease, however, this presents a number of difficulties. What we know about normal adult stem cells indicates that there is likely to be some sort of cancer stem cell niche, whereby the direct environment of the cancer stem cell promotes its existence. What is unknown is whether the niche regulates the stem cells or if the stem cells regulate their own niche. If it is the former then simply killing the cancer stem cells will not have any effect as whichever cell finds itself in the niche will

be driven to become a cancer stem cell. For this reason a greater understanding of the relationship between cancer stem cells and their niches is required in order for this hypothesis to be put to therapeutic use.

Another difficulty commonly encountered when attempting to produce a therapy which specifically targets CSCs, is the similarities between normal ISCs and CSCs. Any treatment which does not distinguish between the two types of cells could cause severe damage to normal intestinal tissue. One recent attempt to expand the differences between the two populations of cells showed that expression of Dclk1 can differentiated between ISCs and CSCs. Using Cre-induced lineage tracing experiments, this study showed that normal intestinal cells which express Dclk1 do not represent the ISC population, whereas tumour cells which express Dclk1 represented a proliferative population of cells at the base of the polyp (Nakanishi *et al.* 2012). Developing this theme, this study then explored how the knowledge of these differences between CSCs and ISCs could be of use to therapy. By specifically ablating Dclk1 positive cells in Min mice, it was shown that normal intestinal epithelium was undamaged, but there were high levels of tumour regression. This example represents how increased understanding of both normal ISCs and CSCs, as well as the relationship between the two, can result in the uncovering of potential therapeutic targets.

Recently there have been some positive outcomes from the use of the CSC hypothesis, namely the development of Metformin (currently a treatment for diabetes) alongside traditional chemotherapeutics to selectively target cancer stem cells, so far with a great deal of success (Cufí *et al.* 2010; Hirsch *et al.* 2009). It is now thought that Metformin functions by inhibiting Transforming Growth Factor-β (TGF-β) driven Epithelial-Mesenchymal Transition (EMT). Metformin is beginning to show its worth as a breast cancer treatment in a variety of trials (Martin-Castillo *et al.* 2010) and as data accumulates it will be interesting to see whether drugs which target CSCs in this way will reduce the risk of relapse post-recovery.

Aims and Objectives

The importance of the relationship between ISCs and intestinal tumourigenesis is clear, not only due to the identification of ISCs as the "cell of origin" of intestinal adenomas (Barker *et al*. 2008), but because conditional homozygous loss of the tumour suppressor gene *Apc* results in an increase in undifferentiated cell types (Sansom *et al.* 2004b). This indicates that an early stage of tumourigenesis may involve an expansion of the intestinal stem cell compartment.

Currently, assessment of the ISC compartment relies on the use of gene expression markers, either by *in situ* hybridisation or qRT-PCR. The specificity of these genes to mark the ISC population is continually debated (Barker *et al*. 2012), and they do not provide a readout of changes in the functional potency of the ISC compartment.

The two main objectives of this thesis are therefore to develop a functional assay for the assessment of the ISC compartment and to apply this assay to a variety of mouse models of colorectal cancer in order to identify how changes in the ISC compartment contribute to tumourigenesis.

To address the first objective I will be utilising the known functional properties of ISCs; the ability to produce daughter cells of all of the intestinal epithelial lineages, and as such, form intestinal organoids in culture (Sato *et al*. 2009). I will use this technique to investigate the potential of organoid formation efficiency as a readout of the functional stem cell compartment.

In order to assess how changes in the ISC compartment contribute to tumourigenesis I will be using a number of novel models. The role of Wnt-signalling in the maintenance of the ISC compartment will be interrogated through loss of the Wnt-target gene *Cited-1*, individual and combined loss of *Apc* and its homologue *Apc2*, and cross talk with the PI3K pathway will be examined using loss of the negative regulators of PI3K, *Pml* and *Pten* on an *Apc* deficient background. The intestinal phenotype of these models will be described, not only by analysing the effect of gene deficiency on tumourigenesis and intestinal homeostasis but in relation to changes within the ISC compartment, as assessed by gene expression patterns and ISC functionality.

2 Materials and Methods

2.1 Experimental Animals

2.1.1 Animal Husbandry

All animals were housed according to UK Home Office Regulations; mice were given access to the Harlan standard diet (Special Diets Service UK, expanded diet) and water *ad libitum*.

2.1.2 Breeding

All mice were maintained on an outbred background. Mice of 6 weeks and older of known genotype were bred in trios of one male and two females. Pups were weaned at approximately 4 weeks old when feeding independently. Pups were sexed and separated at weaning then ear clipped for identification purposes.

2.2 Genetic Mouse Models

A number of transgenic mouse models were utilised within this project, see Table 1. The transgenes used either resulted in a constitutive deletion of the gene of interest or contained exons of the gene of interest flanked with LoxP sites, to enable conditional deletion of the genes. The only Cre-recombinase transgene used in this thesis was VillinCreER which is expressed in the intestinal epithelium where it is inactive whilst fused to a mutated estrogen receptor. This Cre-recombinase becomes active in the presence of tamoxifen.

2.3 Experimental Procedures

All procedures were conducted according to appropriate UK Home Office Regulations, and fell within the remit of the project licence code 30/2737.

2.3.1 Ear biopsy for genotyping

As the tissue from the ear biopsy taken for identification purposes was also used for DNA extraction and genotyping, (see section 2.4.1) the ear biopsy is defined as an experimental procedure. As such it was performed by a licensed individual in a designated procedure room. Ear biopsies were taken using a 2 mm ear punch (Harvard

apparatus). When DNA from ear biopsy was not suitable for genotyping, tail biopsy was utilized to surgically remove 3-5 mm of the tail tip under local anaesthetic.

Transgene	Effect
VillinCre ER^T (El Marjou *et al.* 2004)	Intestinal epithelial cells, tamoxifen inducible
LoxP targeted *Apc* allele (Shibata *et al.* 1997)	Endogenous *Apc* allele bearing LoxP sites flanking exon 14
LoxP targeted *Pten* allele (Suzuki *et al.* 2001)	Endogenous *Pten* allele bearing LoxP sites flanking exons 4 and 5
Pml$^-$ allele (Wang *et al.* 1998)	Constitutive *Pml* knockout.
Cited1$^-$ allele *(*Rodriguez *et al.* 2004)	Constitutive *Cited1* knockout
Apc2 $^-$ allele (Van der Meer *et al.* 2001)	Constitutive *Apc2* knockout

Table 1 Outline of the transgenic mouse models used within this thesis

2.4 Genotyping of mice using Polymerase Chain Reaction (PCR)

PCR was performed to genotype weaned mice using genomic DNA (gDNA) extracted from ear biopsy. Confirmatory genotyping was also performed at time of death to ensure the mouse was assigned to the correct experimental cohort. PCR was kindly performed by Mark Bishop.

2.4.1 DNA extraction

Ear biopsies were placed in a labelled microtube and stored at -20°C until use. Cell Lysis Solution (Gentra, 250 µl) and Proteinase K (Roche, 5 µl of 20 mg/ml) were added and incubated in a shaking incubator at 40°C overnight (O/N). Protein Precipitation Solution (Puregene, 100 µl) was added and mixed by inversion. Following centrifugation for 10 minutes at 13000 rpm, the supernatant was carefully removed and placed in a fresh microtube with 250 µl isopropanol. This was mixed by inversion and centrifuged at 13000 rpm for a further 15 minutes then the supernatant removed and discarded. The pellet containing the precipitated gDNA was resuspended in 250 µl of Ultrapure H_2O (Sigma). gDNA was stored short term at room temperature (RT) and at 4°C for long term storage.

2.4.2 PCR Protocol

PCR was carried out in thin-wall 12-well strip tubes (Grenier, Bio-One). 2.5 µl of gDNA, extracted as described above, was added to each tube with 47.5 µl of PCR mix (described in Table 2) containing the DNA polymerase and buffer appropriate to the PCR (see Table 3), Ultrapure H_2O (Sigma), Magnesium Chloride (Promega), dNTPs (Bioline) and gene specific primers. One control tube, made up as described above but with the DNA replaced with Ultrapure H_2O (Sigma), was run with every PCR reaction. Primers were either designed using Primer3 software (http://primer3.ut.ee/) and specificity confirmed using BLAST engine against the Ensembl database (http://www.ensembl.org/Mus_musculus/Info/Index) or used as described from previous publications. Specific primer sequences used can be found in Table 3.

The caps were then firmly placed on the tubes and the PCR reactions run on a thermocycler (G storm). Conditions are described in Table 3.

	Volume Required
Buffer	10 µl
Mg (25 mM)	5 µl
dNTPs	0.4 µl
Primers (100 µm)	0.1 µl
Taq polymerase	0.2 µl
H_2O (Sigma)	31.8 µl

Table 2 Constituents of PCR mix

Gene	Primers	Taq Polymerase	Buffer	PCR conditions
Apc^{flox}	**F** GTT CTG TAT CAT GGA AAG ATA GGT GGT C R CAC TCA AAA CGC TTT TGA GGG TTG ATT C	DreamTaq	Green	95°C, 3 min (95°C, 30 s; 60°C, 30 s; 72°C 1 min) $_{30}$ 72°C, 5 min.
$Apc2^{-}$	**F1** AGC TGT GTC TGA TGA GGT G **F2** AGG TCT GAA GAG GAG TTT AC **R** CTC CAA ACA CAA GAT GAT CG	GoTaq	Clear	95°C, 3 min (95°C, 30 s; 60°C, 30 s; 72°C 1 min) $_{30}$ 72°C, 5 min.
$Cited^{-}$	**F1** TTA CTT GCA GAC CAA CAG GC **F2** TGT TGC ATC ACC TTC ACC CT **R** TGC TTC TTT GAC CCA TTT CC	GoTaq	Clear	95°C, 3 min (95°C, 30 s; 60°C, 30 s; 72°C 1 min) $_{30}$ 72°C, 5 min.
Cre	**F** TGA CCG TAC ACC AAA ATT TG **R** ATT GCC CCT GTT TCA CTA TC	GoTaq	Clear	95°C, 3 min (95°C, 30 s; 60°C, 30 s; 72°C 1 min) $_{30}$ 72°C, 5 min.
Pml^{-}	**F1** TTT CAG TTT CTG CGC TGC C F2 CGA CCA CCA AGC GAA ACA R TTG GAC TTG CGC GTA CTG TC	DreamTaq	Clear	95°C, 3 min (95°C, 30 s; 60°C, 30 s; 72°C 1 min) $_{30}$ 72°C, 5 min.
$Pten^{flox}$	**F** CTC CTC TAC TCC ATT CTT CCC **R** ACT CCC ACC AAT GAA CAA AC	DreamTaq	Green	95°C, 2 min 30 s (94°C, 1 min; 54°C, 1 min; 72°C 1 min)$_{35}$ 72°C, 5 min.

Table 3 PCR conditions required for genotyping.

2.4.3 Visualisation of PCR products

PCR products were visualised using gel electrophoresis. Agarose gels were made by dissolving 10 g agarose in 400 ml 1 × Tris-Boreate-EDTA (TBE) buffer (Sigma) in a conical flask by heating in a microwave until boiling. The gel was then cooled by running cold water over the base of the conical flask while agitating to prevent uneven cooling. 14 µl of Safe View fluorescent nucleic acid stain (NBS Biologicals) was added to the melted gel and agitated carefully to ensure even distribution of the Safe View without incorporating air bubbles into the gel. 200 ml of gel solution was then poured into each of two moulds (Bio-Rad) and combs inserted to create wells. Once the gels were set, the combs were removed and they were placed into gel electrophoresis tanks and covered with 1 × TBE with Safe View (10 µl Safe View/100 ml 1 × TBE).

5 µl of loading dye (50% Glycerol [Sigma], 50% Ultrapure H_2O, 0.1% bromophenol blue [Sigma]), was added to the PCR product and mixed by pipetting. 20 µl of the coloured

PCR product was added to each well of the agarose gel, and run alongside a molecular weight ladder (Promega) of appropriate size to the estimated PCR product. The gel was run at 120 V until the loading dye had run more than halfway across the gel (approximately 30 minutes) and the gel was visualised using a GelDoc UV trans illuminator (Bio-Rad). Depending on the size of the PCR products produced, the gel was frequently run for longer in order to clearly separate the bands.

2.5 Experimental Cohorts

After the genotype of mice had been ascertained by PCR, Cre-recombinase mediated recombination was induced in appropriate mice around 8-10 weeks of age using tamoxifen administration. Once induced, long term cohorts were monitored closely for signs of ill health, and were culled when they presented either an intestinal tumour phenotype (hunched appearance, piloerection, paling feet, large rectal prolapse which caused discomfort or was ulcerated) or any other signs of loss of condition.

Short term cohorts were induced at 8-10 weeks of age and then sacrificed 3 days after the first induction day to study the short term effects of gene deletion.

2.5.1 Tamoxifen administration

Powdered Tamoxifen (Sigma) was dissolved in corn oil (Sigma) at a concentration of 10 mg/ml in an 80°C water bath. An 80 mg/kg dose of tamoxifen was administered to each experimental mouse via intraperitoneal (I.P.) injection daily, for four consecutive days. For short term cohorts, 3 injections of 60 mg/kg were administered in a single day. I.P. injections were performed using a 1 ml syringe (BD Plastipak) and 25 G needle (BD Microlance3).

2.5.2 5-Bromo-2-deoxyuridine administration

Sort term experimental animals were injected with 250 µl of the thymidine analogue 5-Bromo-2-deoxyuridine (BrDU, Amersham Biosciences) either 2 or 24 hours prior to sacrifice in order to label cells currently undergoing, or which have passed through, S-phase within the 2 hours during which BrDU is bioavailable.

2.6 Tissue Preparation

2.6.1 Tissue Dissection

Mice were culled via cervical dislocation according to Home Office Licence procedures. The mouse was sprayed with 70% EtOH and the skin and muscle wall of the abdomen cut through to open the abdominal cavity. The genitourinary tract, kidneys, pancreas and spleen were fixed together, liver was dissected out and fixed alone, and the small and large intestine and stomach were flushed out using 1 × PBS and fixed as described below.

For the short term cohorts, the small intestine was divided into small sections, with some being snap frozen for RNA extraction, some being opened longitudinally, rolled and placed in formalin and a third section being used for epithelial cell extract using Weiser preparation. All organs were collected into 10% formalin on ice.

For long term cohorts, once sacrificed due to ill health, where possible the cause of death was established. All organs were collected and formalin fixed. The intestine was opened longitudinally and fixed in methacarn.

2.6.2 Tissue Fixation using Formalin

All organs were formalin fixed unless otherwise stated. Small and large intestine were flushed with cold 1 × PBS and opened longitudinally. The gut was then rolled using dissection tweezers and pinned in place using a syringe needle. The gut roll was placed in 10% formalin (Sigma) on ice. Organs were incubated in formalin for 24 hrs at 4°C then stored in 70% EtOH at 4°C until paraffin embedding.

2.6.3 Fixation Using Methacarn

For long term cohorts where an accurate tumour count was required, small and large intestines were flushed with cold 1 × PBS and opened longitudinally on 3MM paper (Whatman). This was then placed in a sealed container of Methacarn (4:2:1 Methanol: Chloroform: Glacial Acetic Acid (Fisher)) and stored overnight (O/N) at RT in a fume hood. Tumour counts and location were then performed and the gut was rolled using dissection tweezers and pinned in place using a syringe needle. This was placed in 70% EtOH at 4°C prior to paraffin embedding.

2.6.4 Paraffin Embedding Fixed Tissue

Fixed tissues were removed from 70% EtOH and placed in a cassette (Fisher) and processed using an automatic processor (Leica TP1050). The tissues were incubated in an increasing gradient of EtOH for dehydration (70% EtOH for 1 hour, 95% EtOH for 1 hour, 2 × 100% EtOH for 1 hour 30 minutes and 100% EtOH for 2 hours), then in 2 × xylene for 2 hours. The tissue samples were then placed in liquid paraffin for 1 hour, followed by 2 × 2 hours. The samples were removed from the cassette and embedded in paraffin wax by hand and left to solidify.

2.6.5 Sectioning Fixed Tissue

In order to enable microscopic analysis of the tissue, sections of tissue were fixed onto slides in preparation for H&Es, cell-specific staining or IHC. Paraffin embedded tissues were cut to 5 μm sections using a microtome (Leica RM2135) and placed on Poly-L-Lysine coated slides (PLLs) and baked at 58°C for 24 hours.

Paraffin embedding and sectioning was performed by Derek Scarborough and Mark Isaac.

2.6.6 Snap freezing tissue

Several sections of normal intestinal tissue and intestinal tumour tissue (approximately 2 mm × 2 mm) were placed in lockable microtubes and placed in liquid nitrogen until frozen then stored at -80°C until required.

2.6.7 Epithelial Cell Extraction using Weiser Preparation

When RNA or protein analysis was required, Weiser preparation was performed in order to extract intestinal epithelium and therefore minimise interference from stromal and smooth muscle compartments. The 10 cm of the small intestinal proximal to the pyloric junction was dissected out, and flushed with ice cold PBS. The gut was opened longitudinally and cut in half longitudinally, and one half rolled and formalin fixed. This enabled direct comparison between gene expression levels and phenotype. The other half was washed 3 × in 15 ml ice cold Weiser solution (Table 4) by shaking in a 50 ml Falcon tube. The sample was then incubated on ice for a maximum of 20 minutes in 15 ml Weiser solution then vortexed for 15 minutes. The solution was removed and retained on ice and a further 15 ml ice cooled Weiser solution added to the sample, this

was repeated twice. The removed fractions were combined and centrifuged at 1500 rpm for 5 minutes at 4°C. The supernatant was discarded and the pellet washed 2 × with 20 mls of ice cold PBS. The pellet was then resuspended in 3 ml PBS and aliquoted into 3 × 1 ml samples in microtubes which were then centrifuged at 13000 rpm and the supernatant removed. Two of these pellets were resuspended in 500 µl Trizol before snap freezing in liquid nitrogen and stored at -80°C for future RNA extraction. The third pellet was snap frozen in liquid nitrogen then stored at -80°C for future protein extraction.

Weiser Solution	Volume required
1M Na_2HPO_4 (Sigma)	2.8 ml
1M KH_2PO_4 (Sigma)	4 ml
5M NaCl (Sigma)	9.6 ml
1M KCl (Sigma)	750 µl
1M $Na_3C_6H_5O_7$ (Sigma)	13.5 ml
Sucrose (Sigma)	7.5 g
D-sorbital (Sigma)	5 g
0.5M EGTA	4 ml
0.5M EDTA	6ml
0.5mM DTT *	39 mg

Table 4 Constituents of Weiser Solution for epithelial extraction. * DTT should only be added on day of use.

2.7 Histological Analysis

2.7.1 De-waxing and Rehydrating PLLs

Prior to IHC or cell staining, PLL sections were de-waxed by 2 × 10 minute submersion in Xylene and rehydrated through 5 minute incubations in each of the following gradients of EtOH; 2 × 100% EtOH, 1 × 95% EtOH and 1 × 70% EtOH. Slides were placed in dH_2O in preparation for IHC or cell staining.

2.7.2 Haematoxylin and Eosin (H&E) staining

Staining with H&E enables the visualisation of tissue morphology. Haematoxylin stains the cell nuclei blue, whereas Eosin stains protein red. PLL sections were de-waxed and rehydrated, as described in section 2.7.1, and then immersed in a bath of Mayer's Haemalum (R.A. Lamb) at RT for 45 seconds. The slides were removed and placed in a fresh bath with running water to remove any excess Haemalum and then placed in a bath of Eosin (R.A. Lamb). The slides were removed and placed in a fresh bath with running water to remove any excess Eosin. Slides were then dehydrated and mounted as described in section 2.8.2.8.

2.8 Cell Type Specific Stains

2.8.1.1 Alcian Blue Staining for Goblet Cells

Alcian blue stain the mucins which are present in the secretory intestinal epithelial cell type, goblet cells.

PLL slides were de-waxed and dehydrated as described in section 2.7.1 then immersed in a bath of alcian blue staining solution (1% Alcian blue (Sigma), 3% Acetic acid (Fisher) in distilled water (dH_2O) at pH 2.5) for 2 minutes then placed in a bath with running water for 5 minutes. Tissue sections were then counter stained with Haemalum (R.A. Lamb) for 45 seconds then returned to a bath with running water for a further 5 minutes. Slides were then dehydrated and mounted as described in section 2.8.2.8.

2.8.1.2 Grimelius Staining for Enteroendocrine Cells

The hormone-secreting enteroendocrine cells of the intestinal epithelium contain argyrophilic granules, which bind silver ions. These can be precipitated in the presence of a reducing solution which results in enteroendocrine cells appearing black.

All glassware was washed in double distilled H_2O (ddH_2O) prior to use to prevent contamination by any reducing agents. Slides were de-waxed and rehydrated as described in section 2.7.1 then incubated in silver staining solution (see Table 5) for 3 hours at 65°C. The slides were then incubated in preheated reducing solution (see Table 5) at 45°C for 1-10 minutes until the tissue sections had a visible yellow background stain, thereby eliminating the need for a counter stain. Slides were then dehydrated and mounted as described in Section 2.8.2.8.

Silver Staining Solution	Volume required
Acetate buffer ph5.6	10 ml
ddH_2O	87 ml
1% Silver Nitrate	3 ml
Acetate buffer	**Volume required**
17.4M Acetic Acid (Sigma)	54 µl
0.2M Sodium Acetate (Sigma	45.2 ml
ddH_2O	54.3 ml
Reducing Solution	**Volume required**
Sodium Sulphite (Hydrated)	2.5 g
Hydroquinone	0.5 g
ddH_2O	50 ml

Table 5 Constituents of Solution required for a Grimelius stain for the presence of enteroendocrine cells.

2.8.2 Immunohistochemistry (IHC)

IHC was performed to enable the visualisation of the presence and location of specific proteins within the tissue sections. The specific conditions for each IHC performed are outlined in Table 6, and a generic protocol is described below.

PLL slides were dewaxed and rehydrated as described in section 2.7.1 prior to antigen retrieval.

2.8.2.1 Antigen retrieval

In order to unmask the antigens, the cross-linking bonds formed between proteins during fixation were broken via antigen retrieval. Slides were boiled in pre-warmed citrate buffer (2.94 g Sodium citrate tribasic dehydrate (Sigma) in 1 L dH_2O, pH 6) in a

pressurized cooker for 10 minutes then left to cool to room temperature and washed in dH_2O.

2.8.2.2 Blocking of endogenous peroxidises

Antibody visualisation involves an enzymatic reaction catalysed by horse radish peroxidise (HRP), and so it was necessary to block the activity of endogenous peroxidises. This was achieved by the incubation of slides in hydrogen peroxide. The slides were either incubated in hydrogen peroxide (Sigma) diluted to the appropriate concentration in dH_2O, or a commercial peroxidise blocking solution (Envision+Kit, DAKO). Hydrogen peroxide concentrations and blocking time can be found in Table 3. Slides were then washed 3 × 5 minutes in wash buffer (Table 6) at RT with agitation.

2.8.2.3 Blocking of non-specific antibody binding

Binding of non-specific antibodies was blocked by incubating the sections with serum derived from a species other than that in which the primary antibody was raised. A hydrophobic barrier pen (Immedge, VectorLabs) was used to draw around the sections and serum diluted in wash buffer to the correct concentration (Table 6) was added to the slides and incubated for 30 minutes at room temperature.

2.8.2.4 Primary Antibody Treatment

Primary antibodies were diluted to the working concentration (Table 6) using the working serum stock used in the previous step. The serum block was removed from the slides and the primary antibody applied and incubated in a moist chamber for the appropriate time.

2.8.2.5 Secondary Antibody Treatment

Slides were washed 3 × 5 minutes in wash buffer at room temperature with agitation then the secondary antibody, which was either a biotinylated antibody diluted to the correct concentration in the working stock of blocking serum, or a HRP-conjugated antibody from the EnVision plus kit (DAKO), was applied and incubated for the appropriate time (Table 6).

2.8.2.6 HRP Conjugation for Signal Amplification

When a biotinylated antibody had been used as a secondary (but not when the EnVision plus kit had been used), a signal amplification step which involves the binding of HRP to

the biotin of the secondary antibody was performed. This was achieved using the Avidin-Biotin Complex (ABC) kit (Vector Labs). The ABC reagent was prepared according to manufacturers' instructions 30 minutes prior to use and stored at RT. Sections were washed 3 × 5 minutes in wash buffer at RT with agitation then the ABC reagent applied and incubated at RT for 30 minutes in a moist chamber.

2.8.2.7 Visualisation of Antibody Binding

Visualisation was achieved by the use of diaminobenzidine (DAB), which is a substrate for HRP, and when catalysed results in a brown coloured stain.

Sections were washed 3 × 5 minutes at RT with agitation and the DAB reagents (DAKO) prepared according to manufacturers' instructions immediately prior to incubation. DAB was applied and incubated for 5-10 minutes until a brown stain could be seen. Tissue sections were then washed in dH_2O, and counterstained in Mayer's Haemulum (R.A. Lamb) for 45 seconds and washed in a bath of running water to remove excess Haemulum.

2.8.2.8 Dehydration and Mounting of slides

Slides were dehydrated by incubation in a series of EtOH baths at an increasing gradient of EtOH. (1× 5 minutes 70% EtOH, 1 × 5 minutes 95% EtOH, 2 × 5 minutes 100% EtOH) then cleared in 2 × 5 minute incubations in xylene. Slides were removed from the xylene and mounted in DPX mounting medium (R.A. Lamb) and coverslips applied and allowed to dry in a fume hood.

Primary Antibody	Manufacturer	Non-specific Signal block	Wash Buffer	Primary Antibody Incubation Conditions	Secondary Antibody	Signal Amplification
Anti-β-catenin	BD Transduction labs # 610154	**Peroxidase**: Envison+ (Dako) 20 mins **Serum:** 5% NRS 30 mins	TBS/T	1:200 O/N 4°C	Envision+ HRP-conjugated anti-mouse (DAKO) 30 mins RT	N/A
Anti-BrDU	BD Bioscience #347580	**Peroxidase**: Envison+ (Dako) 20 mins **Serum:** 1% BSA 1 hr	PBS	1:150 O/N 4°C	Envision+ HRP-conjugated anti-mouse (DAKO) 30 mins RT	N/A
Anti-Cleaved caspase 3 (Asp 175)	Cell Signaling Technlogy #9661	**Peroxidase**: 3% H_2O_2 10 minutes **Serum:** 1% NGS 1 hr	TBS/T	1:20 for 2 days 4°C	1:200 Biotinylated anti-rabbit (Vector labs) 30 mins RT	ABC kit (Vector Labs)
Anti-Ki67	Vector Labs #VPK453	**Peroxidase**: 0.5% H_2O_2 20 minutes **Serum:** 20% NGS 1 hr	TBS/T	1:20 O/N 4°C	1:200 Biotinylated anti-rabbit (Vector labs) 30 mins RT	ABC kit (Vector Labs)
Anti-Lysozyme	Neomarkers #RB372A	**Peroxidase**: 1.5% H_2O_2 15 minutes **Serum:** 20% NGS 1 hr	TBS/T	1:100 1 hr RT	Envision+ HRP-conjugated anti-rabbit (DAKO) 30 mins RT	N/A
Anti-phospho AKT (ser 473)	Cell Signaling Technlogy #4060	**Peroxidase**: 3% H_2O_2 10 minutes **Serum:** 5% NGS 30 mins	TBS/T	1:50 O/N 4°C	1:200 Biotinylated anti-rabbit (Vector labs) 30 mins RT	ABC kit (Vector Labs)

Table 6 Optimised conditions for IHC for the range of antibodies used.

2.8.3 Cell Counting

Unless otherwise stated, all cell counts were performed on 50 half crypt-villus axes per mouse for a minimum of 4 mice per cohort. Positively stained brown cells from IHC were counted in this way, as were black enteroendocrine cells from Grimelius staining and blue goblet cells from alcian blue staining.

2.8.3.1 Crypt/aberrant cell number counts

The number of cells from the base of the crypt were counted per half crypt up to the crypt "shoulder" at the crypt-villus junction using H&E sections. Mice with homozygous deletion of *Apc* did not have clear crypt compartments due to cell mis-regulation, and so the number of cells in the region of aberrant proliferation within the crypt-villus axis were counted in a single line.

2.8.3.2 Apoptosis and Mitosis Scoring

When counting the crypts and the aberrant regions of the intestine, the number of apoptotic bodies and mitotic bodies and their positions were recorded.

2.8.4 Tumour Severity Grading

Tumour grading was carried out on all sections from aged $Apc^{flox/+}$ $Pten^{flox/flox}$ $Pml^{-/-}$ mice and associated control cohorts. From H&E slides from methacarn fixed gut roll, the intestine was examined under the microscope and the number and severity of lesions was counted and graded. Each lesion was graded according to the grading system outlined in Figure 2.1.

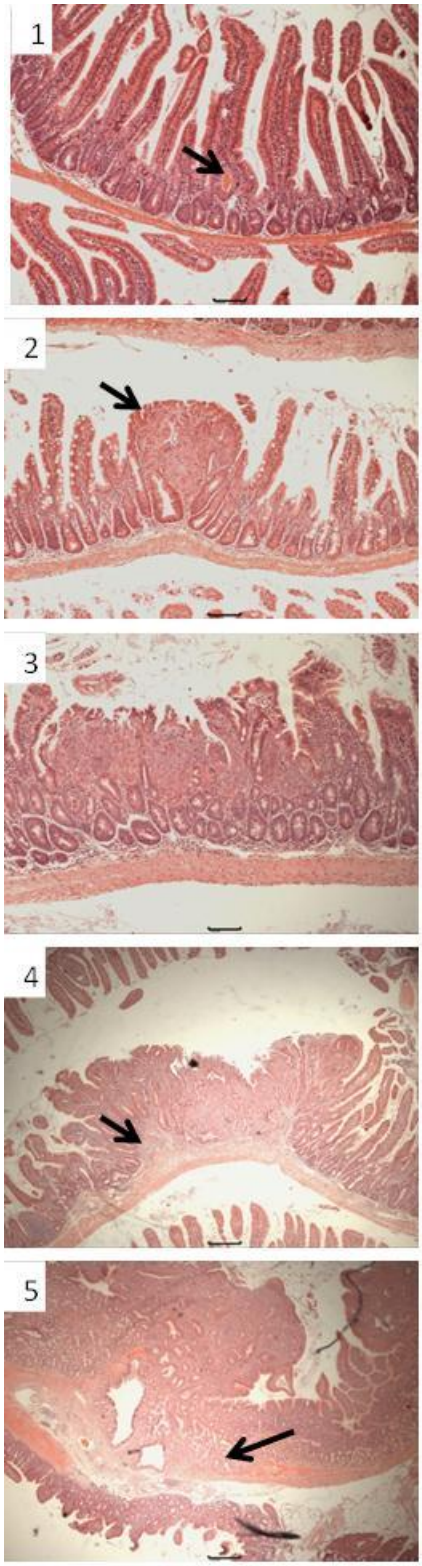

Grade	Description
1	Single crypt lesion
2	Microadenoma
3	Adenoma
4	Adenoma with stromal invasion
5	Adenoma with smooth muscle invasion

Figure 2.1 Tumour grading system. Black arrows indicate aberrant region. Black bar represents 100 μm.

2.9 In Situ Hybridisation

In situ hybridisation was performed on gut PLL slides from formalin fixed tissue in order to assess the location of *Ascl2* and *Olfm4* mRNA, two markers of the ISC compartment. Markers of the ISC compartment are generally expressed at such low levels, and there are few useful antibodies against the proteins, that it is impractical to visualise expression using IHC.

In situ hybridisation uses digoxigenin (DIG) labelled RNA probes (riboprobes) which specifically bind target mRNA due to their complementary sequence. Successful probe binding can be detected using an anti-digoxigenin alkaline phosphatase-conjugated antibody. BM purple, a chromogenic substrate for alkaline phosphatase, is then used to visualise the location of antibody binding through the development of a purple stain. DIG labelled sense RNA probes (of the same, not complimentary sequence to the mRNA) were used as a control.

Previously published probes for *Ascl2* (Guillemot *et al.* 1994) and *Olfm4* (van der Flier et al. 2009a) cloned into a pBluescript vector flanked by a promoter sequence for T3 or T7 RNA polymerase, were used to transform competent *Escherichia coli* (*E.coli*) cells. These were then cultured and the plasmid DNA extracted and linearised and the probe transcribed using the appropriate RNA polymerase.

2.9.1 Transformation of competent cells with cDNA vectors

The probes were supplied integrated into plasmid vector DNA, and so had to be amplified for long term use via transfection into *E.coli* cells. 50 µl of chemically competent JM109 *E.coli* cells (Promega) were incubated on ice for 30 minutes with 1 µg plasmid DNA. The cells were then heat shocked at 42°C for 45 seconds before being returned to ice for 2 minutes. 1 ml SOC medium (Invitrogen) was added to the cells and incubated at 37°C in a shaking incubator for 2 hours. 750 µl of the culture was then plated onto one agar plate containing ampicillin and 250 µl plated onto another. The plates were then incubated O/N at 37°C.

A single colony from this plate, selected using a sterile pipette tip, was streaked onto a separate agar plate containing ampicillin, and incubated O/N at 37°C. Four isolated colonies were selected from this plate using a sterile pipette tip and cultured O/N at

37°C in 10 ml of ampicillin containing LB medium in a 50 ml falcon tube in a shaking incubator. Plasmid DNA was extracted from 3.5 ml of this culture using a Qiagen Mini-prep kit and subjected to an analytical digest to ensure transfection of the correct construct had occurred (see below). Another 100 µl of this culture was then used to inoculate 200 ml of ampicillin containing LB medium which was cultured O/N at 37°C in a shaking incubator to enable large scale plasmid DNA extraction through the use of a midi-prep kit (Qiagen). A glycerol stock of each culture was prepared by mixing 0.5 ml of this culture with 0.5 ml 50% glycerol and freezing at -80°C. Future probe generation was performed by culturing *E.coli* directly from this stock.

2.9.2 Plasmid DNA extraction and probe linearization

Plasmid DNA was extracted using Qiagen mini-prep kit (for the analytical digest) or Qiagen midi-prep kit (for the probe preparation) according to manufacturer's instructions and resuspending extracted DNA in 200 µl 10 mM Tris (pH 8). A NanoDrop machine was used to quantify the DNA.

Analytical digests were performed by digesting the *Ascl2* probe-containing plasmid with EcoR1 (New England Biolabs), which had been used to insert the probe into the plasmid, whilst the *Olfm4* probe-containing plasmid was digested with NotI and SacI (New England Biolabs) (see Table 7 for restriction digest protocol). For both constructs the resultant digestion product was analysed on a 4% agarose gel to assess the fragment size. The *Ascl2* digest was approximately 1,700 bps after analytical digest, and the *Olfm4* digest was approximately 700 bps.

200 µg plasmid DNA was linearised for probe preparation using the appropriate restriction enzyme (seen in Table 8) and the linearised plasmid DNA was phenol/chloroform extracted. This was performed by making the volume of plasmid DNA up to 500 µl with 10 mM Tris (pH 8) and adding an equal volume of phenol. This was then mixed by inversion for 5 minutes at room temperature and centrifuged at room temperature at 13000 rpm for 10 minutes. The upper aqueous phase was carefully pipetted into a clean microtube and an equal volume of chloroform added. This was mixed by inversion for 10 minutes at room temperature then centrifuged again for 10 minutes at 13000 rpm at room temperature. The aqueous phase was then carefully pipetted into a clean microtube and 0.1 volume of 3 M NaOAc (ph 5.2) was added with

2.5 volumes of 100% EtOH. This was incubated at -20°C O/N in order to precipitate the DNA. This was then centrifuged at 4°C for 20 minutes at 13000rpm and the supernatant discarded. The pellet was washed twice with 70% EtOH and allowed to air dry before being resuspended in 40 µl of 10 mM Tris (pH 8). The DNA was quantified using a NanoDrop machine and adjusted to a concentration of 1 µg/µl using 10 mM Tris (pH 8).

Restriction Digest	**Volume**
Rnase Free H_2O	to 200 µl
Plasmid DNA	30 µg
Restriction Enzyme	10 µl
Buffer (10X) (NEB)	20 µl
BSA (1X) (NEB)	1 µl

Table 7 The constituents required to perform a restriction digest of the plasmid DNA.

	Analytical Digest	**Sense (Control) Probe**	**Anti-sense Probe**
Ascl2	EcoRI	ClaI	SmaI
Olfm4	NotI and SacI	SacI	NotI

Table 8 Restriction enzymes required for linearisation of plasmid DNA. All restriction enzymes were purchased from NEB and were associated with a specific buffer. For the analytical digest of *Olfm4*, the combination of two restriction enzymes resulted in the need for an alternative buffer, and buffer 2 (NEB) was used.

2.9.3 Probe Preparation

The probes were prepared using the linearised plasmid DNA as a template for the transcription of DIG-labelled riboprobes using T3 or T7. 1 µg of 1 µg/µl linearised plasmid DNA was labelled using the appropriate RNA polymerase (see Table 9) and a DIG labelling mix (Roche). The transcription reactions were set as detailed in Table 10, and incubated for 2 hours at 37°C and 20 units of DNaseI (Ambion) added and then incubated for a further 15 minutes at 37°C to digest the DNA template.

1/10th of the volume of NaOAc and 2.5 volumes of 100% EtOH were then added to the transcription reaction in order to precipitate out the DIG-labelled riboprobe. This was centrifuged at 13000 rpm for 20 minutes at 4°C and the pellet washed twice with 70%

EtOH and air dried. The pellet was resuspended in 100 µl Ultrapure H_2O (Sigma) and stored at -80°C in 10 µl aliquots until use.

	Sense (control Probe)	Anti-sense Probe
Ascl2	T7	T3
Olfm4	T3	T7

Table 9 RNA polymerase enzymes for probe transcription. DIG-labelled riboprobes were transcribed from linearised plasmid DNA using the appropriate RNA polymerase enzyme.

DIG RNA labelling mix	Volume
Rnase Free H_2O	12 µl
Transcription Buffer (10X) (Roche)	2 µl
DIG RNA labelling mix (Roche)	2 µl
RNasin (Promega)	1 µl
RNA Polymerase (Roche)	2 µl
Linearised plasmid DNA (1µg/µl)	1 µl

Table 10 DIG-labelling mix. Table shows the constituents and volumes for a single reaction to produce a DIG-labelled riboprobe.

2.9.4 Probe hybridisation

Sections were dewaxed, rehydrated, treated with 6% H_2O_2 for 30 minutes, washed 2× in PBS and fixed in 4% paraformaldehyde for 20 minutes on ice. Sections were washed 2× in PBS and digested in Proteinase K solution for 5 minutes (200 µg/ml proteinase K in 50 mM Tris, 5 mM EDTA), washed once in PBS, post-fixed in 4% paraformaldehyde for 5 minutes, and washed in DEPC H_20 for 2 minutes. The slides were then treated in acetic anhydride solution (2 M Acetic anhydride in 0.1 M triethanolamine hydrochloride) for 10 minutes whilst stirring, washed once in PBS and once in 1× saline then dehydrated and allowed to air-dry. The *olfm4* probe was diluted 1 in 100 in hybridisation buffer (5× SSC, 50% formamide, 5% SDS, 1 mg/ml heparin, 1 mg/ml calf liver tRNA) which was heated to 80˚C for 3 minutes. 100 µl of this was applied to each slide which was then covered in parafilm to prevent dehydration of the slide, and incubated overnight in a dark, moist chamber at 65˚C.

2.9.5 Post-hybridisation treatment

Post hybridisation washes were performed 1× in 5× SSC at 65˚C for 15 minutes then 2× in 50% formamide, 5× SSC 1% SDS for 30 minutes at 65˚C. Post hybridisation washes were continued by washing twice in 0.5 M NaCl, 10 mM TrisHCl pH 7.5, 0.1% Tween for 10 minutes, the first at 65˚C and the second at room temperature. Sections were then incubated for 45 minutes in 0.5 M NaCl, 10 mM TrisHCl pH 7.5, 0.1% Tween with 25 µg RNAse A (Qiagen) at 37˚C then washed once in 0.5 M NaCl, 10 mM TrisHCl pH 7.5, 0.1% Tween for 5 minutes at room temperature. Sections were washed 2× in 50% formamide, 5× SSC for 30 minutes at 65˚C and preblocked in 10% sheep serum in PBT in a dark, moist chamber at room temperature for 2-3 hours. Antibody solution was created by pre-absorption of Anti-digoxigenin alkaline phosphatise conjugated antibody (Roche) for 3 hours at 4°C in 1% heat-inactivated sheep serum in PBT containing 5 mg/ml mouse intestinal powder. 100 µl of this antibody solution was applied to each slide which was then covered in parafilm and incubated in a dark, moist chamber at 4°C O/N.

2.9.6 Signal Detection

Sections were washed 3× in PBT for 5 minutes then 3× in PBT for 30 minutes then preconditioned to inhibit endogenous alkaline phosphatase by washing 3× in NTMT buffer for 5 minutes (100 mM NaCl, 100 mM Tris HCl, 50 mM $MgCl_2$, 0.1% Tween, 2 mM Levamisole). The substrate (BM purple, Roche) was added directly to the slides and incubated in the dark at 4˚C for 24-72hrs until a sufficiently strong colour developed. Sections were washed in PBT and counterstained with eosin. Excess eosin was removed by washing in running H_2O and the slides were dipped in xylene prior to air-drying and mounting using DPX.

2.9.7 Preparation of intestinal tissue powder

The small intestines of 5 adult mice were combined and homogenised in the minimum volume of ice cold PBS. 4 volumes of ice cold acetone were added to the homogenised intestine, which was mixed thoroughly and incubated on ice for 30 minutes. This was centrifuged and the pellet was washed using ice cold acetone. This was further centrifuged and the resulting pellet spread onto filter paper and allowed to dry. Once thoroughly dry the material was ground to a fine powder using a pestle and mortar.

2.10 Quantitative Reverse Transcription Polymerase Chain Reaction (qRT-PCR)

qRT-PCR was used to assess the relative expression levels of genes within intestinal epithelial tissue. Intestinal epithelium was isolated using the Weiser preparation method (see section 2.6.7) and stored in Trizol at -80°C prior to RNA extraction. This RNA was used as a template for cDNA synthesis and then the levels of gene expression of a range of Wnt-target genes and ISC markers was compared between a minimum of 4 mice of each genetic cohort.

2.10.1 RNA extraction

Epithelial cell extract was defrosted in 1ml Trizol (Invitrogen) in Precellys® beaded microtubes. Once defrosted, the samples were homogenized using a Precellys®24 homogenizer for 45 seconds followed by 1 minute incubation and a further 45 seconds homogenisation. The samples were removed from the machine and allowed to settle on ice for 5 minutes to remove bubbles. The samples were pipetted into fresh microtubes with 200 µl pre-chilled chloroform. This was incubated on ice with frequent agitation for 10 minutes.

The samples were then centrifuged for 15 minutes at 13000 rpm at 4°C, and the aqueous phase of the supernatant carefully pipetted into fresh microtubes and 700 µl isopropanol added. This was incubated at -20°C O/N for optimal RNA precipitation.

The samples were then centrifuged for 15 minutes at 13000 rpm at RT and the supernatant discarded. The pellets were washed twice with 500 µl pre-chilled 70% EtOH and air dried for 5 minutes then resuspended in 10µl Ultrapure H_2O (Sigma) and incubated for 10 minutes at 65°C. Extracted RNA was quantified using the NanoDrop machine.

2.10.2 DNase Treatment

10 µg extracted RNA was mixed with 5 µl RQ1 buffer (Promega), 10 µl RQ1 DNase enzyme (Promega) and made up to 50 µl with Ultrapure H_2O. This was incubated at 37°C for 30 minutes for optimum DNase activity. 5 µl STOP solution (Promega) was added and the solution heated to 65°C for 10 minutes to prevent further DNase activity. This resulted in DNA-free RNA at a concentration of 10 µg/ 55 µl.

2.10.3 cDNA synthesis

The RNA was used as a template for cDNA synthesis using the reverse transcriptase SuperScript II (Invitrogen). The constituents of the cDNA synthesis mix are outlined in Table 11 and made up in thin-walled 12 well strip tubes (Grenier, Bio-One). This was heated to 65°C for 3 minutes then placed on ice and 1 µl Superscript II (Invitrogen) was added. This was incubated within a thermocycler at 25°C for 10 minutes, 42°C for 1 hour and 65°C for 15 minutes. cDNA samples were stored at -20°C.

cDNA synthesis mix	Volume	Supplier
Random Hexamer Primers (50µM)	4 µl	Invitrogen
5 x SS buffer	4 µl	Invitrogen
0.1 M DTT	2 µl	Invitrogen
Rnase inhibitor	1 µl	Invitrogen
10 mM dNTPs	1 µl	Promega
Ultrapure Water	1 µl	Sigma
10 µg/ 55 µl DNA free RNA	11 µl	

Table 11 Constituents of cDNA synthesis mix.

2.10.4 SYBR Green Gene Expression Analysis

qRT-PCR was carried out in MicroAmp fast optical 96-well reaction plates (Applied Biosystems). All reactions were carried out in duplicate and each cDNA sample was run with primers for the house-keeping gene β-actin in order to normalise the expression levels of target genes. Each well was made up of 10 µl SYBR green fast mix (Invitrogen) 2 µl of cDNA, 0.5 µl of each primer (10 mM) and 8 µl Ultrapure H_2O (Sigma). See Table 12 for primer sequences. The plate was sealed and centrifuged for 1 minute at 8000 rpm.

qRT PCR reactions were carried out using a Step One Plus real-time PCR system (Applied Biosystems). The relative mRNA abundance was determined by incorporation of SYBR green into the PCR product. Thermocycler conditions were: 95°C for 20 seconds followed by 40 cycles of 95°C for 3 seconds (denaturation) and 60°C for 30 seconds. The data were collected automatically using StepOne Software.

When the abundance of the mRNA transcript within the intestinal epithelial extract was particularly low, SYBR green was inefficient at detecting expression levels, and so the more specific, probe based TaqMan assay was used for these genes (see Table 12).

2.10.5 TaqMan Gene Expression Analysis

Each well of the plate was made up of 10 µl TaqMan gene expression master mix (Invitrogen), 2 µl cDNA, 1 µl TaqMan probe (10 mM) and 8 µl Ultrapure H_2O (Sigma). See Table 12 for TaqMan probe details. The plate was sealed and centrifuged for 1 minute at 8000 rpm.

The TaqMan probes are pre-designed and consist of a forward and reverse primer for the gene of interest and a probe complimentary to an internal region of the amplified PCR product with a fluorescent molecule and quencher attached to the 5' end. During thermocycling, the fluorescent molecule is cleaved from any cDNA bound probe by Taq polymerase activity, releasing it from the quencher and enabling fluorescent signal detection.

qRT-PCR reactions were carried out using a Step One Plus real-time PCR system (Applied Biosystems). Thermocycler conditions were: 50°C for 2 minutes, 95°C for 10 minutes followed by 40 cycles of 95°C for 15 seconds and 60°C for 1 minute. The data were collected automatically using StepOne Software.

SYBR GREEN	Forward Primer	Reverse Primer
Axin2	GCA GCT CAG CAA AAA GGG AAA T	TAC ATG GGG AGC ACT GTC TCG T
B-actin	ACC CAG ATC ATG TTT GAG ACC T	AGG GCA TAC CCC TCG TAG AT
Bmi1	AAG CTT GTC TAT TGA GTT CTT TGA	TCT CAA GTG CAT CAC AGT CAT T
Cd44	ATC GCG GTC AAT AGT AGG AGA A	AAA TGC ACC ATT TCC TGA GAC T
Cmyc	CTA CCC TCT CAA CGA CAG CAG	GCC TCT TTT CCA CAG AAA CAA C
Cyclin D1	ACG ATT TCA TCG AAC ACT TCC T	GGT CAC ACT TGA TGA CTC TGG A
Dikkopf	TCA CTA TTC CAA CCA TGA CCT G	CTT CTT GCG TTG TTT GGT ACA G
Epherin B2	AAA CCC TGA TGG ACT CTA CGA C	TTG TTC TGG CTT GAC TCA AAG A
Epherin B3	TAA CGC TGT GGA GGT CTC TGT A	CCT TGC TTT GCT TTG TAA CTC C
Groucho	GGA GAG AGC TCC TGA AGT TTC C	TTC TCT TTG TTC CTC TTC AAT GG
Msi1	CCT GGT TAC ACC TAC CAG TTC C	AGA GCC TGT CCC TCG AAC TAC
Taqman	**Supplier**	
Ascl2	Applied Biosystems	
B-actin	Applied Biosystems	
Lgr5	Applied Biosystems	
Olfm4	Sigma	

Table 12 Primer details for genes analysed by qRT-PCR using the SYBR green and the TaqMan assay.

2.10.6 Analysis of qRT-PCR data

SYBR green melt curves were examined to ensure the presence of a single peak, as double peaks indicate the presence of primers dimers or primer contamination. A fluorescence threshold was set and the number of thermocycles required by each well to reach the threshold in fluorescence was recorded as the cycle threshold (C_T value). Samples were only analysed if they had a single peak in the melting curve and the duplicate repeats were within 1 C_T value of each other.

In each assay, the sample C_T value was calculated as an average of the duplicates, and normalised by the subtraction of the C_T value of β-actin for the same sample, thereby generating a ΔC_T value. The ΔC_T values were used to determine significance of change in gene expression at N=4. If the data was normally distributed (tested by the Shapiro-Wilk test in SPSS) then a two-tailed T-test was performed, whereas if the data was not normally distributed a Mann-Whitney test was performed.

In order to calculate the fold changes in expression levels, the average of the ΔC_T values of the control cohort was subtracted from the average of the ΔC_T values of the test cohort producing a $\Delta\Delta C_T$ value. The equation fold change = $2^{-\Delta\Delta C_T}$ was used to calculate fold change in gene expression levels.

2.11 Western Blotting

2.11.1 Protein Extraction

40-100 mg of frozen intestinal epithelial tissue (prepared by Weiser preparation, see section 2.6.7, and stored at -80°C until use) was resuspended at 100 µl / 10 µg tissue in pre-chilled modified RIPA buffer (see Table 13) with protease inhibitor (Complete protease cocktail mini tablets (Roche), 1 tablet per 5 ml RIPA buffer). This was transferred into Precellys® beaded microtubes and homogenized on the Precellys®24 homogenizer for 2 x 45 seconds. The samples were then stored on ice until the bubbles had settled and then transferred to a fresh microtube and incubated on ice for 20 minutes. Samples were then centrifuged at 13000 rpm for 10 minutes at 4°C and the supernatant containing the protein was aliquoted into 50µl aliquots, snap frozen in liquid nitrogen and stored at -80°C until use.

Modified RIPA buffer	Quantity
1 M Tris pH 7.4	5 ml
10% Nonidet-p40 (IGEPAL)	10 ml
$C_{24}H_{39}NaO_4$	250 mg
5 M NaCl	3 ml
0.25 M EGTA pH8	400 µl
dH_20	up to 100 ml

Table 13 Constituents of modified RIPA buffer

2.11.2 Protein Quantification

Protein was quantified using the bicinchonic acid (BCA) method. This method is based on a biuret reaction whereby the presence of peptide bonds reduces Cu^{2+} ions to Cu^{1+} ions, producing a violet colour. The BCA reagent (Pierce) strongly absorbs light at 562 nm and so the extent to which Cu is reduced (and the quantity of protein present) can be determined through a colourimetric assay.

Protein samples were created by adding 8 µl sample to 192 µl PBS and 2 serial dilutions resulted in 3 protein concentrations (1:25, 1:50, 1:100) in a final volume of 100 µl PBS. Stock Bovine Serum Albumin (BSA) was diluted in RIPA buffer and then PBS to produce 6 standards of known concentration ranging from 0 µg/ml to 25 µg/ml. All samples

were loaded and standards were loaded into a colourless, flat bottom 96-well plate in duplicate.

BCA reagents (Pierce) were made up according to manufacturer's instructions and 100 µl added to each sample. The plate was then sealed and incubated at 37°C for 2 hours. The absorbance of each sample was then read on an ELx800 spectrophotometer (BioTek) at 590 nm. A standard curve of absorbance to concentration was calculated using the absorbance of the BSA standards and the concentrations of the samples calculated.

2.11.3 Sample Preparation

Protein samples were defrosted on ice and 30 µg was resuspended in laemlli buffer (4% SDS, 20% glycerol, 10% 2-mercaptoethanol, 0.004% bromphenol blue and 0.125 M Tris HCl in Ultrapure H_2O, pH 6.8. All reagents were purchased from Sigma) to make up a volume of 25 µl. Samples were heated to 95°C for 5 minutes and quenched on ice before loading into gels.

2.11.4 Gel Casting

Mini-Protein III (Bio-Rad) gel casting apparatus was used to prepare polyacrylamide gels. Solutions for a 5% stacking gel and a 10% resolving gel were made up without the addition of the TEMED (see Table 14). The gel casting apparatus was assembled and TEMED was added to the 10% gel solution which was then mixed and poured between the two glass plates, to 2 cm below the top of the glass plates. 2 ml of H_2O was poured over the top of the gel to prevent drying out and the formation of bubbles. Once the gel was set, (typically 45 minutes) the H_2O was poured off the gel and the TEMED added to the 5% stacking gel solution. This was then mixed and poured on top of the 10% gel until it overflowed the top of the glass plates, and the well comb was inserted.

Once the gel was set, the well comb was removed and the gel placed in sodium dodecyl sulphate-polyacrylamide gel electrophoresis (SDS-PAGE) apparatus and 1× running buffer (see Table 15 Recipes for running buffer and transfer buffer. 500 ml of 1 × running buffer is required per tank, and 1 L of 1 ×transfer buffer required for each transfer tank.) added, and the wells were flushed out using a pipette to remove any excess gel.

2.11.5 SDS-PAGE

Prepared protein samples were loaded into the wells of the gel in the SDS-PAGE apparatus with 1× running buffer. One well was loaded with 7 µl of pre-stained full-range Rainbow molecular weight ladder (GE Healthcare). The gels were then run at 120-200 V until the dye reached the end of the gel.

2.11.6 Protein transfer

The gel containing the separated proteins was removed from the glass plates, the 5% stacking gel removed, and placed in transfer buffer (see Table 15). Amersham Hybond-ECL nitrocellulose filter (GE Healthcare) was then cut to size and dipped in transfer buffer (Table 15) before being placed on top of the 10% gel. This was then sandwiched between two sheets of 3MM blotting paper (Whatman) which had been dipped in transfer buffer, and transfer buffer soaked sponges. This was placed into the plastic transfer supports and placed into the transfer tank so that the filter was between the gel and the positive electrode. Transfer buffer was added to the tank and it was run at 100 V for 1 hour. After transfer, the filter was carefully removed from the transfer supports and placed in Tris Buffered Saline with 0.1% Tween (TBS/T, Sigma) until probing.

2.11.7 Antibody probing of nitrocellulose filter

The nitrocellulose filter was blocked in 5% milk powder in TBS/T for 1 hour at RT with agitation. 3× 5 minute washes in TBS/T were then performed and the primary antibody (diluted in 5% milk powder in TBS/T) was added (see Table 16). This was incubated O/N at 4°C with agitation. The filter was then washed 3× 5 minutes in TBS/T and incubated with HRP-linked secondary antibody in TBS/T for 1 hour at RT with agitation and then washed for a further 3× 15 minutes in TBS/T prior to signal detection.

5 % Stacking Polyacrylamide Gel	Volume required f
ddH_2O	6.9 ml
30 % acrylamide (Sigma)	1.7 ml
1 M Tris-HCl pH 6.8	1.25 ml
10% SDS (Sigma)	100 µl
25% Ammonium Persulphate (Sigma)	66 µl
TEMED (Sigma)	13.2 µl
10 % Resolving Polyacrylamide Gel	Volume required f
ddH_2O	6.8 ml
30 % acrylamide (Sigma)	8.4 ml
1 M Tris-HCl pH 8.8	9.4 ml
10% SDS (Sigma)	250 µl
25% Ammonium Persulphate (Sigma)	72 µl
TEMED (Sigma)	13.2 µl

Table 14 Recipe to make up 5% and 10% polyacrylamide gels for Western blotting.

5 X Running Buffer	Volume required
Tris Base (Sigma)	15.1 g
Glycine (Sigma)	94 g
10% SDS	50 ml
dH2O	to 1 L
1 X Transfer Buffer	Volume required
Tris Base (Sigma)	2.9 g
Glycine (Sigma)	14.5 g
Methanol (Fisher)	200 ml
dH2O	to 1 L

Table 15 Recipes for running buffer and transfer buffer. 500 ml of 1 × running buffer is required per tank, and 1 L of 1 ×transfer buffer required for each transfer tank.

Primary Antibody	Manufacturer	Primary Antibody conditions	Secondary Antibody
Anti- β-actin	Sigma #A5316	1:5000 in 5 % powdered milk in TBS/T	HRP-conjugated anti-mouse (GE Healthcare) 1:2000 in 5% powdered milk in TBS/T
Anti- phospho AKT (ser473)	Cell Signalling Technology #9275	1:1000 in 5% BSA in TBS/T	HRP-conjugated anti-rabbit (GE Healthcare) 1:2000 in 5% powdered milk in TBS/T
Anti- total AKT	Cell Signalling Technology #9272	1:1000 in 5% BSA in TBS/T	HRP-conjugated anti-rabbit (GE Healthcare) 1:2000 in 5% powdered milk in TBS/T

Table 16 Antibody incubation conditions for protein expression analysis using Western Blotting

2.11.8 Signal detection

The standard electrochemiluminescence (ECL) detection reagents (GE Healthcare) were prepared according to manufacturers' instructions. The filter was incubated with 2 ml of the reagents at RT for 1 minute then excess ECL reagent removed and the filter placed in an X-ray cassette. The X-ray film (Fujifilm Super RC, blue background) was exposed in a dark room under safe light conditions and the film processed using an automatic processor (Xograph Compact X4 automatic X-ray film processor). A number of exposure times were attempted to produce a clear image. The developed film was then overlaid onto the filter and the band size measured against the molecular weight ladder to ensure the correct protein had been detected.

2.11.9 Stripping the filter

The filter could be re-used for probing with other antibodies, but if the protein of interest was of a similar size to that previously detected (for example phospho-AKT and total-AKT were the same size) the filter was stripped between probing. 20 ml of stripping buffer (1.2 ml 1 M Tris pH 6.8, 400 mg SDS made up to 20 ml in dH_2O) was added to the membrane with 70 µl β-mercaptoethanol. This was incubated at 55°C for 30 minutes with agitation and then the filter removed and re-probed as described in section 2.11.7.

2.11.10 Confirmation of equal loading

The filter was re-probed with β-actin antibody to ensure any changes in phospho-AKT and total-AKT were not due to unequal protein loading.

2.12 Intestinal organoid culture

The method outlined below for intestinal organoid culture has been adapted from the method originally presented by Sato *et al.,* in order to increase efficiency (Sato et al. 2009).

2.12.1 Isolation of intestinal crypts

15 cm of small intestine was flushed through with HBSS containing 1× penicillin/streptomycin (Invitrogen). The intestine was then opened longitudinally and scraped firmly using a glass cover slip in order to remove the villi. Once scraped, the intestine was chopped into 0.5 mm pieces and placed in 25 ml HBSS containing 1× penicillin/streptomycin and incubated for 15 minutes at RT. This solution was gently shaken then transferred into a primary tissue culture hood. All of the remaining steps were carried out in sterile conditions. The media was removed from the pieces of intestine, which were then washed gently 5 times in HBSS. The intestine was resuspended in 10 ml 8 mM EDTA in HBSS and incubated at RT for 5 minutes. The solution was then shaken vigorously and the EDTA in HBSS removed. The intestine was again suspended in 10 ml 8 mM EDTA in HBSS and incubated on ice for up to 30 minutes. This was shaken vigorously and the solution removed and retained as the first crypt-containing fraction. This fraction was immediately diluted 1:1 in DMEM/F12 containing Glutamax. 15 ml HBSS was added to the intestine and again shaken vigorously, this fraction added to the first and repeated until four fractions had been collected. The collected crypts were then spun at 6000 rpm for 5 minutes to remove single cells and resuspended in 10 ml DMEM/F12 containing Glutamax. This was then spun at 7000 rpm for 3 minutes and the pellet resuspended in 10 ml DMEM containing Glutamax and passed through a 70 μm cell strainer to remove clumps.

2.12.2 Counting and seeding crypts

The number of crypts within three 10μl aliquots were counted and the appropriate volume of solution to seed 60 wells at 200 crypts per well was calculated. This volume was taken then spun at 7000 rpm for 3 minutes and first resuspended in 20 μl DMEM/F12 (Invitrogen) (due to difficulty of resuspending directly into Matrigel) followed by dilution into the appropriate volume of Matrigel (BD Biosciences). Plates were pre-warmed in the incubator prior to seeding. 96 well Nunclon U-bottom plates

were seeded with 10 µl Matrigel, and 24 well Nunc plates were seeded with 50 µl Matrigel.

2.12.3 Organoid growth media

100 µl organoid growth media (Table 17) was then added to each well of 96 well plates, and 500 µl to each well of 24 well plates and the plates returned to the incubator immediately. Media was changed every two days.

Organoid Culture Medium	Volume	Supplier
Penecillin/Streptomycin (100x)	1 ml	Invitrogen
Hepes Buffer (100x)	1 ml	Invitrogen
Glutamax (100x)	1 ml	Invitrogen
Gentamycin (50 mg/ml)	20 µl	Sigma
Fungizone	500 µl	Invitrogen
N2 supplement (100x)	1 ml	Invitrogen
B27 supplement (50x)	2 ml	Invitrogen
Human Recombinant Noggin	10 µg	PeproTechEC
Human Recombinant EGF	5 µg	Sigma
R-spondin (133 µg/ml)	500 µl	R & D Systems
DMEM F/12	to 100 ml	Invitrogen

Table 17 Recipe for 100 ml of complete organoid culture medium including all growth factors.

2.12.4 Organoid formation efficiency assay

30 wells of a 96 well plate were seeded at 200 crypts/well in 10 µl Matrigel per well in each of two plates (one for the organoid formation assay, another for the PrestoBlue viability assay). Three batches of media were made up, one with 665 ng/ml R-spondin (R&D Systems), another with 332 ng/ml and the third with 0 ng/ml. 10 of the seeded wells of the 96 well plate were given each of the three concentrations of media. Media was changed every two days.

The plate was read at day 1, day 3, day 5, day 7, day 9 and day 11 using the Gelcount (Oxford Optronix) machine and software. Data of average size was used from all of the readings in order to produce the growth curves whilst only data from day 1 and day 11 were counted and analysed to produce a readout for the proportion of seeded crypts which grew into organoids. The CHARM settings (which define the thresholds for automated organoid identification through a number of different parameters) for each day and genotype can be seen in Table 18. When high quality images were required, a

preheated 24 well plate was also seeded at a density of 200 crypts per well in 50 µl matrigel per well and images taken daily for 14 days.

2.12.5 PrestoBlue viability assay

10 µl of Prestoblue (Invitrogen) was added per 100 µl media to each of the 30 wells in one of the 96 well plates and 3 extra wells were filled with 100 µl media and 10 µl Prestoblue without any cells as a negative control. This was incubated at 37°C for 2 hrs and then 50 µl of the media removed and placed into a black 96well flat bottomed plate (ThermoScientific 11359163). This was then read in a fluorescence plate reader. Relative fluorescence was calculated by subtracting the average of the negative controls from each of the well readings, then comparing the average of 10 wells from each R-spondin concentration to the average of the wells containing the highest R-spondin levels.

Wildtype or wildtype-like organoids	DAY1	DAY3	DAY5	DAY 7	DAY 9	DAY11
Edge Detection Sensitivity	29.5	40.2	50.8	50.8	20	1
Centre Detection Sensitivity	50.2	70.4	70.4	70.4	35	27.3
Soft Colony Diameter Range						
Lower Diameter µm	40	50	60	70	70	80
Upper Diameter µm	500	500	500	500	500	600
Min Center to Center Seperation	40	30	30	30	30	30
Smoothing	3	3	3	3	3	3
Circularity Factor	0	0	0	0	10	22
Edge Distance Threshold	0.92	0.88	0.88	0.88	0.88	0.89
Number of Spokes	32	32	32	32	32	32
Shape Filtering	3	3	3	3	3	3
Shape Processing	Best Fit Circle	Best Fit Circle	Best Fit Circle	Best Fit Circle	Best Fit Circle	Best Fit Circle
Colony Diameter Filter						
Min Diameter	30	50	50	70	70	70
Max Diameter	600	600	600	600	600	600
Colony Intesity (OD)						
Min Intensity/Density	0.15	0.17	0.18	0.2	0.22	0.23
Max Intensity/Density	2	2	2	2	2	2
Good Edge Factor	0.8	0.5	0.62	0.7	0.75	0.84
Overlapping Threshold	0.67	0.67	0.67	0.67	0.67	0.75

$Apc^{flox/flox}$ or other cyst-like organoids	DAY1	DAY3	DAY5	DAY 7	DAY 9	DAY11
Edge Detection Sensitivity	57.5	40.2	50.8	50.8	20	7.7
Centre Detection Sensitivity	50.2	50.2	50.2	65.3	65.3	65.3
Soft Colony Diameter Range						
Lower Diameter µm	40	50	60	70	90	120
Upper Diameter µm	500	500	500	500	500	700
Min Center to Center Seperation	40	30	30	30	30	30
Smoothing	3	3	3	3	3	3
Circularity Factor	10	10	10	10	10	36
Edge Distance Threshold	0.92	0.88	0.88	0.88	0.78	0.78
Number of Spokes	32	32	32	32	32	32
Shape Filtering	3	3	3	3	3	3
Shape Processing	Best Fit Circle	Best Fit Circle	Best Fit Circle	Best Fit Circle	Best Fit Circle	Best Fit Circle
Colony Diameter Filter						
Min Diameter	30	50	50	50	60	60
Max Diameter	600	600	600	600	600	800
Colony Intesity (OD)						
Min Intensity/Density	0.05	0.07	0.08	0.08	0.09	0.1
Max Intensity/Density	2	2	2	2	2	2
Good Edge Factor	0.86	0.5	0.62	0.7	0.75	0.84
Overlapping Threshold	0.67	0.67	0.67	0.67	0.67	0.95

Table 18 CHARM settings devised for the detection of dissociated crypts and grown organoids over an 11 day period. Different settings were used to detect wildtype-like organoids and cyst-like organoids.

2.12.6 Fixing Intestinal Organoids for Immunohistochemistry

From a 24-well plate, matrigel was disrupted using a 1 ml pipette tip and the matrigel pipetted up and down to free the organoids from the matrigel. It was then pipetted into a microtube. In a 96-well plate the wells were scraped using a 200 µl tip and then pipetted straight into a microtube, disrupting the Matrigel by abrasing the microtube over a microtube rack. When few organoids were present, the pipette tips were soaked in 0.1% BSA in PBS prior to use, to prevent organoid loss to the pipette tip surface.

The organoids were centrifuged at 7000 rpm for 5 minutes then the supernatant and the clear layer of matrigel were carefully removed and discarded. 800 µl of formalin was then added to the organoids and the pellet broken up into the formalin by running along a microtube rack. This avoided unnecessary pipetting, which could cause organoid loss, and sonication, which could disrupt the structure of the organoid. Following 1 hour incubation on ice, the organoids were centrifuged for a further 5 minutes at 7000 rpm and the supernatant and any remaining matrigel removed. The organoids were resuspended in 70% EtOH (avoiding pipetting) and incubated on ice for a further 1 hour.

The organoids were centrifuged for 3 minutes at 7000 rpm and the EtOH removed and the organoids resuspended in 70 µl of Histogel (ThermoScientific) (pre-heated to 70°C) and placed in a specially made mould on top of parafilm and allowed to set (typically 3-5 minutes). The pellet was then removed from the mould and stored in 70% EtOH prior to paraffin embedding and sectioning (see section 2.6.4).

2.13 Data Analysis

Raw data obtained from cell counts, tumour grading and qRT-PCR were input into Excel (Microsoft) for the calculations of means and standard deviations for graphical representation.

Comparison of means was carried out in SPSS data analysis software. All analysed data was tested for normality using the Shapiro-Wilk test. Normally distributed data was tested for significance using a two-tailed T test, and data which was not normally distributed was analysed using Mann-Whitney U Test.

Survival data was analysed using Kaplan-Meier plots to present the data and significance calculated using the Wilcoxon Log Rank test.

3 Development and Optimisation of a novel ISC function assay

3.1 Introduction

The importance of understanding the relationship between changes in the ISC compartment and tumourigenesis was highlighted by the observation by Baker *et al*., that the ISC is the cell of origin of intestinal cancer (Barker *et al.* 2008). This was found by comparing the effects of conditional deletion of the tumour suppressor *Apc* using two different Cre-recombinases. One of these specifically recombined within the ISC compartment (using an Lgr5-linked Cre recombinase). The other Cre drove recombination efficiently within the proliferative crypt compartment but only very inefficiently within ISCs (using AH-linked Cre recombinase and a specially designed induction method). These experiments showed that loss of *Apc* from the ISC compartment initiated the formation and growth of multiple adenomas, whereas loss of *Apc* from the other cell types within the crypt produced fewer, smaller lesions.

In addition to these experiments, it has been observed that in a model of early tumourigenesis, $Apc^{flox/flox}$ mice, one of the earliest characteristics observed following deletion of *Apc* is an increase in undifferentiated cell types (Sansom *et al.* 2004). Taken together, these experiments suggest that perturbation of the ISC compartment could play an essential role in tumourigenesis.

In order to increase our understanding of the relationship between changes in the ISC compartment and tumourigenesis it is necessary to be able to accurately assess the ISC compartment.

As previously discussed in section 1.3.1 there are a range of ISC markers which can be used for the identification of the presumed stem cell population (Barker *et al.* 2007; Besson *et al.* 2011; Potten *et al.* 1974; Sangiorgi and Capecchi 2008; van der Flier *et al.* 2009a; van der Flier *et al.* 2009b). These markers have proven extremely useful when studying the mis-localisation of expression or expansion of the ISC compartment but are informative simply of gene expression patterns, rather than ISC functionality. In order to truly assess any changes occurring in the ISC population it is necessary to combine expression levels and localisation information of published stem cell markers with a

functional assay which can be used to determine whether these cells are capable of functioning as ISCs.

Lineage tracing experiments have been previously very successful in determining whether or not a cell which expresses a particular gene is in fact an ISC due to its ability to produce daughter cells which can form any of the intestinal epithelial lineages. These methods, however, are not capable of comparing the number, location and potency of the ISC populations between individual mice of different genotypes. Furthermore, the necessity of a stem cell specific Cre to drive LacZ expression in order to perform these experiments presents numerous logistical problems, not only with the breeding of many mice, but the interference it may have with the required experimental phenotype. In order to study changes in ISC functionality between specific genotypes it has been necessary to expand our current toolkit for assessing this intestinal compartment. An ideal method would assess the functional capacity of ISCs, while being easily incorporated into traditional tissue harvesting techniques enabling it to be used in conjunction with other mechanisms for assessing the ISC compartment, such as gene expression analysis.

The technique which appeared to hold the most potential as a method for assessing changes in the stem cell compartment was that of intestinal organoid culture. The method of culturing intestinal organoid structures *in vitro*, devised by Sato *et al.*, is now well established as a useful tool to study crypt homeostasis (Sato *et al.* 2009). This method simply isolates intestinal crypts, and using knowledge of intestinal growth *in vivo*, simulates the conditions required for growth with the addition of the growth factors EGF and Noggin. Crypts are cultured in laminin-rich Matrigel in the presence of Rspo1. Epidermal Growth Factor (EGF) is associated *in vivo* with intestinal proliferation, and inhibition of BMP signalling via transgenic expression of Noggin is sufficient to induce a significant expansion in crypt numbers (Haramis *et al.* 2004). Sato *et al*. noted that intestinal cells undergo programmed cell death when isolated from normal intestine, an effect which can be overcome by the addition of laminin, which is present *in vivo* at high levels at the base of the intestinal crypt. Culturing the intestinal organoids in laminin-rich Matrigel not only prevents anoikis by providing the required laminin,

but also supports the 3-dimensional structures of the organoids thereby enabling epithelial cell growth.

R-spondin1 (Rspo1) is a Wnt activator found endogenously at the base of the intestinal crypt. It has been shown that R-spondins interact with Lgr5 (de Lau *et al.* 2011), and it has recently been shown that, *in vivo*, Rspo1 is a ligand of the widely accepted ISC marker Lgr5 and its homologue Lgr4 (Schuijers and Clevers 2012). In organoid culture, the addition of Rspo1 enhances activation of the Wnt-signalling pathway specifically within $Lgr5^{+}$ cells (Sato *et al.* 2010). *Apc* mutants have been shown to be capable of organoid formation in the absence of Rspo1, indicating that reliance on Rspo1 could be used as a measure of Wnt-signalling activation within the intestinal crypt.

Once isolated, the crypts capable of regenerating and producing organoids in culture are able to do so as a consequence of containing functional ISCs. There remains a degree of inefficiency within this system, and consequently not all crypts are capable of producing organoids. However, increases in efficiency of organoid formation are likely to be concomitant with an increase in the number of ISCs per crypt and/or with augmented Wnt-activated stem cells per crypt. This can be extrapolated so that the number of organoids which grow from a known number of crypts seeded may be used to readout a level of "stemness" within each crypt.

Not only is organoid culture a technically challenging method to initially establish within the laboratory, but the use of it in this manner poses more obstacles. The main difficulties that we aim to overcome are;

1. Accurately calculating the number of seeded crypts. This is essential for the calculation of the percentage of seeded crypts which form organoids and subsequent determination of the level of "stemness"

2. Accurately and efficiently counting the number of organoids grown in order to minimise the time outside of the specific culture conditions of the incubator, as organoids are extremely sensitive to changes in culture conditions

3. Accurately quantifying the differences between the types of organoids which can grow. Organoids grown from $Apc^{flox/flox}$ mice are reported to be of a different

morphology to those grown from wildtype, indicating that Wnt-activation alters the way in which organoids grow. Quantifying these differences is required to assess the level of Wnt activation in the ISCs in the crypts

3.2 Results

3.3 Identifying and counting crypts

As previously mentioned, in order to calculate an accurate organoid formation efficiency, it is essential to have reliable data on the number of crypts seeded. In order to do this a counting method was optimised. Once the crypts were isolated and resuspended in 10 ml media, 3 x 10 µl samples were taken and counted. Only parallel rows of epithelial cells with a defined edge were counted (Figure 3.1). Variation in the quality of crypt preparations between mice was large, and the number of non-crypt epithelial cells (such as villus cells) is variable. Hence, by specifically counting crypts, rather than single cells, any other epithelial cells present do not skew the data. A further advantage of seeding crypts rather than single cells is that the efficiency of organoid formation from unsorted single cells is low (efficiency <0.003%, data not shown) such that very small variation can have a huge impact on the data, whereas organoid formation efficiency from crypts is much higher.

Initially 100 crypts were seeded per 50 µl Matrigel in each well of a 24 well plate. The number of crypts per well were counted 3 times manually. Due to the 3-dimensional nature of the Matrigel crypts were present in various planes of vision and this was a source of variation between counts. Furthermore, this method of counting is a slow process, and results in the removal of the plates from the incubator for extended periods of time, thereby potentially affecting their growth.

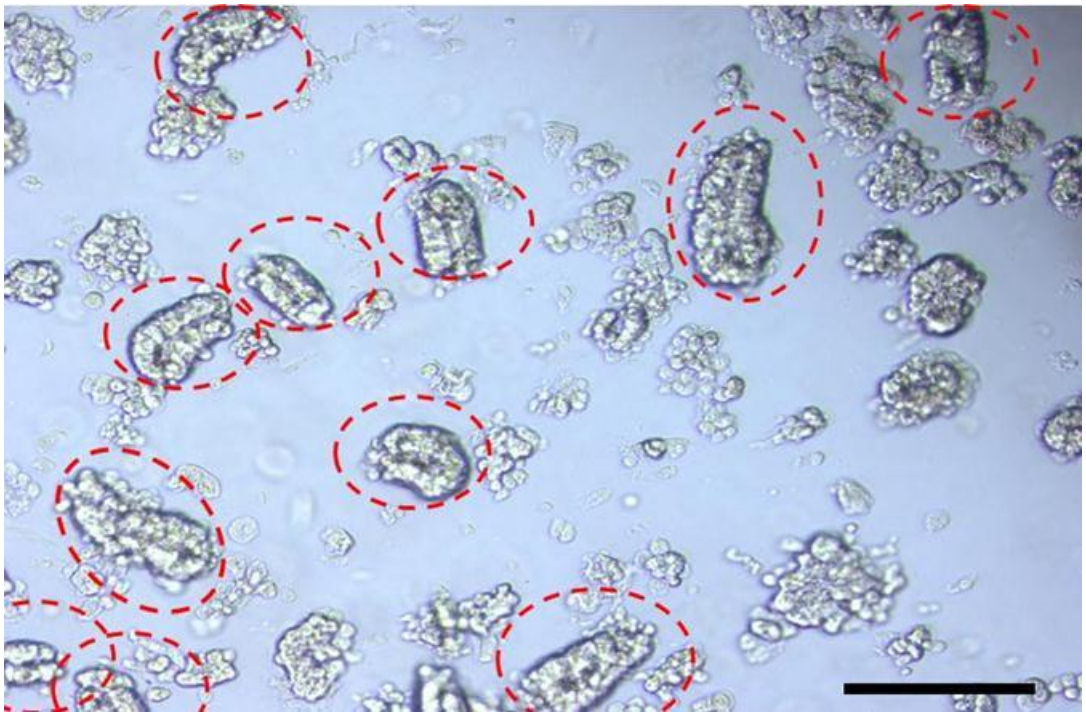

Figure 3.1 A typical crypt faction at counting. Red circles indicate crypts that would be counted. Although there is other cell debris and potentially fractions of intestinal crypts, crypts are only counted when there are clearly two parallel rows of epithelial cells which have a clear and distinct edge. Black bar represents 50 μm.

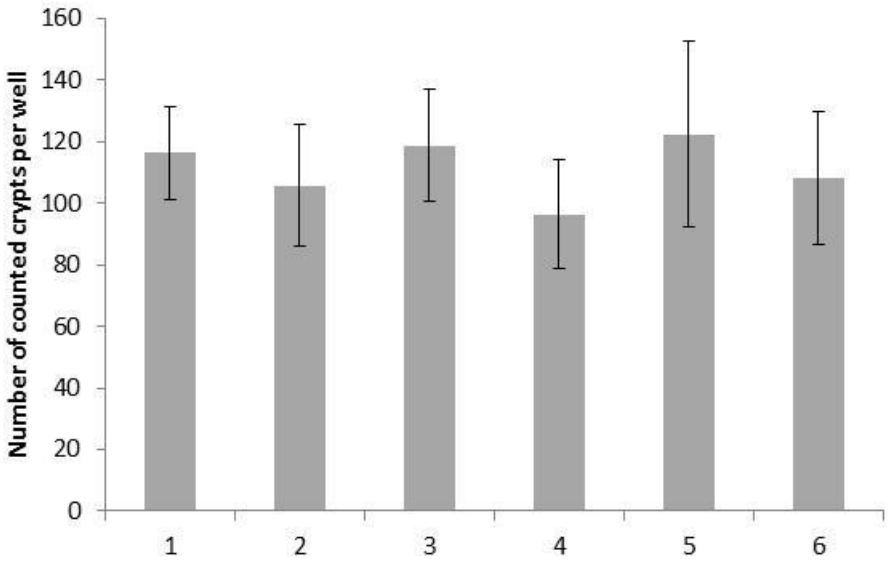

Figure 3.2 The number of crypts counted in 6 wells when seeded at 100 crypts per well. Each was counted 3 times and the bars represent the average of these counts. Error bars represent standard deviation.

The solution to this problem was to use an automated colony counter to count the organoids with greater speed and accuracy. In order to do this, the organoids have to be grown in a single plane of vision. This was achieved by using 96-well U-bottom plates and seeding 10 µl Matrigel per well. Using such a small volume in a U-bottom well prevented the Matrigel from setting in a dome shape. The newly designed plate reader and software used (Gelcount, Oxford Optronix) captured images of each well of the plate and automatically processed these to flatten the images from the U-bottom plate. Transferring the organoid culture from 24-well to 96-well plates, facilitated the production of a high throughput system in which accurate automated counting could be performed, removing much of the propensity for error in the system.

3.4 High variation between seeding densities in wells of 96-well plate

The conversion to growing the organoids in 96 well plates and reducing the seeding volume from 50 µl to 10 µl, resulted in a higher variation in seeding density between wells (Figure 3.3). In order to minimise the variation in organoid formation efficiency between wells, the problem of variations of seeding density between wells had to be addressed. This problem was overcome by using the automated plate reader to count wells individually and provide an accurate day 1 count. The number of organoids grown can thus be expressed, with confidence, as a percentage of the actual (rather than assumed) number of crypts present at day 1 for reach well. In order to assess the utility of this method it was necessary to ascertain whether seeding density, which clearly varied between each well, had an impact on this readout, see section 3.6.

3.5 Establishing CHARM settings for counting initially seeded crypts and number of organoids at day 11

In order to enable the Gelcount machine to perform automated organoid counts on images taken from 96 well plates, a script, entitled CHARM settings, had to be established. In order to establish these CHARM settings, threshold values for specific parameters such as optical density, size, circularity and quality of edge of objects detected within the well were set to enable the Gelcount programme to determine what type of object to count as a live organoid. The number of organoids within a well were manually counted and identified by the presence of an organised structure, and it was decided if they were alive or dead based on the quality of the “edge” of the organoid.

Dead organoids appear to lose the organisation of their outer edge and are less optically dense because of this. The parameters of the CHARM settings were adjusted until the Gelcount programme consistently counted organoids within 10% accuracy of the manual counts (see Figure 3.4). As both the manual counts and the Gelcount generated organoid counts are based on morphological criteria alone, there remains a propensity for error within the system, for example, an organoid may appear alive but actually be dead. In order to overcome this problem, the CHARM settings were adjusted for each day post seeding, and the size threshold altered, so that the only organoids within the well which were counted were those which had actively grown. This gives a level of accuracy and reproducibility which cannot be achieved through the use of manual counts alone, without measuring the size individual organoids. Final CHARM settings can be seen in section 2.12.4.

3.6 Seeding density does not affect the percentage of organoids which grow

The rate of organoid growth is greatly dependent on the presence or absence of the Wnt-activator Rspo1. Furthermore, Paneth cells are known to secrete other Wnt-activators which can impact on ISC function and number and thereby influence organoid growth. It therefore follows that the initiation and subsequent growth rate of organoids could be influenced by the density of the seeded crypts. If the proportion of organoids formed per well is dependent on the initial seeding density, then the seeding density will need to be the same between wells and between mice, which as previously mentioned is difficult to achieve using 96-well plates. Initial counts of actual crypt number seeded into each well of a 96-well plate showed a wide variation in seeding density per well (Figure 3.3). In order to assess any alterations in growth rate due to initial seeding density within this range, 20 wells were seeded with either 100 crypts, or 400 crypts. The number of crypts seeded was counted on the Gelcount machine at day 1 to establish the exact number per well, and the number of organoids over 150μm per well were counted at day 11 using the Gelcount machine. There was no significant difference in the percentage of crypts seeded which grew into organoids by day 11 when wells with an initial seeding density of less than 200 crypts per well (range 27-200) were compared to those with an initial seeding density of 300-500 crypts per well (Figure 3.5). Thus differences in the seeding density within this range do not affect the percentage of organoids which grow.

3.7 Number of wells of each genotype required to produce an accurate readout of stemness

In order to assess the number of wells of organoids required to give an accurate reading of organoid forming efficiency, 20 wells of a 96-well plate were seeded with 200 crypts per well and the percentage of crypts which formed organoids by day 11 was calculated per well. Using the running mean enabled the calculation of the number of wells required for an accurate reading of organoid forming efficiency. As organoid culture is both expensive and labour intensive, it is necessary to seed the least number of wells possible while still seeding enough to get an accurate result. It was found that the running mean had stabilised at around 6-7 wells (Figure 3.6) and so it was decided that 10 wells would be seeded to ensure accuracy.

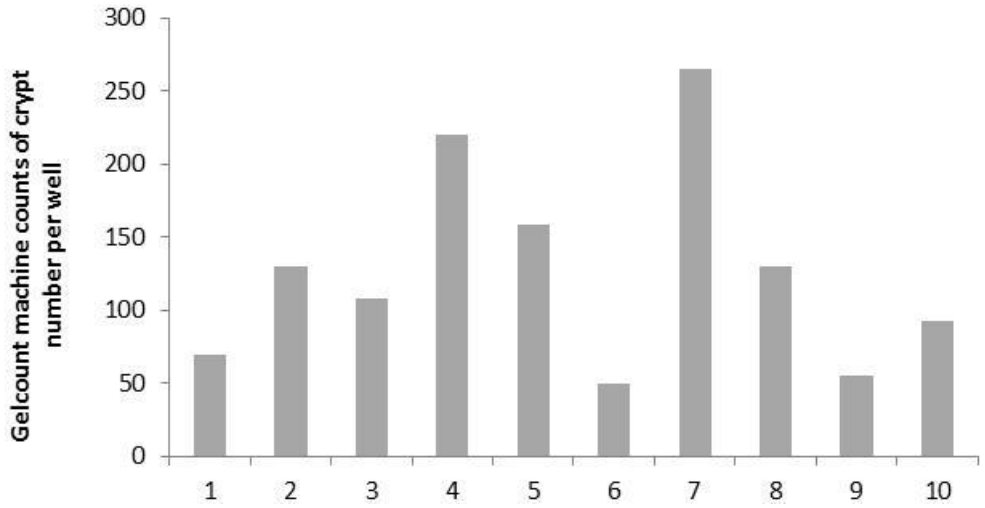

Figure 3.3 GelCount counts of 10 wells of a 96 wells plate were seeded at a predicted 100 crypts per 10 µl in each well. Machine counts showed that the number of crypts actually present within each well was greatly variable, ranging from 50 to 265.

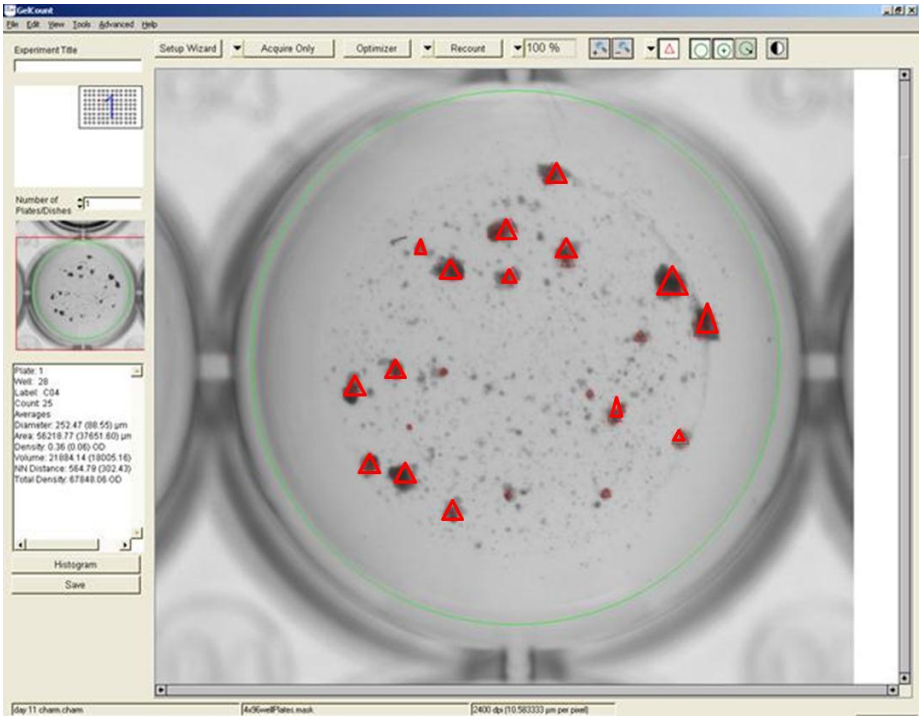

Figure 3.4 Screenshot of GelCount programme when counting organoids using specially selected CHARM settings. The red triangles indicate organoids which have been counted based on their size, density and complete edge. A quantity of cell debris and dead organoids can also be seen within this well.

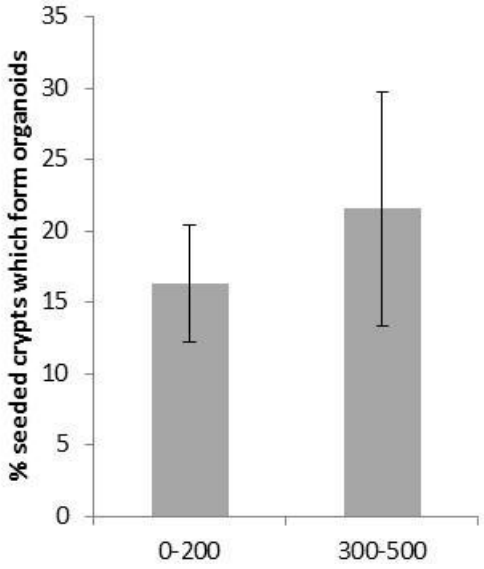

Figure 3.5 Seeding density within a two-fold range does not affect the percentage of crypts which form organoids. 20 wells were seeded with an estimated 100 crypts per well (actual values ranged from 27-200) and 20 wells were seeded with 400 crypts (actual range 300-500). There was no significant difference in the organoid formation efficiency between crypts seeded at 0-200 crypts per well, and those seeded at 300-500 crypts per well, 2-tailed T-test p= 0.086. Error bars represent standard deviation. N=9.

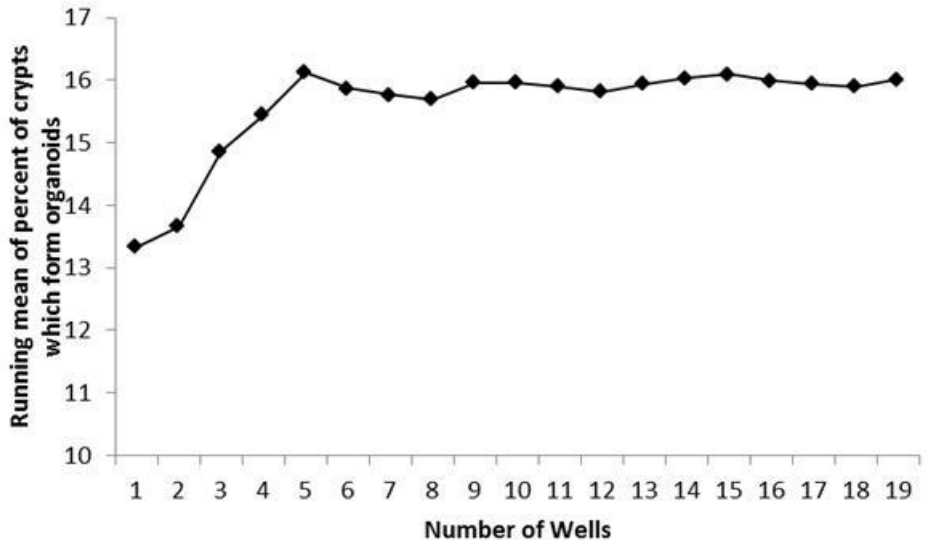

Figure 3.6 Running mean of the percent of crypts which form organoids in 20 wells. The average becomes stable at around 6-7 wells.

3.8 Crypts from induced Apc$^{flox/flox}$ mice form cyst-like organoids

To date, *Apc* deficient organoids have only been studied following the conditional loss of *Apc* within the organoids (Onuma *et al.* 2013). Our aim was to develop a system which permits the measurement of intestinal crypt "stemness" from the quantification of the percentage of seeded crypts which are capable of forming organoids. Therefore, we induced *Apc* loss within the mice using established tamoxifen induction of Cre-combinase under control of a *Villin* promoter in order to induce loss of *Apc* specifically within the intestinal epithelium, 3 days prior to initiating the crypt culture. This method of forming *Apc$^{flox/flox}$* organoids resulted in the development of cyst-like organoids forming at day 1-2 (Figure 3.7). The differences between organoid structure and growth rate can be visually ascertained, but difficult to quantify, due to the requirement for multiple photographs thereby requiring removal of the organoids from the incubator for long periods of time. As the *Apc$^{flox/flox}$* organoids are different in structure from wildtype organoids (Figure 3.8), specific CHARM settings were devised for cyst-like organoids, as they are less optically dense, and are more circular than wildtype. The CHARM settings were developed by altering the detection parameters until the automated counts were consistently within 10% of manual counts. All CHARM setting can be found in section 2.12.4.

3.8.1 Apc$^{flox/flox}$ form two distinct types of organoids

Organoids grown from *Apc$^{flox/flox}$* crypts 3 days post induction form two distinct types of organoids. As can be seen from Figure 3.7, all *Apc$^{flox/flox}$* organoids are cyst-like in structure; however they can be subcategorized into those which have a single layer of undifferentiated cells in a regular structure and those which have thick outer layers of multiple undifferentiated cells in an irregular and disordered structure (Figure 3.9). Both subtypes of *Apc$^{flox/flox}$* organoids grew in the absence and presence of Rspo1 and occured independently of whether recombination was induced *in vivo* or *in vitro* so the differences are not due to differential dependency on Rspo1, or incomplete recombination of *Apc* within the intestinal epithelium. Regions of cells with polarised nuclei were observed in both subtypes of *Apc$^{flox/flox}$* organoids, which contradicts what is observed *in vivo* whereby *Apc* deficiency results in loss of cell polarity within the aberrant proliferative region of the crypts.

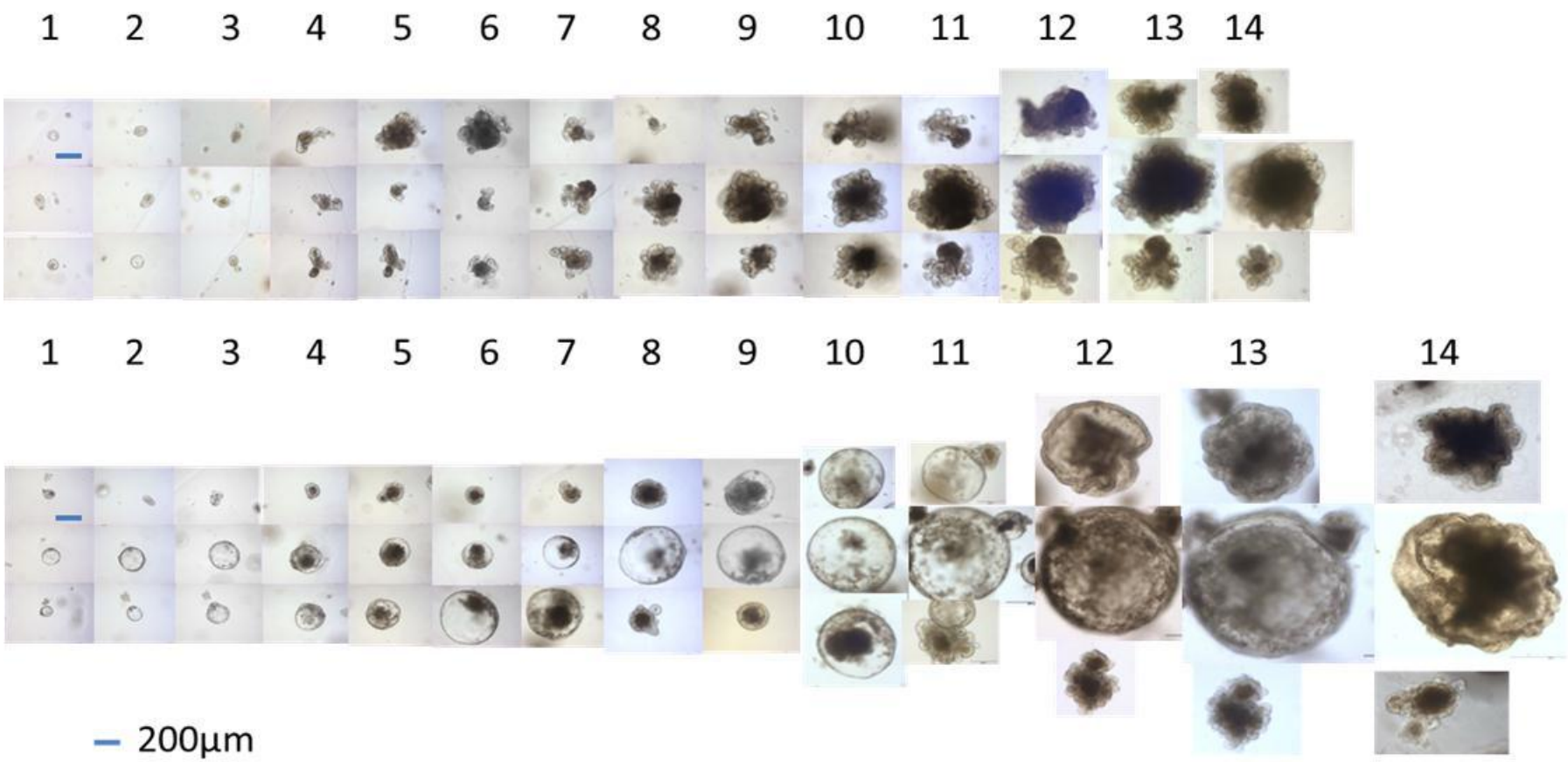

Figure 3.7 Images of organoids grown from the crypts of wild type (top row) and induced *Apc*$^{flox/flox}$ mice taken daily for 14 days. Differences between the two types of organoids are clear, with *Apc*$^{flox/flox}$ organoids having a cyst-like morphology and growing faster and larger than wild type organoids.

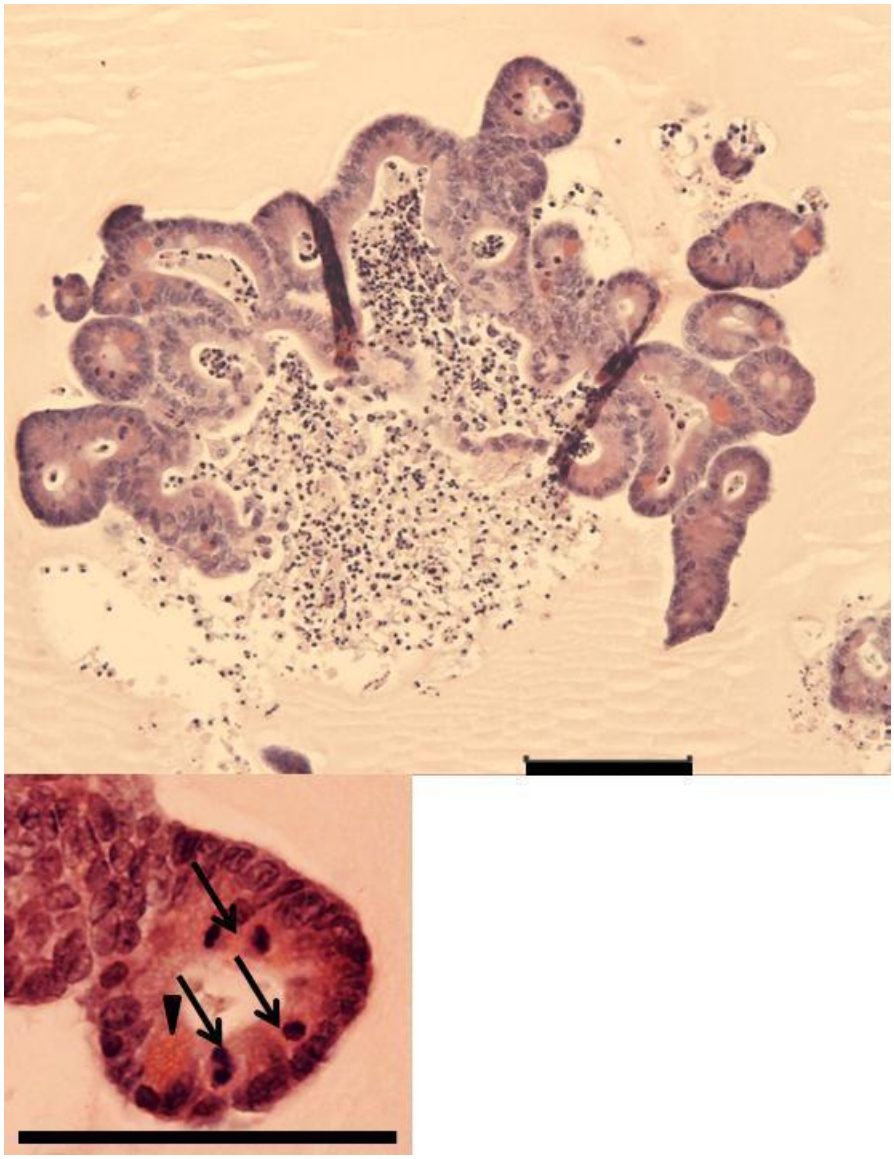

3.8 Wildtype organoids form a regular structure with visible Paneth cells (indicated by the black triangle). The crypt structures protruding clearly display polarised cells with clear organisation enabling mitotic cells to move away from the basement membrane towards the interior of the crypt structure (indicated with arrows) as is seen *in vivo*. Bar represents 100 µm.

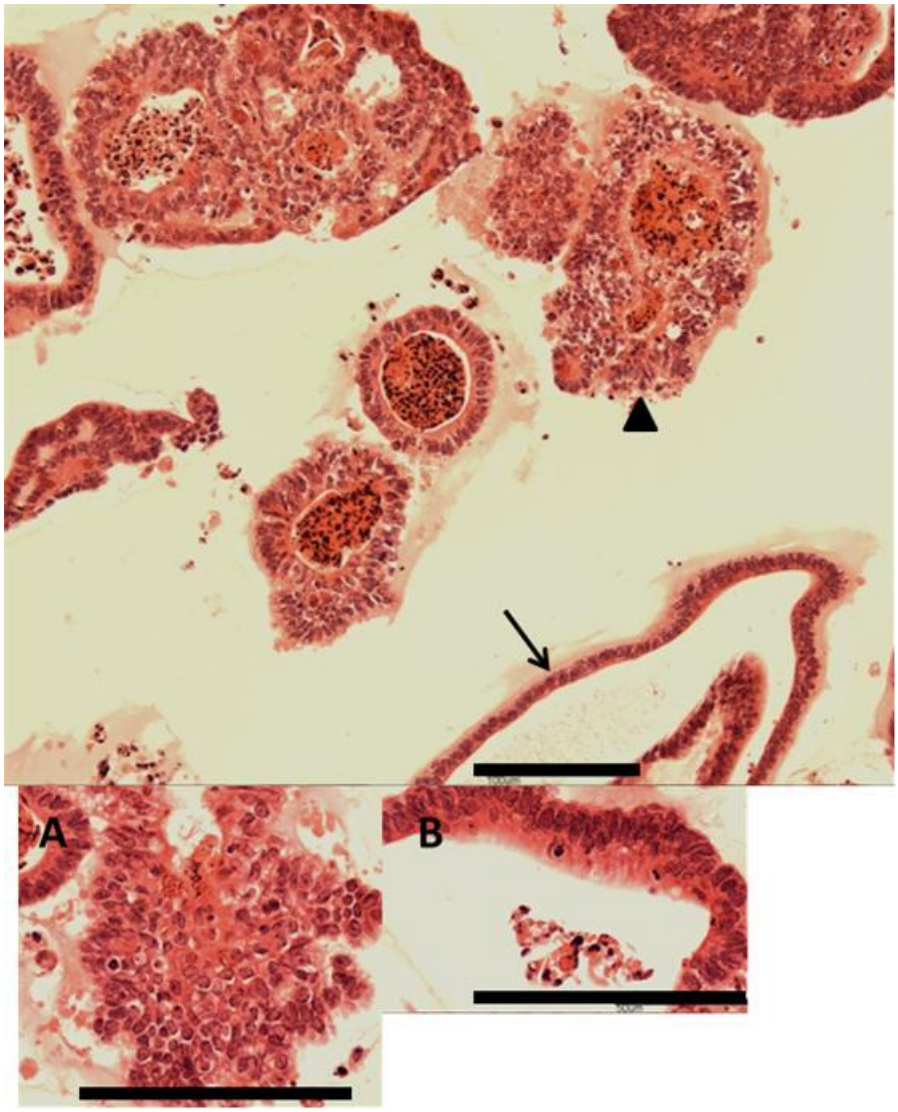

3.9 Organoids derived from *Apc*$^{flox/flox}$ mice form cyst-like structures of two types. This H&E slide shows that many organoids (indicated with a black triangle) display edges which are many cells thick with large patches of unpolarized cells (insert **A**), whereas others have a single cell thickness (indicated with an arrow) with clearly polarized nucei (insert **B**). Bars represent 100 µm.

3.8.2 *Apc$^{flox/flox}$* organoids contain fewer differentiated cell types than wildtype organoids

Wildtype organoids present all the differentiated cell lineages found *in vivo* within the intestinal epithelium. However, organoids derived from *Apc$^{flox/flox}$* mice 3 days post induction, only rarely stain positive for Alcian Blue, a marker of the mucins produced by goblet cells. It must be noted that goblet cells were only observed in *Apc$^{flox/flox}$* organoids which had been cultured in the presence of Rspo1, and may represent organoids derived from intestinal crypts in which there had been incomplete recombination of *Apc* (Figure 3.10). Positive staining for alcian blue was not observed in *Apc$^{flox/flox}$* organoids which had been grown in the absence of Rspo1, thereby selecting for organoids derived from crypts in which recombination of *Apc* was complete.

Enteroendocrine cells were detected in wildtype organoids using Grimelius staining, although they were rare, however they were not observed in *Apc$^{flox/flox}$* organoids under any growth conditions (Figure 3.11).

Interestingly, Paneth cells were observed in *Apc$^{flox/flox}$* organoids, although less frequently than were observed in wildtype organoids (Figure 3.12). Due to the lack of other differentiated cell types in *Apc$^{flox/flox}$* organoids it is likely that rather than these Paneth cells being the result of differentiation in culture, they represent surviving Paneth cells which were present in the crypts when the organoid culture was established. Data courtesy of Nadia Panitz indicates that Paneth cells were not observed in *Apc$^{flox/flox}$* cultures which had been cultured long term and had undergone multiple passages.

These data show that intestinal *Apc$^{flox/flox}$* cells with a stem-like phenotype, i.e. able to form organoids in culture and a high expression of ISC markers, cannot be described as true ISCs due to their inability to produce all of the differentiated cell types of the intestinal epithelia.

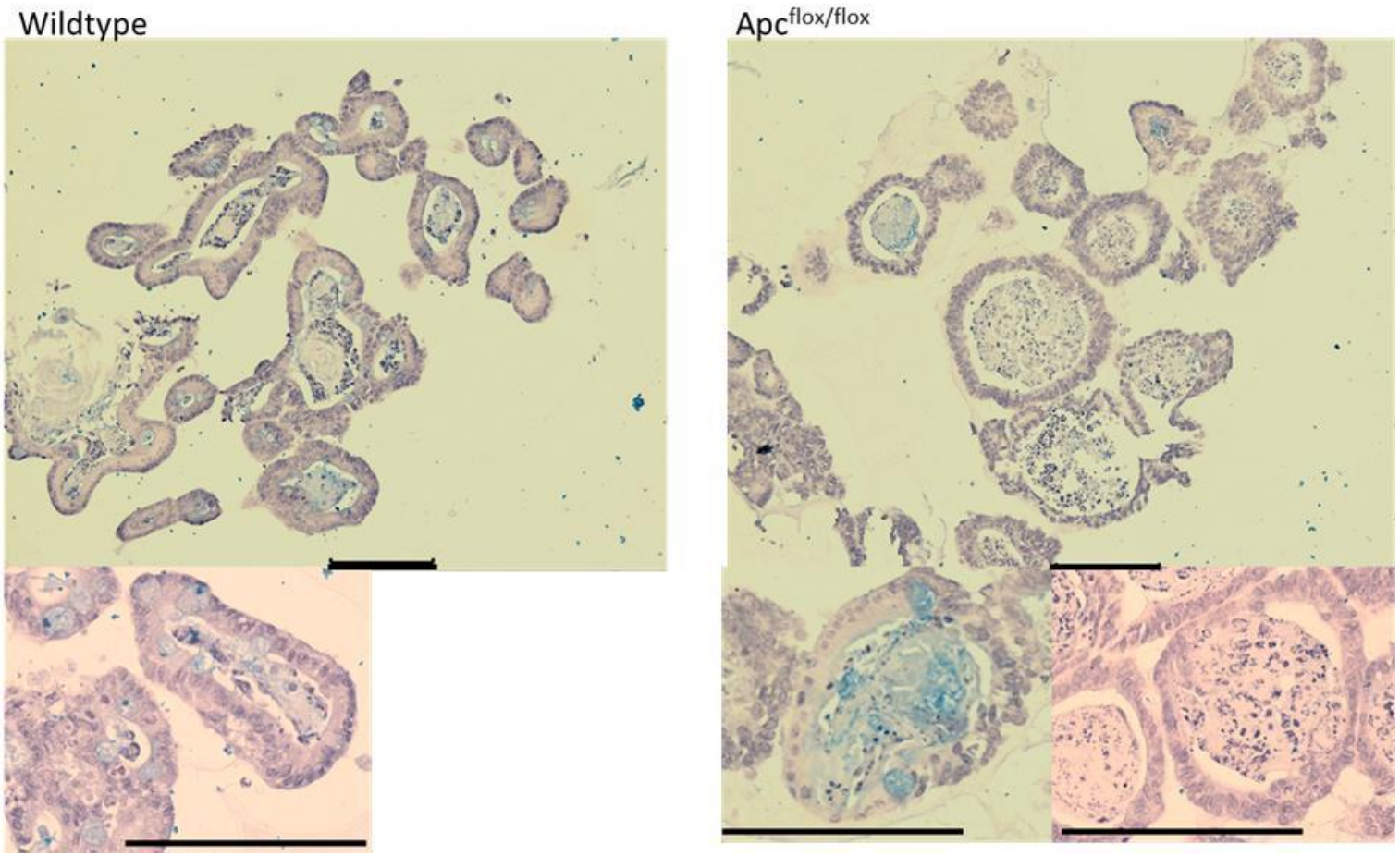

3.10 Alcian Blue stain of wildtype and *Apc*$^{flox/flox}$ organoids. Multiple goblet cells can be seen in wildtype organoids throughout the structures, whereas goblet cells were only observed extremely rarely in *Apc*$^{flox/flox}$ organoids. Bars represent 100 µm.

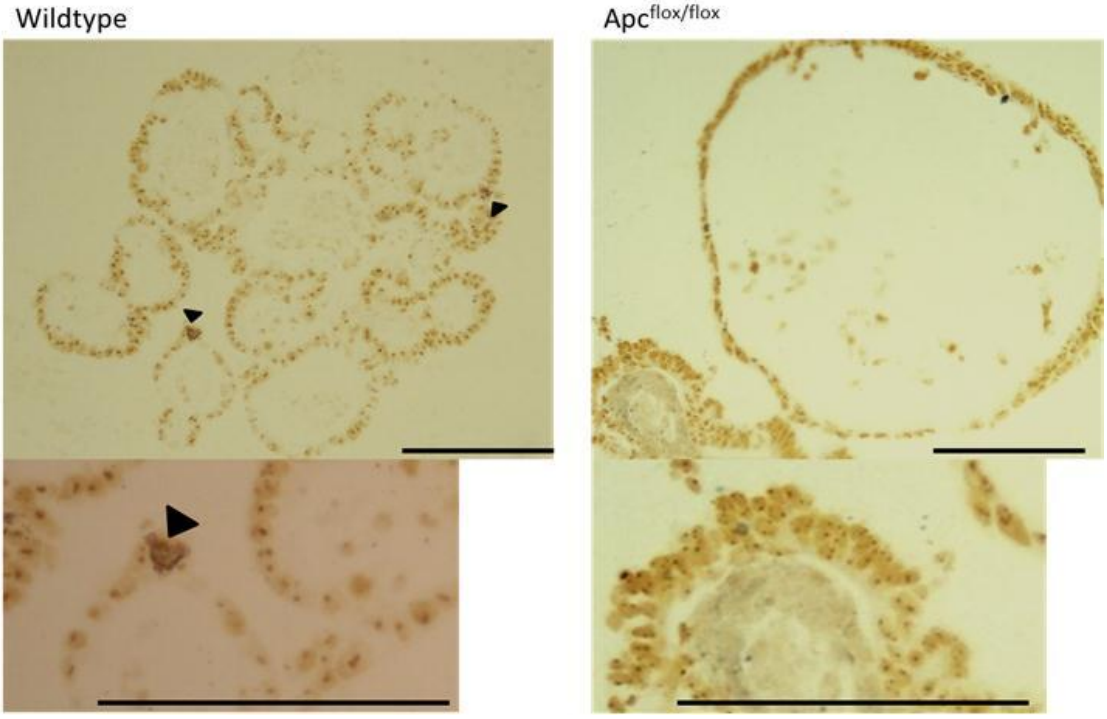

3.11 Grimelius stain of wildtype and *Apc*$^{flox/flox}$ organoids. Black arrows indicate enteroendocrine cells. Black bars represent 100 µm.

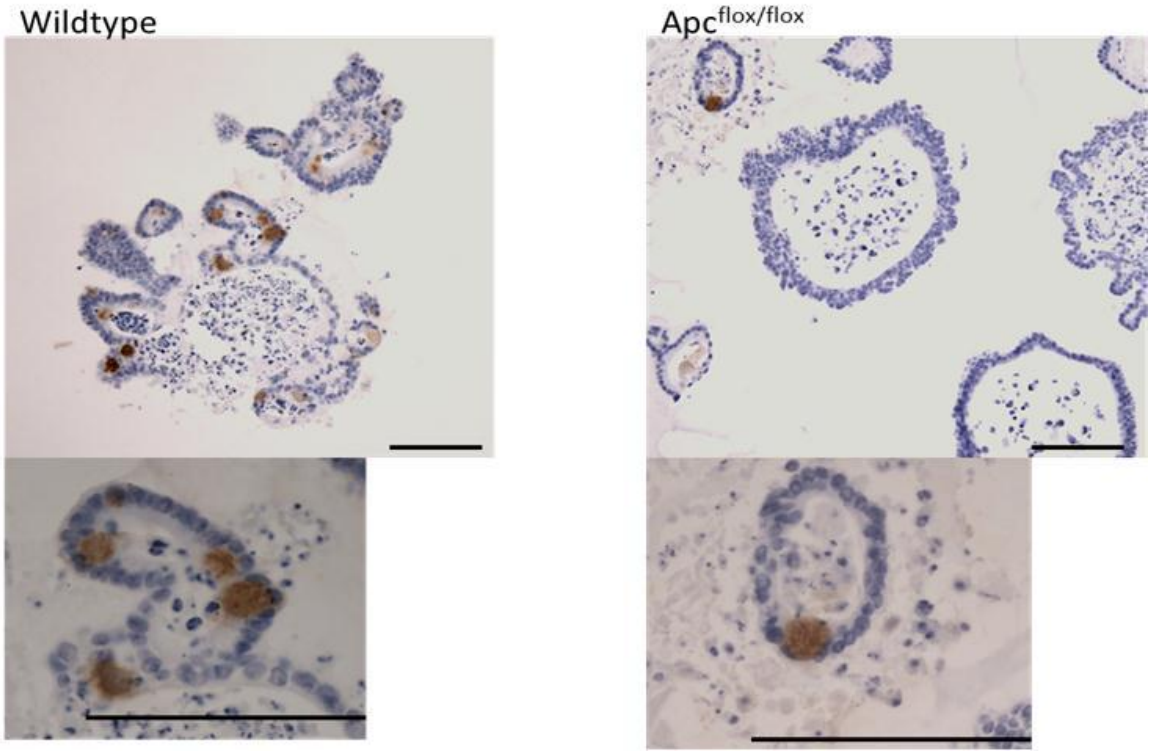

Figure 3.12 Lysozyme IHC of wildtype and *Apc*$^{flox/flox}$ organoids. Paneth cells are stained brown and are seen more frequently in wildtype than *Apc*$^{flox/flox}$ organoids. Black bars represent 100 µm.

3.8.3 Ki67 is expressed from a higher number of cells from wildtype organoids than from Apc$^{flox/flox}$ organoids

It has been shown that conditional homozygous loss of *Apc* from the intestinal epithelium *in vivo* results in an increase in levels of cell proliferation (Sansom et al. 2004). However, counts from IHC staining for the proliferative marker Ki67 in the organoids (Figure 3.13) show that a significantly higher percentage of cells are proliferating in cultured wildtype organoids than in *Apc$^{flox/flox}$* organoids (Figure 3.13) (Wildtype 98±2, *Apc$^{flox/flox}$* 49±29). This was measured by counting the total number of cells per sectioned organoid and representing Ki67 positive cells as a percentage of the total number of cells. Individual organoids were classed as a separate "n" value, although organoids derived from a minimum of 3 mice were counted for each genotype. BrDU stains, (courtesy of Nydia Panitz) show that exposing the organoids to BrDU for 1 hour prior to fixing, results in a similar proliferative readout (Figure 3.15).

3.8.4 Apc$^{flox/flox}$ and wildtype organoid cells undergo similar levels of apoptosis

Levels of apoptosis within the organoids were assessed by expression of the apoptotic marker Caspase 3 (Figure 3.16). The percentage of organoid cells which were Caspase 3 positive showed no significant difference between *Apc$^{flox/flox}$* organoids and wildtype organoids (Figure 3.17) (Wildtype 0.6±0.6, *Apc$^{flox/flox}$* 0.9±0.8). This is in direct contrast to the observation made *in vivo,* namely that loss of *Apc* results in an increase in apoptosis (Sansom et al. 2004).

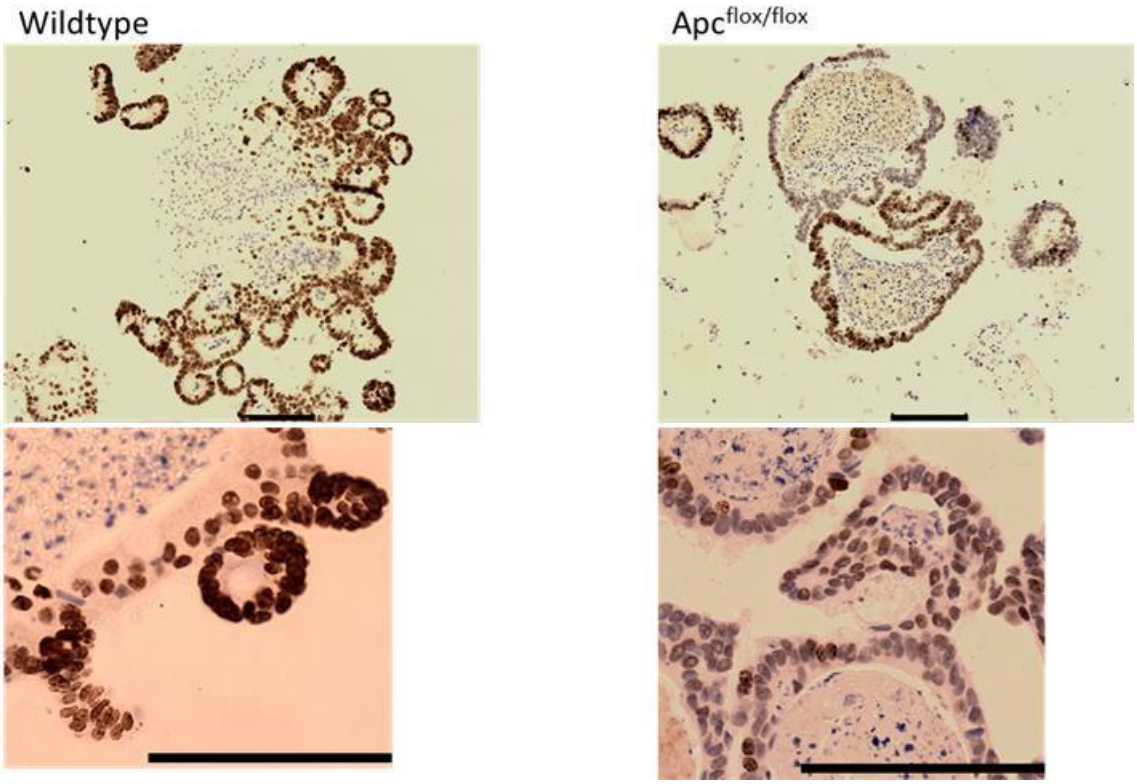

3.13 A Ki67 IHC on wildtype and *Apc*$^{flox/flox}$ organoids. Brown cells represent Ki67 positive cells, c the vast majority of cells from wildtype organoids were Ki67 positive, and non-proliferating cells were extremely rare. In *Apc*$^{flox/flox}$ organoids both Ki67 positive and negative cells were seen frequently. Bars represent 100 µm.

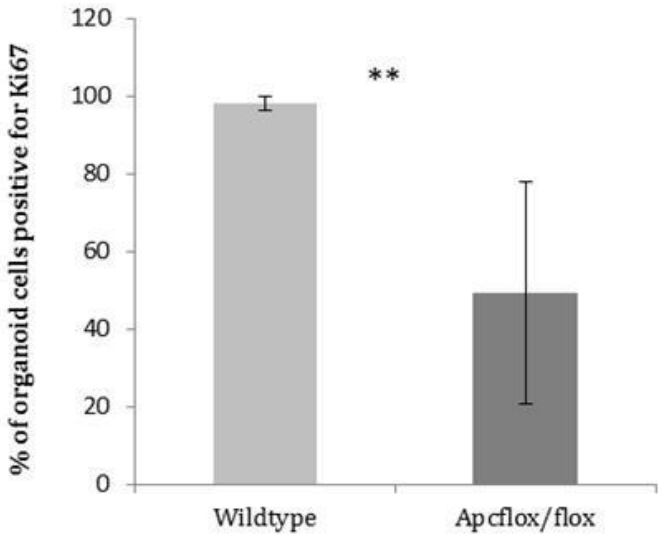

3.14 Percentage of wildtype and *Apc*$^{flox/flox}$ organoid cells which stain positive for Ki67. Error bars represent standard deviation. Wildtype organoids contained significantly more Ki67 cells than *Apc*$^{flox/flox}$ organoids, 2-tailed T-test p=0.00. N>30.

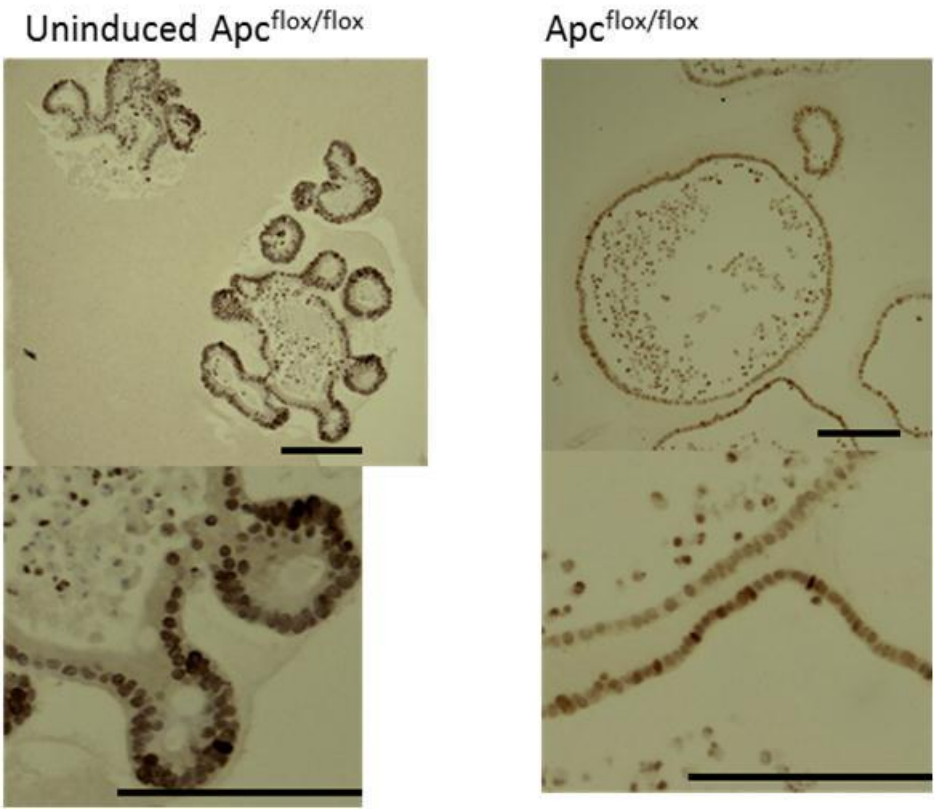

3.15 BrDU IHC of uninduced *Apc*$^{flox/flox}$ organoids (equivalent to wildtype) and induced *Apc*$^{flox/flox}$ organoids after 1 hour of BrDU exposure. Slides courtesy of Nydia Panitz. There is an observable reduction in BrDU uptake from induced Apc$^{flox/flox}$ organoids compared to uninduced. Bars represent 100 μm.

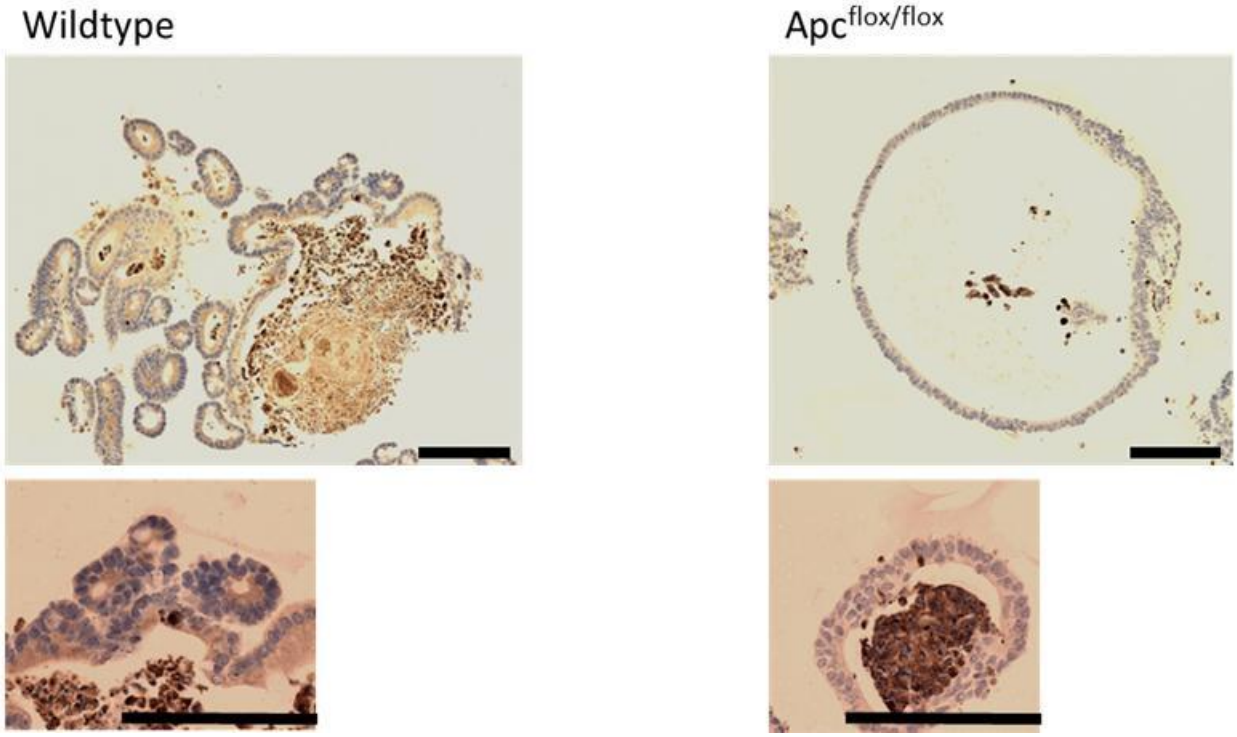

3.16 A Caspase3 IHC on wildtype and *Apc*$^{flox/flox}$ organoids. Caspase 3 positive cells (stained brown) are rare in both genotypes. Bars represent 100 μm.

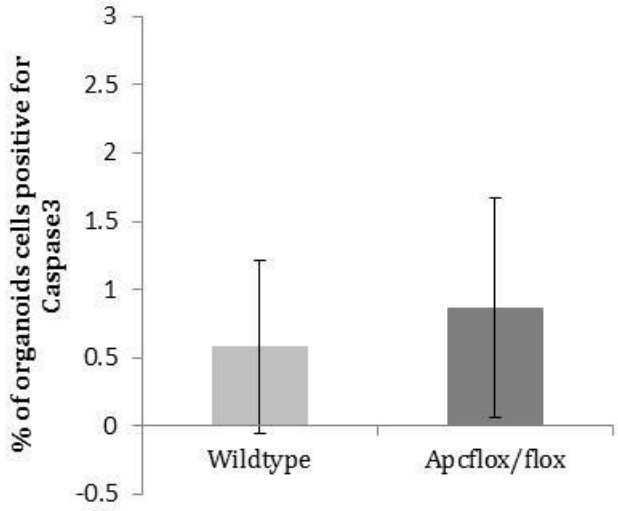

3.17 Percentage of Wildtype and *Apc*$^{flox/flox}$ organoid cells which are Caspase 3 positive. There was no significant difference in the percentage of organoid cells which were caspase positive between the two genotypes, 2-tailed T-test p=0.119. Error bars represent standard deviation. N>30.

3.9 Apc$^{flox/flox}$ organoids grow faster than wildtype

Measuring the average diameter of the organoids on alternate days using the GelCount programme enabled assessment of the growth rate of the intestinal organoids. Organoids derived from *Apc*$^{flox/flox}$ crypts grew faster than those derived from wildtype crypts (Figure 3.18), however, by day 11 the sizes were not significantly different and there was no difference between the numbers of cells per organoid (as counted on H&E sections) at day 11 (Figure 3.19) (Wildtype 172±141, *Apc*$^{flox/flox}$ 159±91). It should be noted that sectioning of paraffin embedded organoids results in a high variation of visible cells per organoid due to differences in the plane of the section.

3.9.1 Apc$^{flox/flox}$ organoids have higher levels of nuclear β-catenin than wildtype

In vivo, loss of Apc is associated with a dramatic increase in Wnt-signalling, which is highlighted by an increase in nuclear β-catenin. This situation is mimicked *in vitro*, where intestinal organoids derived from *Apc* deficient crypts are high in nuclear β-catenin, whereas cells from wildtype organoids have variable levels (Figure 3.20).

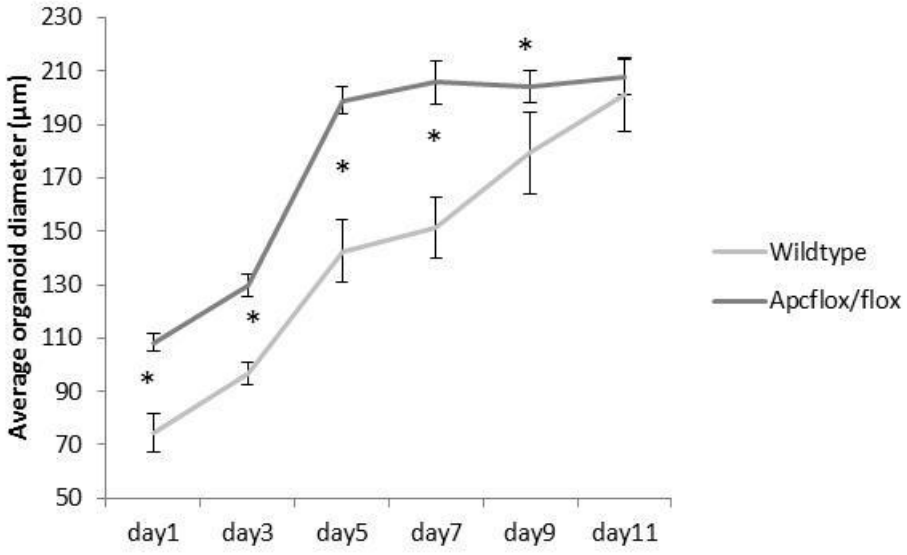

3.18 *Apc*$^{flox/flox}$ organoids grew faster than wildtype, but were not significantly larger at day 11. Average organoid diameter was measured using Gelcount machine. Ten wells of each genotype were measured. Error bars represent standard deviation. * represents $p<0.05$ at that time point using 2-tailed T-test.

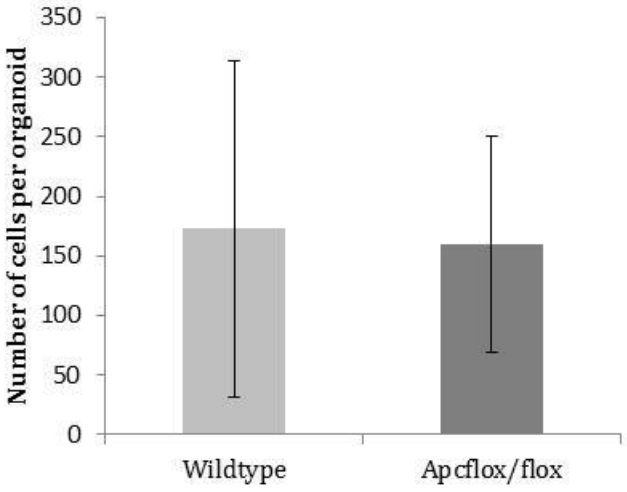

3.19 Wildtype and *Apc*$^{flox/flox}$ organoids have the same number of cells at day 11. Cell counts were performed using H&E sections of paraffin embedded fixed organoids. There was no significant difference in the total cell counts between the two genotypes, 2-tailed T-test $p=0.651$. Error bars represent standard deviation. $N>30$.

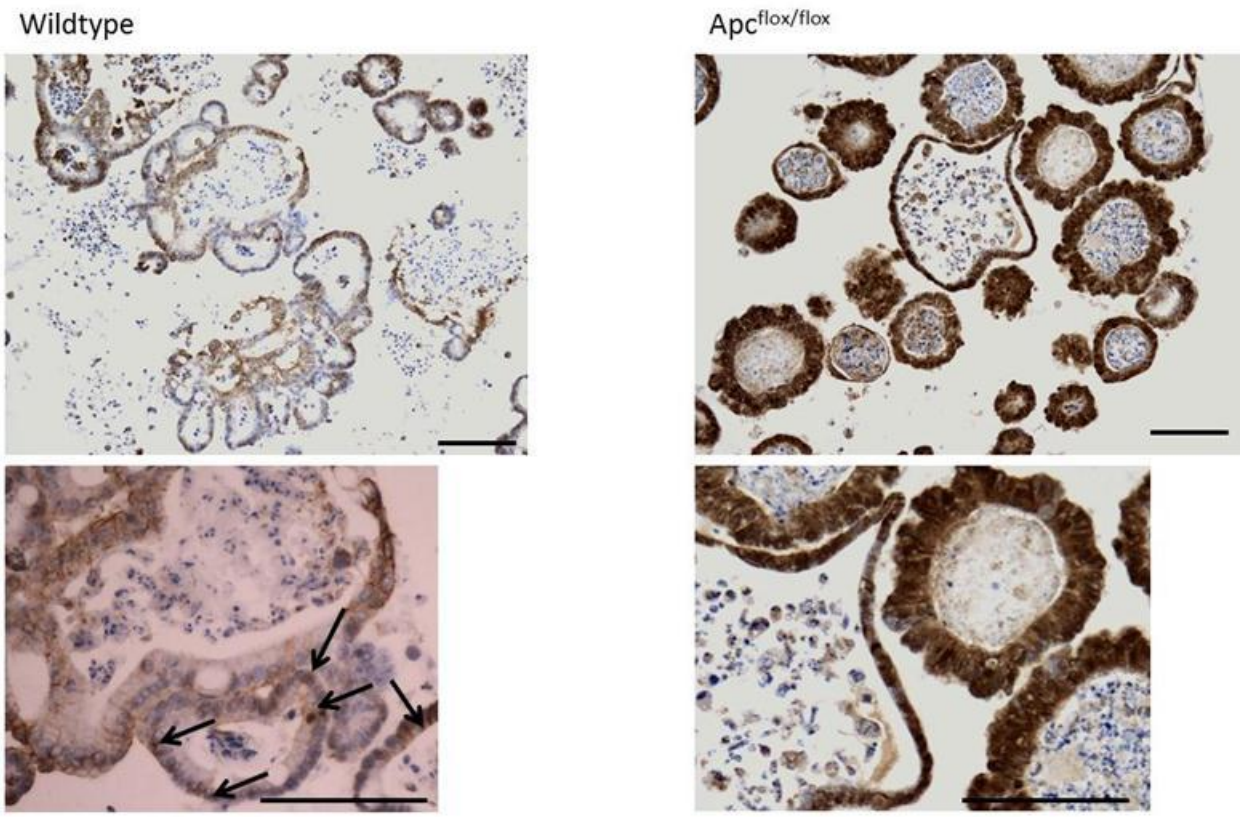

3.20 β-catenin immunohistochemistry on wildtype and *Apc*$^{flox/flox}$ organoids, brown nuclei represent nuclear β-catenin. Nearly 100% of *Apc*$^{flox/flox}$ organoid cells are positive for nuclear β-catenin, whereas the levels of nuclear β-catenin in wildtype organoids are variable. Nuclear β-catenin in wildtype organoids indicated by arrows. Black bars represent 100 μm.

3.10 Assessing changes in the ISC compartment as a result of Apc loss using traditional gene expression methods

Using qRT PCR to determine the relative expression levels of a range of intestinal stem cell markers shows an increased expression of these markers in *Apc$^{flox/flox}$* intestinal tissue when compared to wildtype intestinal epithelium (Figure 3.21). The most commonly used markers of the intestinal stem cell compartment, *Lgr5*, A*scl$_2$*, *Olfm4*, *Msi1* and *Bmi1* (Barker et al. 2007; Kayahara *et al.* 2003; Sangiorgi and Capecchi 2008; van der Flier et al. 2009a; van der Flier et al. 2009b) were all significantly upregulated following loss of *Apc* from the intestinal epithelium. Intestinal epithelium was extracted using Weiser preparation to minimise interference from the stromal and muscle compartments of the intestine.

In situ hybridisation is a commonly used method for identifying the location of the ISC compartment (Ziskin *et al.* 2012). *In situ* hybridisation for the ISC markers *Ascl$_2$* and *Olfm4* shows an expansion of the ISC compartment following *Apc* loss. These *in situ* hybridisations support the qRT-PCR data and indicate that loss of *Apc* does not simply lead to an increase of expression of these markers, but also a mis-localisation. These data taken together indicate an expansion of intestinal stem-like cells as a result of loss of *Apc* as assessed by ISC expression markers (Figure 3.22).

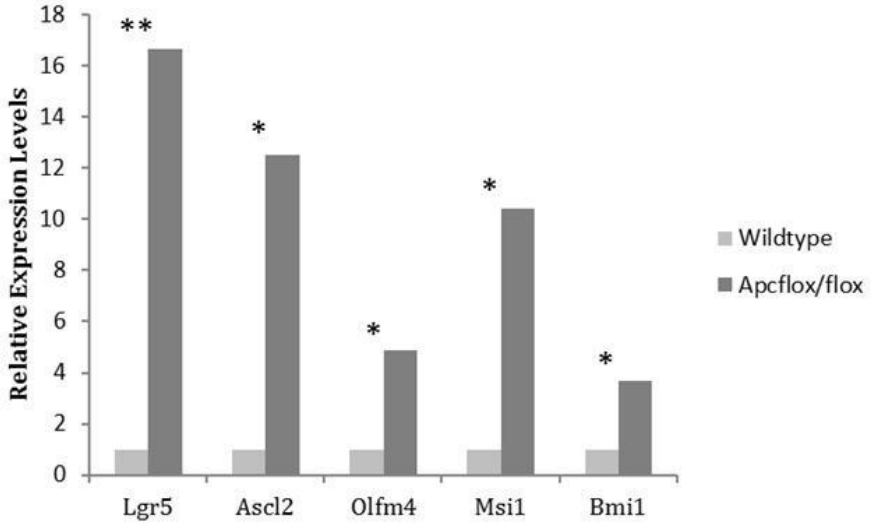

3.21 qRT-PCR results of relative expression levels of a range of proposed intestinal stem cell markers from wildtype versus *Apc*$^{flox/flox}$ intestinal epithelial cell preparation. * indicates $p<0.05$, ** indicates $p<0.01$ using 2-tailed T-test.

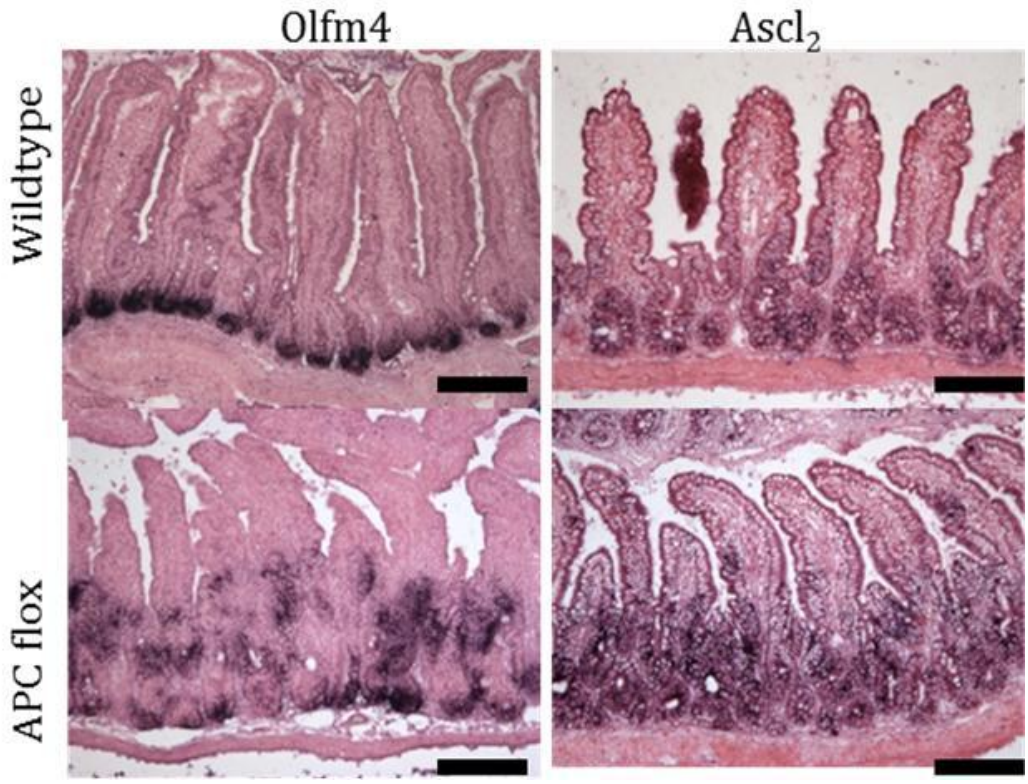

3.22 *In situ* hybridisation for stem cell markers *Olfm4* and *Ascl*$_2$ in wildtype and day 4 *Apc*$^{flox/flox}$ murine intestine. Mis-localisation and increase of expression was observed following *Apc* loss. Bar represents 100 μm.

3.11 A higher percentage of Apc$^{flox/flox}$ crypts are capable of forming organoids than wild type crypts and grow in the absence of Rspo1

Using the specially adapted CHARM settings it was possible to directly compare efficiency of organoid formation between wildtype and *Apc$^{flox/flox}$* crypts. It was found that the percentage of *Apc$^{flox/flox}$* crypts which had formed organoids by day 11 was more than 2 fold greater than that seen in wildtype crypts (Figure 3.23) (Wildtype 16±8, *Apc$^{flox/flox}$* 38±11). These data support the qRT-PCR and *in situ* hybridisation results which suggest an increase in number of functional ISCs.

The number of *Apc$^{flox/flox}$* crypts which form organoids was found to be independent of the presence of Rspo1 in the media, whereas wildtype organoids did not form without Rspo1 (Figure 3.24), demonstrating that not only are there more ISCs in Apc deficient mice, but that these ISCs are highly Wnt-activated.

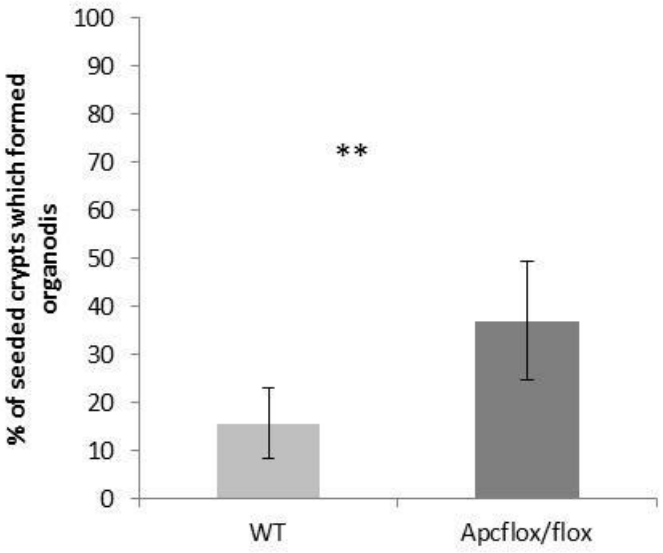

3.23 Organoid forming efficiency of wildtype and *Apc*$^{flox/flox}$ crypts. Crypts deficient for *Apc* are significantly more efficient at forming organoids, 2-tailed T-test p=0.004. N>6.

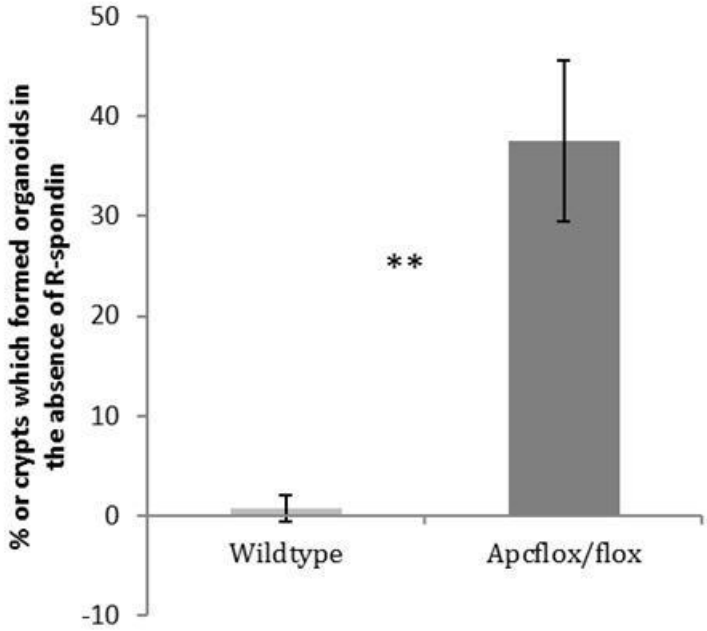

3.24 Organoid forming efficiency of wildtype and *Apc*$^{flox/flox}$ crypts in the absence of Rspo1. Crypts deficient for *Apc* are capable of forming organoids in the absence of Rspo1, whereas wildtype crypts are not. 2-tailed T-test p=0.00. N>6.

3.12 Using the organoid culture method as a readout of Wnt-activation in the Intestinal Stem cell compartment

As the ability to grow *in vitro* independently of Rspo1 concentration could represent a readout of the level of Wnt-activation of the ISCs, the ability to quantify the level of Rspo1 dependency of the crypts of various genotypes became essential. As previously discussed the addition of the growth factor Rspo1 results in the activation of the Wnt-signalling pathway specifically within the $Lgr5^{+}$ ISC population. It can therefore be inferred that genotypes of organoids which are more capable of growing in the absence of Rspo1 contain more highly Wnt-activated ISCs.

Using the plate reader to count the number of organoids each day post seeding when cultured in the absence of Rspo1 is not currently possible, as the CHARM settings cannot differentiate between organoids which are alive or recently dead (as the size and density of organoids does not alter for a few days after death). Therefore in order to quantify the ability of intestinal organoids to grow in the absence of Rspo1 it was necessary to explore the use of cell viability assays.

The PrestoBlue cell viability reagent uses the reducing ability of the cytosol in living cells to reduce a blue, non-fluorescent, cell-permeant compound into a red, highly fluorescent compound, enabling the detection of changes in levels of absorbance without affecting cell viability. This enables the measurement of cell viability in the presence or absence of Rspo1 without damaging the organoids.

Previous culturing of organoids has shown that wildtype crypts can survive for 2 days in the absence of Rspo1, so the PrestoBlue assay was used on day 3 for 2 hours at 3 different Rspo1 concentrations. The normal culture conditions include Rspo1 at 6.5 μg/ml, and the fluorescence produced by PrestoBlue exposure to 10 wells of these organoids was used as a baseline for mitochondrial activity. The fluorescence measured as a result of PrestoBlue exposure to wells containing organoids grown with the other Rspo1 concentrations (3.25 μg/ml and 0 μg/ml) was normalised as relative to those grown at 6.5 μg/ml.

3.13 Mitochondrial activity within Apc$^{flox/flox}$ organoids is not affected by Rspo1 concentration whereas wild type organoids respond in a dose dependant manner

Calculating relative mitochondrial activity using the PrestoBlue assay for wildtype vs *Apc$^{flox/flox}$* organoids shows that loss of *Apc* renders organoids independent of Rspo1 for their survival and growth. As an Lgr4/5 ligand (Wang *et al.* 2013a), Rspo1 activates the Wnt-signalling pathway specifically within Lgr4/5 expressing cells, identified as the ISCs. Ability to grow in the absence of Rspo1 must therefore reflect the presence of ISCs with already highly activated Wnt-signalling, as would be expected from ISCs derived from murine intestinal epithelium in which *Apc* has been homozygously deleted.

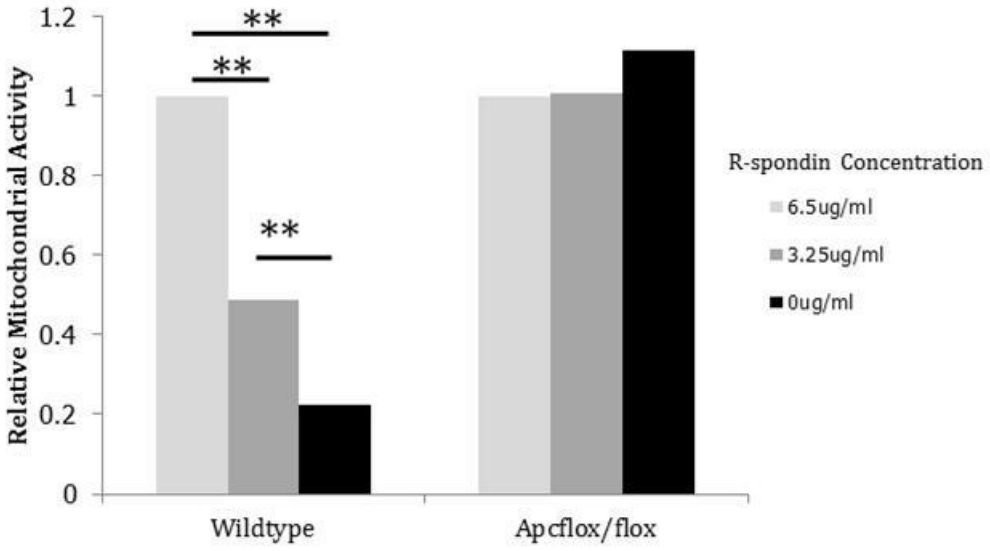

3.25 Relative mitochondrial activity of wildtype and *Apc$^{flox/flox}$* organoids in different Rspo1 concentrations using the PrestoBlue assay. ** indicates $p<0.001$ using 2-tailed T-test.

3.14 Assessing the utility of the organoid formation assay using a Cited-1 deficient mouse model

In order to assess whether the stem cell functionality assay could provide useful insights into the early stages of tumourigenesis, we must be able to demonstrate that it can detect more subtle changes in the ISC compartment than those caused by homozygous deletion of *Apc*. Also, as loss of *Apc* results in large, cyst-like structures as opposed to differentiated organoids, the method must also be able to distinguish between genotypes which have a similar phenotype *in vitro*.

3.14.1 Cited-1

It was shown in a mouse melanoma cell line that the bi-functional transcriptional cofactor encoded by *Cited-1* plays a role in activation and repression of expression of a wide range of target genes (Shioda *et al.* 1996; Yahata *et al.* 2001). The complex role that Cited-1 could play in tumourigenesis was hinted at by its ability to inhibit Wnt signaling but activate Smad-4 dependent transcription resulting in enhanced TGFβ/BMP signaling (Plisov *et al.* 2005). A role for *CITED-1* in tumourigenesis has also been implicated in several human cancers such as nephroblastoma, melanoma and Wilm's tumours where disregulation of *CITED-1* expression is observed (Lovvorn Iii *et al.* 2007; Nair *et al.* 2001). In a mouse model of mammary cancer (MMTV-Cre/FloxNeoNeuNT), it was shown that *Cited-1* expression is elevated within the tumours where it functions alongside Egr2 to drive expression of the oncogene ErbB2 (Dillon *et al.* 2007).

Microarray data from this laboratory has shown that loss of *Apc* immediately results in an increase in expression of the gene *Cited-1*, an upregulation that is dependent on the presence of functional C-myc. Loss of the Wnt target *C-myc* in an $Apc^{flox/flox}$ mouse not only rescues the phenotype of *Apc* loss (Sansom *et al.* 2007), but also returns *Cited-1* expression levels to those found in wildtype. Our laboratory has recently shown that an upregulation of CITED-1 is observed in human colorectal cancers, and that loss of *Cited-1* expression in the *Apc* heterozgygous mouse model of colorectal tumourigenesis, $Apc^{min/+}$, increases survival via a reduced intestinal tumour burden (Méniel *et al.* 2013).

Loss of *Cited-1* alone does not result in intestinal tumourigenesis, but does markedly increase levels of dephosphorylated β-catenin within the intestinal epithelium. Interestingly, loss of *Cited-1* in the context of homozygous *Apc* loss using *AhCre Apc$^{flox/flox}$* mice results in a further increase in both dephosphorylated β-catenin and associated Wnt-target genes (Méniel *et al*. 2013).

The subtle deregulation of Wnt signaling observed in *Cited-1* null intestinal epithelia without grossly affecting the intestinal phenotype, provides a perfect model for testing the ability of the organoid formation assay to analyze small changes in the ISC compartment that may arise as a result of Wnt-deregulation.

3.15 Cited-1 loss and the ISC compartment

qRT-PCR was used to show that expression of the ISC markers *Lgr5*, *Msi1* and *Ascl$_2$* were significantly higher in the intestinal epithelia of *Cited-1* null mice than wildtype ($p<0.05$). There was a trend for increased expression of the markers *Bmi-1* and *Olfm4* but it was not significant at n=6 ($p>0.05$).

In situ hybridisation revealed that expression of the intestinal stem cell marker *Olfm4* was still limited to the crypt base in *Cited-1* null mice, and the probe signal appears no different to that observed in wildtype. This indicates that there is no mislocalisation of the ISC compartment, however, there could be an increase in ISC number around the base of the crypts, which would not be visible from the cross-sections of the crypt structure shown in Figure 3.27. Also, it should be noted that *Olfm4* is one of the ISC markers whose expression is not significantly upregulated as a result of *Cited-1* loss. *Olfm4* was chosen for *in situ* hybridisation as *in situ* hybridisation for this marker results in a tighter staining pattern than that observed with *Ascl2*. In addition to this, *Olfm4*, unlike *Ascl2*, is not a direct Wnt target gene, and so changes in expression pattern are less likely to be due to an increase in Wnt-signalling as opposed to an increase in ISC markers (van der Flier et al. 2009a).

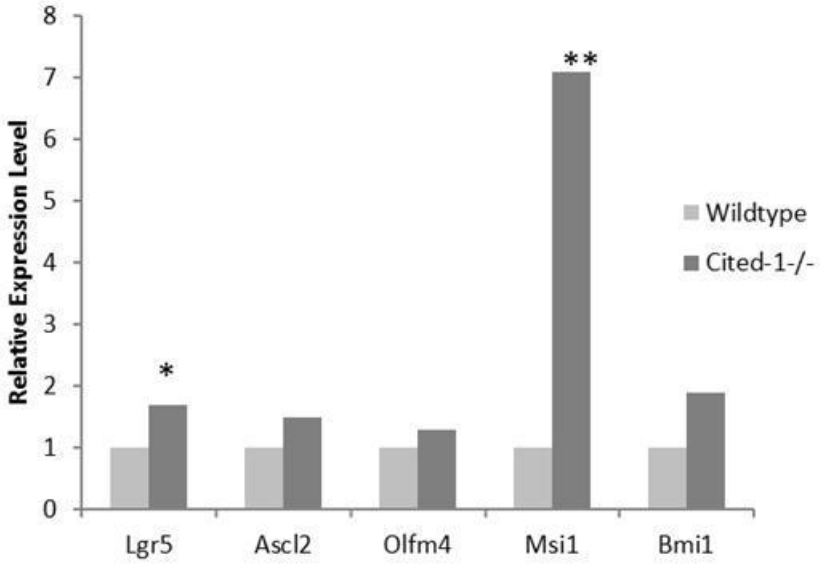

3.26 qRT-PCR results of relative expression levels of a range of proposed intestinal stem cell markers from wildtype versus *Cited-1*$^{-/-}$ intestinal epithelial cell preparation. * indicates $p<0.05$, ** indicates $p<0.01$. N=6

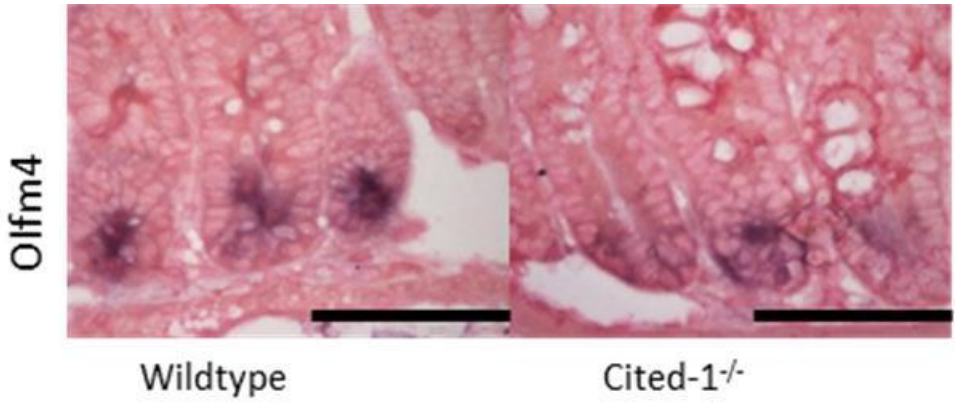

3.27 *In situ* hybridisation for the intestinal stem cell marker *Olfm4* in wildtype and *Cited-1*$^{-/-}$ crypts. Bars represent 100 μm.

3.15.1 Cited-1$^{-/-}$ organoids

Cited-1$^{-/-}$ organoids are phenotypically identical to wildtype (Figure 3.28), displaying multiple crypt-protrusions containing goblet cells, enteroendocrine cells and Paneth cells (images not shown). As there were no gross differences between *Cited-1*$^{-/-}$ organoids and wildtype organoids, the same CHARM setting for organoid counting and measurement of growth rates were used.

3.15.2 Cited-1$^{-/-}$ crypts form organoids more efficiently than wildtype

The organoid formation assay revealed that a significantly higher percentage of *Cited-1*$^{-/-}$ crypts were capable of forming organoids than wildtype (Figure 3.29) (Wildtype 14±5, *Cited*$^{-/-}$ 21±3). This supports the expression marker data which indicates that loss of *Cited-1* results in an expansion of the ISC compartment. The organoid formation efficiency of *Cited-1*$^{-/-}$ crypts was still significantly lower than that seen in *Apc*$^{flox/flox}$ crypts.

3.15.3 Cited-1$^{-/-}$ organoids are Rspo1 dependent

The PrestoBlue mitochondrial activity assay shows that *Cited-1*$^{-/-}$ organoids are dependent on the presence of Rspo1 in the culture medium for their growth and development in a dose dependent manner equivalent to that of wildtype. This indicates that the ISCs of *Cited-1*$^{-/-}$ mice are not significantly more Wnt-activated than wildtype ISCs.

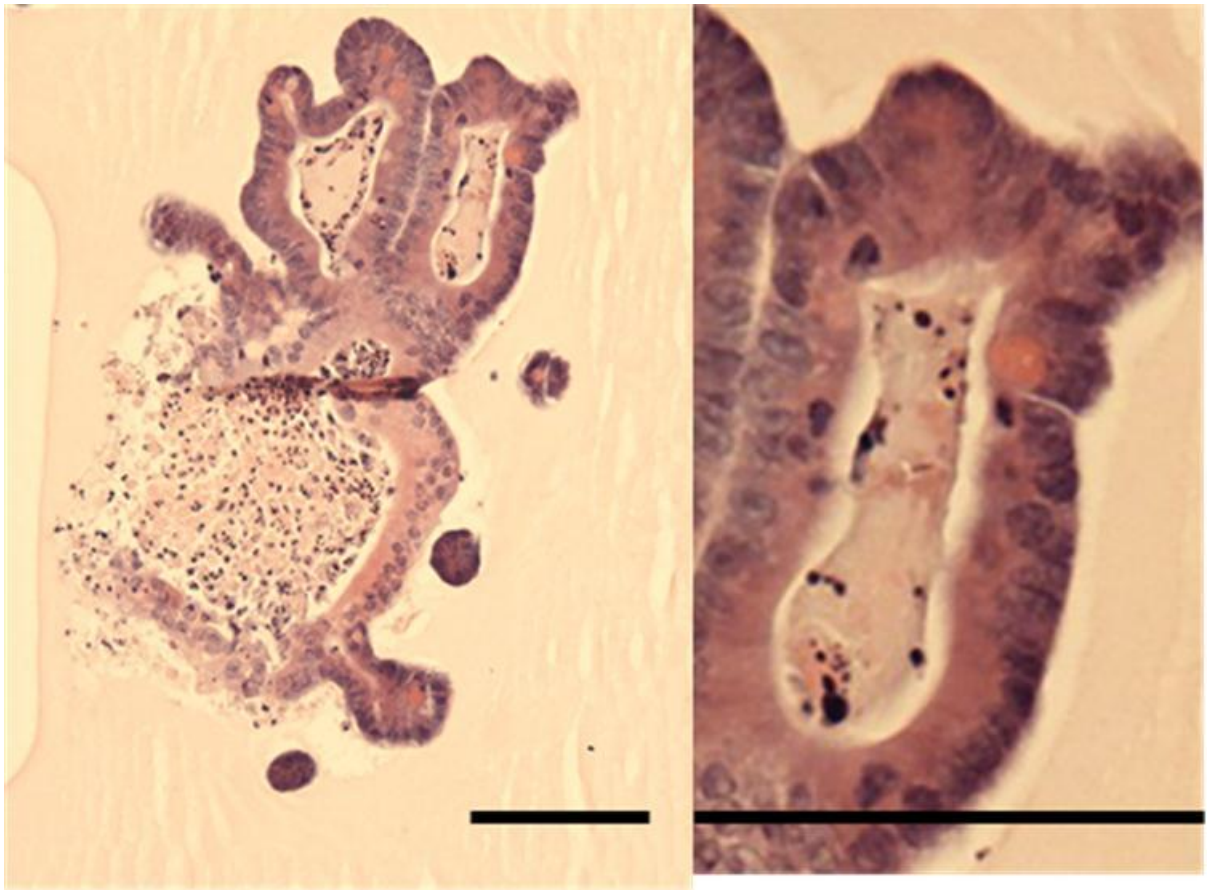

3.28 H&E of a *Cited-1*$^{-/-}$ organoid. *Cited-1*$^{-/-}$ organoids are phenotypically identical to wildtype organoids displaying multiple crypt-like protrusion containing differentiated cell types. Bars represent 100 μm.

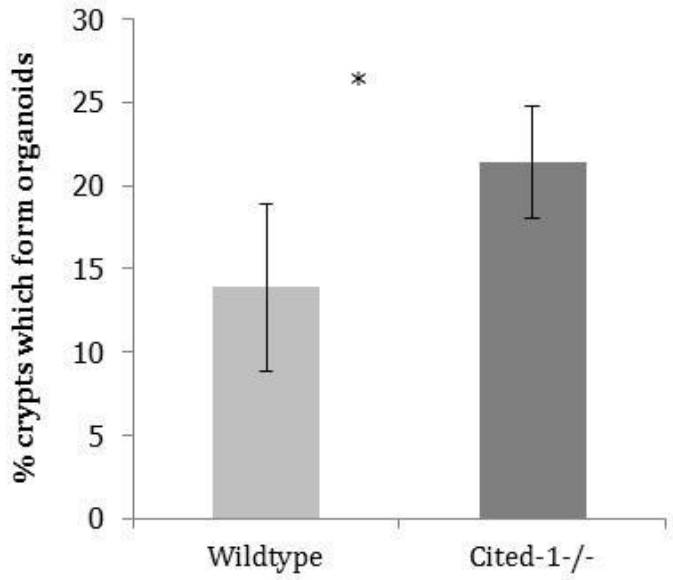

3.29 Organoid formation efficiency of *Cited-1*$^{-/-}$ compared to wildtype crypts. Loss of *Cited-1* resulted in a significant increased organoid formation efficiency, 2-tailed T-test p=0.026. N>4.

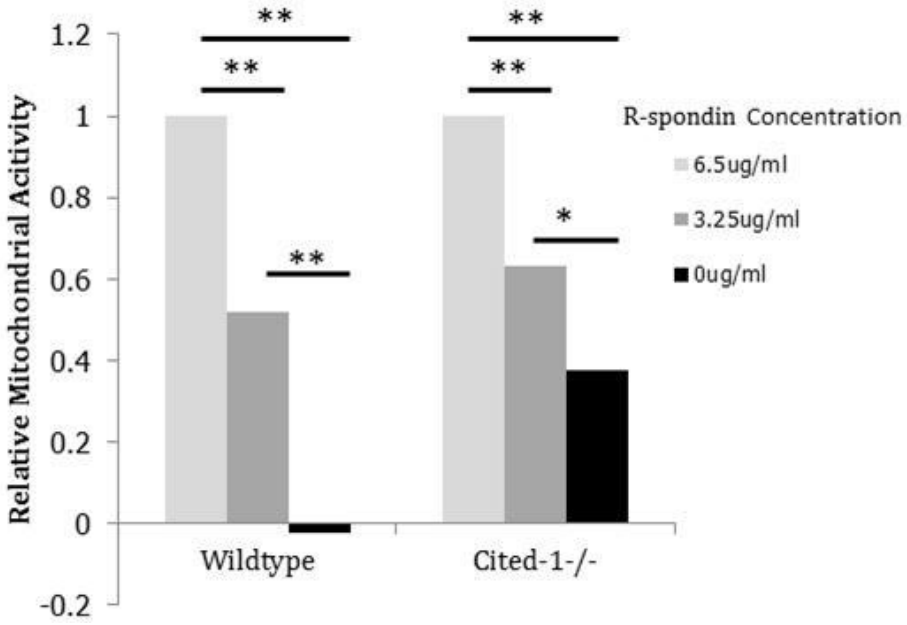

3.30 Relative mitochondrial activity of wildtype and *Cited-1*$^{-/-}$ organoids in differenct Rspo1 concentrations using the PrestoBlue assay. * indicates p<0.05 **indicates p<0.001 using 2-tailed T-test. N=10.

3.16 Discussion

The final protocol for the ISC functionality assay with the CHARM settings used can be found in section 2.12.4 of Materials and Methods.

3.16.1 $Apc^{flox/flox}$ crypts form two distinct types of organoids

The difference between the two types of organoids formed from *Apc* deficient crypts indicates that potentially there are two types of cells in these crypts capable of forming organoids. This could represent the two different ISC populations which, once Wnt-activated as a result of *Apc* loss, can both grow in culture (Yan *et al.* 2012). Alternatively it could represent the difference between organoids grown from Wnt-activated ISCs and those grown from highly Wnt-activated cells of the proliferative compartment of the crypt which are not "true" ISC.

As both types of organoids are observed when *Apc* was recombined *in vitro* as well as *in vivo*, it is difficult to assess why they are different. One potential method would be to sort *Apc* deficient intestinal cells based on expression of $Lgr5^{hi}$ $Ckit^{lo}$ and $Lgr5^{lo}$ $Ckit^{hi}$ using Lgr5 expression as a marker of the ISC population and Ckit expression as a marker of the proliferative zone. This would enable assessment of both the efficiency of organoid formation and the different types of organoid which each cell type can produce. The difficulty of this method is the likelihood of plasticity within the system, especially within *Apc* deficient tissue, whereby stem cells are defined by their microenvironment, and all cells are capable of becoming "stem-like" given exposure to specific conditions. This plasticity means that some cells can be more "stem-like" than others, and measures of "stemness" are difficult to quantify.

It was also noted that $Apc^{flox/flox}$ organoids often contain polarized cells, whereas $Apc^{flox/flox}$ intestinal tissue *in vivo* does not. This is most likely due to the environment *in vitro* whereby sealed cyst-like organoids have a clearly defined "inside" and "outside" with the outside being rich in growth factors and the inside being the area of cell death and so high in apoptotic signals. This clear gradient of signals may give the cells stronger positional cues than occur *in vivo* when a high level of proliferation occurs.

3.16.2 Apc$^{flox/flox}$ organoids contain fewer differentiated cells than wildtype

The observation that *Apc$^{flox/flox}$* organoids contain fewer differentiated cells than wildtype matches the *in vivo* data whereby loss of *Apc* results in an increase in undifferentiated cell types. No enteroendocrine cells were observed in *Apc$^{flox/flox}$* organoids and goblet cells were only observed in *Apc$^{flox/flox}$* organoids which had been cultured in the presence of Rspo1. The organoids containing goblet cells most likely represent organoids derived from crypts in which incomplete recombination of *Apc* had occurred, as these organoids would not survive in the absence of Rspo1.

By contrast, Paneth cells were occasionally observed in *Apc$^{flox/flox}$* organoids which had been cultured in the absence of Rspo1. As these organoids were only cultured for 11 days it is likely that the observed Paneth cells are those from the original crypts which were seeded that survived rather than ones which had differentiated in culture. Paneth cells are long-lived and can survive for up to 20 days (Ayabe *et al.* 2004). This hypothesis is supported by microscopic analysis of fixed *Apc$^{flox/flox}$* organoids which have undergone long-term culture and passage (courtesy of Nydia Panitz) and did not revealed the presence of any Paneth cells.

As previously discussed, the inability of *Apc$^{flox/flox}$* organoids to differentiate indicates that they are not derived from true ISCs, as the definition of an ISC is its ability to produce all the differentiated cell types found within the epithelium. For this reason, despite the utility of comparing wildtype and *Apc$^{flox/flox}$* organoid formation in order to calibrate this assay, the stem cell function assay should only be used to compare formation efficiency of organoids which display a wildtype phenotype with all the differentiated cells present or the formation efficiency of cyst-like structure producing genotypes with that seen in *Apc$^{flox/flox}$* crypts.

3.16.3 Wildtype organoids are more highly proliferative than Apc$^{flox/flox}$ organoids

The interesting and unexpected observation that wildtype organoids express higher levels of the proliferation marker Ki67 and contain more cells in “S”-phase of mitosis (as measured by number of cells which uptake BrDU in a one hour period) indicates that wildtype organoids are proliferating at a greater rate than *Apc$^{flox/flox}$* organoids. This is in direct contrast with *in vivo* data where loss of *Apc* and subsequent Wnt-signalling activation results in a great increase in proliferation (Sansom et al. 2004). This

observation does not fit with the data showing that *Apc*$^{flox/flox}$ organoids grow faster than wildtype. However, as the growth rate data shows, by day 11 (which is when the organoids were fixed) *Apc*$^{flox/flox}$ growth has reached a plateau, whereas wildtype organoids are still growing. This could be due to the lack of organized structure of *Apc*$^{flox/flox}$ organoids, which just form cyst-like sacks of dead matter and toxins. Potentially there is a maximum size the organoids can reach before proliferation is reduced to maintain this size. This is supported by the observation that larger organoids appear to collapse in on themselves by day 12-13 (see Figure 3.7).

The organized structure of wildtype organoids enables them to continue growing despite the large quantity of dead material inside, as a "crypt" can bud further away from the necrotic matter, and often a "leak" of dead matter will form within wildtype organoids with the crypts budding on the opposite side of this "leak". This could explain why proliferation rate of wildtype organoids are so much higher than those seen in *Apc*$^{flox/flox}$ organoids, and could be easily tested by fixing organoids at day 5 when growth rates between genotypes are very different, and assessing proliferation using Ki67 and BrDU. Nearly 100% of wildtype organoid cells are proliferating which indicates that they only represent the proliferative compartment of the intestinal epithelium with the crypt protrusion and there is no compartment of the organoid which represents the non-proliferating villus region.

The observation that loss of *Apc* does not appear to result in an increase in apoptosis (as measured by Caspase 3 expression) *in vitro*, but does *in vivo* (Sansom et al. 2004), could be explained by the presence of laminin within the cultures, which prevents cell anoikis (Sato et al. 2009). The loss of cellular organisation seen *in vivo* as a result of *Apc* loss, may interfere with cell-cell contact and positional cues, thereby resulting in cellular anoikis. An alternative hypothesis is that *in vivo*, mice do not survive loss of *Apc* using *Villin-Cre* for more than 5-6 days and so the increase in apoptosis may be an earlier phenotype. This could again be assessed by fixing organoids at earlier time-points and assessing Caspase 3 expression.

These data not only show the differences between wildtype and *Apc*$^{flox/flox}$ organoids but also highlight that despite the utility of this *in vitro* system to recapitulate aspects of

in vivo work, there are still many areas in which it does not truly represent the situation seen in the mouse intestine.

3.16.4 Development of a functional stem cell assay

By testing this method using *Apc*$^{flox/flox}$ mice as an example of a Wnt activated mutant, we have developed a sound methodology to examine ISC functionality which is capable of determining changes in the ISC population due to aberrations in Wnt signalling. The changes in ISC compartment can be supported by *in situ* hybridisation to determine whether the number of stem cells, or simply their potency, has changed.

There is one major drawback to this technique which is currently being addressed, namely that in order for it to be a true representation of "stemness", the ability of the organoids to self-renew would need to be assessed. At present, this has not been possible due to the inefficiencies of passage. The major difficulty of gaining a readout of the number of organoids which grow after passage is the variability in the passage preparation. In order to passage intestinal organoids, it is necessary to manually disrupt their structures until they are once more single crypts. In published data this is often taken down to single cells using trypsin or similar in order to disassociate the cells, then passed through a 40μm filter to ensure that only single cells are seeded. However, due to the nature of this assay, it is necessary to seed crypts as opposed to single cells. This is due to the inefficiency of organoid growth from unsorted single epithelial cells, as sorting for a specific marker, such as Lgr5, would impose pre-selection for defined parameters of "stemness", and what is required from this assay is a global analysis of ISC functionality within the whole intestinal crypt. Passage involving the breakdown of organoids and re-seeding of crypts as opposed to single cells is routinely done for the long term maintenance of intestinal organoid cultures, but not in a manner whereby the quality of crypt preparation is essential, or the number of single crypts seeded needs to be quantified. When this was attempted, it was found that the quality of the crypt preparation was variable, with many individual crypts, or partial organoids, and other complete organoids which were undisrupted by the passage process.

The problem lies in both the difficulty of extracting a large quantity of organoids from cultures grown in a 96 well plate, and the inability to consistently break these organoids down to a single crypt level. In order to confirm that only single crypts (and not large

chunks of organoids, or whole organoids) have been seeded it is necessary to pass the sample through a 70 μm filter (pre-soaked in PBS + 0.1%BSA), which results in a great reduction in crypt numbers. At present the maximum number of crypts successfully passaged from a culture which was originally seeded with approximately 75,000 crypts, is 400 crypts. This has meant that incorporating a self-renewal assay into this method has as yet been unfeasible.

It must also be taken into consideration that intestinal organoid function and phenotype is not always a direct representation of that seen *in vivo*. For example, Farin *et al*., recently showed that despite the dispensable nature of Wnt3 in the intestinal epithelium *in vivo*, the loss of Wnt3 cannot be supported in intestinal organoids (Farin *et al.* 2012).

Other methods for using the intestinal organoid method to assess the ISC compartment in vivo have previously been suggested, and other laboratories are using the number of crypt-like protrusions as a readout of "stemness", due to the clear difference between wildtype and $Apc^{flox/flox}$ organoids in this characteristic (Ernlund 2011). However, these protrusions arise via crypt fission (Sato et al. 2009), and there is no evidence that crypt fission occurs as a result of an expansion of the ISC compartment. Furthermore, measuring organoid formation efficiency more accurately recapitulates the "gold standard" of stem cell assays used in other tissues, such as the neurosphere or cleared fat pad transplant assay (Deome *et al.* 1959; Reynolds and Weiss 1992), whereby cells capable of forming a differentiated tissue structure *in vitro* are measured as stem cells.

3.16.5 The effect of Cited-1 loss on the ISC compartment

The data presented here showing that loss of *Cited-1* results in an increased organoid forming efficiency indicates the potential utility of this method for gaining an understanding of the effect of subtle deregulations of Wnt on the intestinal stem cell compartment. Although loss of *Cited-1* is not alone sufficient to cause intestinal tumourigenesis, the subtly increased Wnt-signalling levels, as observed by increased nuclear β-catenin, are resulting in an increase in ISCs. Despite this increase in the pool of potential "cells of origin" of colorectal cancer, there is not an increase in tumourigenesis as these cells are not highly Wnt-activated, as determined by their dependency on Rspo1.

These data show that a small expansion of the ISC compartment is not alone sufficient to drive tumourigenesis, as transforming mutations must still occur within these ISCs which result in high levels of nuclear β-catenin.

The increased number of ISCs should theoretically increase the likelihood of tumourigenesis as the number of potential "cells of origin" has increased, however, as spontaneous colorectal tumourigenesis in mice is very rare, the number of mice required in order to see such an effect would be large. Recently, it has been shown that *Cited-1* loss is not sufficient for the initiation of intestinal tumourigenesis (Méniel et al. 2013). Interestingly, despite loss of *Cited-1* resulting in an apparent expansion in the ISC compartment, *Cited-1* loss in a model of Wnt-driven intestinal tumourigenesis, $Apc^{min/+}$ mice, results in a decrease in tumour burden and a significant increase in survival. This is thought to be due to *Cited-1* loss resulting in an increase in Wnt signalling, which when coupled with Wnt-activation due to *Apc* deficiency results in an over activation of this pathway and an associated increase in apoptosis. This is thought to cause Wnt signalling to elevate above tumour-permissive levels, and therefore actually decrease tumourigenesis (Méniel et al. 2013). This indicates the complexity of intestinal tumourigenesis, and shows that if changes within the ISC compartment are playing a role in potential for tumour initiation, then that role may be overridden by alterations in Wnt signalling levels.

3.17 Summary

This is the first time that an assay to determine the functionality of ISCs has been developed and, despite some drawbacks, could prove itself to be an exceptionally useful technique. In order to overcome these drawbacks, the assay should always be used in a combined approach to assess changes to the ISC compartment, in conjunction with qRT-PCR data of ISC marker expression levels and *in situ* hybridisation techniques.

Apc loss results in such a gross alteration in organoid phenotype that comparisons of organoid formation efficiency between organoids of a wildtype phenotype and those of an *Apc* deficient phenotype may be irrelevant. However, it is possible to draw comparisons between genotypes which present a similar organoid phenotype.

3.18 Future Work

Growing organoids from single cells would be arguably led to more accurate quantification of organoids grown. Single cell organoid culture was attempted (with the addition of Wnt3a and the Rho kinase inhibitor Y-27632 to the growth media) however, the organoid formation efficiency was so low (<0.03%) that very few total organoids grew (typically about 1 per animal) leading to very high variability as well as preventing the use of the Rspo1 dependency test. Sato *et al*., were able to grow organoids at a higher efficiency by sorting for the expression of Lgr5 using an Lgr5-GFP transgene (Sato et al. 2010). However, efficiency was still low unless co-cultured with Paneth cells and for the purposes of a stem cell function assay this method would not be viable, as it would involve artificial selection of proposed ISCs prior to seeding. Ideally, sorting cells on the basis of expression of Lgr5 would also enable a cell count of total number of epithelial cells compared to $Lgr5^{hi}$ expressing cells, however, as currently no reliable antibodies exist for Lgr5, this method would rely on the use of the Lgr5-GFP linked transgene (which is also linked to a Cre-recombinase for lineage tracing experiments). One of the main technical issues experienced in using the Lgr5-GFP transgene is that it is expressed in a mosaic manner, meaning that counts between mice cannot be compared.

However Wang *et al*. recently published a method of sorting out single intestinal cells based on a combination of stem cell associated cell surface markers. When single intestinal epithelial $CD44^{+}$ $CD24^{lo}$ $CD166^{+}$ $GRP78^{lo/-}$ $ckit^{+}$ cells are FACs sorted they are reported to grow into organoids in culture at an efficiency of more 20% (Wang *et al.* 2013b). This is a vast improvement on what was published from $Lgr5^{hi}$ sorted cells and could represent a much purer population of ISCs. If this is shown to be correct, and that $CD44^{+}$ $CD24^{lo}$ $CD166^{+}$ $GRP78^{lo/-}$ $ckit^{+}$ cells are in fact representative of the ISC population, then using FAC sorting to count the percentage of epithelial cells which meet these expression requirements could also prove useful as a readout of changes in the ISC compartment due to genetic mutations. This method would be cheaper than assessing organoid formation efficiency but would miss out on the functional aspect of assessing the ISC compartment as it is a method based purely on expression of ISC

markers, as opposed to interrogation capacity of intestinal epithelium cells to function as ISCs.

In order to develop the organoid formation efficiency assay into a more accurate readout of ISC capability, self-renewal must be assessed. One of the attributes of a stem cell is its ability to self-renew, and so assessing organoid formation efficiency over a series of passage events would provide a more comprehensive ISC function assay.

4 The roles of Pml in the context of Apc and Pten dependent colorectal tumourigenesis

4.1 Introduction

APC is an important negative regulator of the Wnt-signalling pathway, and mutations of this gene are known to initiate colorectal tumourigenesis (Lamlum *et al.* 2000). However, tumourigenesis is a multistep process in which many other gene mutations and mis-regulations play significant roles. One pathway which is known to be important in the progression of tumour development is the PI3K pathway. Activation of the PI3K pathway results in activation of mTOR as well as inhibition of the pro-apoptotic factor BAD (She *et al.* 2005) and the Wnt regulator GSK3, all of which cause increased cell growth and survival (see Section 1.4.1.1). Understandably, tumour cells containing mutations which result in constitutive activation of PI3K have a selective advantage within a tumour and so may drive clonality within that tumour. More than 40% of human colorectal cancers contain mutations which in constitutive activation of this pathway.

The inhibition of GSK3 via activation of the PI3K pathway highlights the potential of crosstalk between the Wnt and the PI3K signalling pathways, as GSK3 forms part of the β-catenin destruction complex which is an integral regulator of Wnt-signalling (Voskas *et al*. 2010).

4.1.1 PTEN in tumourigenesis

The important role of PTEN as a tumour suppressor is well known through its function as a negative regulator of the PI3K pathway. PTEN converts PIP_3 into PIP_2, thereby preventing the recruitment of AKT to the membrane where it is activated by phosphorylation. In this way PTEN negatively regulates the amount of the oncogenic factor phosphorylated AKT (pAKT) available within the cell, see Section 1.1.1.1, (Cully *et al.* 2006).

Germ line *PTEN* mutations are known to play a role in a number of autosomal dominant syndromes such as Cowden's syndrome, which predisposes patients to the development of multiple hamartoma growths (Liaw *et al.* 1997). *PTEN* mutations have also been

identified in many sporadic tumour types such as glioblastoma (Wang *et al.* 1997) and prostate cancer (Cairns *et al.* 1997). Interestingly, loss of an allelic region close to that of *PTEN* has been associated with up to 30% of human colorectal cancers (Frayling *et al.* 1997), although the frequency of *PTEN* mutations observed in sporadic colorectal cancers has been controversial. It has previously been shown that *PTEN* mutations are relatively common, with 19.5% of microsatellite stable human sporadic colorectal cancers displaying a *PTEN* mutation, (Nassif *et al.* 2004) whilst hypermethylation and subsequent inactivation of PTEN is associated with 19.1% of microsatellite instability-high sporadic colorectal tumours (Goel *et al.* 2004). However, there is contradictory evidence which shows that this hypermethylation may not be associated with a decrease in expression, as it refers to the methylation status of a *PTEN* pseudo gene, and not *PTEN* itself (Zysman *et al.* 2002).

Nassif *et al*. showed that reduced *PTEN* expression was associated with a later clinical stage in human colorectal tumours, indicating that *PTEN* loss may not be an initiating mutation in sporadic colorectal tumourigenesis, but a driver of clonality within the tumour (Nassif *et al*. 2004). This theory was supported through the use of Cre-Lox technology to cause homozygous disruption of *Pten* alleles in a specific tissue, as homozygous knockout of the gene is embryonic lethal (Cristofano *et al.* 1998). Homozygous loss of *Pten* within mouse intestinal epithelium had no effect on the homeostasis of normal mouse intestine, but did cause accelerated tumourigenesis when coupled with deficiency of *Apc,* showing the importance of the PI3K pathway as a driver of tumour progression (Marsh et al. 2008). Interestingly, He *et al.* found that *Pten* deletion from the ISC compartment of the intestinal epithelium was sufficient to initiate tumourigenesis (He *et al.* 2007).

4.1.2 PML in tumourigenesis

The oncogenic effect of *Pten* loss is reportedly exacerbated by the loss of another tumour suppressor gene; *Pml* (promyelocytic leukaemia protein) (Trotman *et al.* 2006). In this study Trotman *et al.* demonstrated that in a mouse model with heterozygous deletion of *Pten*, *Pml* deficiency resulted in a higher tumour burden, earlier onset and notably reduced survival due to the formation of colorectal and prostate tumours (Trotman et al. 2006).

PML was originally identified as a potential gene of interest in tumourigenesis due to its association with acute promyelocytic leukaemia (APL) where it is disrupted in 99% of all cases (Goddard *et al.* 1991). For many years the treatment of this disease was retinoic acid (RA), arsenic trioxide or a combination of the two, which seemed to cure most APL patients. It is now known that the mechanism of this cure is through targeting of the PML/RARα (retinoic acid receptor alpha) fusion protein (Chen 2010).

The protein encoded by *PML* localizes to the subnuclear structure of the PML-nuclear body (PML-NB), which interacts with a vast number of proteins *ex vivo* but only a small number of these interactions are fully understood. Using microarray techniques, Gurrieri *et al.* showed that levels of PML protein were reduced or lost in 31% of colon adenocarcinomas, and this was associated with reduced number of PML-NBs (Gurrieri *et al.* 2004).

The function of these PML-NBs is largely unknown although it has been shown to be required for the nuclear localization of PTEN (Song *et al.* 2008), as well as being involved in the inhibition of nuclear function of pAKT by actively recruiting pAKT and the AKT phosphatise, PP2a (Trotman *et al.* 2006). It is important to note that PML also plays a crucial role within apoptosis, modulating calcium release at the endoplasmic reticulum (Giorgi *et al.* 2010) and that lack of *Pml* can protect cell lines and mice from apoptosis resulting from a range of apoptotic stimuli (Bernardi *et al.* 2008). The link between *PML* and apoptosis may be an important factor in its role as a tumour suppressor.

PML has also been linked to a role in cellular senescence, and overexpression of *PML* increases levels of cellular senescence through a p53 dependent pathway (Pearson *et al.* 2000). As cell senescence is an important mechanism for minimising the effects of DNA damage, it could therefore contribute to the role of *PML* as a tumour suppressor (Collado *et al.* 2007).

4.1.3 PTEN, PML and stem cells

PTEN and *PML* have been described as playing some role in the maintenance of adult stem cell compartments, and as such their role within intestinal tumourigenesis could be of great importance. The role of *PTEN* within the maintenance of the ISC

compartment has been explored by He *et al*. who found that knocking out *Pten* in the ISC compartment initiated intestinal polyposis and also resulted in reduced levels of nuclear ß-catenin, an important regulator in ISC self-renewal, within the stem cells (He et al. 2007). *Pml* on the other hand has been shown to inhibit mTOR, which is an important driver of the ISC regulator STAT3 (Bernardi *et al.* 2006; Matthews *et al.* 2011). Bernardi *et al*. showed that inhibition of mTOR by Pml occurred under hypoxic conditions, and not only could this affect the ISC compartment, but could also play a role by inhibiting angiogenesis, a process which is essential for the growth of solid tumours.

Interestingly, PML has more recently been shown to play a role in the maintenance of "stemness" of hematopoietic stem cells (HSCs) and leukaemia-initiating cells (Ito *et al.* 2008; Ito and Ito 2013; Zhou and Bao 2013). In this case, PML deletion results in inhibition of the PPAR-δ and fatty acid oxidation (FAO) pathways which cause an increase in symmetric division of HSCs (Ito *et al.* 2012). The role of PML in the regulation of the PPAR-δ-FAO pathway has also been shown to play an important part in supporting cell survival in breast cancer cells, so also has a relevance to solid tumours (Carracedo *et al.* 2012).

Pml and *Pten* have previously been shown to interact in their suppression of the PI3K pathway (Trotman *et al*. 2006). Here the role of *Pml* and its synergy with *Pten* in Wnt-dependent tumourigenesis has been investigated, with a view to establishing the nature of the relationship between these two genes. As these genes have both been implicated as regulators of stem cell compartments, their role in maintenance of the ISC compartment will be assessed in the context of aberrant Wnt-signalling.

4.2 Results

4.2.1 Pml deficiency does not affect survival, tumour burden or tumour grade, but results in increased intussusception in $Apc^{flox/+}$ mice

Villin $CreER^T$ positive mice carrying one floxed allele of *Apc* (Shibata et al. 1997) with or without an additional homozygous constitutive knockout of *Pml* (created and kindly gifted to us by Pier Pandolfi) were induced with tamoxifen I.P. injection at 8-10 weeks of age and aged for survival analysis. At signs of loss of condition, mice were culled and the size, location and number of intestinal and colon tumours were recorded.

Loss of *Pml* resulted in no change in either survival ($Apc^{flox/+}$=345±123, $Apc^{flox/+}Pml^{-/-}$ =295±21) or tumour burden (Figure 4.1). Interestingly, 3/7 of the $Apc^{flox/flox}$ $Pml^{-/-}$ mice displayed gross intussusception upon dissection, whereas none of the 9 $Apc^{flox/flox}$ mice displayed this phenotype. This change in frequency of intussusceptions was found to be significant when tested using Chi-squared[1] (Chi-squared value=6.7, the 0.05 significance chi value for n=1 being 3.8). Intussusception has previously been associated with *Pten* deficiency in Apc^{min} mice and was reported to be coupled with the presence of particularly large tumours (Shao *et al.* 2007). Although all 3 cases of intussusception were associated with the presence of a large tumour at the start point of the intestinal involution, the tumours were not the largest found in the small intestine (maximum size 7 mm x 6 mm).

As *Pml* deficiency has no effect on overall tumour burden, the level of progression was assessed using a tumour grading system. Tumours were divided into 5 categories; grade 1: single crypt lesions, grade 2: microadenomas, grade 3: adenomas, grade 4: adenocarcinoma with submucosal invasion and grade 5: adenocarcinomas with smooth muscle invasion (see Section 2.8.4). Loss of *Pml* had no significant effect on the level of tumour progression (Figure 4.2).

[1] The significance of this change was assessed using Chi-squared, however, Chi-squared cannot be performed if any of the categories (i.e. intussusceptions or no intussusception) of the expected cohort (which in this case was the $Apc^{flox/+}$ mice) were equal to 0. As no cases of intussusception were observed in this cohort, the $Apc^{flox/+}$ $Pml^{-/-}$ cohort had to be used as the basis for the expected results. So in effect, the frequency of cases of intussusception in $Apc^{flox/+}$ mice was compared to that seen in $Apc^{flox/+}$ $Pml^{-/-}$ mice. A more accurate readout of significance could be obtained with a higher N-number, which would enable the use of higher powered statistical tests such as a Mann-Whitney using a binomial distribution function.

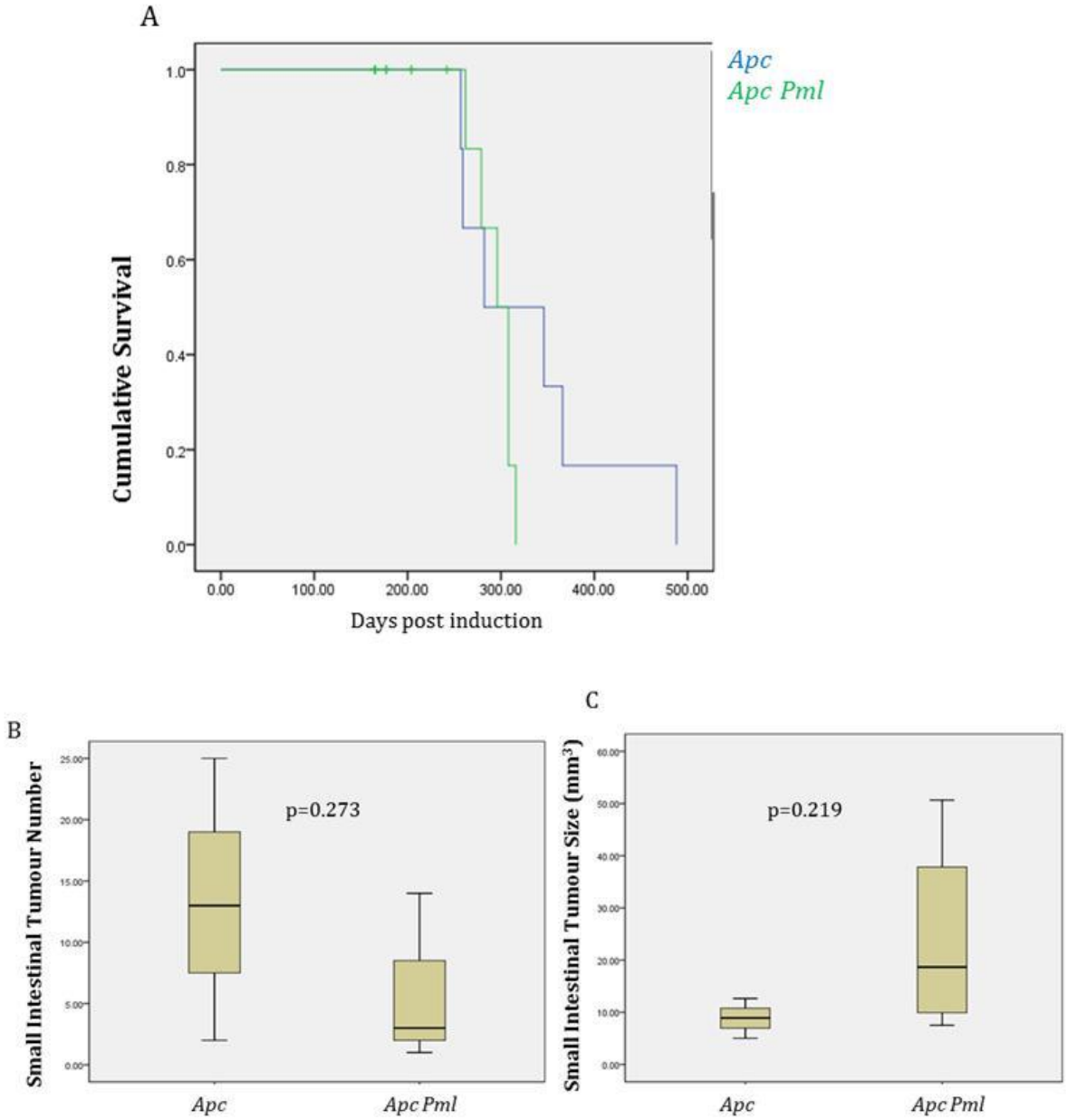

4.1 **A** Survival Plot of *Apc*$^{flox/+}$ mice with or without *Pml* deletion, cross represents mouse still living. No significant difference in survival between the two cohorts was observed (Wilcoxon p=0.748); **B** Comparison of tumour number in *Apc*$^{flox/+}$ mice with *Apc*$^{flox/+}$ *Pml*$^{-/-}$ mice, there was no significant difference in tumour number between the two cohorts (2-tailed T-Test p=0.273); **C** Comparison of average tumour size in *Apc*$^{flox/+}$ mice with *Apc*$^{flox/+}$ *Pml*$^{-/-}$ mice, there was no significant difference in tumour number between the 2 cohorts (2-tailed T-test p=0.251). N>5.

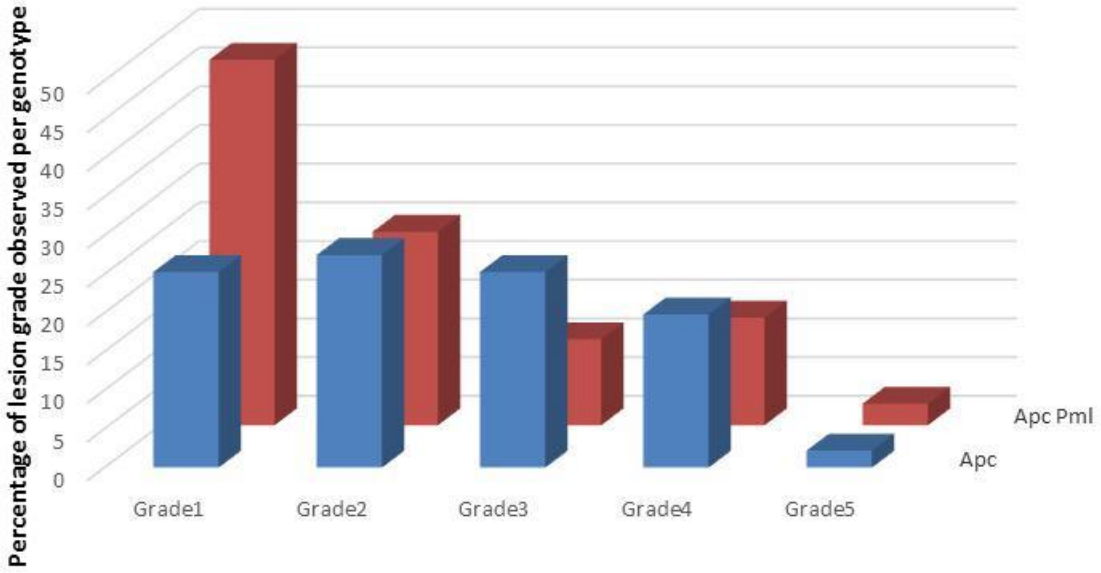

4.2 Graphical representation of the proportion of each lesion type found per genetic cohort. N>5. Chi-squared test showed no significant difference in proportion of tumour grade between the two cohorts.

4.2.1.1 Pml loss has no effect on the survival of Apc$^{flox/flox}$ mice

As no role was found for *Pml* as a tumour suppressor in a long term model of Wnt-dependent tumourigenesis, the potential role of *Pml* as a regulator of PI3K was interrogated using a short term model of early tumourigenesis, the *Apc$^{flox/flox}$* mouse. After induction of *Apc* loss from the intestinal epithelium using tamoxifen injection, the mice were monitored closely (twice daily) for signs of loss of condition. At signs of ill health the animals were culled and the survival time recorded. Additional deficiency of *Pml* resulted in no change in mean survival time of *Apc$^{flox/flox}$* mice (*Apc$^{flox/flox}$*=4.6±0.7, *Apc$^{flox/flox}$ Pml$^{-/-}$*=4.6±0.4) *(*Figure 4.3).

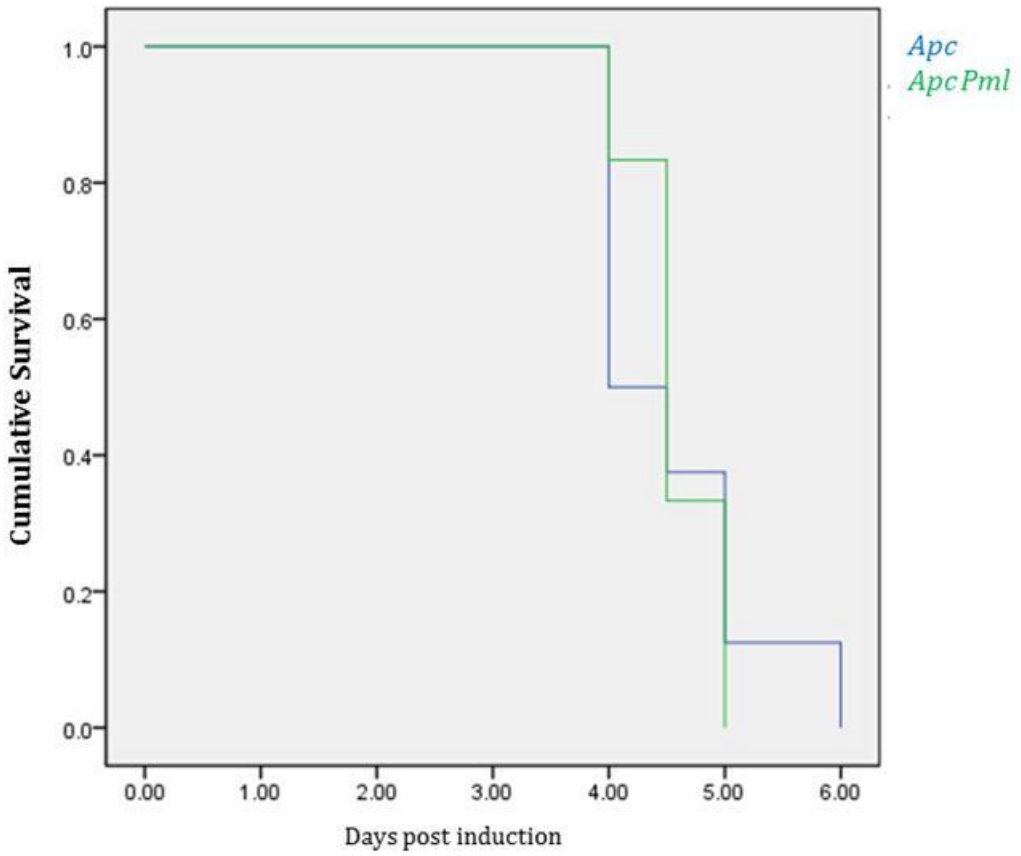

4.3 Cumulative survivals of *Apc$^{flox/flox}$* and *Apc$^{flox/flox}$ Pml$^{-/-}$* mice after administration of tamoxifen. There was no significant difference in mean survival times between the two cohorts (Wilcoxon p=0.639). N>5.

4.2.2 Pml deficiency does not alter the phenotype of Apc$^{flox/flox}$ mice

Mice were induced with tamoxifen on day 0 and injected with BrdU on day3, they were then culled 2 hours later to analyse the short term effect of *Pml* deletion on the *Apc$^{flox/flox}$* phenotype. There was no obvious phenotypic difference between the intestinal compartments of *Apc$^{flox/flox}$* and *Apc$^{flox/flox}$ Pml$^{-/-}$* mice (Figure 4.4).

The number of cells within the zone of aberrant intestinal epithelial cells was determined by counting cells in a single line from the base of the crypt to the top of the zone of aberrant cells (as defined by larger, darker, unpolarized and disordered cells). There was no difference in the number of aberrant cells due to additional loss of *Pml* (*Apc$^{flox/flox}$*= 45.8±5.3, *Apc$^{flox/flox}$Pml$^{-/-}$*= 49±3.4) (Figure 4.5).

Because subtle changes in intestinal homeostasis can be identified by alterations in the numbers and distributions of differentiated cell types, paraffin sections of intestine taken from *Apc$^{flox/flox}$* and *Apc$^{flox/flox}$ Pml$^{-/-}$* mice were stained for markers of differentiated cells, and the numbers of these cell types counted. No difference in the number of goblet cells as marked by staining of mucins by alcian blue was observed (*Apc$^{flox/flox}$*= 7.2±1.1, *Apc$^{flox/flox}$Pml$^{-/-}$*= 8.1±3.1) (Figure 4.6), nor the number of Paneth cells as detected by lysozyme IHC (*Apc$^{flox/flox}$*= 1.4±0.3, *Apc$^{flox/flox}$Pml$^{-/-}$*= 1.4±0.1). Loss of *Pml* did result in a trend for an increased number of enteroendocrine cells as detected by Grimelius staining (*Apc$^{flox/flox}$*= 0.13±0.05, *Apc$^{flox/flox}$Pml$^{-/-}$*= 0.18±0.03), however, this was not significant at N=4 (Figure 4.8).

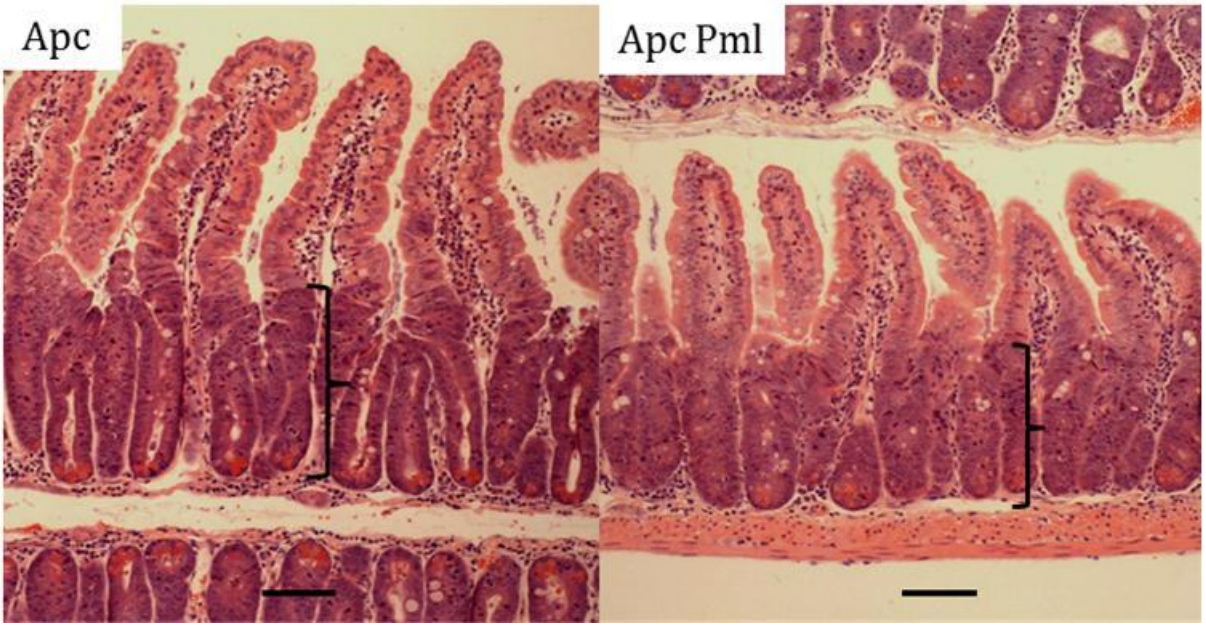

4.4 H&E Stain of *Apc*$^{flox/flox}$ and *Apc*$^{flox/flox}$ *Pml*$^{-/-}$ mouse intestine day 3 post induction with tamoxifen. The region of aberrant proliferation is indicated by the black brackets. There was no gross morphological difference between the two genotypes. Black bars represent 100 µm.

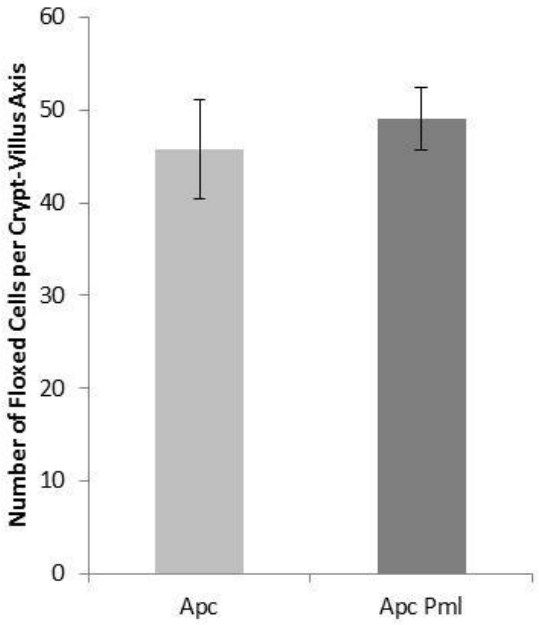

4.5 Counts of the number of cells in the region of aberrant proliferation per crypt-villus axis in *Apc*$^{flox/flox}$ and *Apc*$^{flox/flox}$ *Pml*$^{-/-}$ mice. There was no significant difference in number of aberrant cells between the two genotypes 2-Tailed T-test p=0.406, N=4. Error bars represent standard deviation.

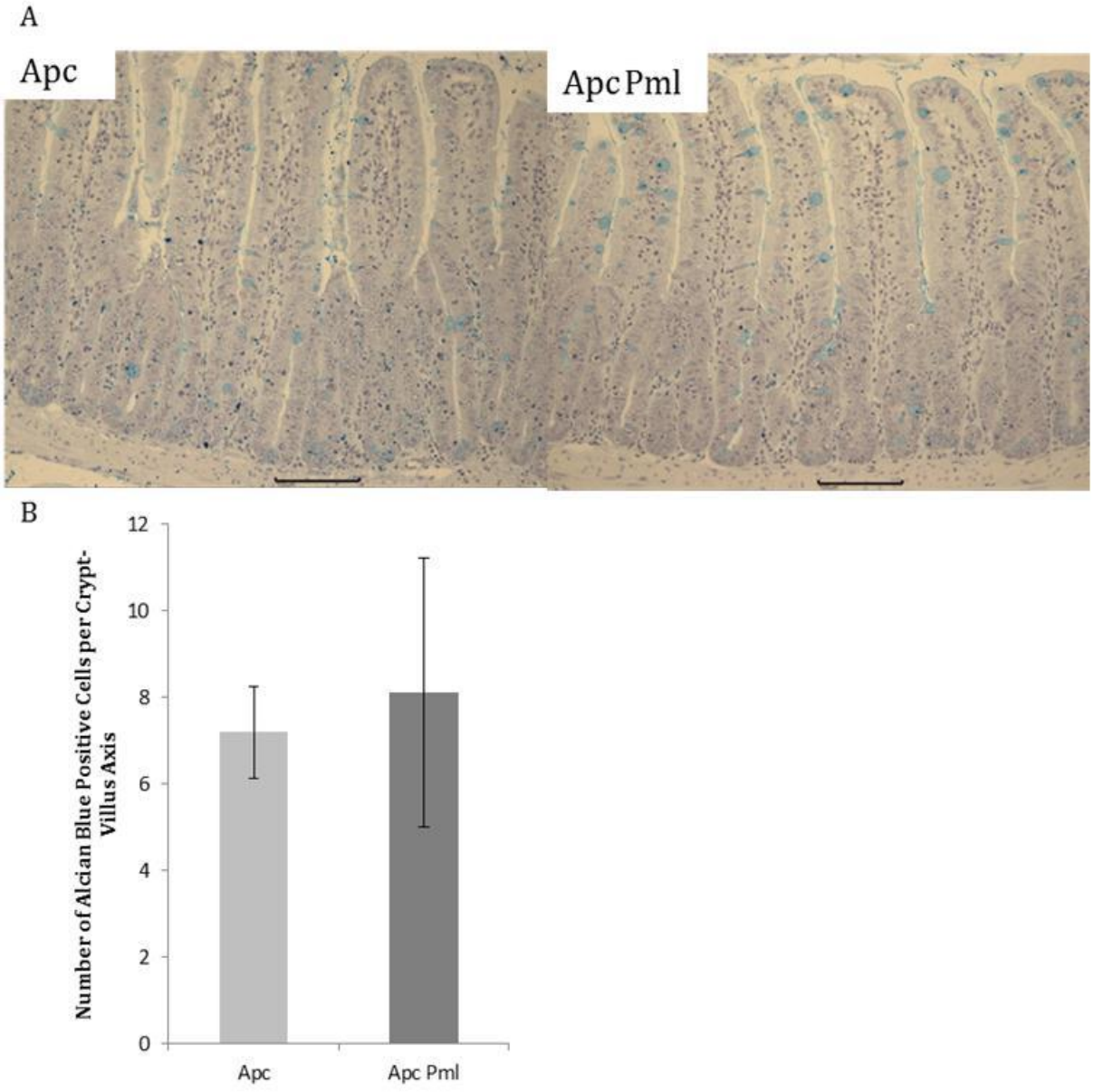

4.6 **A** Alcian Blue IHC of *Apc*$^{flox/flox}$ and *Apc*$^{flox/flox}$ *Pml*$^{-/-}$ intestine. Black bars represent 100 μm; **B** Counts of the number of alcian blue positive cells per crypt-villus axis in *Apc*$^{flox/flox}$ and *Apc*$^{flox/flox}$ *Pml*$^{-/-}$ mice. There was no significant difference in number of goblet cells between the two genotypes, 2-Tailed T-test p=0.28, N=4. Error bars represent standard deviation.

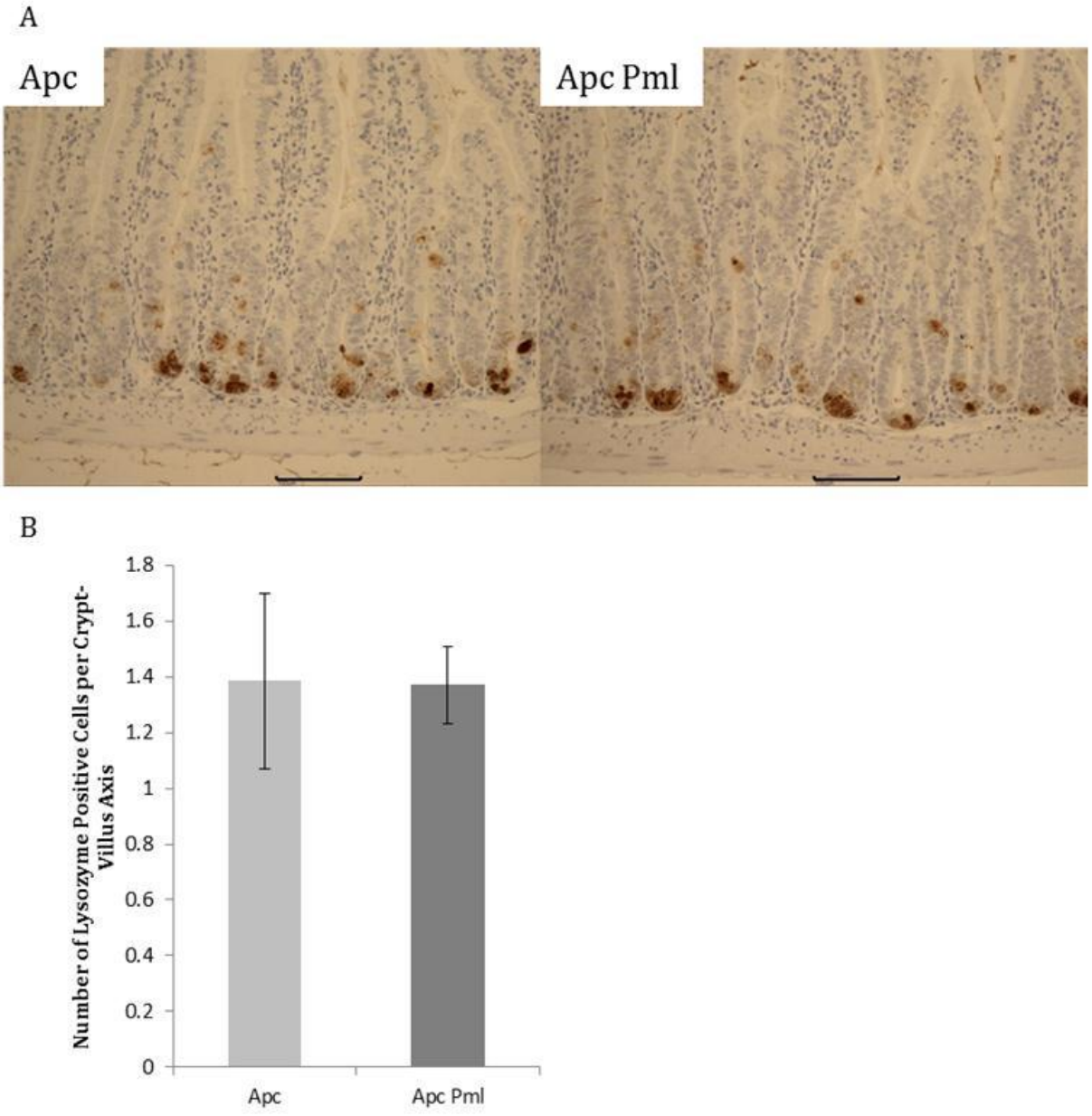

4.7 **A** Paneth cell IHC of *Apc*$^{flox/flox}$ and *Apc*$^{flox/flox}$ *Pml*$^{-/-}$ intestine, brown stained cells represent Paneth cells. Black bars represent 100 µm; **B** Counts of the number of brown cells per crypt-villus axis in *Apc*$^{flox/flox}$ and *Apc*$^{flox/flox}$ *Pml*$^{-/-}$ mice. There was no significant difference in number of Paneth cells between the two genotypes, 2-Tailed T-test p=0.28, N=4. Error bars represent standard deviation.

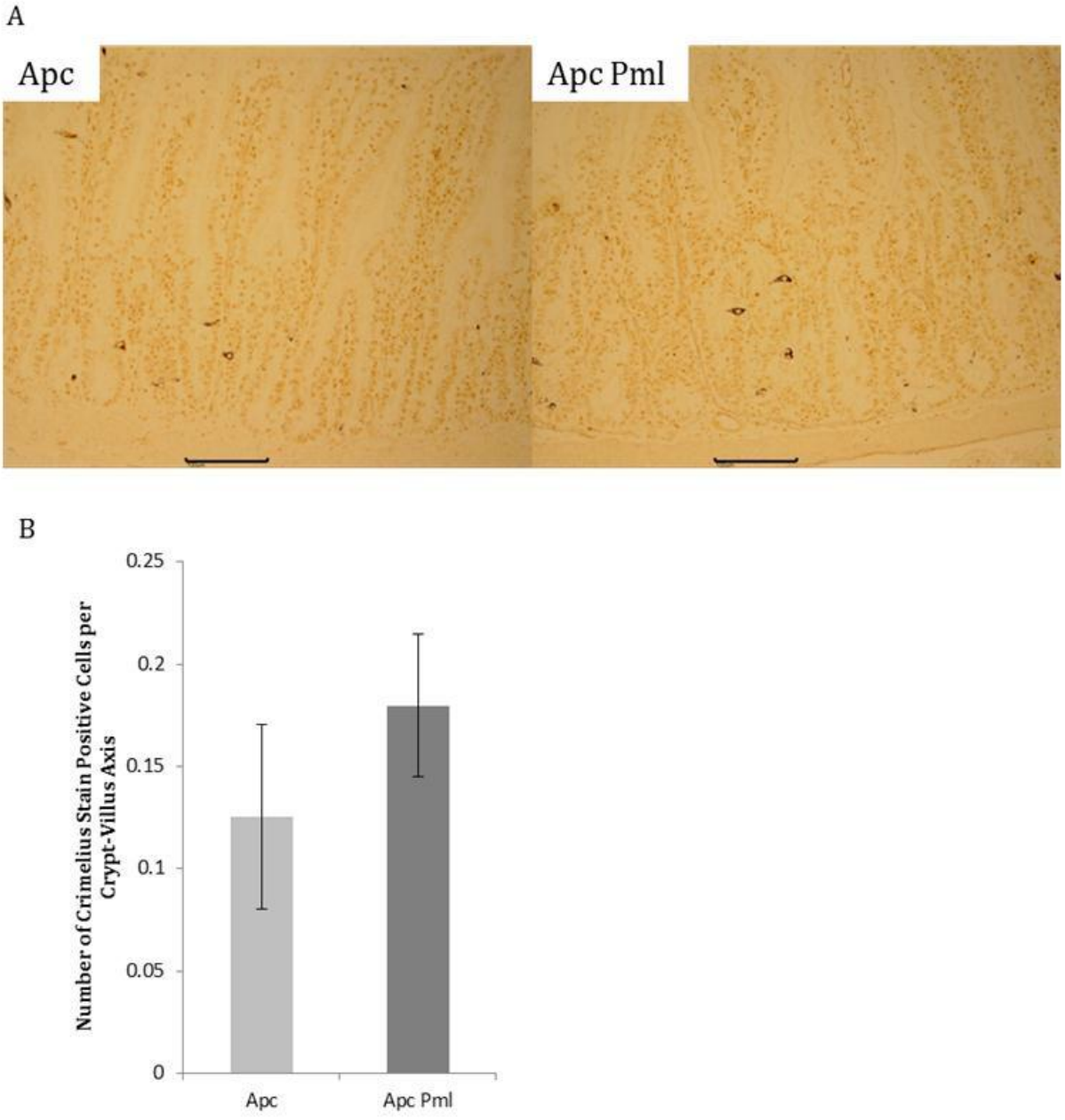

4.8 **A** Grimelius stain of *Apc*$^{flox/flox}$ and *Apc*$^{flox/flox}$ *Pml*$^{-/-}$ intestine, black stained cells represent enteroendocrine cells. Black bars represent 100 µm; **B** Counts of the number of enteroendocrine cells per crypt-villus axis in *Apc*$^{flox/flox}$ and *Apc*$^{flox/flox}$ *Pml*$^{-/-}$ mice. There was no significant difference in number of enteroendocrine cells between the two genotypes, 2-Tailed T-test p=0.105, N=4. Error bars represent standard deviation.

4.1.1.1 *Pml* loss results in no effect on apoptosis in $Apc^{flox/flox}$ intestinal epithelium

Despite the reported role of *Pml* in protecting cells from apoptosis (Bernardi *et al*. 2008; Giorgi *et al.* 2010), *Pml* loss did not result in an increase in number or location of apoptotic bodies in $Apc^{flox/flox}$ mice ($Apc^{flox/flox}$ 0.03±0.01, $Apc^{flox/flox}$ $Pml^{-/-}$ 0.03±0.002), results were normalised for the number of cells within the aberrant region. This was confirmed using a Caspase 3 IHC and counting positively stained cells ($Apc^{flox/flox}$ 0.61±0.1, $Apc^{flox/flox}$ $Pml^{-/-}$ 0.67±0.03) (Figure 4.9).

4.1.1.2 *Pml* loss results in increased mitosis in $Apc^{flox/flox}$ intestinal epithelium

Counting the number and location of mitotic bodies revealed no significant change in number of mitotic bodies as a result of *Pml* loss in $Apc^{flox/flox}$ intestine ($Apc^{flox/flox}$ 2.4±0.01, $Apc^{flox/flox}$ $Pml^{-/-}$2.5±0.8) (Figure 4.10). However, IHC for the presence of incorporated BrDU after a 2 hour exposure to BrDU prior to mouse sacrifice revealed a significant increase in BrDU uptake due to additional *Pml* loss ($Apc^{flox/flox}$ 11.6±1.6, $Apc^{flox/flox}$ $Pml^{-/-}$ 20.7±2.8) (Figure 4.10). This indicates a higher number of cells at "S" phase of mitosis due to *Pml* loss. IHC for the more generic marker of proliferation, Ki67, was conducted in order to confirm this finding. The Ki67 IHC corroborated the observation that loss of *Pml* resulted in an increased level of proliferation ($Apc^{flox/flox}$ 22.8±3.1, $Apc^{flox/flox}$ $Pml^{-/-}$ 28.8±1.5. 2-tailed T-test p= 0.029), data not shown.

4.2.3 *Pml* loss does not activate the PI3K pathway in $Apc^{flox/flox}$ intestinal epithelium

As *Pml* has been reported to play a role as a negative regulator of the PI3K pathway, protein was extracted from the intestinal epithelium of mice from the two genotypes, and analysed for changes in levels of phosphorylated-AKT (pAKT) compared to total-AKT (tAKT) using western blotting analysis. As pAKT is the downstream effector of the PI3K pathway, levels can be used as a direct readout of PI3K activity. Western blotting revealed no evidence of pAKT in either $Apc^{flox/flox}$ or $Apc^{flox/flox}$ $Pml^{-/-}$ mice, and no change in the levels of tAKT. This indicates that in the context of *Apc* deletion, *Pml* does not play a role in the regulation of this pathway (Figure 4.11). IHC for pAKT was performed and supported the evidence from western blotting that loss of *Pml* does not result in an increase in pAKT (Figure 4.11).

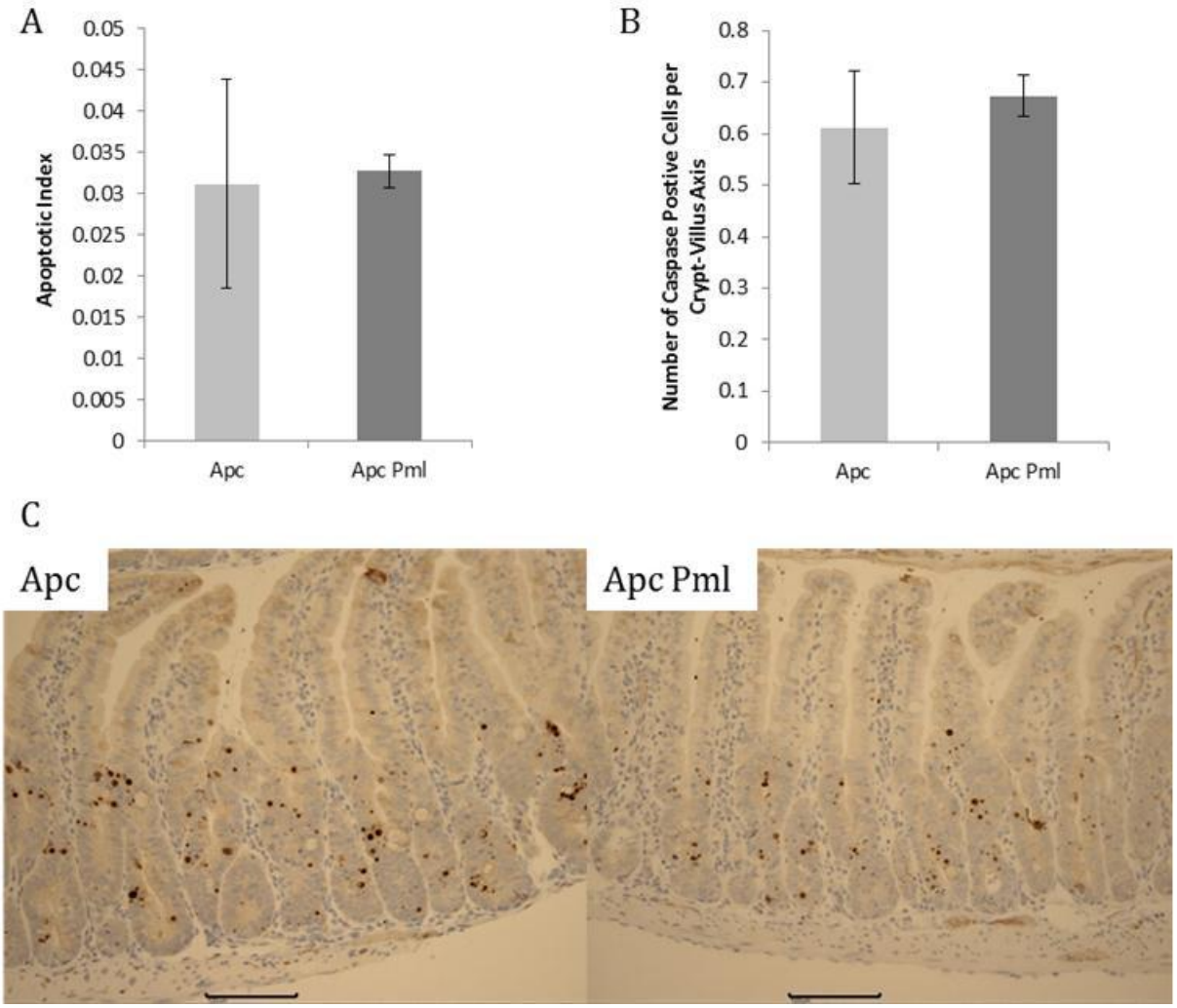

4.9 Comparison of levels of apoptosis in *Apc*$^{flox/flox}$ and *Apc*$^{flox/flox}$ *Pml*$^{-/-}$ mice. **A** Apoptotic Index as measured by number of apoptotic bodies per crypt-villus axis and normalised for the number of cells in the region aberrant proliferation. There was no significant difference between the two genotypes, 2-tailed T test p=0.842, N=4; **B** Number of Caspase positive cells as counted from Caspase IHC. There was no significant difference between the two genotypes, 2-tailed T test p=0.411, N=4; **C** Caspase 3 IHC on *Apc*$^{flox/flox}$ and *Apc*$^{flox/flox}$ *Pml*$^{-/-}$ intestine. Brown cells represent Caspase 3 positive cells. Black bars represent 100 μm.

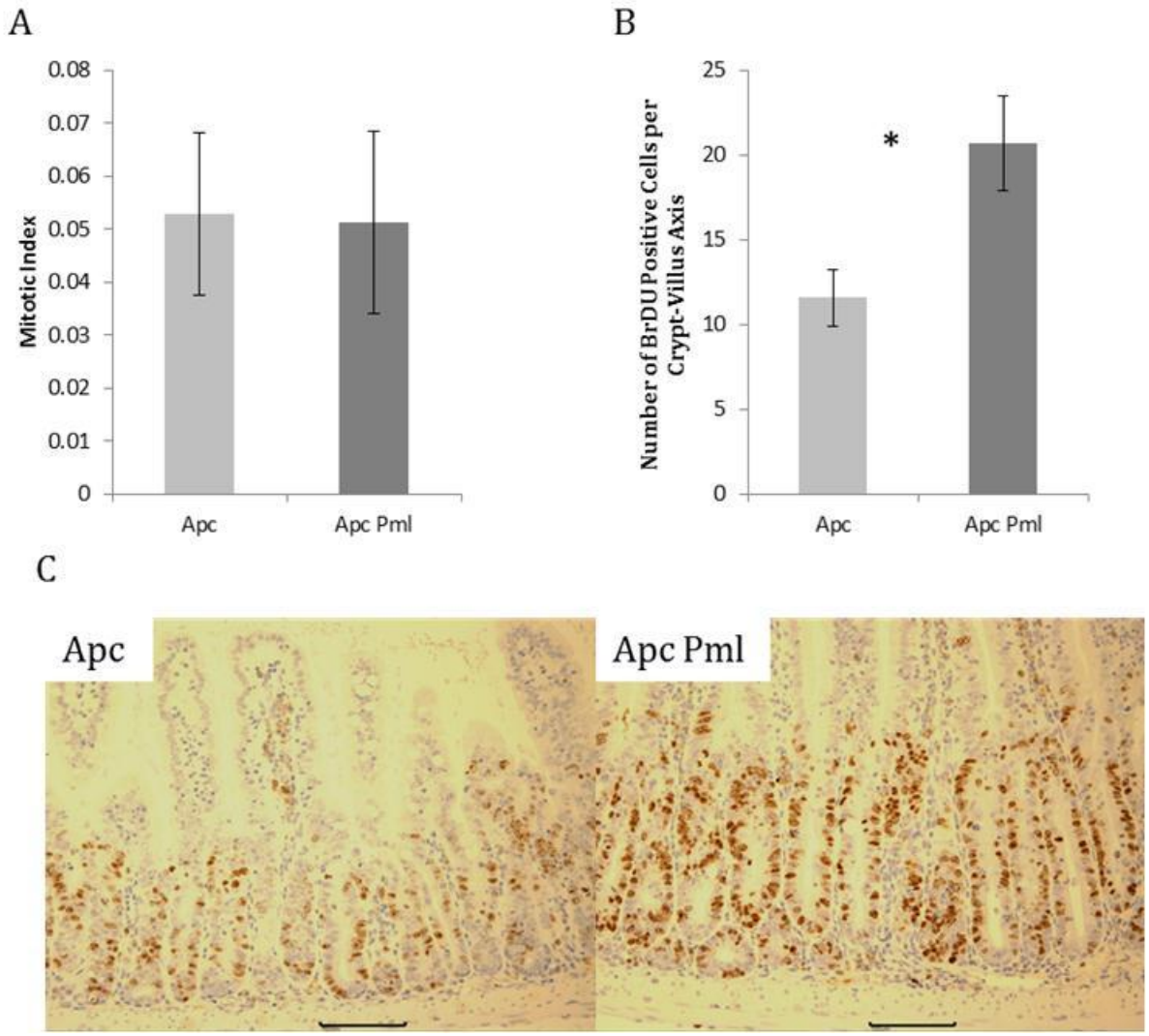

4.10 Comparison of levels of mitosis in *Apc*$^{flox/flox}$ and *Apc*$^{flox/flox}$ *Pml*$^{-/-}$ mice. **A** Mitotic Index, as measured by number of mitotic bodies per crypt-villus axis and normalised for the number of cells in the region aberrant proliferation. There was no significant difference between the two genotypes, 2-tailed T test p=0.789, N=4; **B** Number of BrDU positive cells as counted from BrDU IHC after a 2 hour BrDU exposure. Pml loss led to a significant increase in BrDU uptake 2-tailed T test p=0.001, N=4; **C** BrDU IHC on *Apc*$^{flox/flox}$ and *Apc*$^{flox/flox}$ *Pml*$^{-/-}$ intestine. Brown cells represent BrDU positive cells. Black bars represent 100 μm.

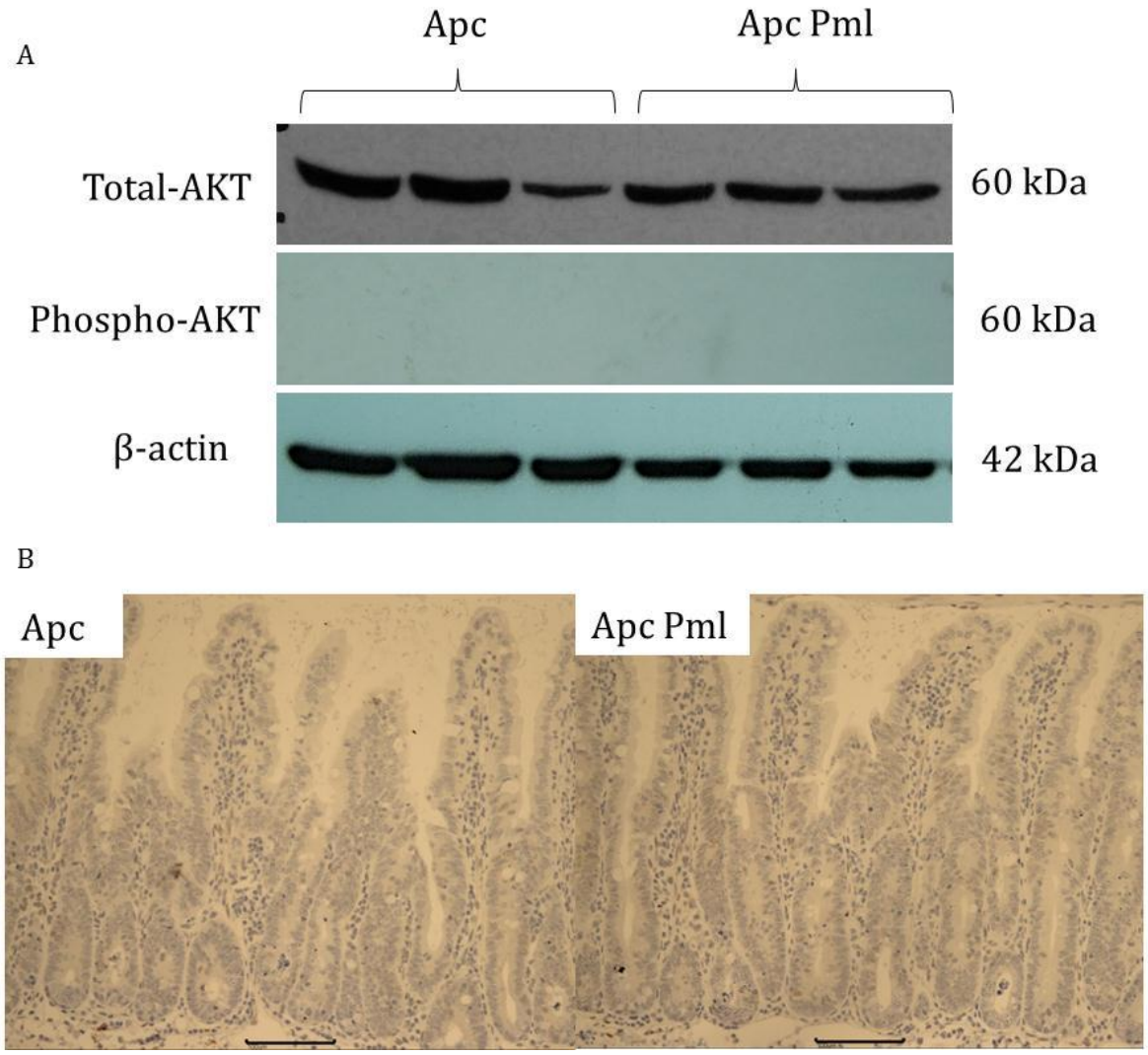

4.11 Phospho-AKT levels as a measure of activation of the PI3K pathway due to additional deletion of *Pml* form $Apc^{flox/flox}$ mice. **A** Western blot analysis shows that total levels of Akt protein within the protein extracted from intestinal epithelium of the two genotypes was high, but no phospho-Akt was detected; **B** IHC for phospho-Akt confirmed that the PI3K pathway was not activated, as phospho-Akt was not observed. Black bars represent 100 μm.

4.2.4 *Pml* loss results in a significant increase in expression of ISC markers in *Apc*$^{flox/flox}$ mice

Given that *Pml* is cited as a tumour suppressor, and that mis-regulation of the ISC compartment may play an important role in tumourigenesis, the ISC compartments of *Apc*$^{flox/flox}$ and *Apc*$^{flox/flox}$ *Pml*$^{-/-}$ mice were analysed.

qRT-PCR for a number of published ISC markers was performed and revealed a significant increase in expression of *Lgr5* due to *Pml* loss (Figure 4.12). Trends for increased expression of the ISC markers *Ascl2, Olfm4, Msi1* and *Bmi1* were found not to be significant at N=6.

As changes in the expression levels could indicate either an increase in expression by the same number of ISCs or a loss of localisation of expression, *in situ* hybridisation was performed using an anti-*Olfm4* riboprobe on paraffin embedded intestinal tissue of *Apc*$^{flox/flox}$ and *Apc*$^{flox/flox}$ *Pml*$^{-/-}$mice. *In situ* hybridisation revealed an apparent increase in the zone of *Olfm4* expression due to additional *Pml* loss (Figure 4.13). However, due to the tissue disruption caused by the proteinase K step of *in situ* hybridisation, this method is not quantifiable and trends can only be determined through the use of a representative image.

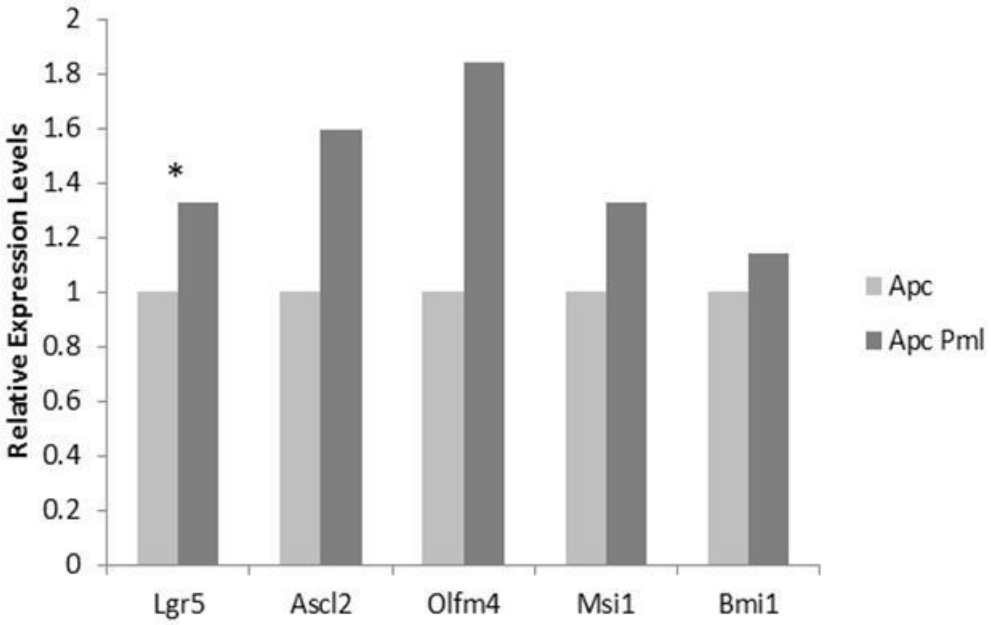

4.12 qRT-PCR analysis of selected ISC markers showed a trend for increased expression due to *Pml* loss in $Apc^{flox/flox}$ mice. * Indicates significance at $p<0.05$ using a 2-tailed T-test. N=6.

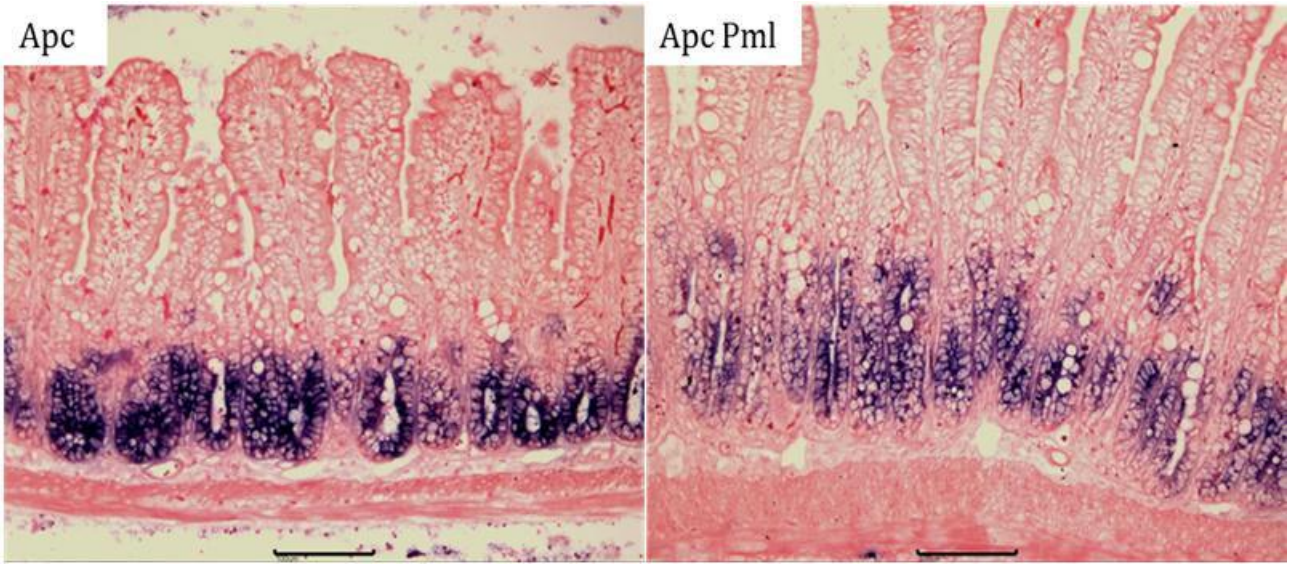

4.13 *In situ* hybridisation to visualise *Olfm4* mRNA expression location. Loss of *Pml* results in an apparent increase in the zone of expression. Black bars indicate 100 μm.

4.2.5 Pml deficiency does not affect the survival or tumour burden in Apc$^{flox/+}$ Pten$^{flox/flox}$ mice

Mice were induced at 8-10 weeks old (+/- 10 days) and aged until displaying loss of condition, when they were culled. Using Wilcoxon survival analysis it was demonstrated that the survival of *Apc*$^{flox/+}$ *Pten*$^{flox/flox}$ *Pml*$^{-/-}$ mice is not significantly different from *Apc*$^{flox/+}$ *Pten*$^{flox/flox}$ mice (*Apc*$^{flox/+}$ *Pten*$^{flox/flox}$ 136 days ± 97, *Apc*$^{flox/+}$ *Pten*$^{flox/flox}$ *Pml*$^{-/-}$ 97 days ± 42 days) (Figure 4.14). Intussusception was only observed in 1/12 of the *Apc*$^{flox/+}$*Pten*$^{flox/flox}$ mice (where it was associated with a large tumour, 9mm x 9mm in size), and 0/16 of the *Apc*$^{flox/+}$*Pten*$^{+/+}$ *Pml*$^{-/-}$ mice.

Tumour counts in both the small and large intestine were performed, and the tumour size recorded. It was found that loss of *Pml* resulted in no change in the numbers of tumours found in the small and large intestine or the size of tumours in *Apc*$^{flox/+}$ *Pten*$^{flox/flox}$ mice.

4.2.6 Pml deficiency increases tumour progression Apc$^{flox/+}$ Pten$^{flox/flox}$ mice

The tumours seen on one section of H&E per mouse were graded using the tumour grading system explained in Section 3.8.2. Using Chi-squared it was possible to determine that there was a significant difference in the ratios of tumour grades observed, with loss of *Pml* resulting in a higher proportion of tumours displaying submucosal and smooth muscle invasion, and therefore fewer lower grade lesions ($P<0.01$) (Figure 4.15) .

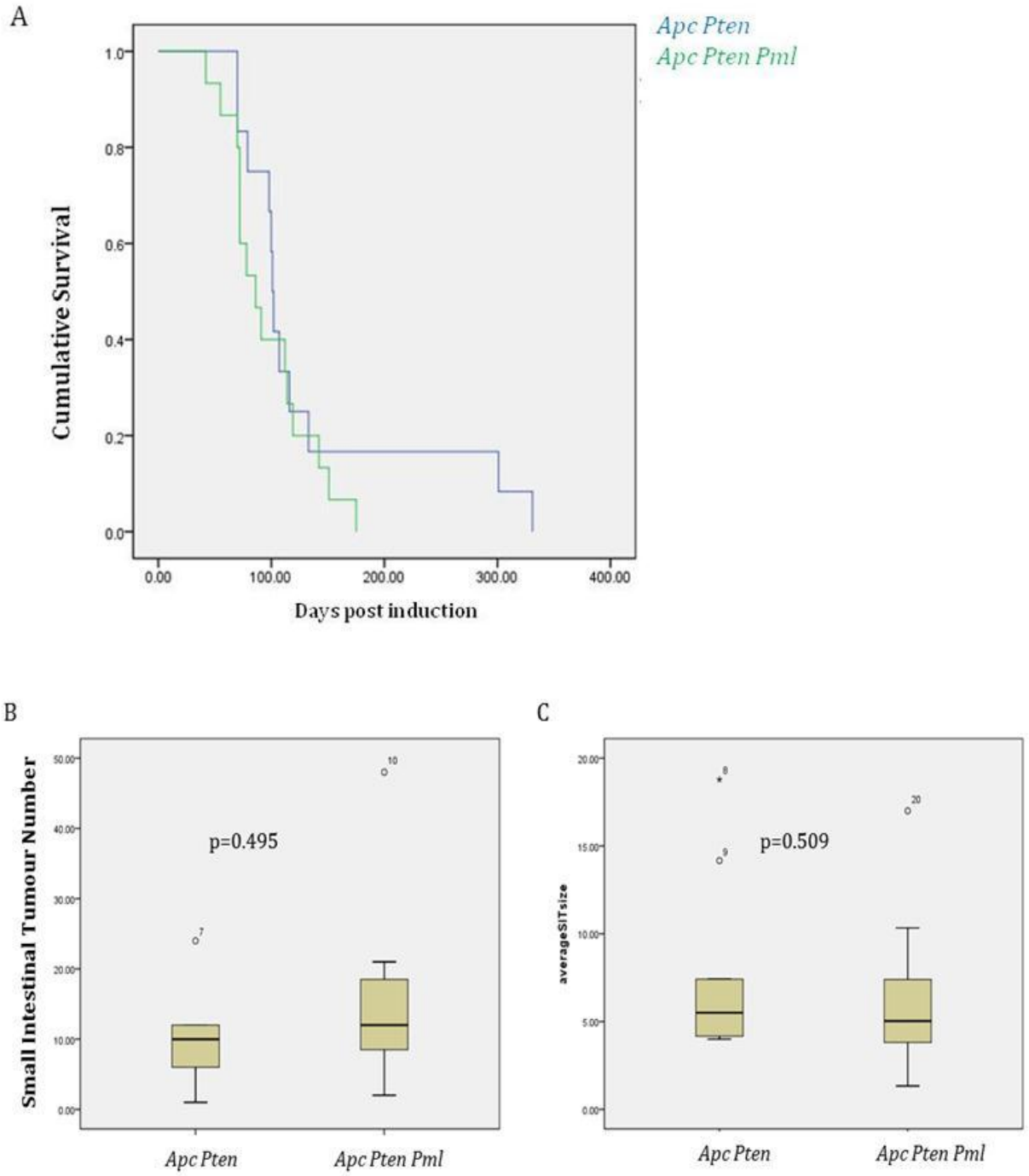

4.14 **A** Survival Plot of *Apc*$^{flox/+}$ *Pten*$^{flox/flox}$ mice with or without *Pml* deletion, there was no difference in survival times between the two cohorts (Wilcoxon p=0.478); **B** Comparison of tumour number in *Apc*$^{flox/+}$ *Pten*$^{flox/flox}$ mice with *Apc*$^{flox/+}$ *Pten*$^{flox/flox}$ *Pml*$^{-/-}$ mice, no significant difference was seen between the two cohorts (2-tailed T-test p=0.495) ; **C** Comparison of average tumour size in *Apc*$^{flox/+}$ *Pten*$^{flox/flox}$ mice with *Apc*$^{flox/+}$ *Pten*$^{flox/flox}$ *Pml*$^{-/-}$ mice, no significant difference was seen between the two cohorts (2-tailed T-test p=0.509). N>10.

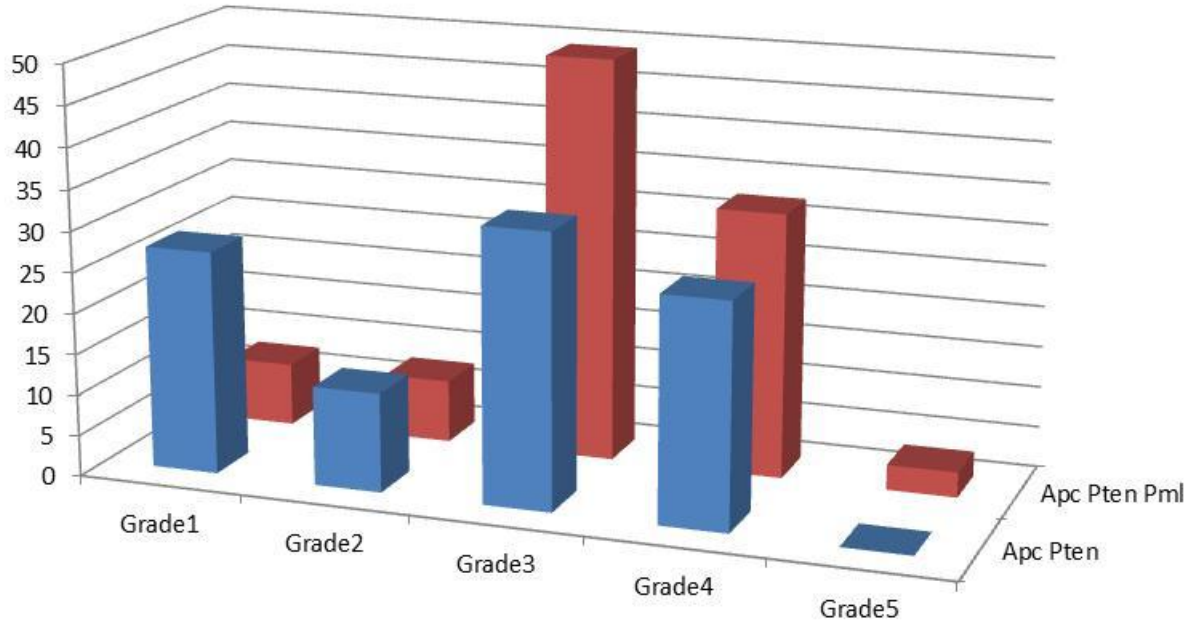

4.15 Graphical representation of the numbers of each lesion type found per genetic cohort. N>10. Chi-squared test showed a significant difference in proportion of tumour grade between the two cohorts, Chi-squared value=34.3 (greater than the Chi-squared given value for $p<0.001$, 6.64).

4.2.7 Pml deficiency significantly reduces survival of Apc$^{flox/flox}$ Pten$^{flox/flox}$ mice

Following induction of Villin-CreER via injection of tamoxifen, *Apc$^{flox/flox}$ Pten$^{flox/flox}$* mice have a median survival time of 4.5 days. In mice carrying the additional *Pml* mutation, median survival following tamoxifen injection was reduced to 3 days (mean values *Apc$^{flox/flox}$ Pten$^{flox/flox}$* 4.5±0.4, *Apc$^{flox/flox}$ Pten$^{flox/flox}$* 3.2±0.4). Upon dissection there was no discernible difference in phenotype between the two cohorts, except that the gut of *Apc$^{flox/flox}$ Pten$^{flox/flox}$Pml$^{-/-}$* mice was noticeably more vascularised. However, this was not quantified.

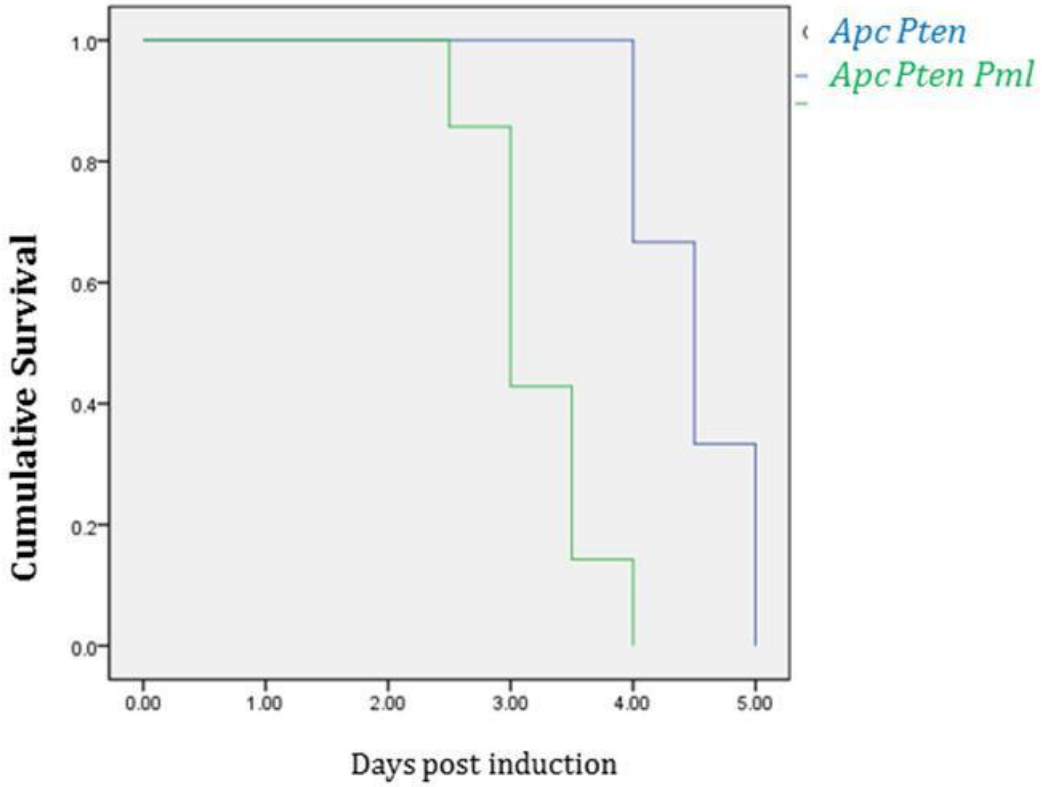

4.16 Cumulative survival of *Apc$^{flox/flox}$ Pten$^{flox/flox}$* and *Apc$^{flox/flox}$ Pten$^{flox/flox}$ Pml$^{-/-}$* mice after administration of tamoxifen. Loss of Pml significantly reduced the survival time of Apc$^{flox/flox}$ *Pten$^{flox/flox}$* mice (Wilcoxon p=0.002). N>5.

4.2.8 Pml deficiency does not alter the histological phenotype of Apc$^{flox/flox}$ Pten$^{flox/flox}$ mice

Despite the decrease in survival of *Apc Pten*-deficient mice due to loss of *Pml,* there was no gross difference in intestinal phenotype (Figure 4.17). Counting the number of aberrant intestinal epithelial cells per crypt-villus axis showed that *Pml* deficiency does not affect the number of cells in this region in *Apc$^{flox/flox}$ Pten$^{flox/flox}$* mice (*Apc$^{flox/flox}$ Pten$^{flox/flox}$* 65±4.5, *Apc$^{flox/flox}$ Pten$^{flox/flox}$* 62±10.7) (Figure 4.18).

Pml deficiency resulted in no significant alteration in the differentiated cell composition of the intestinal epithelium when associated with additional *Pten* loss. In *Apc$^{flox/flox}$ Pten$^{flox/flox}$* mice, *Pml* deficiency had no effect on the number of alcian blue positive goblet cells (*Apc$^{flox/flox}$ Pten$^{flox/flox}$* 8.2±0.7, *Apc$^{flox/flox}$ Pten$^{flox/flox}$* 8.7±2.1) (Figure 4.19), but did result in a trend for decreased numbers of Paneth cells (*Apc$^{flox/flox}$ Pten$^{flox/flox}$* 1.5±0.25, *Apc$^{flox/flox}$ Pten$^{flox/flox}$* 1.3±0.04) (Figure 4.20), and enteroendocrine cells (*Apc$^{flox/flox}$ Pten$^{flox/flox}$* 0.32±0.001, *Apc$^{flox/flox}$ Pten$^{flox/flox}$* 0.21±0.0001) (Figure 4.21).

Similarly, *Pml* loss had no effect on levels of apoptosis in *Apc* and *Pten* deficient mice, as determined by counting the number of apoptotic bodies per half-crypt (*Apc$^{flox/flox}$ Pten$^{flox/flox}$* 0.024±0.006, *Apc$^{flox/flox}$ Pten$^{flox/flox}$* 0.038±0.009), and confirmed by Caspase 3 IHC (*Apc$^{flox/flox}$ Pten$^{flox/flox}$* 0.69±0.09, *Apc$^{flox/flox}$ Pten$^{flox/flox}$* 0.68±0.05)(Figure 4.22). Levels of mitosis were also unaffected, as determined by counting mitotic bodies (*Apc$^{flox/flox}$ Pten$^{flox/flox}$* 2.8±1.2, *Apc$^{flox/flox}$ Pten$^{flox/flox}$* 2.5±0.9), and confirmed by BrDU IHC following a 2hour BrDU exposure prior to animal sacrifice (*Apc$^{flox/flox}$ Pten$^{flox/flox}$* 19.9±4.3, *Apc$^{flox/flox}$ Pten$^{flox/flox}$* 20.4±4.9) (Figure 4.23).

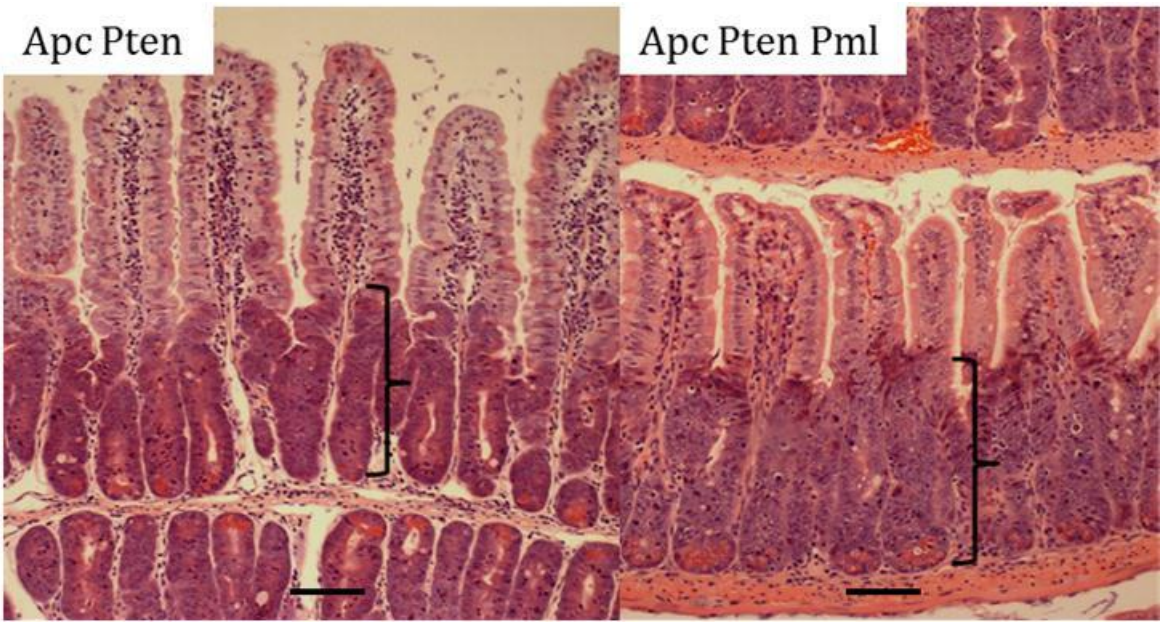

4.17 H&E Stain of *Apc*$^{flox/flox}$ *Pten*$^{flox/flox}$ and *Apc*$^{flox/flox}$ *Pten*$^{flox/flox}$ *Pml*$^{-/-}$ mouse intestine day 3 post induction with tamoxifen. The region of aberrant proliferation is indicated by the black brackets. There was no obvious morphological difference between the two genotypes. Black bars represent 100 µm.

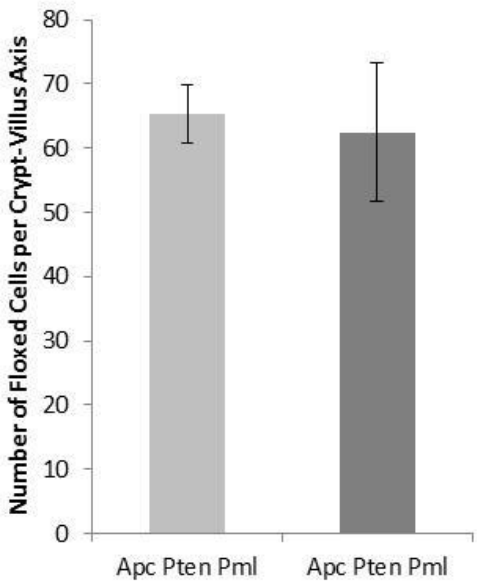

4.18 Counts of the number of cells in the region aberrant proliferation per crypt-villus axis in *Apc*$^{flox/flox}$ *Pten*$^{flox/flox}$ and *Apc*$^{flox/flox}$ *Pten*$^{flox/flox}$ *Pml*$^{-/-}$ mice. There was no significant difference in number of aberrant cells between the two genotypes, 2-Tailed T-test p=0.634, N=4. Error bars represent standard deviation.

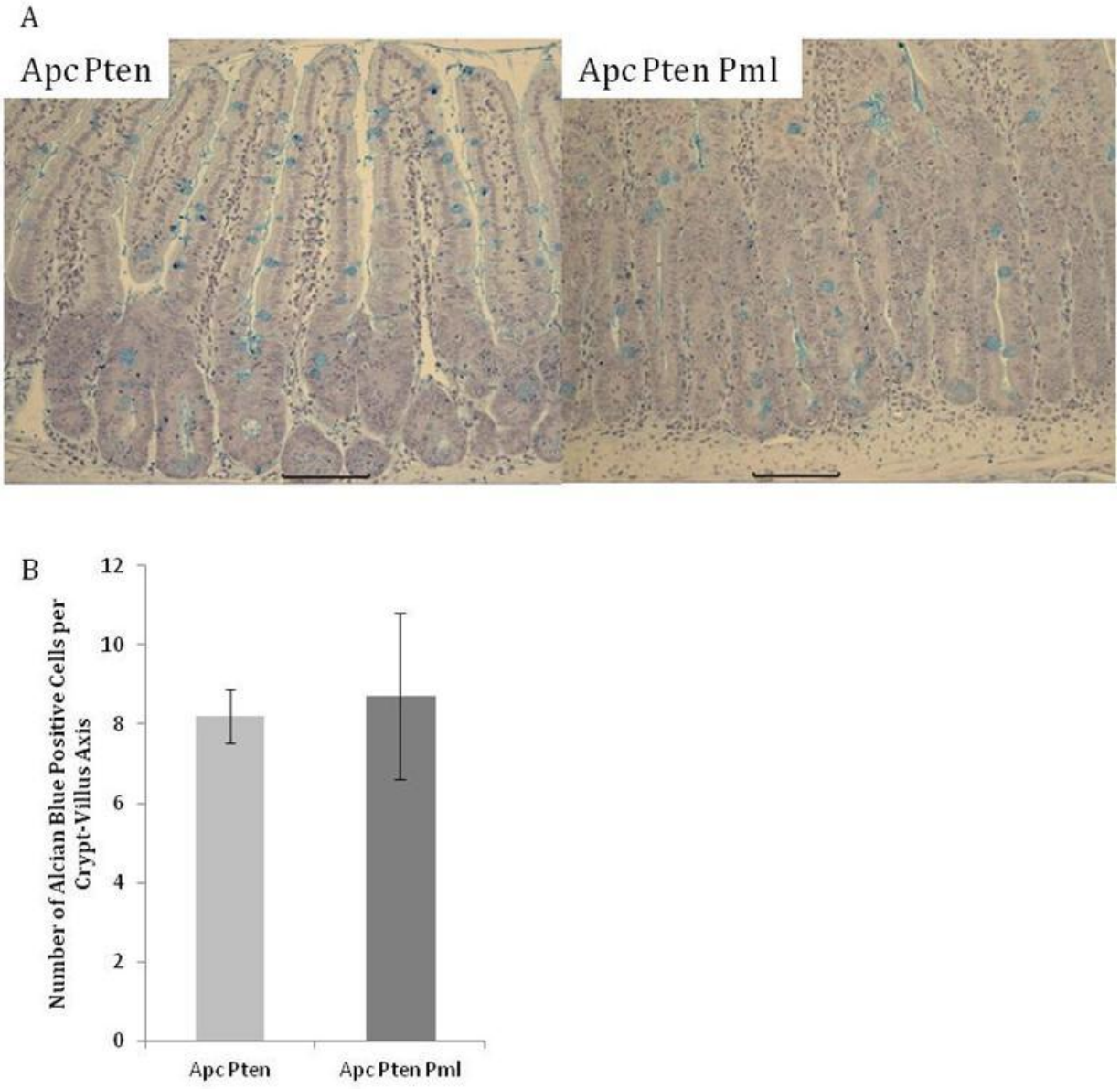

4.19 **A** Alcian Blue IHC of *Apc*$^{flox/flox}$ *Pten*$^{flox/flox}$ *and Apc*$^{flox/flox}$ *Pten*$^{flox/flox}$ *Pml*$^{-/-}$ intestine. Black bars represent 100 μm; **B** Counts of the number of alcian blue positive cells per crypt-villus axis in *Apc*$^{flox/flox}$ *Pten*$^{flox/flox}$ *and Apc*$^{flox/flox}$ *Pten*$^{flox/flox}$ *Pml*$^{-/-}$ mice. There was no significant difference between the two cohorts, 2-tailed T-test p=0.705, N=4.

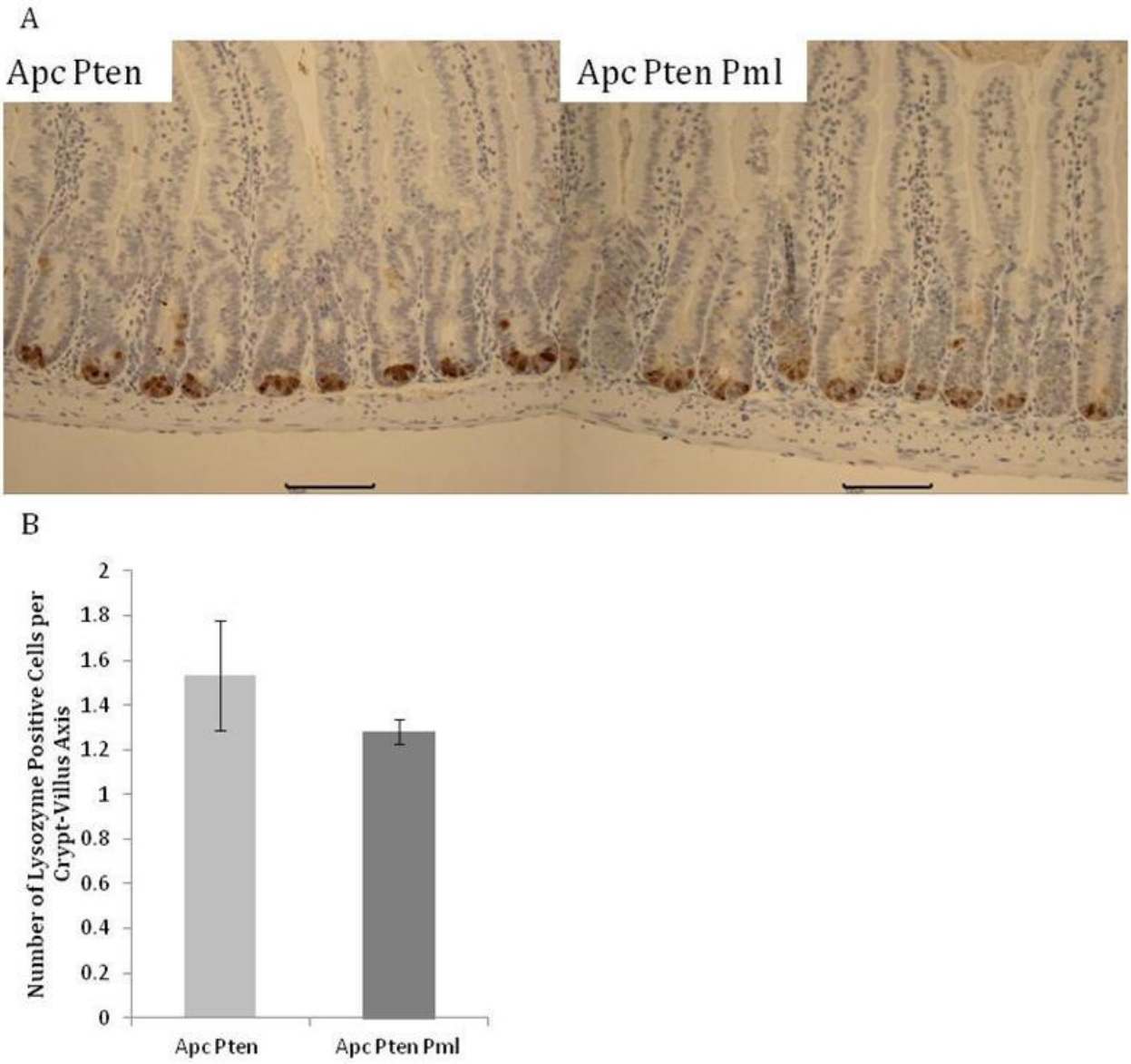

4.20 **A** Lysozyme cell IHC of *Apc*$^{flox/flox}$ *Pten*$^{flox/flox}$ and *Apc*$^{flox/flox}$ *Pten*$^{flox/flox}$ *Pml*$^{-/-}$, brown stained cells represent Paneth cells. Black bars represent 100 μm; **B** Counts of the number of brown cells per crypt-villus axis in *Apc*$^{flox/flox}$ *Pten*$^{flox/flox}$ and *Apc*$^{flox/flox}$ *Pten*$^{flox/flox}$ *Pml*$^{-/-}$ mice. Despite a clear trend, the difference was not significant at N=4, 2-Tailed T-test p=0.146.

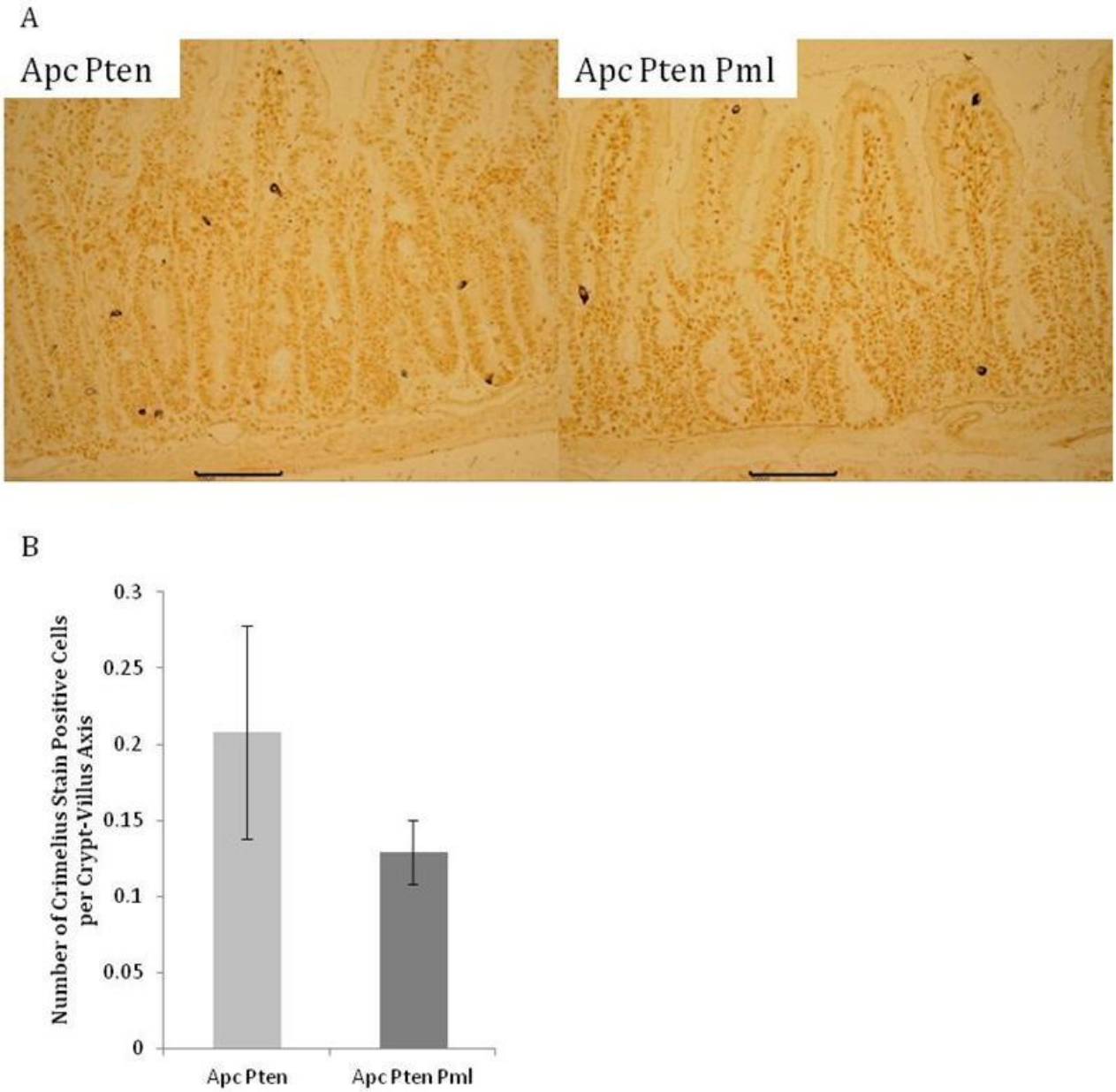

4.21 **A** Grimelius stain of *Apc*$^{flox/flox}$ *Pten*$^{flox/flox}$ and *Apc*$^{flox/flox}$ *Pten*$^{flox/flox}$ *Pml*$^{-/-}$, black stained cells represent Grimelius containing enteroendocrine cells. Black bars represent 100 µm; **B** Counts of the number of black cells per crypt-villus axis in *Apc*$^{flox/flox}$ *Pten*$^{flox/flox}$ and *Apc*$^{flox/flox}$ *Pten*$^{flox/flox}$ *Pml*$^{-/-}$ mice. Despite a clear trend, the difference was not significant at N=4, 2-Tailed T-test p=0.135.

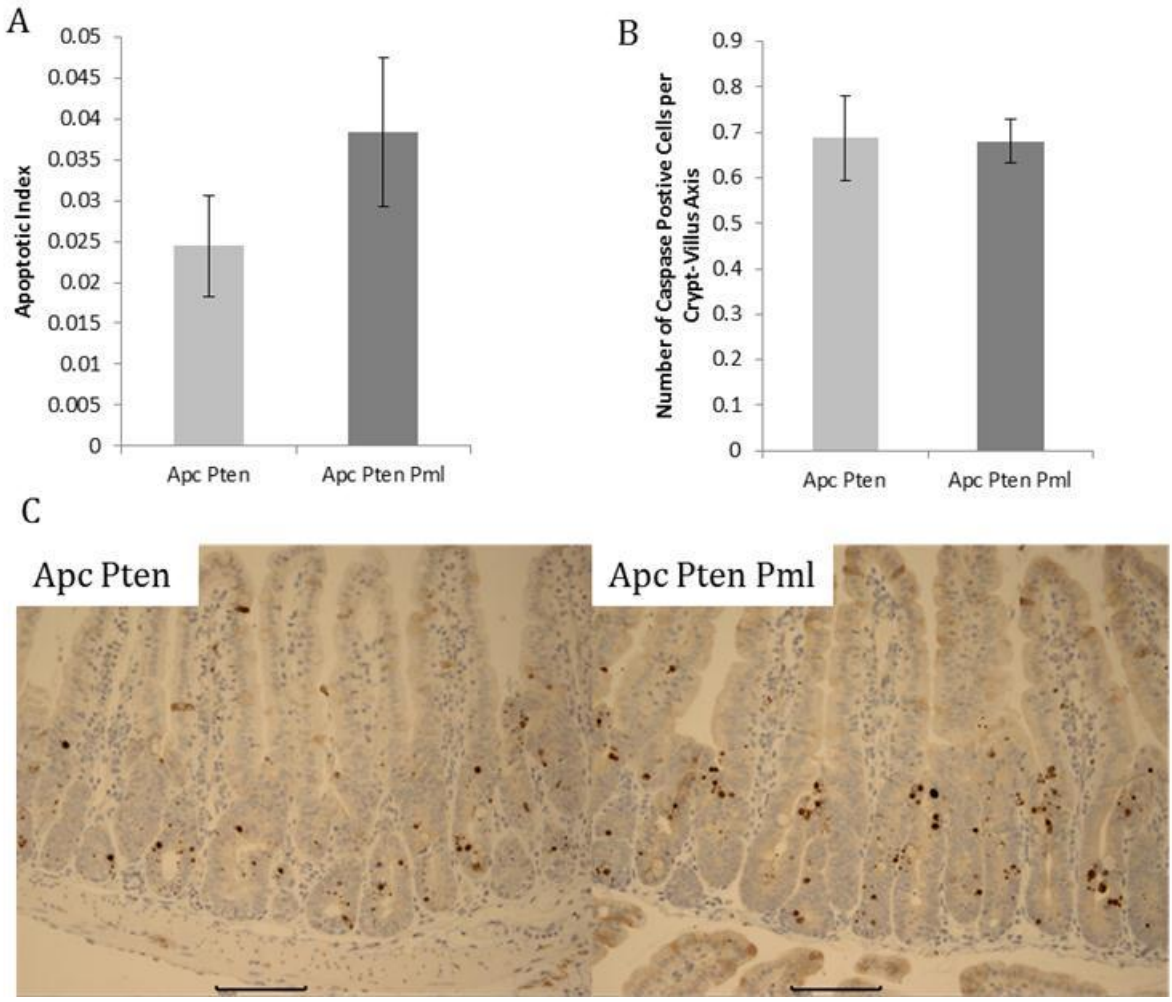

4.22 Comparison of levels of apoptosis in *Apc*$^{flox/flox}$ *Pten*$^{flox/flox}$ and *Apc*$^{flox/flox}$ *Pten*$^{flox/flox}$ *Pml*$^{-/-}$ *mice.* **A** Apoptotic Index, as measured by number of apoptotic bodies per crypt-villus access and normalised for the number of cells in the region aberrant proliferation. There was no significant difference between the two genotypes, 2-tailed T test p=0.059, N=4; **B** Number of Caspase positive cells as counted from Caspase IHC There was no significant difference between the two genotypes, 2-tailed T test p=0.411, N=4; **C** Caspase 3 IHC on *Apc*$^{flox/flox}$ *Pten*$^{flox/flox}$ and *Apc*$^{flox/flox}$ *Pten*$^{flox/flox}$ *Pml*$^{-/-}$ intestine. Brown cells represent Caspase 3 positive cells. Black bars represent 100 µm.

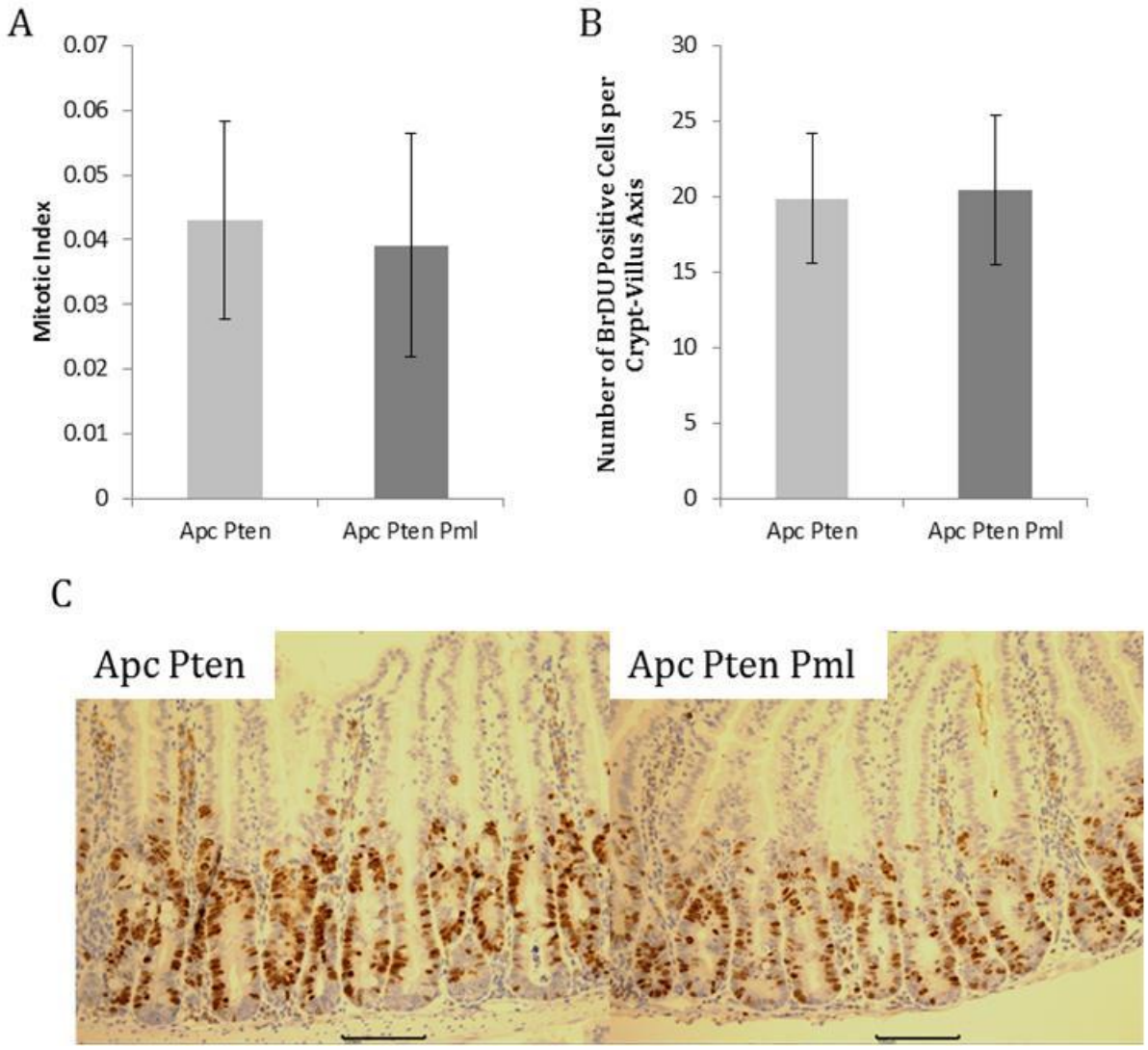

4.23 Comparison of levels of mitosis in *Apc*$^{flox/flox}$ *Pten*$^{flox/flox}$ and *Apc*$^{flox/flox}$ *Pten*$^{flox/flox}$ *Pml*$^{-/-}$ mice**. A** Mitotic Index, as measured by number of mitotic bodies per crypt-villus access and normalised for the number of cells in the region aberrant proliferation. There was no significant difference between the two genotypes, 2-tailed T test p=0.672, N=4; **B** Number of BrDU positive cells as counted from BrDU IHC after a 2 hour BrDU exposure. There was no significant difference in BrDU uptake between the two genotypes, 2-tailed T test p=0.895, N=4; **C** BrDU IHC on *Apc*$^{flox/flox}$ *Pten*$^{flox/flox}$ and *Apc*$^{flox/flox}$ *Pten*$^{flox/flox}$ *Pml*$^{-/-}$ intestine. Brown cells represent BrDU positive cells. Black bars represent 100 µm.

4.2.9 *Pml* loss does not activate the PI3K pathway in $Apc^{flox/flox}$ $Pten^{flox/flox}$ intestinal epithelium

Western-blot analysis of protein extracted from intestinal epithelial cells of $Apc^{flox/flox}$ $Pten^{flox/flox}$ and $Apc^{flox/flox}$ $Pten^{flox/flox}$ $Pml^{-/-}$ mice showed that additional *Pml* deficiency had no effect on the levels of pAKT. This result was confirmed by IHC, which showed no visible change in levels of pAKT between the two genotypes (Figure 4.24).

4.2.10 *Pml* loss results in a significant increase in expression of ISC markers in $Apc^{flox/flox}$ $Pten^{flox/flox}$ mice

Due to loss of *Pml* resulting in an increased tumour grade in *Apc* and *Pten* deficient mice, the ISC compartment was analysed. ISCs have been shown to be the cell of origin of intestinal tumourigenesis, and loss of *Apc* specifically within ISCs results in more aggressive adenomas than when *Apc* is lost from other intestinal epithelial cell types (Barker et al. 2008), hence once possible reason for the observed increase in the grade of adenomas may be a change in the ISC compartment.

Loss of *Pml* in the context of combined *Apc* and *Pten* deficiency had a clear effect on the ISC compartment, with a trend for increased expression of the ISC markers *Ascl2*, *Msi1* and *Bmi1*, and a significant increase in the expression of the markers *Lgr5* (t-test p=0.03) and *Olfm4* (t-test p=0.03) at N=6 (Figure 4.25).

Interestingly, *in situ* hybridisations for the ISC marker *Olfm4* did not display any change of location of expression (Figure 4.26).

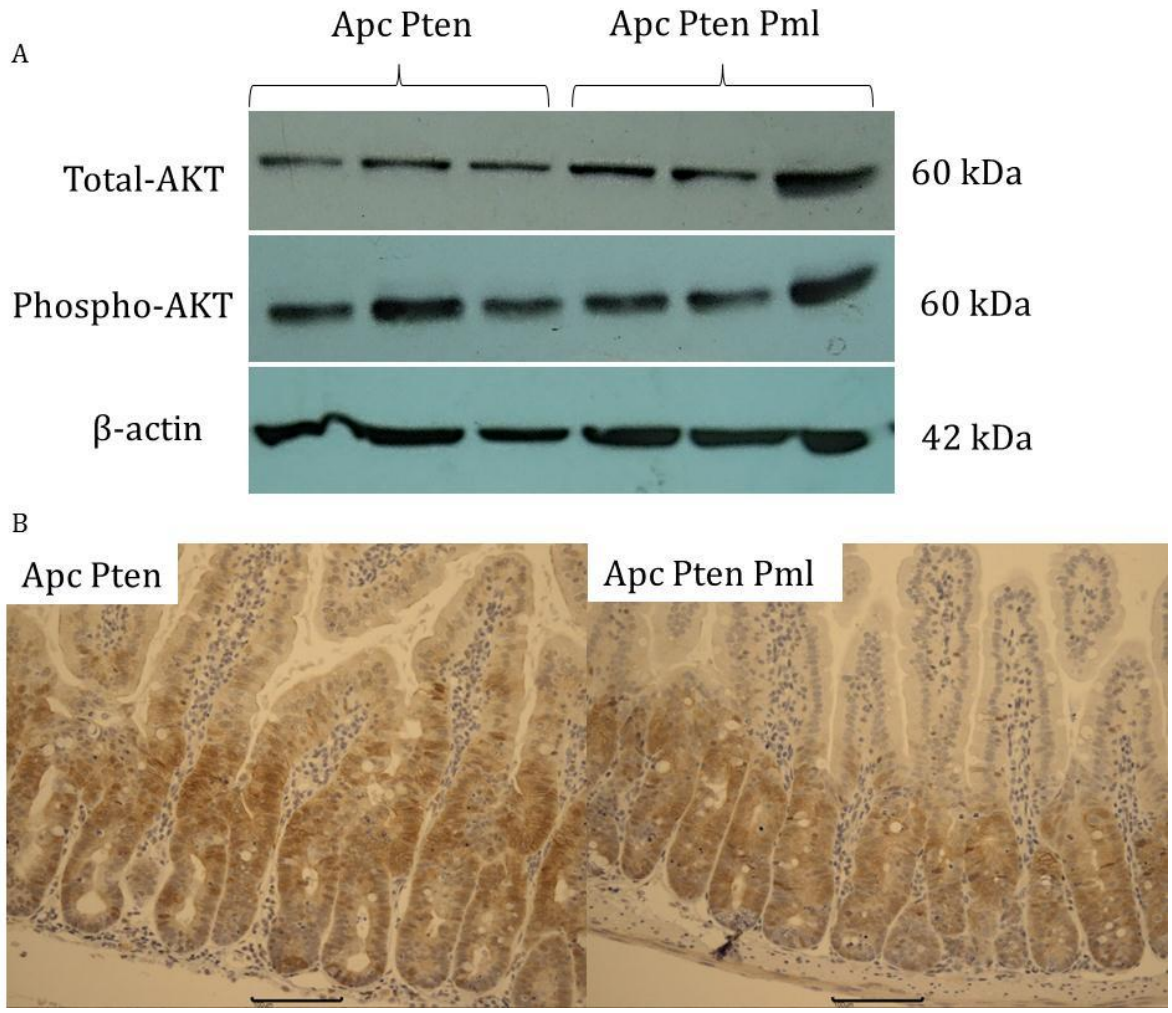

4.24 Phospho-AKT levels as a measure of activation of the PI3K pathway due to additional deletion of *Pml* from $Apc^{flox/flox}$ $Pten^{flox/flox}$ mice. **A** Western blot analysis shows that total levels of both total- Akt protein and phospho-Akt were high in both cohorts with no difference between the two cohorts; **B** IHC for phospho-Akt confirmed that the PI3K pathway was activated equally in both genotypes. Black bars represent 100 μm.

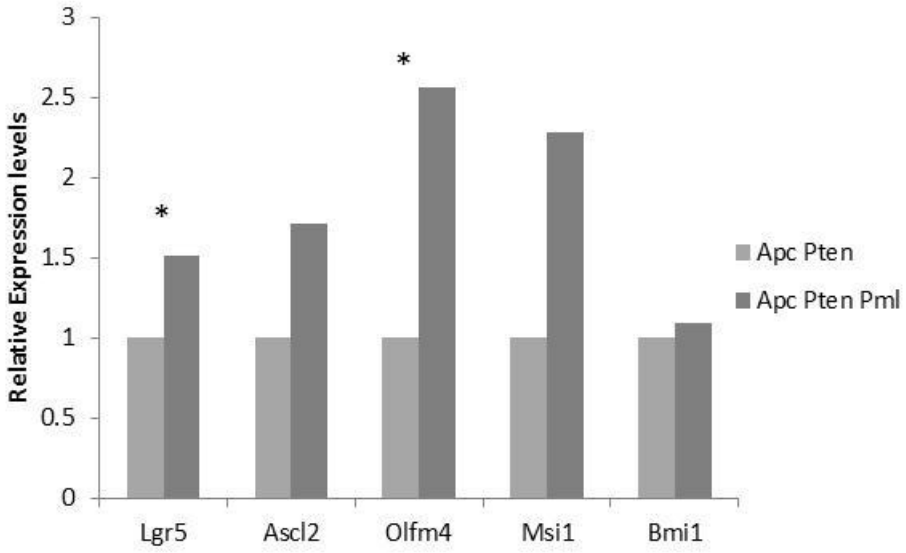

4.25 qRT-PCR analysis of selected ISC markers showed a trend for increased expression due to *Pml* loss in *Apc*$^{flox/flox}$ mice. * Indicates significance at $p<0.05$ using a 2-tailed T-test. N=6.

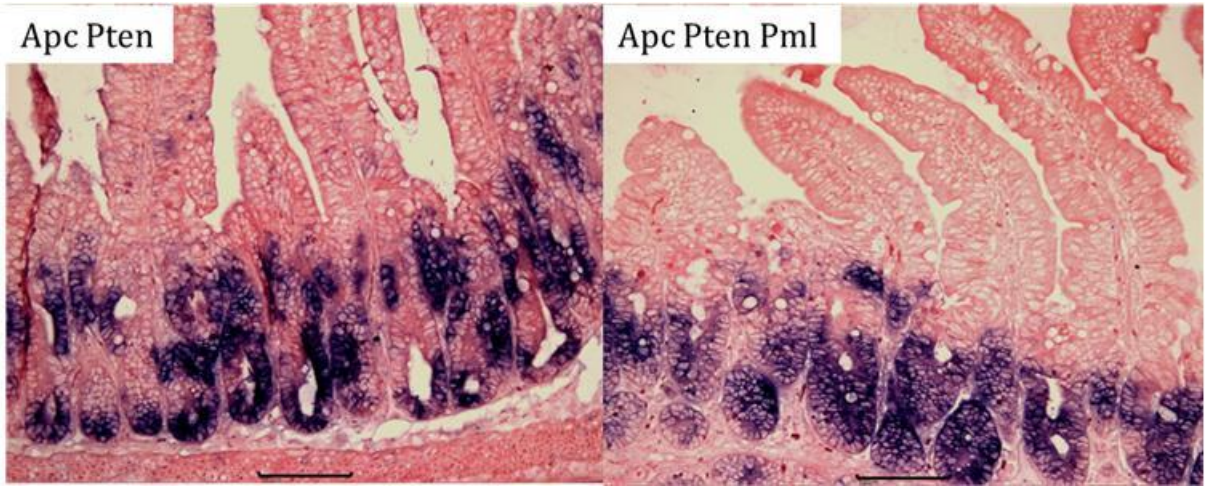

4.26 *In situ* hybridisation to visualise *Olfm4* mRNA expression location. Loss of *Pml* results in no gross change in the zone of expression. Black bars indicate 100 μm.

4.2.11 Organoids from all cohorts are cyst-like, with few differentiated cell types

The ability of *Pml* loss to seemingly expand the ISC compartment, and therefore the potential number of "cells of origin" of intestinal tumourigenesis, without having an impact on the number of tumour initiation "events" is contradictory and so it is necessary to assess the effect of *Pml* loss on the functional ISC compartment separately from its effect on the expression of ISC markers.

$Apc^{flox/flox}$ $Pml^{-/-}$, $Apc^{flox/flox}$ $Pten^{flox/flox}$ and $Apc^{flox/flox}$ $Pten^{flox/flox}$ $Pml^{-/-}$ intestinal crypts all produced organoids which were cyst-like with few differentiated cells, which were indistinguishable from $Apc^{flox/flox}$ organoids (Figure 4.27). Due to the similarities with $Apc^{flox/flox}$ organoids, the $Apc^{flox/flox}$ $Pml^{-/-}$, $Apc^{flox/flox}$ $Pten^{flox/flox}$ and $Apc^{flox/flox}$ $Pten^{flox/flox}$ $Pml^{-/-}$ organoids were analysed using the $Apc^{flox/flox}$ CHARM programme. See section 2.12.4.

4.2.12 Pml loss does not affect organoid formation efficiency in $Apc^{flox/flox}$ or $Apc^{flox/flox}$ $Pten^{flox/flox}$ mice

In contradiction to the *in vivo* results which showed that *Pml* loss resulted in an increased expression of *Lgr5*, loss of *Pml* had no effect on the organoid forming efficiency of intestinal crypts from any of these cohorts (Figure 4.28). All organoid cultures were completely Rspo1 independent due to *Apc* deficiency.

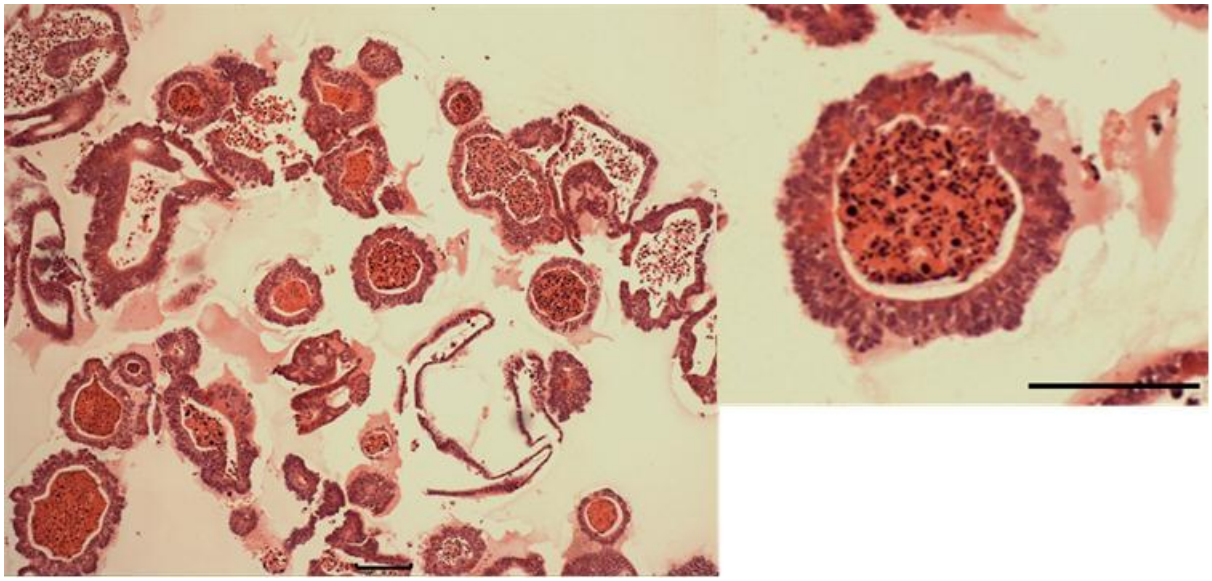

4.27 H&E displaying organoids representative of *Apc*$^{flox/flox}$ *Pml*$^{-/-}$, *Apc*$^{flox/flox}$ *Pten*$^{flox/flox}$ and *Apc*$^{flox/flox}$ *Pten*$^{flox/flox}$ *Pml*$^{-/-}$ organoids. Image actually taken of fixed *Apc*$^{flox/flox}$ *Pten*$^{flox/flox}$ *Pml*$^{-/-}$ organoids. Black bars represent 100 µm.

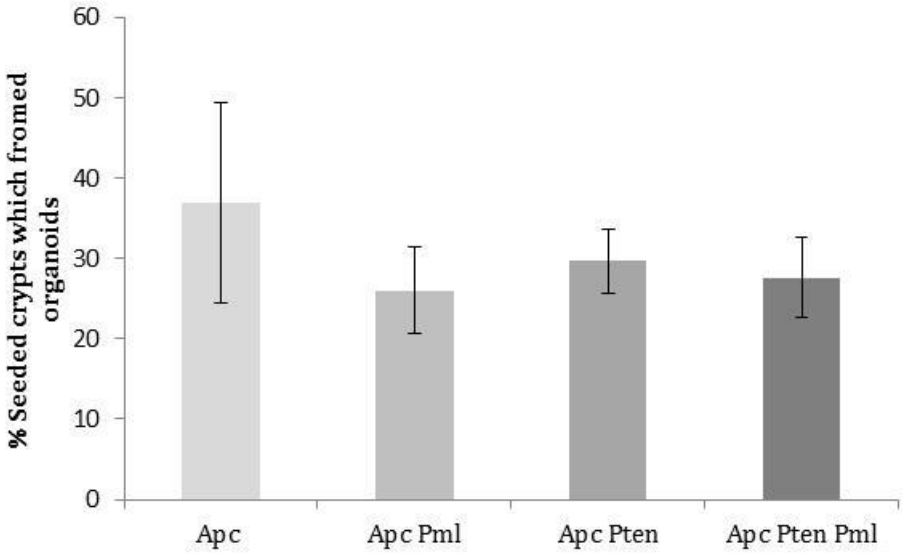

4.28 Intestinal organoid formation efficiency of *Apc*$^{flox/flox}$, *Apc*$^{flox/flox}$ *Pml*$^{-/-}$, *Apc*$^{flox/flox}$ *Pten*$^{flox/flox}$ and *Apc*$^{flox/flox}$ *Pten*$^{flox/flox}$ *Pml*$^{-/-}$ intestinal crypts. No significant difference was observed between any of the genotypes (2-tailed T-test $p>0.05$ for all comparisons).

4.3 Discussion

4.3.1 Pml deficiency results in subtle phenotypic changes in $Apc^{flox/+}$ and $Apc^{flox/flox}$ mice, but no change in survival or tumour burden

Despite *Pml* loss resulting in no change in survival or tumour burden of $Apc^{flox/+}$ mice, there was an increase in the levels of intussusception observed upon dissection. Heterozygous loss of *Pten* has been previously shown to increase levels of intussusceptions in an Apc^{min} model of colorectal tumourigenesis (Shao et al. 2007). Although intussusception is normally viewed as a result of the presence of large tumours, rather than a tumour independent phenotype, this was not the case in the $Apc^{flox/+}$ $Pml^{-/-}$ mice, which did not have significantly larger tumours than were seen in $Apc^{flox/+}$ mice alone. In order to assess whether the observed intussusception is due to a mechanism which is independent of tumour size, it would be necessary to generate a much higher N-number and record the size and location of the tumour associated with it.

Shao *et al*. noted that in Apc^{min} $Pten^{+/-}$ mice where intussusception was observed, expression of the gene *Osteopontin* (*Opn*) was significantly upregulated (Shao *et al.* 2007). *Opn* is a secreted phosphoglycoprotein which plays important roles in cell adhesion, motility, apoptosis and inflammation. Furthermore, high levels of OPN are associated with tumour progression in colorectal and breast cancers (Yeatman and Chambers 2003). Interestingly, *Opn* is an important driver of *Interleukin17* (*Il17*) expression, which in turn regulates inflammation and immune response. It is currently believed that intussusception which is not tumour associated is likely to be induced by infection and inflammation (Nissan *et al.* 1997). Pml-NBs have been implicated in the inflammatory process through their association with inflammatory tissue, and have been observed at high levels in macrophages (Terris *et al.* 1995). In order to assess the role inflammation is playing in intussusception caused by *Pml* deletion in $Apc^{flox/+}$ mice, expression levels of *Opn*, *Il17* and *Tumour Necrosis Factor-α* (*TNFα*) could be assessed.

There is evidence that one of the ways in which PML regulates the PI3K pathway is through its role in regulating the localisation of PTEN. Specifically, this occurs within the nucleus where loss of *Pml* is associated with mis-localization of Pten (Song *et al*. 2008;

Trotman et al. 2006), and mis-localization of PTEN is associated with disease progression in CRC (Zhou *et al.* 2000). Despite the role of Pten within the PI3K pathway taking place at the cell membrane, mis-localisation of Pten may explain the proposed role of *Pml* in intestinal tumourigenesis. However, the work presented here shows that loss of *Pml* alone had no effect on the survival of either $Apc^{flox/+}$ or $Apc^{flox/flox}$ mice, indicating that any mis-localisation of Pten is not comparable to loss of *Pten* function, which decreased survival time of these mice (Marsh et al. 2008).

In our $Apc^{flox/flox}$ model it is clear that *Pml* is not playing a significant role in the regulation of the PI3K pathway, as loss of *Pml* does not result in any increase in levels of pAKT. It is therefore unsurprising that loss of *Pml* does not result in a change in survival or tumour burden of these mice, as in this context it is not regulating PI3K upstream of pAKT (Trotman *et al*. 2006). However, *Pml* may be playing a role downstream of pAKT, due to the ability of Pml-NBs to sequester mTOR (Bernardi *et al.* ; Carracedo and Pandolfi 2008). In order to test this in our model, levels of mTOR could be assessed using Western blotting, however, any significant increase in mTOR due to loss of *Pml* would presumably result in increased tumourigenesis and decreased survival of $Apc^{flox/+}$ mice, which we did not observe.

As PML-NBs are known to play a role in apoptosis, and loss of PML from cell lines resulted in decreased apoptosis (Bernardi *et al*. 2008; Gao YM *et al.* 2013), it was expected that loss of *Pml* from an $Apc^{flox/flox}$ model of acute Wnt activation would protect cells from apoptosis. However, this was not the case, and potentially the mechanism which drives apoptosis in $Apc^{flox/flox}$ mice, which is likely the result of highly activated Wnt-signalling increasing genetic damage, may be Pml-NB independent.

In $Apc^{flox/flox}$ mice, we showed that loss of *Pml* results in increased mitosis, which supports the previously described role of *Pml* as a promoter of cell senescence, with loss of *Pml* resulting in increased proliferation (Ferbeyre *et al.* 2000; Melnick and Licht 1999), although we have no evidence for senescence occurring in the intestinal epithelium of $Apc^{flox/flox}$ mice.

4.3.2 *Pml* deficiency does not affect the survival or tumour burden in $Apc^{flox/+}$ $Pten^{flox/flox}$ but results in increased tumour progression

As it had previously been published that *Pml* deficiency increased tumour initiation, burden and progression in $Pten^{+/-}$ mice (Trotman et al. 2006), it was thought that a similar effect would be observed in a Wnt-driven model of intestinal tumourigenesis with homozygous *Pten* loss. Surprisingly, neither survival or tumour burden were affected by additional *Pml* loss, however, there are a number of potential mechanisms which would cause this effect.

In the work presented by Trotman *et al*. a heterozygous model of *Pten* deletion is used, resulting in *Pten* deficiency in all tissues (Trotman *et al*. 2006). Heterozygosity for this allele of *Pten* alone, has already been shown to be adequate to drive the development of microscopic benign colonic polyps (Suzuki *et al.* 1998), whereas the conditional homozygous deletion of $Pten^{flox/flox}$ using Villin-CreER does not result in any immediate change in intestinal or colonic homeostasis (Langlois *et al.* 2009; Marsh et al. 2008). These bodies of work suggest that any role played by *Pten* in initiating intestinal tumourigenesis in these models may occur outside of the intestinal epithelium, and may be due to changes in gene expression within the stromal compartment of the intestine. Consistent with this, conditional homozygous deletion of *Pten* using a fibroblast specific Cre-recombinase (Col1A2CreER (Zheng *et al.* 2002)), which specifically recombined in the intestinal stroma and smooth muscle compartments, resulted in tumourigenesis throughout the small intestine and colon (Davies 2011). However, He *et al.* found that *Pten* deletion from the ISC compartment was sufficient to induce intestinal tumourigenesis (He et al. 2007). The mechanism for *Pten* deletion in this instance was through the use of a Cre-recombinase linked to expression of *Mxi1*, which is upregulated due to interferon expression (Kühn *et al.* 1995). The use of this Cre means that not only is there a lack of specificity (with *Pten* recombination appearing to occur within the stromal compartment as well as the ISC compartment) but that the Cre is induced by the injection of polyinosinic-polycytidylic acid (pipC), which stimulates inflammation and immunity in order to upregulate interferon levels. This means that *Pten* loss within the intestinal epithelium may not be responsible for tumour initiation in this model as it

could either be due to *Pten* deletion within the stroma, or due to the stimulation of inflammation and the immune response.

Potentially, the network through which *Pten* and *Pml* interact to suppress intestinal tumourigenesis is a stromal specific one, and as Villin-CreER recombines between LoxP sites of *Pten* specifically within the intestinal epithelium, the model used here is not an accurate representation of the interactions between *Pten* and *Pml* within the intestinal stroma. Alongside the cohorts shown here, $Pten^{flox/flox}$ $Pml^{-/-}$ mice were also generated and aged (in the absence of *Apc* mutations), and they showed no decrease in survival compared to wildtype mice or any instances of intestinal tumourigenesis at death (data not shown).

In our model, tumourigenesis is initiated by loss of *Apc*, but progression is driven by loss of *Pten* from the intestinal epithelium. In this context, constitutive loss of *Pml* does not play a role in tumourigenesis, and therefore does not increase tumour number. However, loss of *Pml* results in increased tumour progression. This supports the finding of Bernardi *et al.* that *Pml* acts to repress tumour progression in a mouse model of kidney cancer (Bernardi *et al*.). In this study it was shown that this repression of tumour progression was due to the role of *Pml* as an inhibitor of mTOR. Increased tumour progression in our $Apc^{flox/+}$ $Pten^{flox/flox}$ due to *Pml* loss could be a result of hyperactivation of the PI3K pathway specifically within the tumours.

4.3.3 Pml deficiency significantly reduces survival of $Apc^{flox/flox}$ $Pten^{flox/flox}$ mice but does not grossly alter intestinal phenotype

Despite *Pml* deficiency resulting in no change in survival in an $Apc^{flox/+}$ $Pten^{flox/flox}$ model of long term tumourigenesis, the effect on survival of the short term model of early tumourigenesis, $Apc^{flox/flox}$ $Pten^{flox/flox}$ mice, was dramatic. *Pml* deficiency resulted in a more than 25% decrease in survival, despite no gross microscopic gut phenotype when assessed at day 3 post induction. There was also no change in the number of cells in the region aberrant proliferation, apoptosis, mitosis or differentiated cell types. The health status of mice following combined loss of *Apc* and *Pten* is severely compromised, the supposed cause of death in $Apc^{flox/flox}$ mice is dehydration caused by complete intestinal failure. Furthermore, the intestine undergoes a gross immune response following loss of *Apc,* with visible gut inflammation. *Pml* has been shown to play an important role in

innate immunity, and *Pml*$^{-/-}$ mice have previously been found to develop lethal botryomycosis (BTM), which are granulomatous lesions caused by an inability to clear pathogenic microorganisms (Lunardi *et al.* 2011). Potentially, the decrease in survival time due to *Pml* loss in these models is due to an abnormal immune response.

Despite the proposed role of Pml as a negative regulator of phosphorylation of AKT, loss of *Pml* did not result in any increase in pAKT in *Apc*$^{flox/flox}$ *Pten*$^{flox/flox}$ mice, as confirmed by Western blots and IHC. Trotman *et al.* showed that Pml-NBs specifically recruit both PP2a (an Akt phosphatase) and pAKT, and that loss of *Pml* results in an increase in nuclear pAKT. This is directly contradictory to our observations. However, it should be noted that nuclear pAKT levels have not been analysed directly, rather pAKT levels were from complete intestinal epithelial extract. As the proposed roles of *Pml* in regulating the PI3K pathway are diverse, it is possible that loss of *Pml* in the epithelium is not increasing pAKT levels, but may be increasing mTOR activity (Bernardi *et al.* 2011; Carracedo and Pandolfi 2008; Ito *et al.* 2009). IHC for phosphorylated mTOR could help elucidate this function.

4.3.4 Pml loss results in a significant increase in expression of ISC markers in both Apc$^{flox/flox}$ and Apc$^{flox/flox}$ Pten$^{flox/flox}$ mice

The role of *Pml* as a promoter of quiescence (Ito et al. 2008), is particularly relevant when considering its role in maintaining the ISC compartment. Cell quiescence is commonly associated with stem cells, as adult stem cells generally rarely divide as a protective mechanism against genetic damage. However, Lgr5^{+} ISCs have been shown to proliferate rapidly and so cannot be said to be quiescent (Lopez-Garcia et al. 2010; Schepers *et al.* 2011). This is clear since loss of *Pml,* in the context of both conditional homozygous deletion of *Apc* alone and *Apc* and *Pten* loss, results in an increase in expression of the ISC marker *Lgr5*, and a trend for increased expression of the other ISCs examined.

The increased expression of ISC markers observed due to loss of *Pml* supports its role as an inhibitor of mTOR, which has a reported role in the maintenance of breast cancer stem-like cells through its interactions with Stat3 signalling (Zhou *et al.* 2007). The increase in ISC marker expression due to *Pml* loss could provide a mechanism for how *Pml* loss results in an increased level of tumour progression in *Apc*$^{flox/flox}$ *Pten*$^{flox/flox}$ mice.

In another mouse model of intestinal tumourigenesis, the *Apc*^{min} mouse, it has been shown that Stat3 regulates tumour progression (Musteanu *et al.* 2010). Stat3 is also an important regulator of the ISC compartment, and may provide a link between changes in tumour grade and expansion of the ISC compartment (Matthews et al. 2011).

ISCs, specifically the Lgr5^{+} population, are known to be the cell of origin of intestinal tumourigenesis (Barker *et al.* 2008). As such, it would be expected that an expansion of the ISC population (as evidenced by an increase in expression of ISC markers) would result in an increased level of "cells of origin" and therefore an increased level of tumourigenesis. However, there is a great deal of controversy surrounding the relevancy of many of the ISC markers previously published (Barker et al. 2012; Muñoz et al. 2012). One of the main concerns with the use of many of these ISC markers is that they do not play a functional role in the maintenance of the ISC population. For example, the most commonly used marker of the ISC population is *Lgr5*, yet *Lgr5* expression is dispensable for the maintenance of intestinal homeostasis (Tian et al. 2011). This highlights the fact that the ISC markers used here are not an adequate readout of changes in the ISC compartment.

Despite the increased expression of ISC markers as a result of *Pml* loss in both *Apc*$^{flox/flox}$ and *Apc*$^{flox/flox}$ *Pten*$^{flox/flox}$ mice, this did not translate into an increase in organoid formation efficiency. This paradox highlights one of the pitfalls of assessing the ISC compartment using gene expression markers alone, as they do not relate to a function capacity of ISCs. Loss of *Pml* in these contexts increased expression of ISC markers, but had no quantifiable effect on the functional ISC compartment (as assessed by organoid formation efficiency). This may explain why an increase in ISC marker expression did not correspond with an increase in tumourigenesis in these models.

Equally, the result could indicate that organoid formation efficiency is not a relevant readout of changes in the ISC compartment within *Apc*$^{flox/flox}$ mice, as potentially, over-activation of the Wnt-signalling pathway enables non-ISCs to form organoids in culture. As previously discussed, organoids derived from *Apc*$^{flox/flox}$ mice do not differentiate and therefore may not be derived from a population of true ISCs, and so potential changes in the ISC compartment due to *Pten* and *Pml* loss, may be being masked in this assay by the gross phenotypic change resulting from *Apc* deletion.

4.4 Summary

Much of the research regarding *Pml* has struggled to produce confident mechanisms for its role as a tumour suppressor due to its diverse interactions and seemingly tumour-specific functions. The primary role of *Pml* as a tumour suppressor within the intestine was thought to be due to its role in interacting with *Pten* to regulate the PI3K pathway (Trotman *et al*. 2006). However, in the context of Wnt-driven tumourigenesis, *Pml* has not been shown to play a role in either survival or tumour burden. It is possible that the interaction between *Pml* and *Pten,* which drives tumourigenesis, occurs in the stroma, as epithelial *Pten* loss is not tumour initiating, whereas stromal *Pten* does result in tumourigenesis. Any interaction between *Pten* and *Pml* in the model presented here (where *Pten* is lost specifically within the intestinal epithelium and tumourigenesis is initiated by *Apc* loss) results in an increase in tumour progression, but not tumour formation.

Interestingly, constitutive loss of *Pml* did result in an increased tumour grade in a model of *Apc* heterozygous and *Pten* homozygous deletion from the intestinal epithelium. This increase in tumour grade due to *Pml* loss correlated with an increase in expression of ISC markers, both of which may be being controlled by changes in Stat3 levels, but not an increase in ISC functionality as assessed by the organoid formation efficiency assay.

Pml loss, in the context of *Apc* and *Pten* homozygous deletion, resulted in a significantly decreased survival time, without altering the gross intestinal phenotype. It is thought that in this context, immune-deficiency brought about by *Pml* loss maybe causing decreased survival by increasing the susceptibility to and the severity of innate infectious reagents. However, there is no evidence for this as cause of ill health of these animals remains unclear.

4.5 Future Work

In order to ascertain the mechanism by which loss of *Pml* is resulting in an increase in both expression of ISC markers and invasion, levels of both phospho-mTOR and Stat3 will be studied in both the intestinal epithelium and within tumours via IHC and Western blotting.

In order to understand the mechanism by which *Pml* loss resulted in a decreased survival of $Apc^{flox/flox}$ $Pten^{flox/flox}$ mice, the immune response of these mice could be analysed, by looking at levels of gut inflammation and plasma macrophage levels. The effect any changes in immune response may be having on survival could be tested by challenging the immune system of $Apc^{flox/+}$ $Pten^{flox/flox}$ mice with a known pathogen, and assessing the response with or without additional *Pml* loss.

It is thought that one reason why our model did not recapitulate the results observed by Trotman *et al.,* may be due to the importance of the relationship between *Pten* and *Pml* in tumour initiation within the stromal rather than the intestinal epithelium. Therefore it would be interesting to study the effect of *Pml* deletion when recombination of $Pten^{flox/flox}$ mice are induced using a stromal-specific Cre such as Col1A2CreER.

5 Investigating the effects of loss of *Apc2* on the ISC compartment

5.1 Introduction

The identification of the APC homologue APC2, which shares many structural similarities with APC, led to the hypothesis that these two genes may share certain functions (Nakagawa et al. 1998; Van Es et al. 1999). One of these structural similarities, the presence of a 20-amino acid repeat motif, was shown to be capable of binding β-catenin, and as a result APC2 is capable of depleting the levels of intracellular β-catenin, albeit less efficiently than APC (Nakagawa et al. 1998). The drosophila homologue of Apc2 has also been shown to rescue mis-expression of Wnt-target genes due to loss of Apc (Kunttas-Tatli *et al.* 2012), and in *APC* deficient colorectal cancer cell lines, transient expression of *APC2* was shown to result in a reduced TCF-Topflash readout equivalent to that seen as a result of transient expression of *APC* (Van Es et al. 1999).

As well as a potential role as a negative regulator of Wnt-signalling, either in co-operation with or independently from APC, it has emerged that APC2 may play a role as a tumour suppressor independently from APC.

APC2 has been fine mapped to a region of chromosome 19p13.3, which contains the markers *D19S883* and *WI-19632*, which are frequently lost in a range of different cancer types, most markedly in ovarian cancer (Jarrett *et al.* 2001; Sobottka *et al.* 2000). Patients with Peutz-Jeghers syndrome (PJS), a heritable condition causing multiple intestinal polyps and increasing susceptibility to colon cancer, are missing this chromosome region. PJS patients also show an increased susceptibility to a range of other cancer types including breast, ovarian and testis. Loss of heterozygosity (LOH) of this region of chromosome 19p13.3 is also observed in certain sporadic cancers (Sobottka et al. 2000).

Despite the rarity of known *APC2* mutations, loss of gene function can occur through other mechanisms. Epigenetic regulation of gene expression by methylation is an extremely important means of controlling gene expression. Methylation is a process by which a methyl group is attached to a CpG sequence in the gene's promoter region, thereby preventing transcription of the gene, and is an essential process during

development. Hypermethylation of tumour suppressor gene promoters is commonly seen in a variety of cancers and is how many of these genes are down regulated without having been identified as commonly mutated (Baylin 2005; Das and Singal 2004; Ehrlich 2002).

Hypermethylation of *APC2* has been recorded in a number of different cancer types including neurological, breast and colorectal cancer (Nakagawa et al. 1998; Schuebel *et al.* 2007). Interestingly, hypermethylation of *APC2* is also associated with the progression from inflammatory bowel disease (IBD) to IBD associated neoplasia (Dhir *et al.* 2008). Chan *et al*. demonstrated that hypermethylation of *APC2* was seen in 100% of primary colon tumours and that increased methylation directly correlated with a decrease in levels of APC2 protein (Chan *et al.* 2008). Studies by (Mokarram *et al.* 2009) confirmed that hypermethylation of *APC2* occurs in 90-98% of colorectal tumour samples. Hypermethylation is associated with decreased gene expression, and previous work within our laboratory has shown that APC2 expression is indeed significantly down regulated in human colorectal tumours (Figure 5.1).

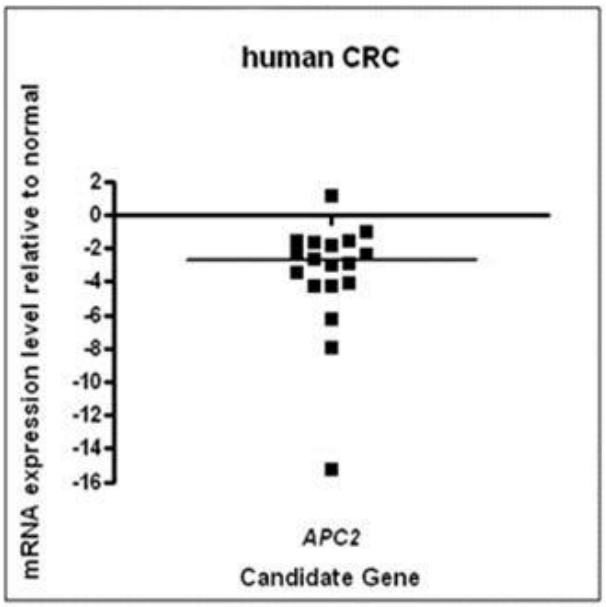

5.1 Expression of *Apc2* is downregulated in the majority of human colorectal cancers. Median fold change -2.754, $p<0.01$. Tumour samples and qRT-PCR analysis courtesy of Fei Song.

Despite the embryonic lethality of a constitutive knockout of *Apc* in mice (Moser *et al.* 1995), a constitutive *Apc2* mutant is viable, and such a mouse was produced by Professor Hans Clevers' laboratory and gifted to us for analysis of the intestinal phenotype. The *Apc2*$^{-/-}$ mouse was produced by the insertion of a stop codon into the open reading frame of the gene, resulting in a shortened protein which is lacking the β-catenin and axin binding sites (Van der Meer et al. 2001).

Previous work conducted by Carl Daly within this laboratory has shown that loss of *Apc2* in the mouse results in no obvious phenotype and no change in the numbers of differentiated cell types, but does result in an increase in expression of Wnt target genes, and an increase in nuclear β-catenin (Daly 2013). However, despite this increase in Wnt-signalling levels, it was shown that in *Apc*$^{fl/+}$ mice, additional loss of *Apc2* had no effect on survival or tumour burden. This unexpected result highlights the need for a thorough examination of the *Apc2*$^{-/-}$ phenotype, alone and in the context of homozygous *Apc* deletion, especially with regards to the intestinal stem cell compartment.

5.2 Results

5.3 Analysis of Apc2$^{-/-}$ intestinal phenotype in vivo and in vitro

5.3.1 Apc2 loss results in significantly shorter crypt lengths

Despite no obvious difference in structure of the intestinal crypts between wildtype and *Apc2*$^{-/-}$ crypts (Figure 5.2), cell counts revealed that loss of *Apc2* results in significantly shorter crypt lengths (24.9±1.97 for *Apc2*$^{-/-}$ compared to 28.1±1.25 for wildtype, $p<0.05$) (Figure 5.3). There was no significant difference observed in the length of villi between the two genotypes.

5.3.2 Apc2 loss does not affect levels of apoptosis or mitosis but does alter the location of apoptotic bodies

As levels of apoptosis and mitosis are reportedly increased due to loss of *Apc in vivo*, increases in the levels of cell death and proliferation are seen as early markers of Wnt-activation (Sansom et al. 2004b). Using H&E slides the apoptotic and mitotic indices were calculated by counting the number of apoptotic and mitotic bodies per 50 half crypts and then calculating the percentage of these cells based on average crypt length. It was found that *Apc2* loss has no effect on levels of mitotic cells (Figure 5.4), or their position (Figure 5.5). Interestingly, previous work performed by Carl Daly showed that uptake of BrDU in a two hour period was increased by loss of *Apc2* (data not shown), indicating an increase in cells at "S" phase of mitosis.

There was a trend for increased apoptosis in the *Apc2*$^{-/-}$ mice (wildtype 0.55±0.37, Apc2$^{-/-}$ 0.93±0.4) (Figure 5.6), however this was not significant (Independent sample T-test $p=0.166$). Positional information on the location of the apoptotic bodies showed that loss of *Apc2* resulted in apoptosis occurring further down the crypt towards the stem cell compartment than seen in wildtype (Figure 5.7). This change in location was found to be significant using the Kolmogorov-Smirnov Z test ($p=0.042$).

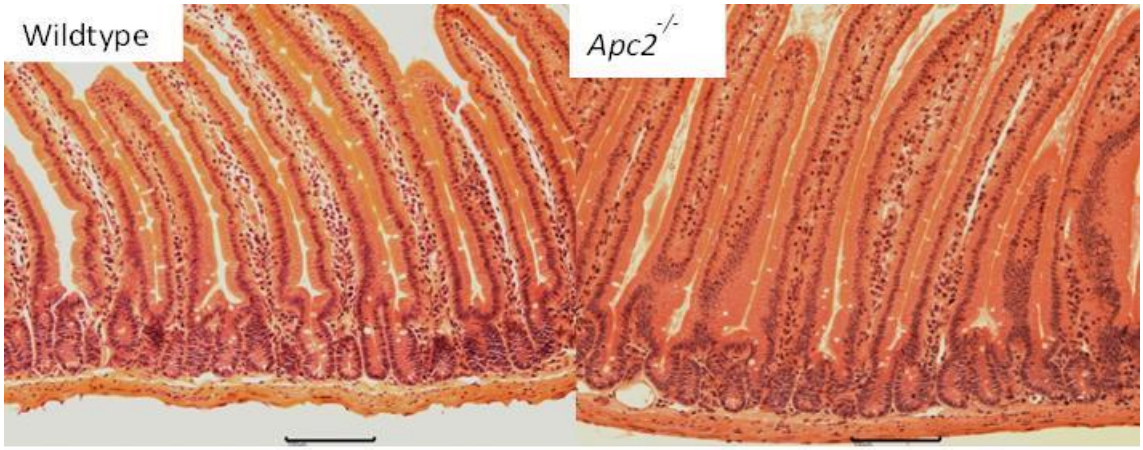

5.2 H&E of crypt villus structure of wildtype and *Apc2*$^{-/-}$ intestine. There is no gross intestinal phenotype observed due to loss of *Apc2.* Black bars indicate 100μm.

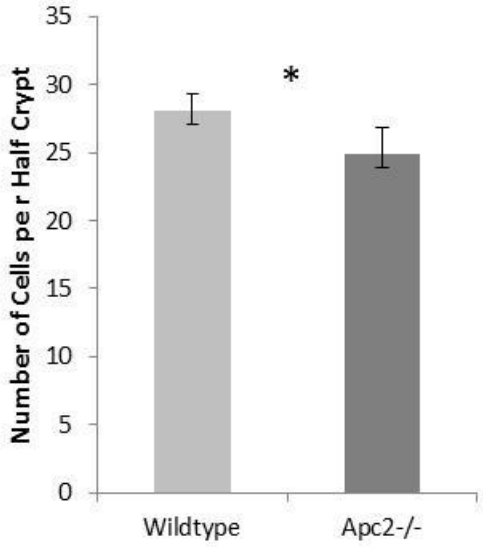

5.3 Cell counts for wildtype and *Apc2*$^{-/-}$ intestinal crypts. There was a significant decrease in crypt cell number due to loss of *Apc2*. Two tailed T-test p=0.016. N>5

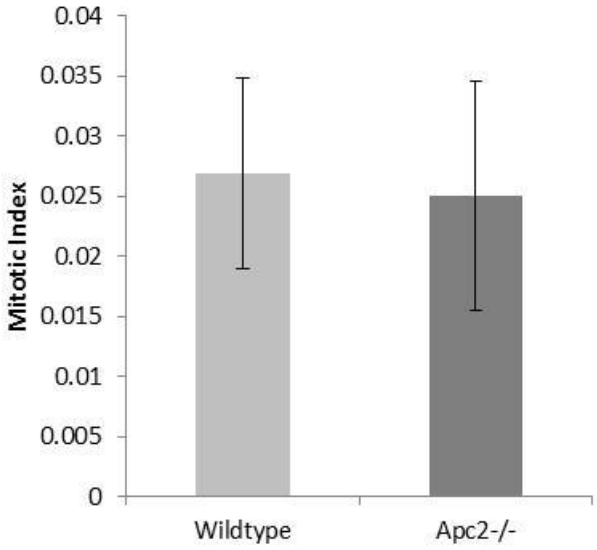

5.4 Mitotic Index of wildtype versus *Apc2*$^{-/-}$ crypts. This was calculated by counting the number of mitotic bodies per crypt and normalising it to the number of cells per crypt. No significant difference was seen in the mitotic index between the two genotypes, two tailed T-test p=0.782. N>5.

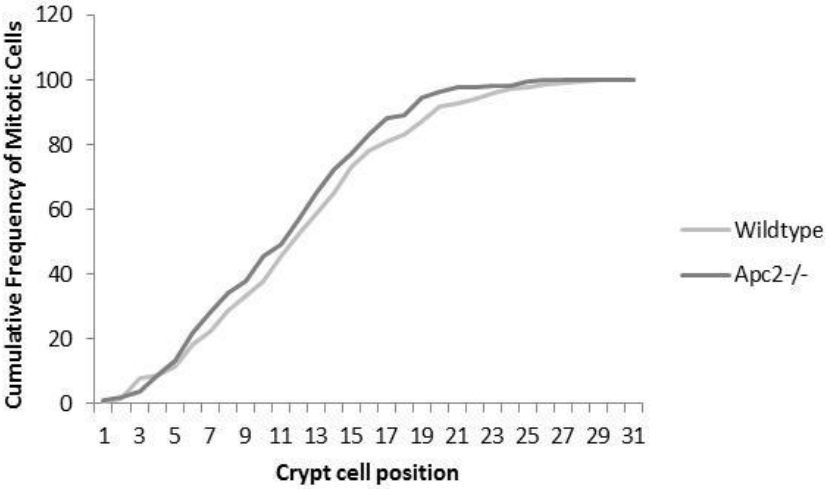

5.5 Cumulative distribution of mitotic cells within the intestinal crypt of wildtype and *Apc2*$^{-/-}$ mice. The positions were not significantly different, Kolmogorov-Smirnov Z-test p=0.072. N>5.

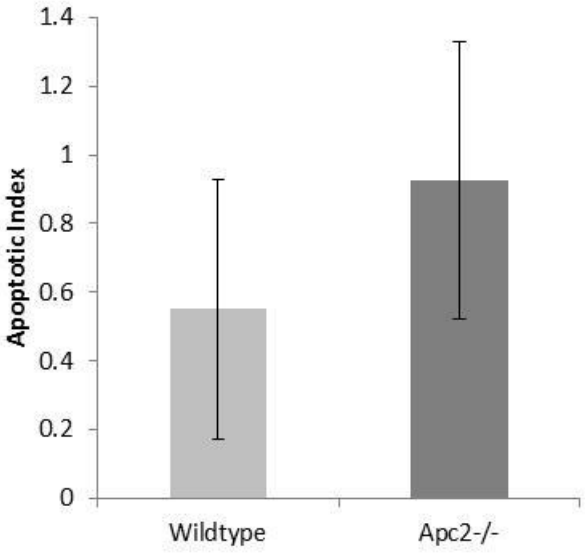

5.6 Apoptotic Index of wildtype versus *Apc2*$^{-/-}$ crypts. This was calculated by counting the number of apoptotic bodies per crypt and normalising it to the number of cells per crypt. No significant difference was seen in the mitotic index between the two genotypes, two tailed T-test p=0.166. N>5.

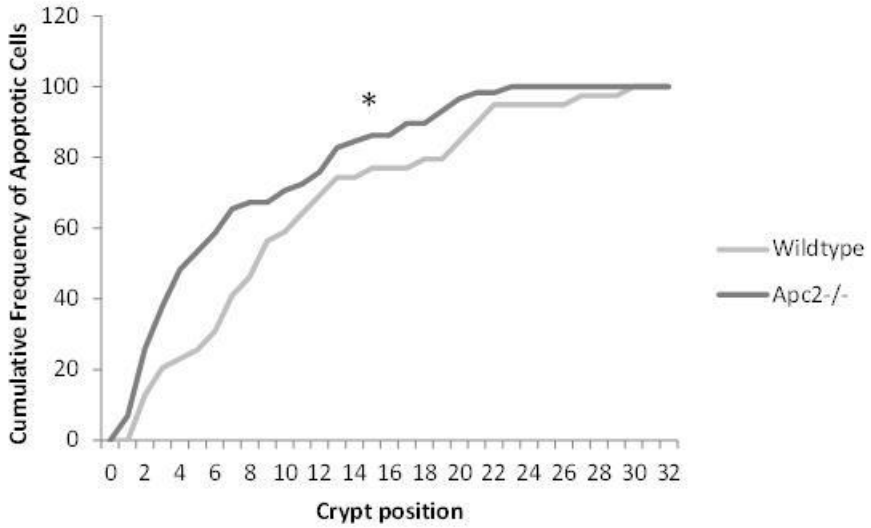

5.7 Cumulative distribution of apoptotic cells within the intestinal crypt of wildtype and *Apc2*$^{-/-}$ mice. The positions were significantly different Kolmogorov-Smirnov Z-test p=0.042.

5.3.3 Loss of Apc2 results in an increased level of Wnt-signalling within the intestinal epithelium

Loss of *Apc* from the intestinal epithelium results in a failure to form the β-catenin destruction complex, leading to a build-up of nuclear β-catenin and increased Wnt-signalling. This increase in Wnt-signalling is thought to be responsible for the severity of the $Apc^{flox/flox}$ phenotype, as additional loss of the Wnt-target *C-myc* attenuates the phenotype (Sansom et al. 2007; Wilkins and Sansom 2008). It was predicted that loss of Apc2, which can also bind β-catenin, would also result in increased expression of a range of Wnt-target genes.

Intestinal epithelium was extracted using the Weiser preparation method (see section 2.6.7) and RNA extracted for qRT-PCR analysis. This enabled the investigation of the effect of loss of *Apc2* on Wnt-signalling levels specifically within the intestinal epithelia without interference from the stromal or muscle compartments of the intestine. However, it should be noted that as $Apc2^{-/-}$ is a constitutive knockout, it is also lost from these extra-epithelia compartments as well as the intestinal epithelium.

As predicted, the loss of *Apc2* results in an increased level of Wnt-signalling within the intestinal epithelium as measured by expression levels of a number of Wnt-target genes. Loss of *Apc2* resulted in a significant upregulation of *Axin2*, *Ephb3* and *C-myc* ($p<0.05$), a trend for increased expression of *CyclinD1* and *Ephb2* ($p>0.05$) and no change in expression levels of *Cd44* (Figure 5.8). These results support the observation made by Carl Daly that loss of *Apc2* results in an increased level of nuclear β-catenin (Figure 5.9).

Due to the increase in Wnt-signalling levels as a result of *Apc2* loss, the expression levels of the Wnt-inhibitors Groucho and Dikkopf were investigated. Expression of Groucho was found to be more than 4fold upregulated whereas there was no significant change in expression levels of Dikkopf (Figure 5.10).

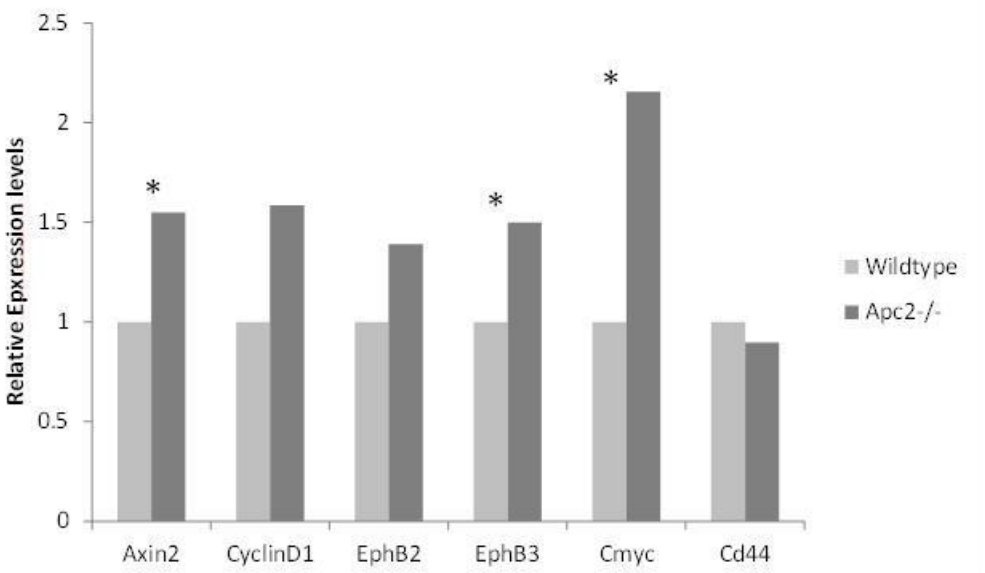

5.8 qRT-PCR results showing the relative expression levels of Wnt-target genes in wildtype and *Apc2*$^{-/-}$ intestinal epithelium. Loss of *Apc2* resulted in significant upregulation of *Axin2, Ephb3* and *Cmyc* (Two sample independent T-test p=0.0401, 0.0472 an d0.0439 respectively). N<4

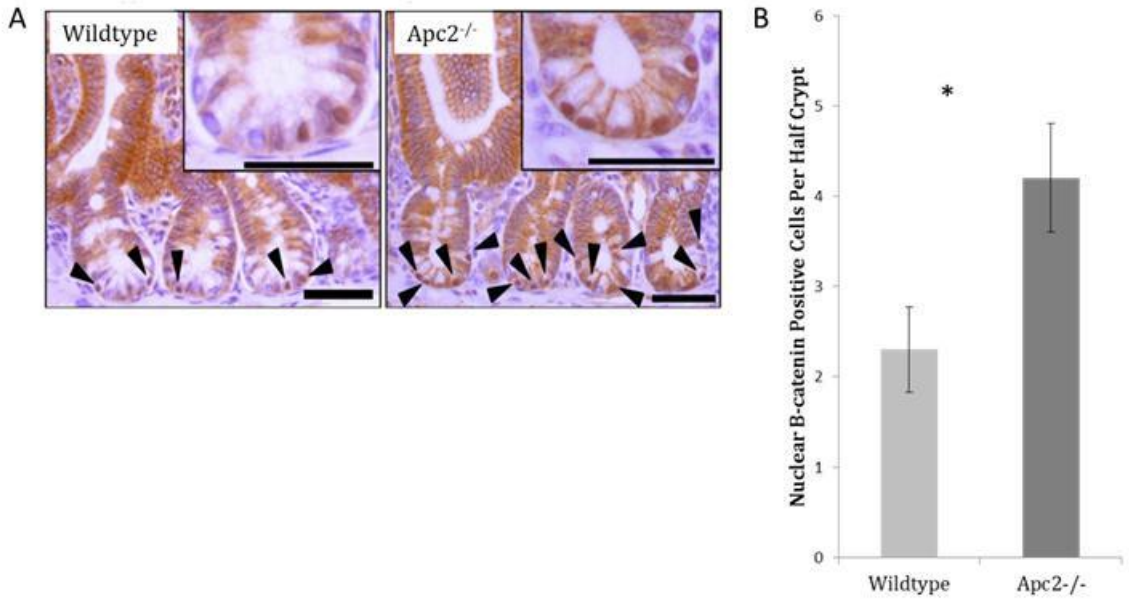

5.9 **A** Immunohistochemistry for β-catenin showing increased nuclear localisation in wildtype and *Apc2*$^{-/-}$ intestinal crypts. Black arrows indicate nuclear β-catenin, black bars represent 50μm; **B** Counts of cells with nuclear β-catenin show significantly increased levels as a result of *Apc2* loss (Mann-Whitney U-test p<0.01). IHC performed by Carl Daly.

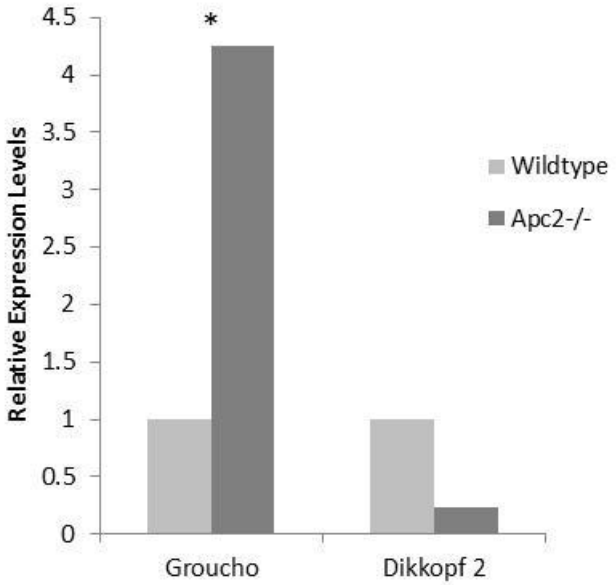

5.10 qRT-PCR results showing the relative expression levels of Wnt-inhibitor genes in wildtype and *Apc2*$^{-/-}$ intestinal epithelium. Expression of *Groucho* was found to be significantly upregulated due to *Apc2* loss (Mann-Whitney U-test p=0.27) whereas there was no significant difference in expression of *Dikkopf2*. N=4.

5.3.4 Loss of Apc2 results in an increased level of expression of intestinal stem cell markers, but no mis-localisation of expression

The importance of Wnt-signalling in the maintenance of the ISC compartment (Reya and Clevers 2005) and the observation that loss of *Apc2* results in increased nuclear β-catenin and expression of Wnt-target genes indicates that loss of *Apc2* may result in expansion of the ISC compartment.

qRT-PCR analysis examining a range of published ISC markers within the intestinal epithelium demonstrated that expression of the ISC markers Lgr5 and Ascl2 was significantly upregulated (independent sample T-test $p<0.01$). Furthermore, there was a trend for increased expression of the markers Olfm4 and Bmi1, although this was not significant at n=5 (independent sample T-test $p>0.05$). Interestingly, expression of *Msi1* was found to be more than 5 fold down regulated (independent sample T-test $p<0.05$) (Figure 5.11).

In situ hybridisation was used to assess the location of expression of the ISC markers. An anti-*Olfm4* riboprobe on paraffin embedded sections of fixed wildtype and *Apc2*$^{-/-}$ intestine, showed that expression of this representative ISC marker was still limited to the base of the intestinal crypt (Figure 5.12). It should be noted that as the *in situ* hybridisations were performed on cross-sections of the crypt-villus axis, it cannot be determined from these images whether the qRT-PCR results indicate an increased expression of stem cell markers from the same number or fewer cells, or an increase in the number of cells expressing these markers as a result of increase ISCs around the base of the crypt.

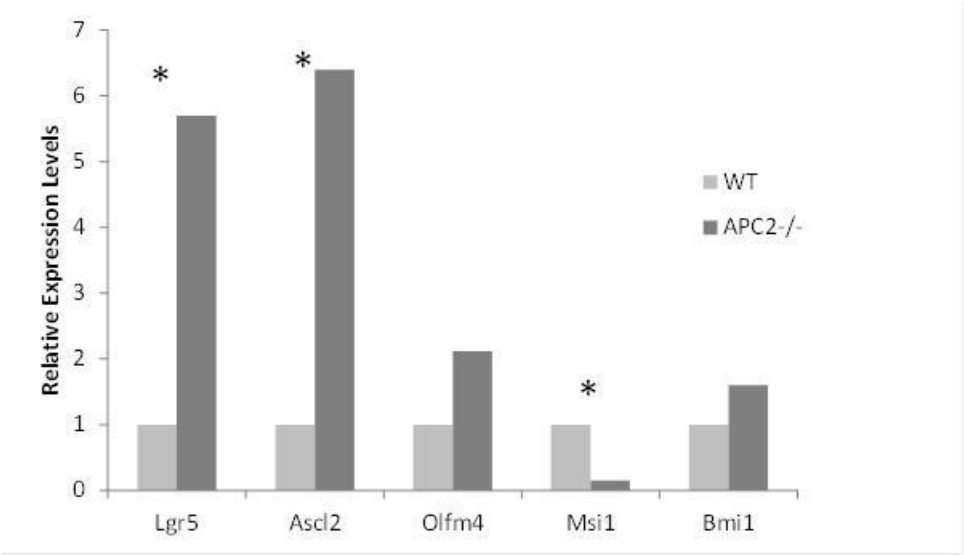

5.11 qRT-PCR results showing the relative expression levels of intestinal stem cell marker genes in wildtype and *Apc2*$^{-/-}$ intestinal epithelium. *Lgr5* and *Ascl2* were significantly upregulated due to *Apc2* loss (Independent samples T-test p=0.0089 and 0.0077 respectively) whereas *Msi1* was significantly downregulated (Independent samples T-test p=0.038). N>4

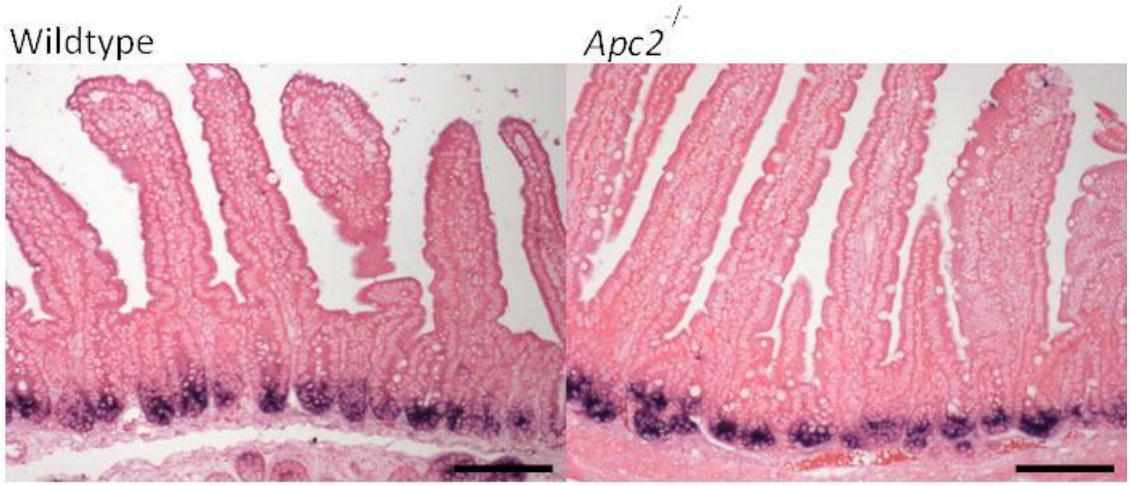

5.12 *In situ* hybridisation for *Olfm4* expression in Wildtype and *Apc2*$^{-/-}$ intestine. Expression remains limited to the crypt base. Black bars represent 100μm.

5.3.5 Apc2$^{-/-}$ organoids are phenotypically identical to wildtype

Increased expression of ISC markers and Wnt-signalling targets within the crypt due to *Apc*-loss is associated with a cyst-like phenotype when cultured *in vitro*. In order to test the level of Wnt-activation of *Apc2*$^{-/-}$ crypts by assessing their phenotype in orgnoid culture, *Apc2*$^{-/-}$ crypts were disassociated and cultured and found to form organoids with crypt like protrusions and all of the differentiated cell types in a manner phenotypically identical to wildtype (Figure 5.13). These organoids grow at the same rate as wildtype and to the same size by day 11 (Figure 5.14).

5.3.6 Apc2$^{-/-}$ crypts form organoids at a lower efficiency than wildtype

Due to increased expression of ISC markers it was predicted that *Apc2*$^{-/-}$ crypts would form organoids at a higher efficiency than wildtype. This, however, did not occur. *Apc2*$^{-/-}$ crypts form organoids only rarely with just 5.2% of crypts (±2.51) capable of forming organoids compared to 15.59% (±7.46) of wildtype (Figure 5.15). This difference was found to be significant using independent sample T-test ($p=0.014$). This indicates that loss of *Apc2* results in a reduction in functional ISCs.

5.3.7 Apc2$^{-/-}$ organoids are less dependent on R-spondin than wildtype

Both wildtype and *Apc2*$^{-/-}$ organoids were cultured in 6.5µg/ml, 3.25µg and 0µg/ml R-spondin, and it was observed that although wildtype crypts die in culture in the absence of R-spondin by day 2-3, many *Apc2*$^{-/-}$ organoids survived until day 3 and only began to die by day 4 (Figure 5.16). The Prestoblue assay, a mitochondrial activity assay used in order to test the survival of organoids at different R-spondin concentrations (see section 2.12.5), was therefore performed on both day 3 and day 4 and showed that mitochondrial activity of *Apc2*$^{-/-}$ organoids is still high in the absence of R-spondin at day 3, but has dropped to wildtype levels by day 4 (Figure 5.17). This indicates that despite an apparent decrease in the number of functional stem cells, the ISCs which remain are more highly Wnt-activated than wildtype.

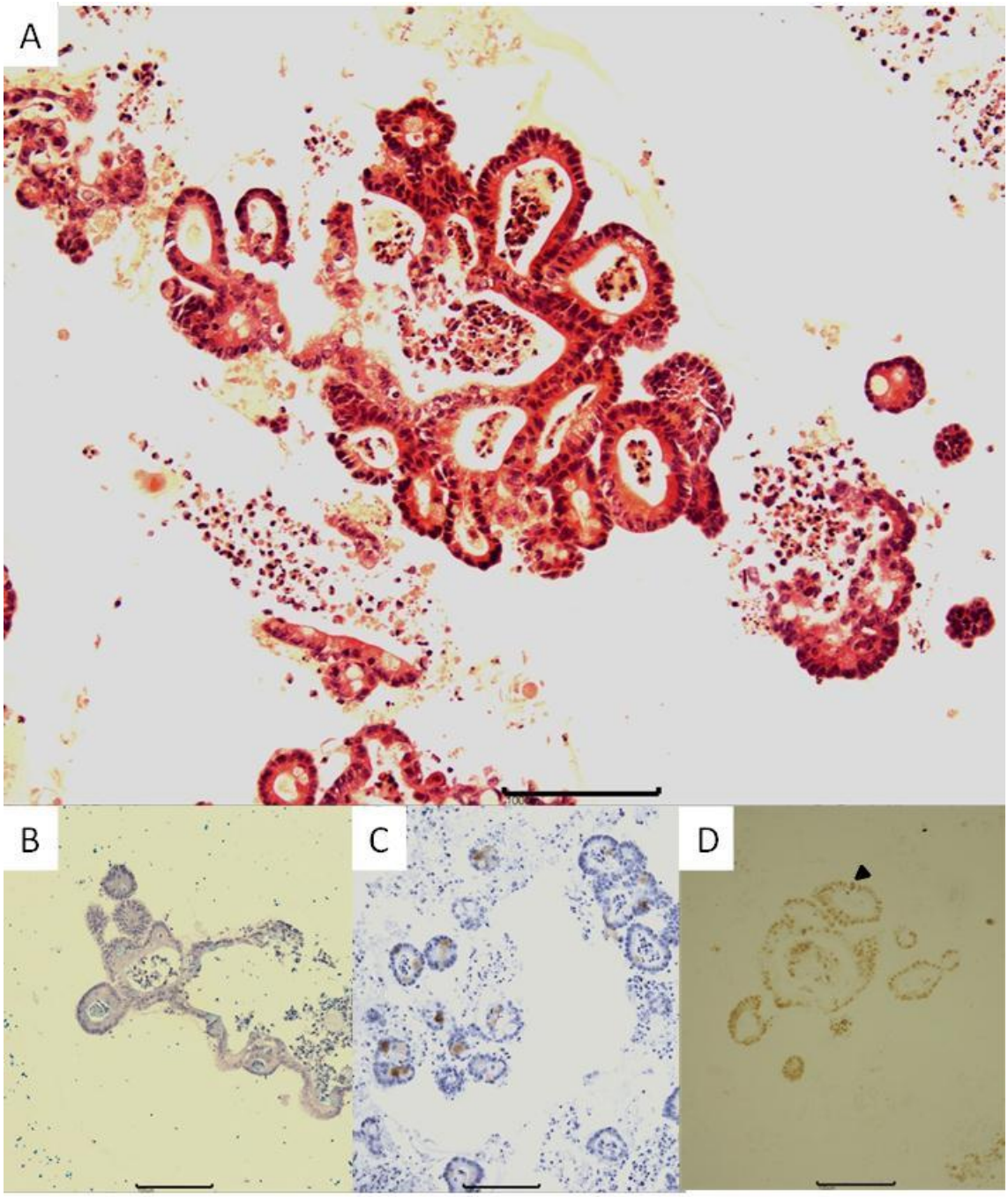

5.13 Phenotype of *Apc2*$^{-/-}$ intestinal organoids. **A**, H&E slide displaying mutliple crypt protrusions. **B**, Alcian blue stain showing presence of blue goblet cells. **C,** Lysozyme immuno of *Apc2*$^{-/-}$ organoids showing the presence of brown Paneth cells. **D**, Grimelius stain of *Apc2*$^{-/-}$ organoids showing intense staining on few rare enteroendocrine cells. Black bars represent 100μm.

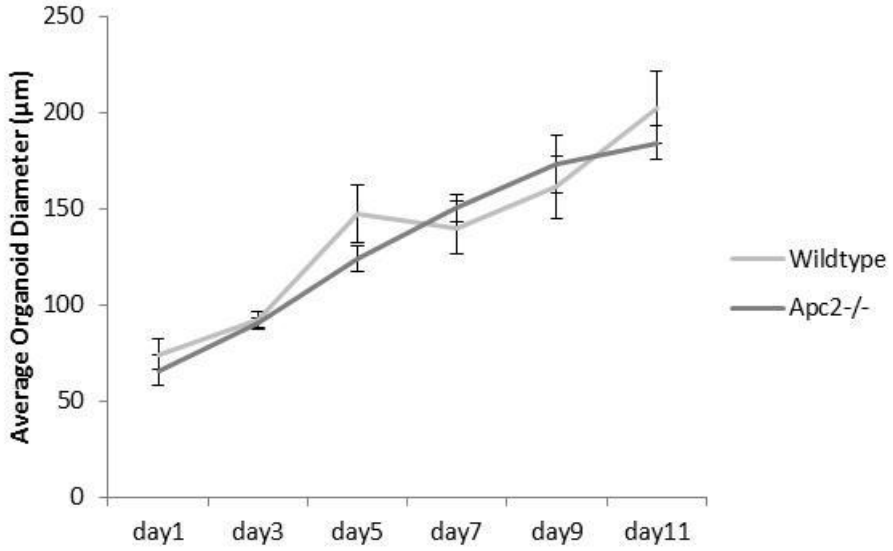

5.14 Growth rates of wildtype and *Apc2*$^{-/-}$ organoids. There was no difference between the average diameters of the organoids at any of the timepoints measured. N<20 (10 wells of organoids were measured for a minimum of 2 mice).

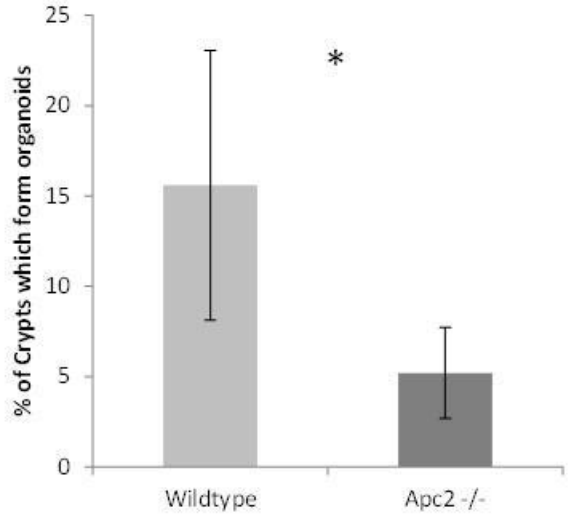

5.15 Organoid formation efficiency of wildtype and *Apc2*$^{-/-}$ crypts. *Apc2*$^{-/-}$ crypts formed organoids significantly less efficiently than wildtype (Independent sample T-test p=0.014). n>5.

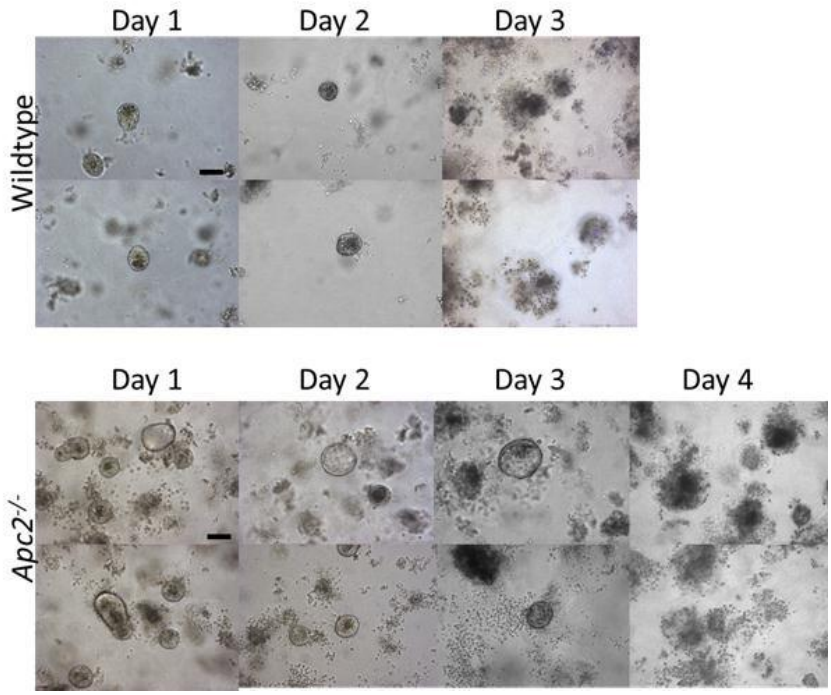

5.16 Wildtype crypts die by day 3 post seeding in the absence of R-spondin, whereas *Apc2*$^{-/-}$ crypts survive until day 4. Black bars represent 50µm.

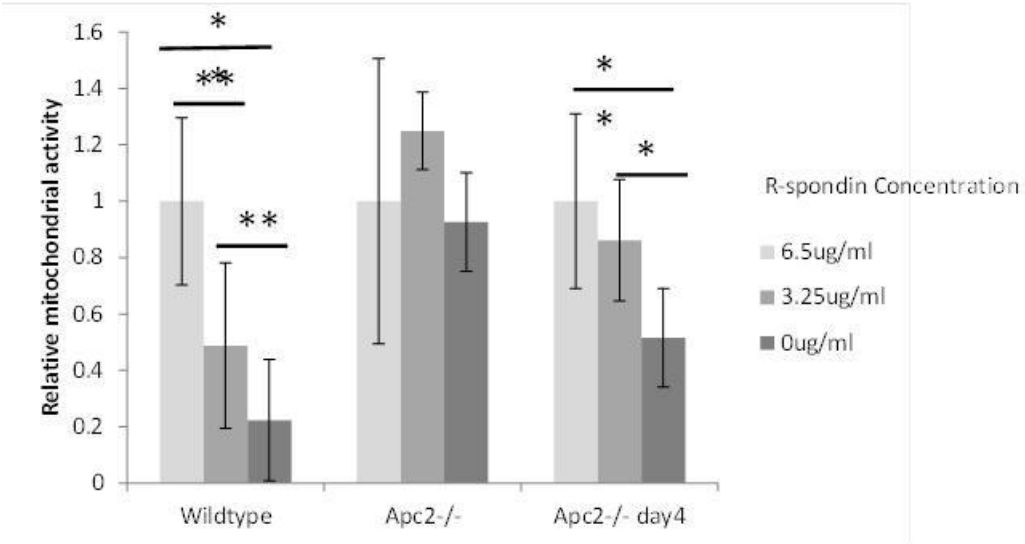

5.17 Prestoblue assay showing the mitochondrial activity of wildtype and *Apc2*$^{-/-}$ organoids day 3 post seeding as well as *Apc2*$^{-/-}$ organoids at day 4 in various R-spondin concentrations. The relative mitochondrial activity of wildtype organoids at day 3 responded to R-spondin concentration in a dose dependent manner, whereas *Apc2*$^{-/-}$ organoids do not show a response to R-spondin concentration via a change in mitochondrial activity at day 3, but did show a dose dependent response by day 4. Using independent samples T-test, * represents p,0.05 and ** represents p<0.01.

5.4 *Analysis of Apc2$^{-/-}$ intestinal phenotype in the context of Apc homozygous deletion, in vivo and in vitro*

As the loss of *Apc2* appears to result in a reduced yet more highly activated ISC compartment, it could be assumed that there would be some effect on Wnt-dependent tumourigenesis. As was observed previously in the lab, loss of *Apc2* does not affect tumour burden or survival of *Apc$^{fl/+}$* mice (Daly 2013). In order to further elucidate the role of *Apc2* in intestinal tumourigenesis, it was necessary to investigate the effect of *Apc2* loss on the early phenotype of intestinal tumourigenesis. The model used to recapitulate the early phenotype of intestinal tumourigenesis is the *Villin-CreER^{+} Apc$^{flox/flox}$* mouse, whereby *Apc* is homozygously deleted from the intestinal epithelium upon injection with tamoxifen. It has been previously published that loss of *Apc* from the intestine results in an increase in Wnt-signalling, an increase in apoptosis and mitosis and an increase of undifferentiated cell types (Sansom et al. 2004b). As previously shown in section 3.11, this expansion of undifferentiated cell types and increase in expression of ISC markers is associated with an increased efficiency of organoid formation.

Here we used two cohorts of mice, *Villin-CreER^{+} Apc$^{flox/flox}$ Apc2$^{wt/wt}$* (referred to as *Apc$^{flox/flox}$*) and *Villin-CreER^{+} Apc$^{flox/flox}$ Apc2$^{-/-}$* (referred to as *Apc$^{flox/flox}$ Apc2$^{-/-}$* or double mutants). Mice were induced using tamoxifen and sacrificed at day 4. For the purposes of the organoid experiments they were sacrificed on day 3.

Previous work within the laboratory has shown that additional loss of *Apc2* resulted in an increased survival of *Apc$^{flox/flox}$* mice post induction. Conditional homozygous loss of Apc alone using Villin-CreER resulted in a median survival of 4.5 days (n=8), whereas additional loss of Apc2 extended the median survival to 6 days (n=5) (Figure5.18). In order to understand the mechanism by which Apc2 loss increases survival in Apc$^{flox/flox}$ mice, the intestinal phenotype of both cohorts were closely analysed.

5.4.1 *Additional loss of Apc2 does not alter the intestinal morphology resulting from Apc deletion*

The increased survival observed in double mutants indicates that disregulation of the intestinal tissue may not be as severe as that seen due to Apc loss alone. As loss of Apc results in loss of distinct crypt structures the crypt length cannot be measured (Sansom

et al. 2004b). In order to overcome this problem, the severity of tissue disregulation was assessed by counting the number of cells in the aberrant region of the intestinal tissue in a straight line from bottom to top (Figure 5.19). 50 half "crypts" were counted per mouse and a minimum of 5 mice were counted. The aberrant region can be identified by the disordered, larger cells which stain slightly darker using H&E (as indicated in Figure 5.19). There was no significant difference in number of cells in the region of aberrant proliferation between genotype on day 4 post induction (Figure 5.20). However, further counts of the number of cells in the zones of abberant proliferation within the crypt show that by day5 post induction, the region of aberrant proliferation is significantly shorter by day 5 post induction (Figure 5.21).

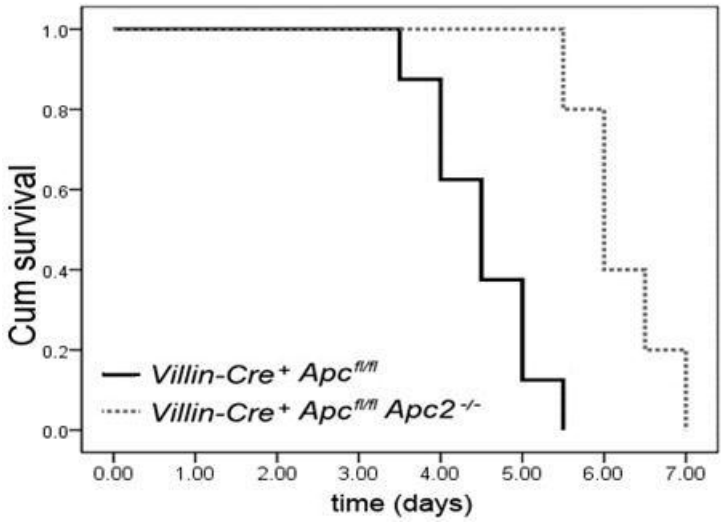

5.18 Cumulative survival plot of *Apc*$^{flox/flox}$ and *Apc*$^{flox/flox}$ *Apc2*$^{-/-}$ mice post tamoxifen induction. Median lifespan was increased by 1.5 days by additional *Apc2* mutation. Work conducted by Carl Daly.

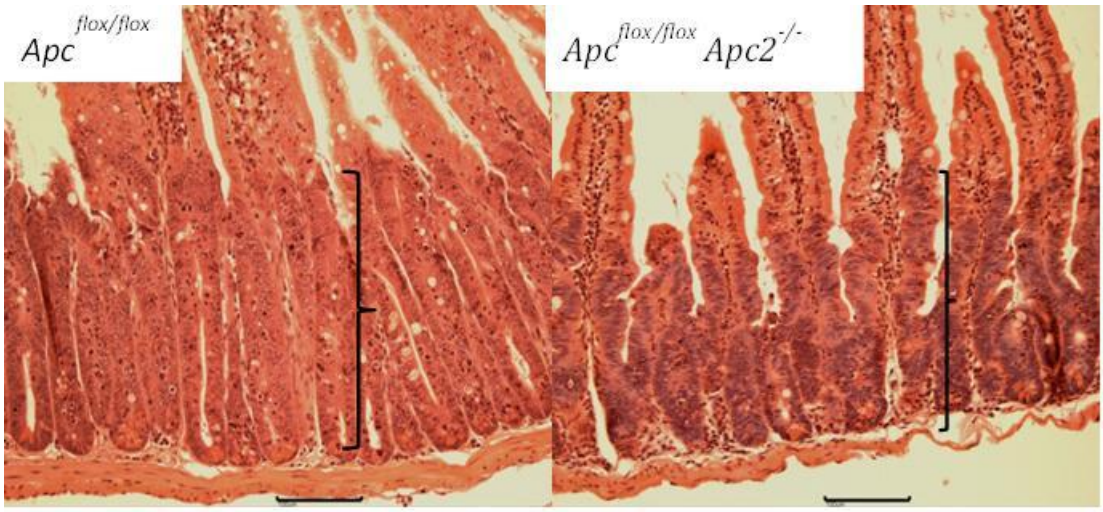

5.19 H&Es of *Apc*$^{flox/flox}$ and *Apc*$^{flox/flox}$ *Apc2*$^{-/-}$ intestine at day 4 post induction. The vertical black bars indicate the region of aberrant proliferation, with darker, disordered and undifferentiated cells with unpolarised nuclei. The scale bar represents 100μm.

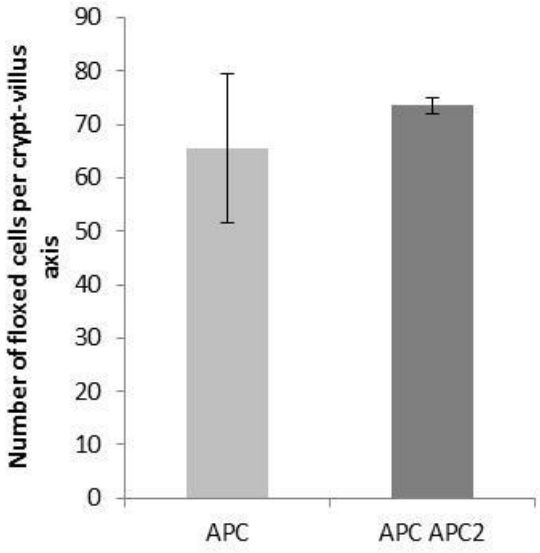

5.20 Number of cells in the region of aberrant proliferation per crypt-villus region of *Apc*$^{flox/flox}$ (Apc) and *Apc*$^{flox/flox}$ *Apc2*$^{-/-}$ (ApcApc2) intestine at day 4 post induction. The number of cells in a direct line from the crypt base to the top of the visible region of aberrant proliferation were counted. There was no significant difference between the two genotypes. N=4

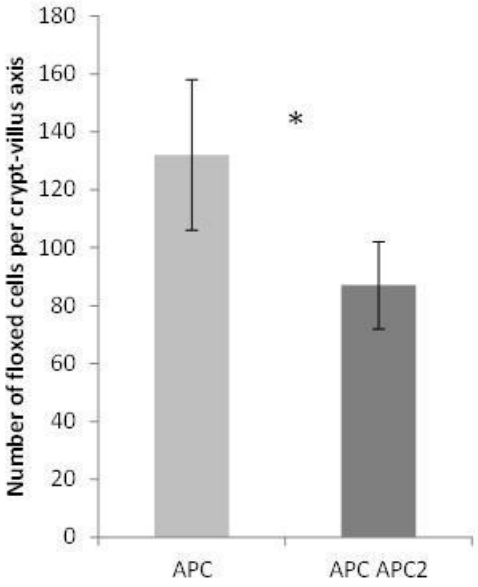

5.21 Number of cells in the region of aberrant proliferation per crypt-villus region of *Apc*$^{flox/flox}$ (Apc) and *Apc*$^{flox/flox}$ *Apc*$^{-/-}$ (ApcApc2) intestine at day 5 post induction. Additional deletion of *Apc2* resulted in a significant decrease in the number of cells within the region of aberrant proliferation by day 5 (Mann-Whitney p=0.016). N=3.

5.4.2 Additional loss of Apc2 results in increased apoptosis

There was no change in levels of mitosis (Figure 5.22) or location of mitotic bodies (Figure 5.23) as a result of the additional loss of *Apc2*.

The increase in apoptosis which is observed after the *Apc* loss *in vivo* is a result of increased proliferation and genetic damage, resulting in more cell death, and appears to be a natural defence mechanism against increased Wnt-signalling which is not potent enough to override the phenotype. This effect is augmented in the double mutants resulting in even higher levels of apoptosis as measured by the number of apoptotic bodies counted in the region of aberrant proliferation in 50 crypts/villus structures (Figure 5.24). The number of apoptotic bodies was normalised to account for the average number of cells within this region to produce an apoptotic index. Interestingly, apoptosis was found to be significantly higher up the crypt-villus axis (Figure 5.25).

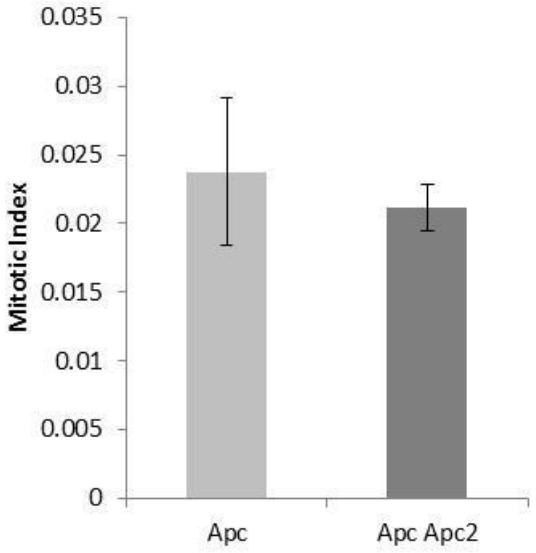

5.22 Mitotic Index of *Apc*$^{flox/flox}$ versus *Apc*$^{flox/flox}$ *Apc2*$^{-/-}$. Counts were normalised using the average number of cells per region of aberrant proliferation. There was no significant difference between the two genotypes (Independent sample T-test p=0.402). N=4.

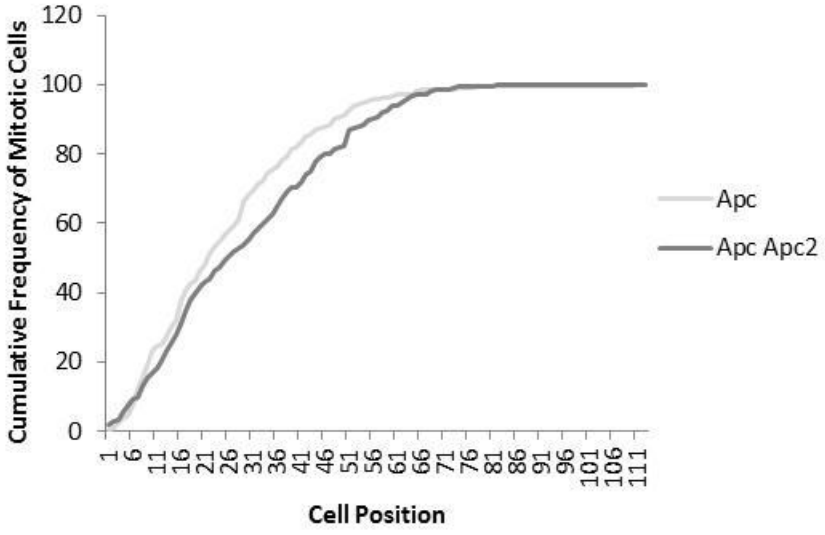

5.23 Cumulative frequency graph showing the location of mitotic bodies within the region of aberrant proliferation of *Apc*$^{flox/flox}$ (Apc) and *Apc*$^{flox/flox}$ *Apc2*$^{-/-}$ (ApcApc2) intestines. There was no significant difference in the location of mitotic bodies between the two genotypes using Kolmogorov-Smirnov Z-test p=0.074. N=4.

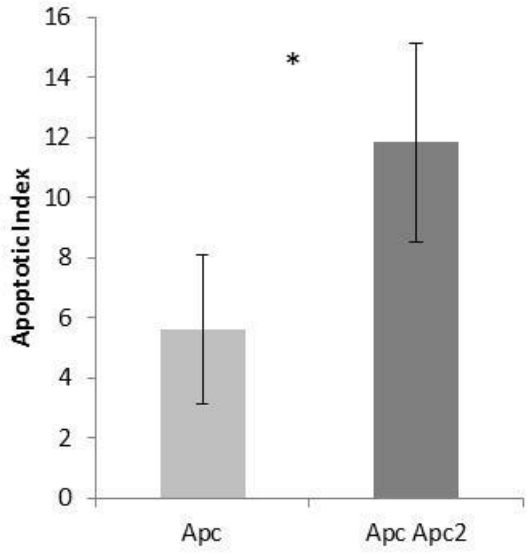

5.24 Apoptotic Index of *Apc*$^{flox/flox}$ versus *Apc*$^{flox/flox}$ *Apc2*$^{-/-}$ at day 4 post induction. Counts were normalised using the average number of cells within the region of aberrant proliferation. Additional loss of *Apc2* resulted in a significant increase in apoptosis (independent sample T-test, p=0.034). N=4.

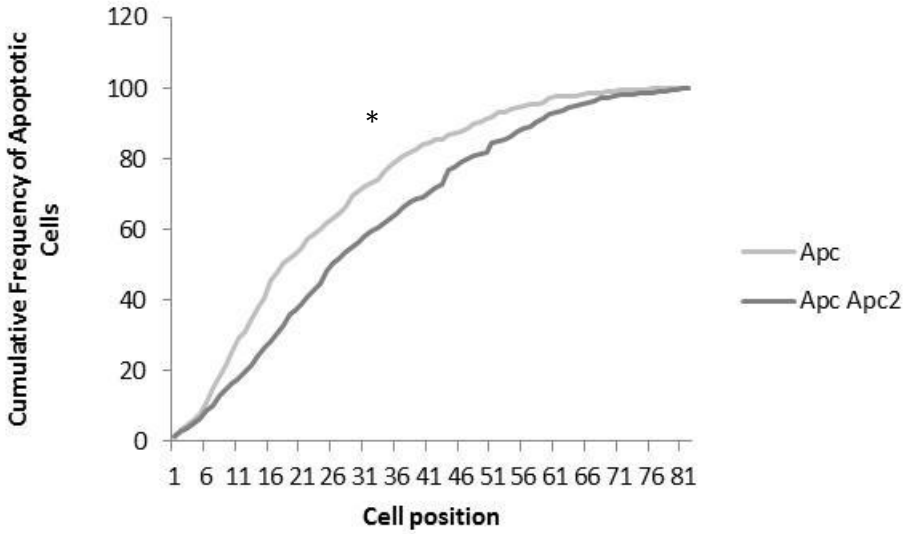

5.25 Cumulative frequency graph showing the location of apoptotic bodies within the region of aberrant proliferation of *Apc*$^{flox/flox}$ (Apc) and *Apc*$^{flox/flox}$ *Apc2*$^{-/-}$ (ApcApc2) intestines. The Kolmogorov-Smirnov Z-test showed that additional loss of *Apc2* resulted in apoptosis occurring further up the crypt-villus axis in *Apc*$^{flox/flox}$ mice (p=0.042). N=4.

5.4.3 Additional loss of Apc2 attenuates the increased Wnt-signalling phenotype of $Apc^{flox/flox}$ mutants

As loss of *Apc2* alone results in a small increase in Wnt signalling, and *Apc* loss results in a large increase in Wnt-signalling, it was predicted that combined loss of *Apc2* and *Apc* would result in augmented expression of Wnt-target genes. Interestingly, combined loss of *Apc* and *Apc2* resulted in an attenuated Wnt-signalling phenotype compared to that of *Apc* alone (Figure 5.26). The Wnt-target genes *Axin2*, *EphB2*, *Cmyc* and *Cd44* were all expressed at a significantly lower level in double mutants than in $Apc^{flox/flox}$ intestinal epithelia (Independent sample T-test $p<0.05$), whereas there was no significant difference in expression levels of *EphB3* and *CyclinD1*.

5.4.4 Additional loss of Apc2 attenuates expansion of the ISC compartment associated with Apc loss

As previously discussed, loss of *Apc* results in an expansion of the ISC compartment, with an increase in undifferentiated cell types, an increase in expression of ISC markers and a mis-localisation of expression of the stem cell markers *Ascl2* and *Olfm4*. qRT-PCR analysis of cDNA synthesised from RNA extracted from epithelial cell extracts from $Apc^{flox/flox}$ mutants and double mutants reveals that additional loss of *Apc2* results in reduced expression of the ISC markers *Ascl2*, *Olfm4* and *Msi-1* ($p<0.05$) with no change in expression of *Lgr5* or *Bmi-1* at n=5 (Figure 5.27).

In situ hybridisations for *Olfm4* revealed that the expression of *Olfm4* in double mutants is still mislocalised, but both the mislocalisation of expression and the intensity of the staining do not appear as severe as seen in the $Apc^{flox/flox}$ gut alone (Figure 5.28). The images shown are representative of the genotypes (n=3), however, as *in situ* hybridisation is not quantifiable it is impossible to say if this difference is significant.

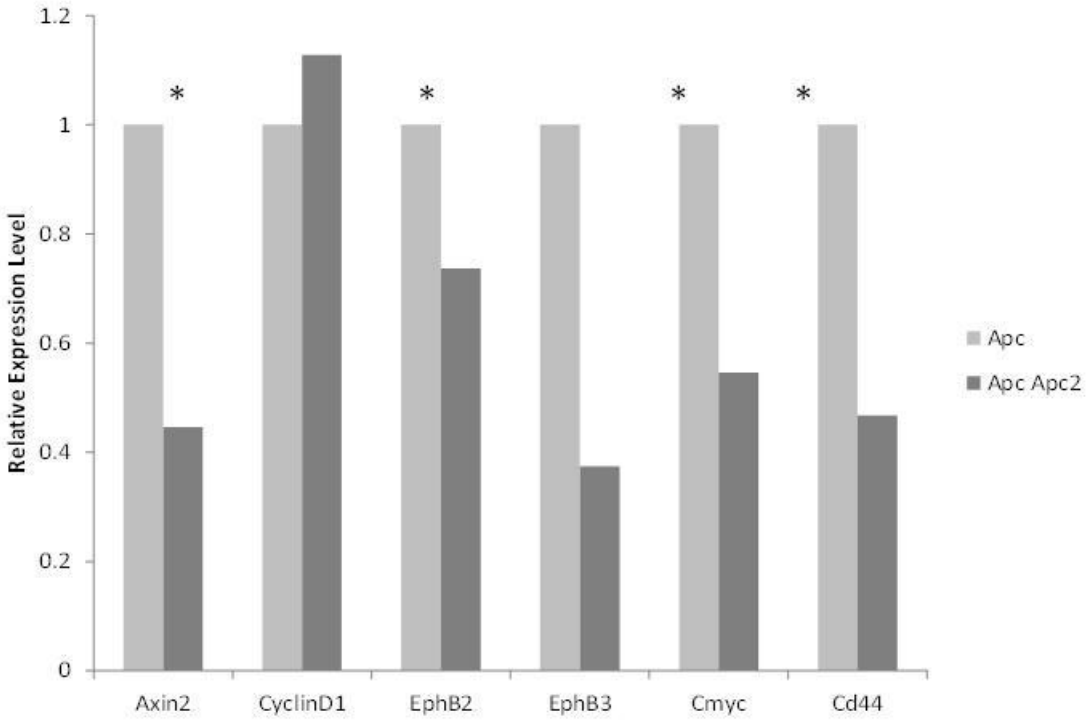

5.26 qRT-PCR results showing the relative expression levels of Wnt-target genes in *Apc*$^{flox/flox}$ (Apc) and *Apc*$^{flox/flox}$ *Apc2*$^{-/-}$ (Apc Apc2) intestinal epithelium. Additional loss of Apc2 resulted in significant down-regulation of the Wnt-targets *Axin2, EphB2, Cmyc* and *Cd44*, independent sample T-test p=0.02, 0.046, 0.046 and 0.034 respectively. N=5.

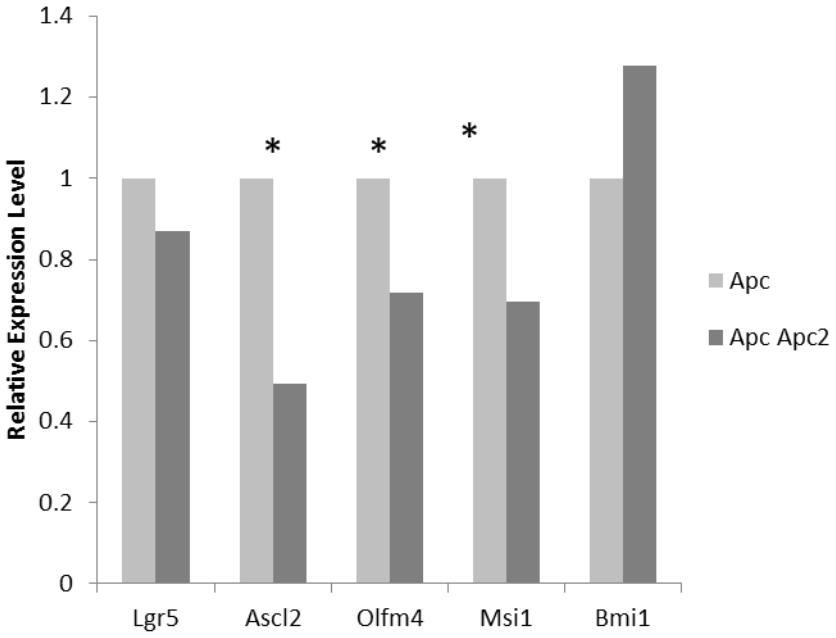

5.27 qRT-PCR results showing the relative expression levels of ISC marker genes in *Apc*$^{flox/flox}$ (Apc) and *Apc*$^{flox/flox}$ *Apc2*$^{-/-}$ (Apc Apc2) intestinal epithelium. *Ascl2, Olfm4* and *Msi1* expression are all significantly lower due to additional loss of *Apc2* independent sample T-test p=0.047,0.029 and 0.04 respectively. N=5.

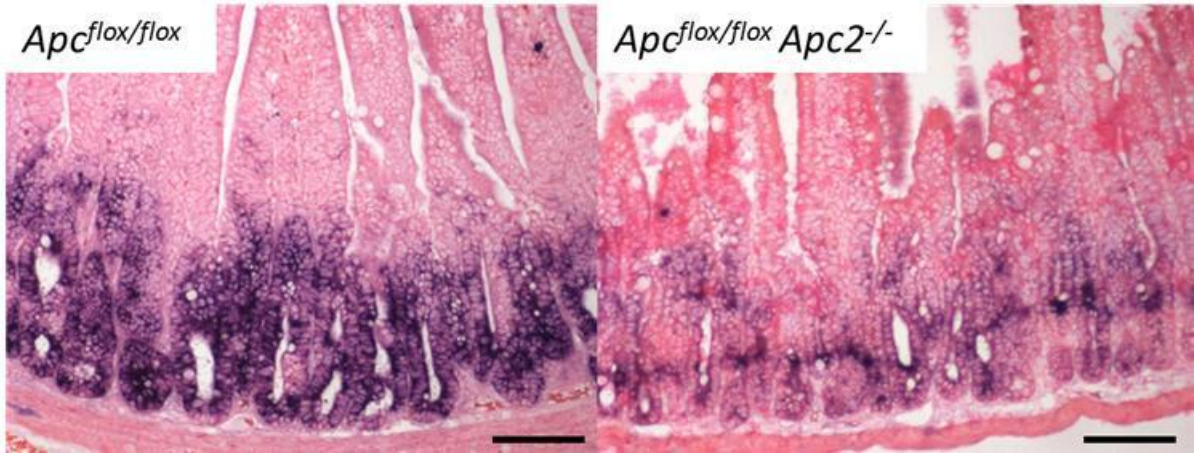

5.28 *In situ* hybridisation for *Olfm4* expression in *Apc*$^{flox/flox}$ and *Apc*$^{flox/flox}$*Apc2*$^{-/-}$ intestine. Expression is still mis-localised due to *Apc* loss, but intensity of staining is dramatically reduced due to additional *Apc2* deletion. Black bars represent 100μm.

5.4.5 Organoids derived from Apc$^{flox/flox}$ Apc2$^{-/-}$ crypts are phenotypically identical to Apc$^{flox/flox}$ organoids

In order to assess any changes in the number functional stem cells using the organoid formation assay, it was necessary to determine which of the CHARM settings (the parameters used to define an organoid on the GelCount machine which vary between wildtype and *Apc$^{flox/flox}$* –like organoids, see section 2.12.4) to use in order to analyse the organoids. This required establishing whether the organoids formed from *Apc$^{flox/flox}$Apc2$^{-/-}$* crypts were more like *Apc$^{flox/flox}$* organoids (large, cyst-like with few differentiated cell types) or more like wildtype organoids with discrete crypt protrusions containing all of the differentiated cell types.

Organoids derived from double mutant mice, were instantly recognisable as similar to *Apc$^{flox/flox}$* organoids in structure and organisation (Figure 5.29) and so the *Apc$^{flox/flox}$* CHARM settings were used for their analysis. The organoids grew at the same rate as *Apc$^{flox/flox}$* and showed the same undifferentiated cell types with patches of polarised and unpolarised nuclei.

5.4.6 Apc$^{flox/flox}$Apc2$^{-/-}$ crypts form organoids less efficiently than Apc$^{flox/flox}$ crypts

Using the organoid formation assay as a readout of functional stem cell activity within the intestinal crypts showed that additional loss of *Apc2* attenuates the *Apc$^{flox/flox}$* phenotype of increased organoid formation efficiency (Figure 5.30). Interestingly, the organoid formation efficiency was not significantly higher than that of wildtype.

This indicates that the number of functional stem cells in *Apc$^{flox/flox}$* intestine is reduced by the additional loss of *Apc2*. However, as previously discussed, since the organoids formed do not present differentiated cells types it is not possible to describe them as "true" stem cells in this instance.

5.4.7 Apc$^{flox/flox}$Apc2$^{-/-}$ organoids are R-spondin independent

Using the PrestoBlue assay of relative mitochondrial activity, it was possible to demonstrate that despite double mutants having lowered Wnt-signalling levels in the intestinal epithelium, the organoids they form still retain high enough levels of Wnt-signalling to enable their survival and growth in the absence of R-spondin, and are as equally R-spondin independent as *Apc$^{flox/flox}$* organoids (Figure 5.31).

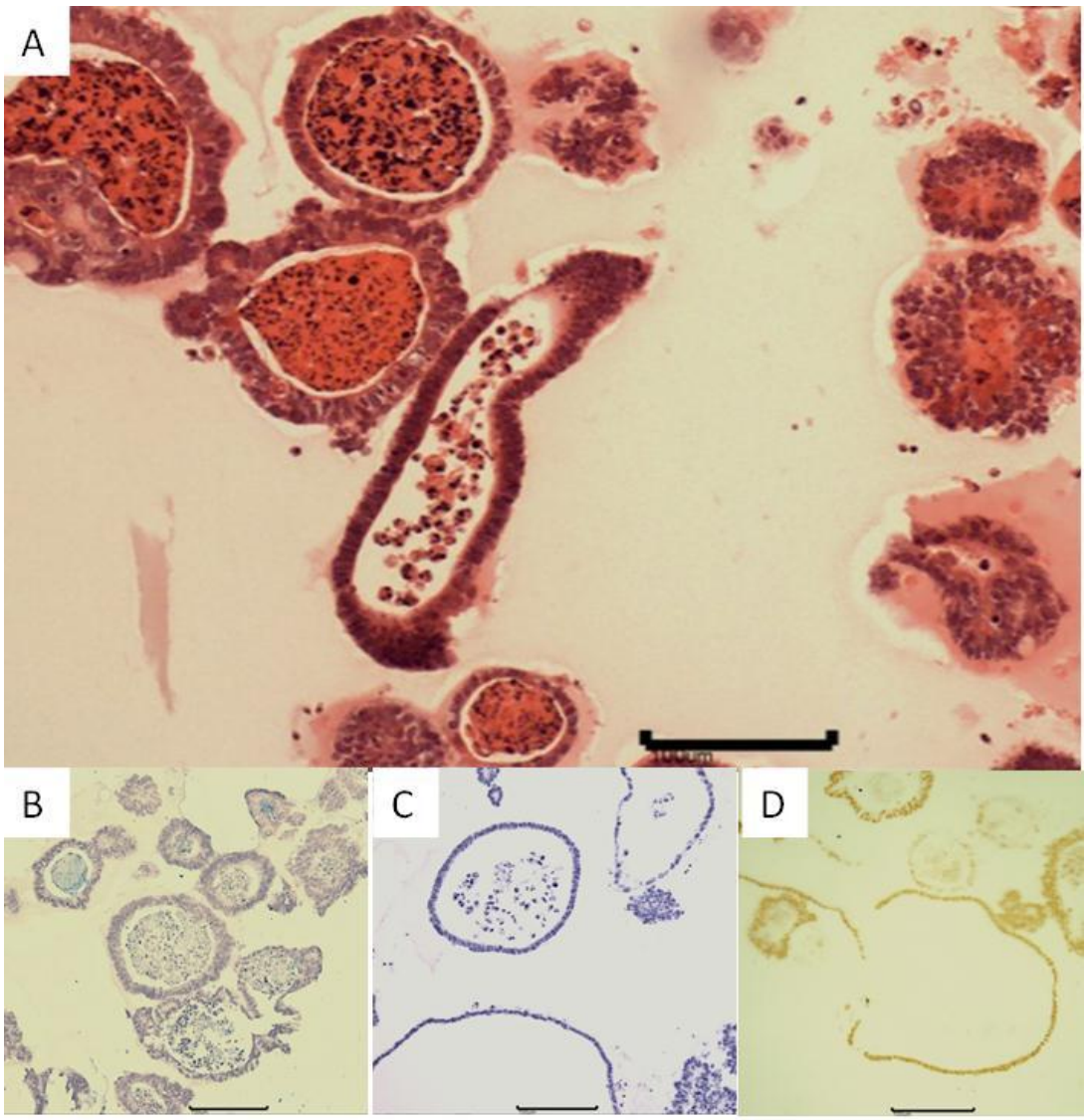

5.29 Phenotype of *Apc*$^{flox/flox}$ *Apc2-/-* intestinal organoids. A, H&E slide displaying large cyst-like organoids. B, Alcian blue stain showing no visible blue goblet cells. C, Lysozyme IHC of *Apc2*$^{-/-}$ organoids showing the absence of brown Paneth cells. D, Grimelius stain showing no intensely stained enteroendocrine cells. Black bars represent 100μm.

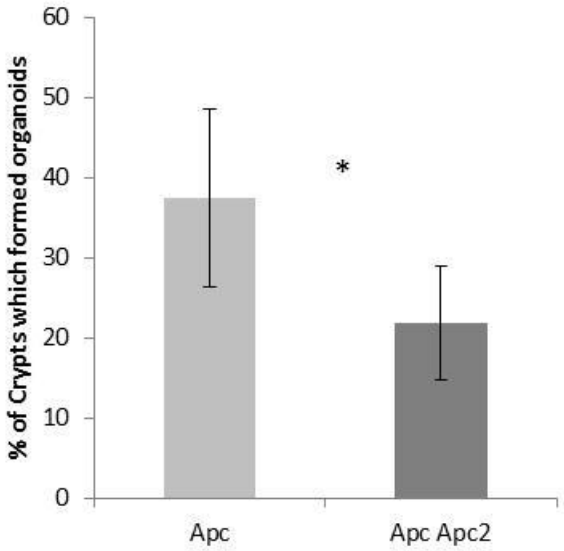

5.30 Organoid formation efficiency of *Apc*$^{flox/flox}$ (Apc) and *Apc*$^{flox/flox}$ *Apc2*$^{-/-}$ (Apc Apc2) crypts. *Apc2*$^{-/-}$ crypts formed organoids significantly less efficiently than wildtype. Independent sample T-test p=0.047. N>4.

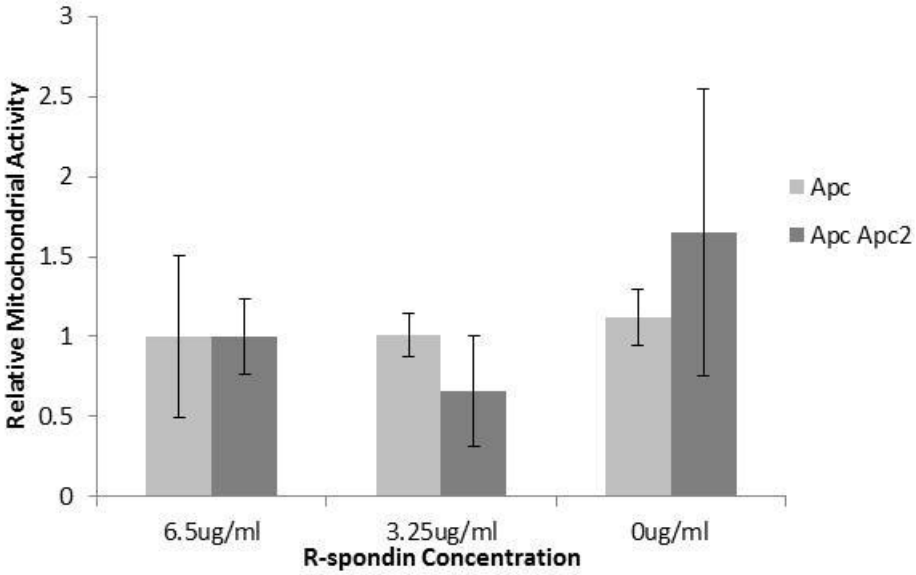

5.31 Prestoblue assay displaying mitochondrial activity of *Apc*$^{flox/flox}$ versus *Apc*$^{flox/flox}$ *Apc2*$^{-/-}$ organoids at a range of R-spondin concentrations. Organoids of both genotypes can grow entirely independently from the presence of R-spondin.

5.5 Discussion

5.5.1 Loss of Apc2 alone subtly alters intestinal homeostasis

An interesting phenotype of *Apc2* loss alone was the increased levels of apoptosis at the base of the crypt. This indicates that apoptosis is occurring at a higher level in either the ISC compartment or the ISC niche. While homozygous loss of *Apc* from the intestinal epithelium results in increased apoptosis, there is no evidence that location of apoptotic bodies is altered. However, loss of *Apc2* in this model is constitutive and universal throughout the mouse, and so it is possible that the subtly increased levels of Wnt-signalling as a result of *Apc2* deletion within the stromal compartment as well as the intestinal epithelium can disrupt the regulation of the ISC niche. The ISC niche plays an important role in intestinal homeostasis by regulating the number of daughter cells which retain stem cell identity thereby blocking the expansion of the stem cell compartment. There is already known to be a gradient of Wnt-signalling from the base of the crypt to the villus and it is easy to suppose that an increase in Wnt-signalling within the stromal compartment could affect the ISC niche.

5.5.2 Loss of Apc2 results in increased Wnt-signalling

As *Apc2* is capable of forming a β-catenin destruction complex independent from that formed by *Apc*, it was assumed that loss of *Apc2* would result in increased Wnt-signalling levels. As shown here, this is indeed the case and indicates that in normal intestinal homeostasis *Apc2* plays a role in regulating levels of nuclear β-catenin.

5.5.3 Loss of Apc2 results in increased expression of intestinal stem cell markers but less efficient organoid formation

As Wnt-signalling plays such an integral role in maintaining the ISC compartment, it is not surprising that a subtle increase in Wnt-signalling results in an increased expression of some ISC markers. However, this did not translate to an increased organoid formation efficiency, and *Apc2*$^{-/-}$ crypts were less efficient than wildtype at growing into organoids in culture. In order to explain this observation, it is necessary to develop our understanding of the ISC markers and their physiological function with regards to the maintenance of the ISC population.

Lgr5, which is significantly upregulated as a result of loss of *Apc2*, is widely regarded as the most accurate marker of the crypt-base columnar stem cell. It was recently identified that Lgr5 interacts with R-spondins in order to increase Wnt-signalling within Lgr5 expressing cells. However, it has also been shown that despite marking the ISC, it has no essential functional role in the maintenance of the ISC. Using a diphtheria toxin receptor knocked into the Lgr5 locus, it was found that Lgr5 is dispensable for intestinal homeostasis (Tian et al. 2011). This was used as evidence of the ability of second ISC population, the +4 stem cells, to compensate for the loss of CBC SCs. However, it should be noted that use of diphtheria toxin would not have resulted in 100% $Lgr5^{+}$ cell death and that single ISCs are capable of repopulating a great deal of damaged intestinal epithelium.

It could be argued that increased expression for Lgr5 is the result of increased Wnt-signalling and confers no added ISC functionality benefit as it is a marker of the ISC population and not a definer of "stemness". Indeed, conditional homozygous deletion of *Lgr5* alone does not result in a loss of intestinal homeostasis, and it is loss of its homologue *Lgr4* that results in an intestinal phenotype of loss of crypts, although this effect is accentuated by additional loss of *Lgr5* (de Lau et al. 2011). This indicates that redundancy in the system may cause expression levels of *Lgr5* to be uninformative about ISC functional status when not combined with *Lgr4* expression levels.

Ascl2 expression levels were also significantly increased due to loss of *Apc2*. *Ascl2* is also a Wnt-target gene, however, it appears that Ascl2 plays an important functional role in maintaining the ISC compartment. Ascl2 is a basic helix-loop-helix transcription factor with a tightly restricted expression pattern which is controlled by imprinting during embryonic development (Miyamoto *et al.* 2002). Despite the lack of knowledge concerning the interactions of *Ascl2*, the importance of this gene in regulating the ISC compartment has been convincingly demonstrated. Transgenic over expression of *Ascl2* within the intestinal epithelium resulted in crypt expansion and hyperplasia, as well as mislocalisation of crypts, whereas loss of *Ascl2* within the intestinal epithelium resulted in crypt ablation (van der Flier et al. 2009b).

However, despite this evidence of *Ascl2's* role in maintaining the ISC compartment, mis-expression of *Ascl2* in these experiments was induced throughout the entire intestinal

epithelium and so does not represent what is observed in the *Apc2* model. In the *Apc2* model we observe elevated expression, but the *in situ* hybridisation indicates that expression is still limited to the crypt base. This is more accurately represented by our 2012 paper in which *Ascl2* was entopically overexpressed at physiologically relevant levels and showed no significant intestinal phenotype (Reed *et al.* 2012). This demonstrates that despite the importance of *Ascl2* in maintaining the ISC population, it is a question of localisation of expression, and despite loss of *Apc2* causing an increase in levels of expression of *Ascl2,* there is no mislocalisation, and so could represent the same number of or even fewer ISCs than wildtype expressing higher levels of markers.

Olfm4 encodes an anti-apoptotic factor that has been shown to promote tumour growth and facilitate cell adhesion and is associated with the $Lgr5^{+}$ intestinal epithelium cells (van der Flier et al. 2009a). There was no significant increase for expression of *Olfm4* due to loss of *Apc2*, although there was a trend for increased expression at n=5. *In situ* hybridisations also showed that the expression pattern was unaltered. This is interesting as *Olfm4* is the only ISC marker used here which is not a direct target of Wnt-signalling (van der Flier et al. 2009a). The *in situ* hybridisations indicate that there is no significant expansion of the ISC compartment, but as *in situ* hybridisation is not a quantifiable technique, it is impossible to tell whether there is in fact an increased expression of *Olfm4* in fewer cells. This is made more difficult by the crypt-villus cross sections taken on the slides, as it is possible that there are in fact fewer ISCs around the base of the crypt. Despite the trend for increased expression of *Olfm4* as detected by mRNA levels, levels of the protein were not examined, and the increased levels of apoptosis seen at the base of the crypt are not indicative of an increased level of an anti-apoptotic factor such as *Olfm4*.

Bmi1 is also a Wnt-target gene, however, its role as a marker of ISCs is controversial. The gene encodes a Polycomb Repressing Complex 1, which is essential in maintaining chromatin silencing. *Bmi1* was initially examined as a potential marker of the ISC population as it has been shown to play a role in self renewal in a variety of different cell types (Lessard and Sauvageau 2003; Molofsky *et al.* 2003). It has more recently been cited as a definitive marker of the +4 population of ISCs (Sangiorgi and Capecchi 2008; Yan et al. 2012),however, it has been shown many times that *Bmi1* is expressed

throughout the crypt and although it is more frequently located at the +4 position(Sangiorgi and Capecchi 2008; Yan et al. 2012). $Bmi1^{+}$ cells are capable of forming organoids in culture. However, from the literature it is not known whether or not $Bmi1^{+}$ $Lgr5^{-}$ epithelial cells are capable of forming organoids, and *Bmi1* and *Lgr5* expression overlaps within the intestinal crypt (Barker et al. 2012). In *Apc2* null mice, there was no significant change in expression of *Bmi1*, however, as *Bmi1* is such a broad marker of the intestinal crypt, this alone cannot be used as evidence that there has been no change to the ISC compartment.

Msi1 encodes an RNA binding protein which plays an important role in the asymmetric division in neural progenitor cells (Okano *et al.* 2002). The role of *Msi1* as a marker of the ISC population is interesting for two reasons, one being that its role as a marker has only ever been shown by localisation of expression using *in situ* hybridisation which revealed expression to be localised to the crypt base and upregulated in tumours. The second reason is that as well as being a Wnt-signalling target gene, *Msi1* is involved in a double-negative feedback loop which results in increased Wnt-signalling (Spears and Neufeld 2011). This double-negative feedback loop was discovered by the observation that Msi1 binds to Apc mRNA and so negatively regulates *Apc* translation. This results in reduced Apc protein available for formation of the β-catenin destruction complex and so an increase in nuclear β-catenin and an increased level of expression of Wnt-target genes such as *Msi1*. Interestingly, *Msi1* was the only ISC marker examined which was significantly down regulated. This means that Wnt-levels had not reached the threshold at which Wnt-signalling becomes self-perpetuating. The role of Msi1 in repressing translation of certain mRNAs has been associated with the ability to maintain the stem-cell state of cells by controlling differentiation and tumourigenesis (Okano et al. 2002). It is possible that the reduced expression of Msi1 observed in $Apc2^{-/-}$ intestinal epithelium is representative of a loss of maintenance of the stem-cell population, which could explain the reduced organoid formation efficiency.

As discussed here, the entopic over-expression of any of the ISC markers examined plays no recognized role on the functionality of ISCs. Therefore, I propose that subtly increased Wnt-signalling as a result of *Apc2* loss has resulted in increased expression of ISC markers, but also induced ISC death via apoptosis. Loss of a number of ISCs is

supportable by the intestine, and this apoptosis has masked the true increase in expression of ISC markers. The combined results from the organoid formation efficiency assay and the R-spondin dependency assay supports the hypothesis that there are fewer functional ISCs present within the *Apc2*$^{-/-}$ intestine, but that those which survived the apoptotic influence of a change in Wnt-signalling levels are more highly Wnt-activated than wildtype, as seen by their decreased dependency on R-spondin.

This proposed mechanism could be tested by making a single cell suspension of intestinal epithelium cells then using antibodies for ISC specific surface markers to FACs sort out Cd44^{+} Cd24^{lo} Cd166^{+} Grp78$^{lo/-}$ Ckit^{+} as recently described in (Wang et al. 2013b). This would enable RNA extraction from ISCs and non-stem epithelial cells from both wildtype and *Apc2*$^{-/-}$ mice in order assess the levels of Wnt-signalling using qRT-PCR. This method would also enable a discreet count of the proportion of epithelial cells which express these markers. Despite not being a functional assay, this could support the organoid formation assay.

5.5.4 Additional loss of Apc2 results in increased survival of Apc$^{flox/flox}$ mice

Interestingly, the loss of *Apc2* resulted in an increased survival of the *Apc$^{flox/flox}$* mice despite having no effect on the number of cells within the region of aberrant proliferation at day 4 post induction. Also, double mutants survived for significantly longer than *Apc$^{flox/flox}$* mice. This can be attributed to the increased apoptosis which results from additional deletion of *Apc2*, and is attested by the significantly lower number of cells in the region of aberrant proliferation at day 5 (counted by Carl Daly, data not shown). This indicates that the combined deletion of the two genes increases Wnt-signalling to such a level that the increased apoptosis acts as a compensatory mechanism to control for the increased proliferation due to *Apc* loss.

Another hypothesis is that as the *Apc2* mutation is a constitutive knockout which results in elevated Wnt-signalling levels, the cells are already acclimatised to increased Wnt-signalling. This would mean that they are better equipped to respond to the gross elevation of the Wnt-signalling pathway which occurs after induction of *Apc* loss via tamoxifen injection. This is supported by the observation that *Apc2*$^{-/-}$ intestinal epithelium expresses the Wnt-inhibitor *groucho* at a higher level than is seen in wildtype and so are more prepared to cope with a change in Wnt-signalling levels.

5.5.5 Additional loss of Apc2 results in attenuated the Wnt-signalling and stem cell phenotype in Apc$^{flox/flox}$ crypts

Despite the observation that double mutants have a reduced Wnt-expression readout in comparison to *Apc$^{flox/flox}$* mice, it is likely that this is actually a side effect of increased apoptosis. We propose that the high levels of Wnt-signalling resulting from combined deletion of *Apc* and *Apc2* results in apoptosis of the most highly activated cells, thereby causing a detectable decrease in measured Wnt-signalling. This supports the "just-right" hypothesis of Wnt-signalling which proposes that levels of Wnt-signalling must reach a certain threshold before they drive a tumourigenic phenotype, and there is a higher threshold over which levels of apoptosis are so high that they counter-act the phenotype (Figure 5.32) (Albuquerque *et al.* 2002).

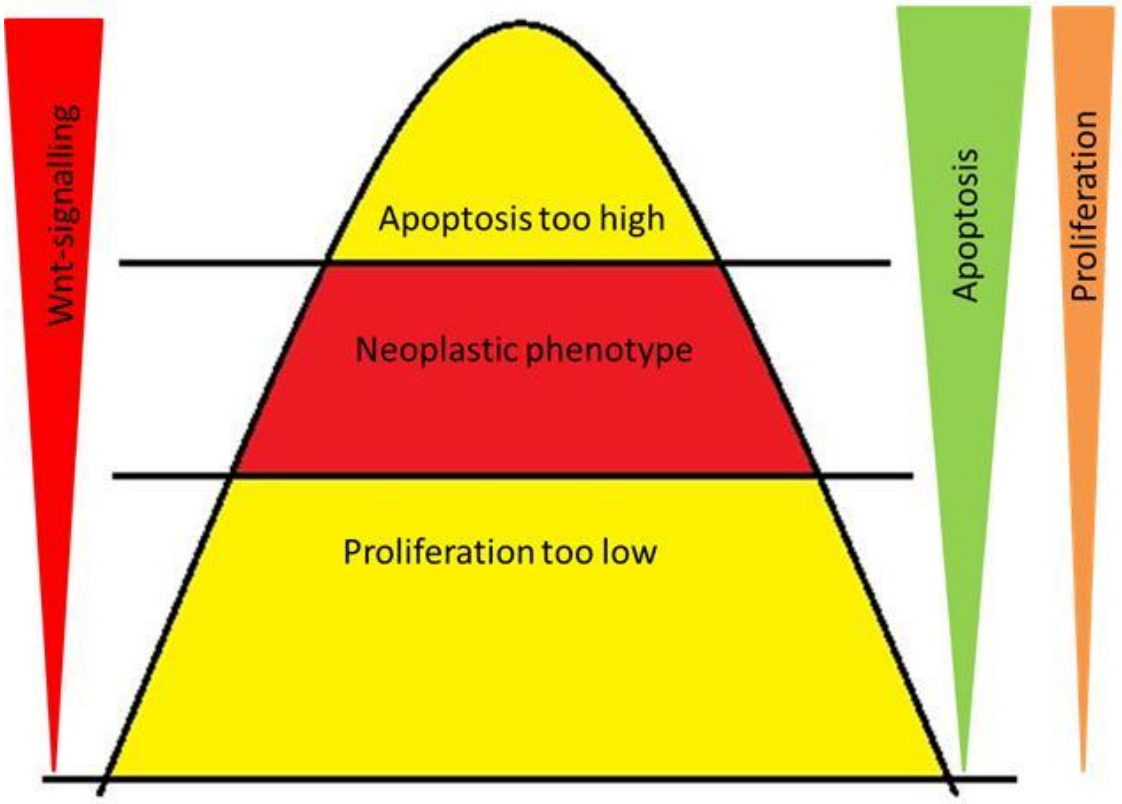

5.32 Diagrammatic representation of the "just-right" hypothesis of neoplasia. As the levels of Wnt-signalling increase, the levels of proliferation and apoptosis increase as well, but the balance of apoptosis and mitosis is only suitable for driving tumourigenesis within certain thresholds.

This would also explain the observation that loss of *Apc2* resulted in reduced expression of ISC markers in $Apc^{flox/flox}$ intestinal epithelium as increased levels of Wnt-signalling induced apoptosis of intestinal stem cells. This is supported by the reduced efficiency of organoid formation of double mutant crypts.

However, as previously discussed, the upregulation of expression of the Wnt-inhibitor *groucho* seen as a result of $Apc2^{-/-}$ alone, may be priming $Apc2^{-/-}$ cells to attenuate the Wnt-signalling and therefore ISC phenotype due to loss of *Apc*. This would explain why additional deletion of *Apc2* reduces the Wnt-signalling levels within the intestinal epithelium.

5.5.6 Loss of Apc2 does not impact tumourigenesis despite affecting the ISC population

The effects on the epithelial Wnt-signalling levels of *Apc2* loss alone and in conjunction with *Apc* loss would suggest that *Apc2* would play some role in intestinal tumourigenesis. However, as previously discussed, it was observed that loss of *Apc2* was not sufficient to induce tumourigenesis, and that deletion of *Apc2* on an *Apc* heterozygous background ($Apc^{flox/+}$) had no effect on either survival or tumour burden. As Wnt-activated ISCs are the "cells of origin" of intestinal cancer (Barker et al. 2008), the changes on the ISC compartment as a result of *Apc2* deletion could be expected to alter the number of tumours formed. However, despite loss of *Apc2* resulting in the presence of fewer functional stem cells, the R-spondin dependency assay indicates that the stem cells remaining are more highly Wnt-activated. As it is only Wnt-activated ISCs which can act as the "cells of origin" of intestinal adenomas, these changes could effectively balance each other out, meaning that although the number of ISCs has changed, the number of "cells of origin" has not.

It is also possible that in the $Apc^{flox/+}$ model, the increased Wnt-signalling observed due to loss of Apc2 is resulting in a selective pressure for the change of location of the spontaneous second mutation of Apc, as described by the "just-right" hypothesis. The "just –right" models of Wnt-signalling in tumourigenesis recognises that in FAP patients who carry a germ line mutation in one copy of *APC*, the sporadic mutation which occurs and results in tumourigenesis is not a random mutation, but is dependent on the position and function of the germ line mutations (Clarke 2006; Clevers 2006; Polakis

2007). Most *APC* mutations result in truncated APC protein missing all the axin/conductin binding regions, but the mutations generally differ in the number of the β-catenin regulating 20-amino acid repeats which are retained. It has been shown that if the germ line mutation retains none of these 20-amino acid repeats then the sporadic point mutation will most frequently result in the retention of one or two of these 20-amino acid repeats, whereas if the germ line mutation results in retention of one or more of these repeats, then the sporadic mutation will generally result in a complete loss of all of the repeats (Albuquerque et al. 2002). This shows how the second hit to *APC* is strongly influenced by the germ line mutation. This is most likely because only Wnt-levels within certain threshold boundaries drive tumourigenesis. Below the lower threshold Wnt-signalling levels are not adequate to drive the levels of proliferation required for tumourigenesis, and above the upper threshold, the apoptosis levels are so high that they counteract the tumourigenic phenotype (see Figure 5.24). This results in a selective pressure for the survival of tumours driven by mutations which facilitate the "just-right" levels of Wnt-signalling.

Recently, the "just-right" hypothesis of Wnt-dependent tumourigenesis was further interrogated by the assessment of the phenotype following β-catenin stabilisation throughout the intestine. It has previously been shown that in normal tissue there is a gradient of Wnt-signalling levels from the proximal intestine to the distal intestine. Stabilisation of β-catenin resulted in a "graduated neoplastic response" ranging from complete transformation of proximal intestine to a neoplastic phenotype to enlarged crypts at the distal intestine where entopic Wnt-levels are relatively low (Leedham *et al.* 2012). This supports the hypothesis that intestinal tumourigenesis is dependent on a fine balance of Wnt-signalling.

Loss of Apc2 alone does not increase Wnt signalling levels high enough to reach the lower threshold required for tumourigenesis to occur and requires loss of Apc to do so. However, in the $Apc^{flox/+}$ mouse, the "second hit" of *Apc*, according to the "just-right" hypothesis, is localised to enable the tumourigenic levels of Wnt-signalling to be achieved. When coupled with *Apc2* loss, LOH mutations of *Apc* which result in complete Apc loss of function may be causing Wnt-levels to soar above the maintainable threshold, and apoptosis to be induced in mutated cells so that tumourigenesis does not

occur. This means that there could be a selective pressure for the *Apc* LOH mutations to be less severe in the absence of *Apc2*, and thereby preventing the manifestation of any phenotype due to *Apc2* loss.

This hypothesis could be tested by deep sequencing of intestinal tumours derived from both $Apc^{flox/+}$ and $Apc^{flox/+}$ $Apc2^{-/-}$ mice in order to determine if the absence of *Apc2* has resulted in a change in location of the "second-hit" of *Apc*.

However, as $Apc^{flox/flox}$ $Apc2^{-/-}$ mice display both reduced ISC marker expression and a decreased organoid formation efficiency than $Apc^{flox/flox}$ it can be assumed that the additional loss of *Apc2* attenuates the expansion of the ISC compartment seen in $Apc^{flox/flox}$ mice. As ISCs are known to be the cell of origin for intestinal adenomas, it could be assumed that a reduced ISC population would result, purely by probability, in a reduced tumour burden. However, this phenotype is the result of the loss of *Apc2* on an $Apc^{flox/flox}$ background, where both *Apc* mutations are severe. The ISC compartment of normal tissue within $Apc^{flox/+}$ $Apc2^{-/-}$ mice would have to be assessed in order to make assumptions about the number of "cells of origin" and therefore the probability of transformation of cells.

5.6 Summary

As *Apc2* is an *Apc* homologue, and as such can deplete cytoplasmic β-catenin levels, albeit less efficiently than *Apc* (Schneikert *et al.* 2013), loss of *Apc2* results in a slight increase in Wnt-signalling levels. This increase in Wnt-signalling is not enough to reach the threshold and drive tumourigenesis, but does cause an increase in apoptosis within the ISC compartment. Cell death within the ISC compartment as a result of Apc2 loss appears to result in fewer ISCs which are more Wnt-activated, although this hypothesis requires further examination. The contradictory results between qRT-PCR for ISC expression markers and the efficiency at which the crypts form organoids in culture highlight the utility of the organoid formation efficiency assay in assessing the functional ISC compartment. *Msi1* was the only ISC marker which followed an expression pattern which represented the results of the organoid formation efficiency assay, and so further investigation of the utility of using *Msi1* expression as a surrogate marker of functional stem cell capacity could be useful.

The decreased number of ISCs as a result of *Apc2* loss does not result in a decrease in tumour burden in an $Apc^{flox/+}$ model, as the ISCs are more Wnt-activated than wildtype and so the actual number of Wnt-activated ISCs (cells of origin) has not altered.

The constitutive loss of *Apc2* developmentally conditions intestinal epithelial cells to maintain homeostasis in the presence of elevated Wnt-signalling levels. This means that $Apc2^{-/-}$ cells are more prepared to deal with the gross increase in Wnt-signalling resulting from *Apc* loss, and therefore additional deletion of *Apc2* attenuates the Apc phenotype.

This fine balance of Wnt-signalling required for tumourigenesis may result in a selection pressure for less aggressive LOH mutations in an $Apc^{flox/+}$ $Apc2^{-/-}$ model, thereby explaining how loss of *Apc2* in this context has no apparent effect on survival or tumour burden.

5.7 Future work

In order to corroborate the "just-right" theory of the relationship between Wnt-signalling and tumourigenesis, the locations of the "second hit" of *Apc* in both $Apc^{flox/+}$ and $Apc^{flox/+}$ $Apc2^{-/-}$ intestinal tumours must be determined via deep sequencing. It will also be important to assess the ISC compartment within normal tissue of these two models in an attempt to determine the role of Apc2 in the maintenance of the ISC compartment.

As previously discussed it will also be essential to FACs sort out the ISCs of $Apc2^{-/-}$ and wildtype mice and perform qRT-PCR to assess how Wnt-signalling levels have actually changed between the ISC populations of the two genotypes. This could be achieved using antibodies for the ISC specific cell surface markers described by Wang *et al,* for FACs sorting, which would also enable be possible to use the proportion of epithelial cells expressing these markers as a readout of ISC number to support the data from the organoid formation efficiency assay (Wang et al. 2013b).

It would also be interesting to further explore the role of *Msi1* not only as an activator of the Wnt-pathway via repression of Apc translation, but also as a regulator of stem cell state. This could be achieved through the use of siRNA to interrupt *Msi1* expression within intestinal organoid in culture, and assess the effect on nuclear β-catenin levels as

well as expression of markers of cell differentiation. This experiment, alongside analysis of the effect of overexpression of *Msi1* in culture using a pcDNA vector coupled with a CMV promoter could help clarify the role which *Msi1* is playing in regulating the ISC compartment within the *Apc2*$^{-/-}$ mouse model.

6 General Discussion

In order to begin developing more targeted drugs for the treatment of colorectal cancer, it is necessary to gain a better understanding of the genetic mutations and processes which occur at an early stage of colorectal tumourigenesis. Conditional homozygous deletion of the important tumour suppressor gene *Apc* enables the modelling of the initial stages of tumourigenesis within the intestine, and indicates that one of the earliest stages of tumourigenesis is a loss of differentiation and an expansion of cell types with an intestinal stem-like phenotype (Sansom *et al.* 2004). As ISCs have been shown to be the cell of origin of intestinal tumourigenesis (Barker *et al.* 2007), it is thought that changes within the ISC compartment may play a role in determining both risk of development of CRC, and potential severity of disease, and expansion of the ISC compartment is one of the earliest stages of tumourigenesis.

To gain insight into the potential of using changes within the ISC compartment as a predictor of disease, it is necessary to develop our current methods for assessing these changes. Currently, the principle way of studying the ISC compartment (without additional genetic alterations) is through the use of gene expression analysis, either using qRT-PCR or *in situ* hybridisation. Multiple genes have been proposed as potential markers of the ISC population, however there is a great deal of controversy regarding both the specificity and the location of expression of these markers (Barker *et al.* 2012). This situation is made additionally complicated by the evidence that there may actually be two distinct ISC populations which play very different roles in the maintenance of intestinal homeostasis, with CBC being responsible for intestinal homeostasis and the +4 cells playing an essential role in intestinal repair following damage (Yan *et al.* 2012).

A variety of assays for assessing the stem cell compartments of other adult tissues based on the functional properties of those stem cells have previously been proposed. In order to assess the stem cell compartment of mammary tissue either a cleared fat-pad assay or a “mammosphere” assay can be used. The cleared fat-pad assay involves the disassociation of mammary glands from donor mice, and then transplanting them into the cleared mammary fat pads of young recipient mice (DEOME *et al.* 1959) . As these mice mature and are subsequently bred, the transplanted cells produce fully

differentiated mammary glands. By transplanting limiting dilutions of the disassociated cells into recipient mice, it is possible to use this as a readout of the levels of mammary repopulating units (MRUs) within the mammary gland, which are proposed to be representative of mammary stem cells (Stingl *et al.* 2006). In order to enable a more high-throughput approach to assessing the mammary stem cell population, an *in vitro* assay was also developed. The mammosphere assay involves the culture of single mammary cells in non-adherent conditions which enables mammary stem cells to survive and proliferate, but results in the cell death of other mammary cell lineages. These stem cells grow into spheroids which can be passaged and so represent a self-renewing population of mammary cells (Dontu *et al.* 2003), and the number of spheroids which form can be used as a representation of the number of stem cells within the mammary gland (Stingl et al. 2006). Both of these mechanisms have been useful, however, it is argued that mammospheres which form in culture are not derived from single cells as they are not clonal in nature, but are the result of cell aggregation of seeded cells (Liao *et al.* 2007). This indicates that the ability of cells to form mammospheres may not be directly linked to the ability of those cells to function as stem cells. Mammary glands grown from transplantation into cleared fat pads have been shown to be of clonal origin, but it could be suggested that the ability of a cell to grow in the artificial environment of a cleared fat pad does not represent the cells ability to function as a true mammary stem cell *in vivo*.

The mammosphere stem cell assay was inspired by work on the central nervous system which showed that a sub-population of neuronal precursor cells are capable of survival, expansion, self-renewal and differentiation in non-adherent culture conditions in the form of neurospheres (Reynolds and Weiss 1992). The efficiency of neurosphere formation has been widely used as an assay of the neural stem cell compartment, but must be used with care, as like other stem cell function assays, they may represent an ability of neural cells to behave like stem cells *in vitro* in an artificial environment rather than representing an actual stem cell population, and it has been shown that the majority of neurospheres are not of clonal origin (Singec *et al.* 2006).

Functional stem cell assays are therefore widely used to gain insight into the both the neural and mammary stem cell compartment, and classify stem cells not on their

expression of markers but on their actual ability to proliferate, differentiate and self-renew. The only system which models all of these functions from cells derived from intestinal epithelium, is that of organoid culture (Sato *et al.* 2009), and so this system was used to develop a novel method to assess the ISC compartment. The ability to form these organoids represents the functional capacity of cells to function as ISCs, i.e. the ability to produce all of the different intestinal epithelial lineages and to self-renew.

Here, intestinal organoid formation efficiency was used as a mechanism for assessing the stem cell compartment as it represented a stem cell assay most similar to the gold standard assays used in other tissues, discussed above. Other methods for using the organoid system to assess ISC capacity would be possible, such as the use of the number of protrusions formed per organoid, however there are difficulties associated with this method. Counting the number of protrusions per organoid is difficult to achieve due to the 3-dimensional nature of the organoids and the great variability in protrusion numbers between organoids of the same genotype. Problems would also arise using this method due to the fact that protruding crypts are formed by crypt fission, and so the number of crypt protrusions formed in culture may bare little relationship to the number of ISCs in the disassociated crypt prior to seeding, but be more representative of conditions favouring crypt fission. By assessing the organoid formation efficiency of various mouse models of CRC we have been able to determine the utility of this method in a variety of different settings. Organoid formation efficiency proved to aid understanding of changes in the ISC compartment that were not detectable by qRT PCR and *in situ* hybridisation alone, such as in the *Apc2*$^{-/-}$ mouse model, where the organoid formation efficiency was in direct contradiction to the expression data for ISC markers.

6.1 Loss of Cited-1 results in an increase in expression of ISC markers and higher organoid formation efficiency

Using the *Cited-1*$^{-/-}$ mouse it had previously been shown that loss of Cited-1 resulted in a subtle increase in Wnt signalling, one of the most important signalling pathways involved in maintaining the ISC compartment. Assessing the ISC compartment of this mouse model using traditional gene expression methods hinted that there may be some subtle expansion of the ISC compartment due to increased Wnt signalling levels. By using the organoid formation efficiency assay on disassociated intestinal crypts derived

from wildtype and *Cited-1*$^{-/-}$ mice it was possible to determine the potential utility of this method in assessing subtle changes in the ISC compartment. In this model, loss of *Cited-1* resulted in an increased organoid formation efficiency, which supported the increased expression of ISC markers to indicate an expansion of the functional ISC compartment. This expansion of the ISC compartment was not sufficient to initiate intestinal tumourigenesis, indicating that an expansion of the ISC compartment alone, and therefore an increase in potential adenoma "cells of origin", without a tumour initiating event, such as loss of *Apc*, has no effect on tumourigenesis. Interestingly, *Cited-1* loss in an *Apc* heterozygous model of tumourigenesis actually decreased tumourigenesis despite this expansion in the ISC compartment (Méniel *et al.* 2013). This indicates that the status of the ISC compartment alone is not an accurate predictor of risk of tumourigenesis in this model.

6.2 Loss of Pml results in an increase in expression of ISC markers but no change in organoid formation efficiency

Interestingly, when studying the role of *Pml* in the maintenance of the ISC compartment in both *Apc*$^{flox/flox}$ mice and *Apc*$^{flox/flox}$ *Pten*$^{flox/flox}$ mice, the loss of *Pml* resulted in an increase in expression of ISC markers which, like that seen in the *Cited-1* model, was not associated with an increase in intestinal tumourigenesis. Interestingly, the organoid formation efficiency assay showed that despite an increase in expression of the markers there was no change in functional capacity, which potentially explains why there was no change in tumourigenesis. By analysing these models in this way it was possible to hypothesise why an increase in expression of ISC markers did not translate into increased tumourigenesis, as the changes within the ISC compartment due to *Pml* loss did not result in a functional change. In this model, assessment of the functional ISC compartment using organoid formation efficiency proved a more accurate indicator of tumourigenesis than using the expression levels of ISC marker genes.

6.3 Loss of Apc2 results in an increase in expression of ISC markers but a lower organoid formation efficiency

In the mouse model of *Apc2* loss, it was shown that despite an increase in expression of ISC markers, there was a significant decrease in organoid formation efficiency. This indicated that there were fewer functional ISCs which were expressing the ISC markers

at a higher level. It would not have been possible to determine this without the use of the organoid formation assay, which also enabled (through the use of the associated PrestoBlue R-spondin dependency assay) the generation of qRT-PCR evidence which showed that loss of *Apc2* results in an increase in expression of Wnt-target genes. Despite the further work required in order to elucidate the mechanism behind the changes in the ISC compartment due to *Apc2* loss and their effect on tumourigenesis, use of the organoid formation efficiency assay has enabled the separation of expression levels of ISC markers, and the functional capacity of the cells which they mark. Loss of *Apc2* resulted in a decreased functional capacity of the ISC compartment, but with no effect on levels of tumourigenesis or tumour burden.

The examples used within this thesis highlight the potential utility of the organoid formation assay in assessing the ISC compartment as an additional technique to be combined with ISC marker expression analysis. However, the ability of crypts to form organoids in culture may not be a true readout of ISC capacity within the crypt, and potentially we are selecting for a subpopulation of intestinal epithelial cells which does not represent the *in vivo* ISC population, but are capable of forming organoids *in vitro*. Because of this, the assay needs to be developed to produce a readout of self-renewal potential of the organoid forming cells via passage efficiency.

Here, through the use of a number of different mouse models of tumourigenesis, I have shown that, despite their role as the cell of origin of intestinal tumourigenesis, the functional status of the ISC compartment is not necessarily an accurate predictor of disease (see Table 19). This appears to reflect the complexity of the relationship between number, ISC marker expression, functional capacity and Wnt-signalling levels of the ISCs. However, the ISC compartment can still be informative of changes in homeostasis within the intestine, and the ability to accurately assess this cellular compartment remains important. The organoid formation assay presented here enables a certain level of insight into the ISC compartment, but remains an expensive and time consuming method, whereas gene expression analysis may not be a good indicator of ISC functionality. The use of gene expression analysis to assess the ISC compartment would be a more reliable method if expression levels of that gene were shown to consistently represent the organoid formation efficiency of that genotype.

6.4 The potential of Msi-1 as a marker of the functional ISC population

Of the ISC markers which were assessed, expression levels of *Msi1* was the only one which consistently translated into equivalent organoid formation efficiency between different models (see Table 19). Loss of *Cited-1* resulted in an increase in *Msi1* expression and increased organoid formation efficiency. Loss of *Pml* in both *Apc* and *Apc Pten* deficient mice resulted in no significant change in *Msi1* expression and no change in organoid formation efficiency. Interestingly, *Msi1* was the only ISC marker analysed which was down regulated due to loss of *Apc2*, associated with decreased organoid formation efficiency. This may mean that *Msi1* expression levels could provide a more accurate readout of changes within the ISC compartment.

Msi1 was originally proposed as a marker of the ISC population due to the location of its expression within the developing and adult intestine and its upregulation in tumours derived from Apc^{min} mice (Potten *et al.* 2003). It has been shown more recently that *Msi1* expression marks both the CBC cells and the +4 cells, the two populations of cells which have been identified as possible constituents of the ISC compartment (Kayahara *et al.* 2003; Muñoz *et al.* 2012). CBC cells are thought to represent a proliferative ISC population responsible for maintenance of intestinal homeostasis, whereas the +4 cells are thought to represent a more quiescent ISC type, and are responsible for gut repair after injury (Takeda *et al.* 2011). Furthermore, FAC sorting for GFP positive cells from a recently developed mouse model which expresses GFP under the control of an Msi1 promoter, demonstrates the ability to isolate two populations of intestinal epithelial cells which differentially express the proposed markers of CBC and the +4 cell types (Cambuli *et al.* 2013).

Genotype	Stem Cell Markers			Organoids		Phenotype
		qRT PCR	In Situ	Organoid formation efficiency	R-spondin dependency	
Cited$^{-/-}$ compared to wildtype	Lgr5	1.7*	Olfm4 expression is limited to the crypt base	21.4% *, significantly higher than wildtype	Same as wildtype	Decrease in tumourigenesis and increase in survival in an Apc$^{flox/+}$ model
	Ascl2	1.5				
	Olfm4	1.3				
	Msi1	7.1*				
	Bmi1	1.9				
Apc2$^{-/-}$ compared to wildtype	Lgr5	5.7*	Olfm4 expression is limited to the crypt base, lower down than is seen in wildtype	5.2% *, significantly lower than wildtype	Survive a day longer than wildtype in the absence of R-spondin	No change in tumourigenesis in an Apc$^{flox/+}$ model
	Ascl2	6.4*				
	Olfm4	2.1				
	Msi1	0.2*				
	Bmi1	1.6				
Apc2$^{-/-}$ compared to Apc$^{flox/flox}$	Lgr5	0.9	Olfm4 expression closer the the crypt base than seen in Apc$^{flox/flox}$	21.1% *, significantly lower than Apc$^{flox/flox}$	R-spondin independent, like Apc$^{flox/flox}$	Increased survival, increased apoptosis,decreased number of abberent cells by day 5 post induction
	Ascl2	0.5*				
	Olfm4	0.7*				
	Msi1	0.7*				
	Bmi1	1.3				
Apc$^{flox/flox}$ Pml$^{-/-}$ compared to Apc$^{flox/flox}$	Lgr5	1.3*	Expanded zone of Olfm4 expression compared to Apc$^{flox/flox}$	25.70%	R-spondin independent, like Apc$^{flox/flox}$	No change in survival, subtle increase in BrDU uptake
	Ascl2	1.6				
	Olfm4	1.8				
	Msi1	1.3				
	Bmi1	1.2				
Apc$^{flox/flox}$ Pten$^{flox/flox}$ Pml$^{-/-}$ compared to Apc$^{flox/flox}$ Pten$^{flox/flox}$	Lgr5	1.5*	Olmf4 expression spread across the region of abberent proliferation	27.40%	R-spondin independent, like Apc$^{flox/flox}$	Reduced survival, no clear phentoypic difference
	Ascl2	1.7				
	Olfm4	2.6*				
	Msi1	2.3				
	Bmi1	1.1				

Table 19. Summary of observed phenotypes, comparing gene expression analysis to organoid formation efficiency and effect on tumourigenesis.

Interestingly, *Msi1* plays a role within the ISC compartment beyond that of a simple marker of locations. *Msi1* encodes an RNA-binding protein, which has been described in Drosophila as essential for the maintenance of stem cell identity (Siddall *et al.* 2006). In mammals, *Msi1* tightly regulated levels of *p21* via transcriptional repression (Battelli *et al.* 2006) and *Msi1* levels are inversely correlated with that of *p21* in intestinal epithelial cells in which *Msi1* is overexpressed (Rezza *et al.* 2010). *P21* has been shown to play an important role in maintenance of the ISC compartment with loss of *p21* enhancing ISC survival following radiation injury (George *et al.* 2009).

As well as potentially playing a direct role maintaining the ISC compartment, *Msi1* has been shown to be a potent regulator of both the Notch and the Wnt signalling pathways. Notch signalling, which is thought to be a major constituent of the ISC niche, has been shown to be activated by *Msi1* overexpression in intestinal epithelial cultures (Rezza *et al*. 2010). Overexpression of *Msi1* via infection with *Msi1* encoding viral particles was shown to increase the number of cells expressing the Notch receptor NICD, as well as its target, Hes1. The importance of Notch signalling as a niche regulator has been supported by evidence that in order to form organoids in culture, single ISCs require the addition of a Notch ligand, and that organoid formation efficiency can be increased by the co-culture of ISCs with Paneth cells, which express Notch ligands (Sato *et al.* 2010). This could indicate why *Msi1* expression levels correlate with organoid formation efficiency, as they could be a representation of Notch signalling levels within the crypt. This could indicate that organoid formation efficiency is not an accurate representation of the number of the ISCs within a crypt, but rather represents a readout of the status of the ISC niche. This issue could be addressed by assessing the Notch signalling status within the models presented here to determine if Notch signalling levels are a better indication of organoid formation efficiency than expression levels of ISC markers. The use of Notch inhibitors would enable subtle manipulation of the Notch signalling pathway within organoid culture, and could enable the interrogation of potential role of Notch signalling in the maintenance of the ISC compartment.

As previously mentioned, *Msi1* is a Wnt-target gene, and interestingly, it is also a negative regulator of Apc via transcriptional regulation (Spears and Neufeld 2011). In this way, an increase in Wnt signalling results in an increase in expression of *Msi1*,

which in turn binds to *Apc* mRNA and reduces translation, thereby resulting in a further increase in Wnt signalling levels. *Msi1* is also able to regulate Wnt signalling indirectly, since *Msi1* induces *Frat1* expression which in turn increases β-catenin stabilisation, thereby increasing Wnt activation (Rezza *et al*. 2010). Due to the seemingly direct relationship between *Msi1* and Wnt signalling levels, it is surprising that in our $Apc2^{-/-}$ model, Wnt signalling was increased but *Msi1* expression was significantly down regulated. One explanation for this seemingly contradictory evidence is that perhaps Wnt signalling levels need to reach a certain threshold before it induces *Msi1* expression and therefore becomes self-regulating.

The evidence presented here supports the idea that *Msi1* expression is representative of organoid formation efficiency, although whether this is due to an expansion of the ISC compartment itself or a more highly activated niche component of the intestinal epithelium is unclear. It is however clear that *Msi1* potentially may be of great interest in this field and that more work into the precise nature of its role in maintenance of the ISC compartment is required. An *Msi1* knockout mouse is available, and it has been shown using this model that loss of *Msi1* does not result in an increase in intestinal Apc levels, but does result in a decreased ISC compartment (Ernlund 2011). An interesting experiment would be to transfect disassociated intestinal crypts with either *Msi1* siRNA or *Msi1* expressing viral particles prior to crypt seeding to assess the effect of down regulation or overexpression of *Msi1* on organoid formation efficiency. If the *Msi1* knockout does result in a decreased ISC population without affecting Wnt-signalling levels, it would be interesting to breed these mice with $Apc^{flox/+}$ mice, to establish if a decreased ISC compartment translates into decreased tumourigenesis. It would be predicted that with fewer "cells of origin" the LOH event would be less common and so tumour burden would decrease, and survival increase due to loss of *Msi1*. Ideally, the production of an *Msi1* allele flanked by LoxP sites would enable a higher level of control of gene expression.

The work presented here indicates that changes in the number of ISCs does not translate well as a predictor of disease, as ISCs are only "cells of origin" once they have been malignantly transformed. Because of this, the levels of Wnt signalling specifically within the ISCs may prove more indicative of tumourigenesis. The R-spondin

dependency assay, when used on organoids derived from mice wildtype for *Apc*, may prove more useful in this instance. By assessing the dependency of organoids on R-spondin, we may be able to assess the levels of Wnt signalling within the ISC compartment in order to gain further understanding into the genetic pathways involved in this complex disease.

References

Al-Hajj, M., Becker, M. W., Wicha, M., Weissman, I. and Clarke, M. F. (2004). Therapeutic implications of cancer stem cells. *Current opinion in genetics & development* **14:**43-47.

Al-Hajj, M., Wicha, M. S., Benito-Hernandez, A., Morrison, S. J. and Clarke, M. F. (2003). Prospective identification of tumorigenic breast cancer cells. *Proceedings of the National Academy of Sciences* **100:**3983.

Albuquerque, C., Breukel, C., Van Der Luijt, R., Fidalgo, P., Lage, P., Slors, F. J. M., Leitão, C. N. *et al.* (2002). The 'just-right'signaling model: APC somatic mutations are selected based on a specific level of activation of the β-catenin signaling cascade. *Human molecular genetics* **11:**1549-1560.

Artavanis-Tsakonas, S., Rand, M. D. and Lake, R. J. (1999). Notch signaling: cell fate control and signal integration in development. *Science* **284:**770-776.

Ayabe, T., Ashida, T., Kohgo, Y. and Kono, T. (2004). The role of Paneth cells and their antimicrobial peptides in innate host defense. *Trends in microbiology* **12:**394-398.

Barker, N., Ridgway, R. A., van Es, J. H., van de Wetering, M., Begthel, H., van den Born, M., Danenberg, E. *et al.* (2008). Crypt stem cells as the cells-of-origin of intestinal cancer. *Nature* **457:**608-611.

Barker, N., Van Es, J. H., Kuipers, J., Kujala, P., Van Den Born, M., Cozijnsen, M., Haegebarth, A. *et al.* (2007). Identification of stem cells in small intestine and colon by marker gene Lgr5. *Nature* **449:**1003-1007.

Barker, N., van Oudenaarden, A. and Clevers, H. (2012). Identifying the stem cell of the intestinal crypt: strategies and pitfalls. *Cell Stem Cell* **11:**452-460.

Barnard, J. A., Warwick, G. J. and Gold, L. I. (1993). Localization of transforming growth factor beta isoforms in the normal murine small intestine and colon. *Gastroenterology* **105:**67.

Bastide, P., Darido, C., Pannequin, J., Kist, R., Robine, S., Marty-Double, C., Bibeau, F. *et al.* (2007). Sox9 regulates cell proliferation and is required for Paneth cell differentiation in the intestinal epithelium. *The Journal of cell biology* **178:**635-648.

Battelli, C., Nikopoulos, G. N., Mitchell, J. G. and Verdi, J. M. (2006). The RNA-binding protein Musashi-1 regulates neural development through the translational repression of p21WAF-1. *Mol Cell Neurosci* **31:**85-96.

Baylin, S. B. (2005). DNA methylation and gene silencing in cancer. *Nature clinical practice oncology* **2:**S4-S11.

Behrens, J., von Kries, J., Kühl, M., Bruhn, L., Wedlich, D., Grosschedl, R. and Birchmeier, W. (1996). Functional interaction of -catenin with the transcription factor LEF-1. *Nature* **382:**638-642.

Bernardi, R., Guernah, I., Jin, D., Grisendi, S., Alimonti, A., Teruya-Feldstein, J., Cordon-Cardo, C. *et al.* (2006). PML inhibits HIF-1 translation and neoangiogenesis through repression of mTOR. *Nature* **442:**779-785.

Bernardi, R., Papa, A., Egia, A., Coltella, N., Teruya Feldstein, J., Signoretti, S. and Pandolfi, P. P. Pml represses tumour progression through inhibition of mTOR. *EMBO Molecular Medicine*.

Bernardi, R., Papa, A., Egia, A., Coltella, N., Teruya Feldstein, J., Signoretti, S. and Pandolfi, P. P. (2011). Pml represses tumour progression through inhibition of mTOR. *EMBO Molecular Medicine*.

Bernardi, R., Papa, A. and Pandolfi, P. P. (2008). Regulation of apoptosis by PML and the PML-NBs. *Oncogene* **27:**6299-6312.

Besson, V., Smeriglio, P., Wegener, A., Relaix, F., Nait Oumesmar, B., Sassoon, D. A. and Marazzi, G. (2011). PW1 gene/paternally expressed gene 3 (PW1/Peg3) identifies multiple adult stem and progenitor cell populations. *Proceedings of the National Academy of Sciences* **108:**11470.

Bevins, C. L. and Salzman, N. H. (2011). Paneth cells, antimicrobial peptides and maintenance of intestinal homeostasis. *Nature Reviews Microbiology* **9:**356-368.

Bienz, M. and Clevers, H. (2000). Linking Colorectal Cancer to Wnt Signaling Review. *Cell* **103:**311-320.

Bjerknes, M. and Cheng, H. (1981). The stem-cell zone of the small intestinal epithelium. I. Evidence from paneth cells in the adult mouse. *American Journal of Anatomy* **160:**51-63.

Bjerknes, M. and Cheng, H. (2006). Intestinal epithelial stem cells and progenitors. *Methods in enzymology* **419:**337-383.

Bonnet, D. and Dick, J. E. (1997). Human acute myeloid leukemia is organized as a hierarchy that originates from a primitive hematopoietic cell. *Nature medicine* **3:**730-737.

Booth, C. and Potten, C. S. (2000). Gut instincts: thoughts on intestinal epithelial stem cells. *Journal of Clinical Investigation* **105:**1493-1500.

Buczacki, S. J. A., Zecchini, H. I., Nicholson, A. M., Russell, R., Vermeulen, L., Kemp, R. and Winton, D. J. (2013). Intestinal label-retaining cells are secretory precursors expressing Lgr5. *Nature* **495:**65-69.

Cairns, P., Okami, K., Halachmi, S., Halachmi, N., Esteller, M., Herman, J. G., Jen, J. *et al.* (1997). Frequent inactivation of PTEN/MMAC1 in primary prostate cancer. *Cancer research* **57:**4997-5000.

Cambuli, F. M., Rezza, A., Nadjar, J. and Plateroti, M. (2013). Musashi1-Egfp Mice, a New Tool for Differential Isolation of the Intestinal Stem Cell Populations. *Stem Cells*.

Carracedo, A. and Pandolfi, P. P. (2008). The PTEN–PI3K pathway: of feedbacks and cross-talks. *Oncogene* **27:**5527-5541.

Carracedo, A., Weiss, D., Leliaert, A. K., Bhasin, M., de Boer, V. C. J., Laurent, G., Adams, A. C. *et al.* (2012). A metabolic prosurvival role for PML in breast cancer. *The Journal of clinical investigation* **122:**3088.

Chan, T. A., Glockner, S., Yi, J. M., Chen, W., Van Neste, L., Cope, L., Herman, J. G. *et al.* (2008). Convergence of mutation and epigenetic alterations identifies common genes in cancer that predict for poor prognosis. *PLoS medicine* **5:**e114.

Chen, Z. (2010). Acute promyelocytic leukaemia: novel insights into the mechanisms of cure. *Nature Reviews Cancer* **10:**775-783.

Clarke, A. R. (2006). Wnt signalling in the mouse intestine. *Oncogene* **25:**7512-7521.

Clevers, H. (2006). Wnt/β-catenin signaling in development and disease. *Cell* **127:**469-480.

Clevers, H. and Van de Wetering, M. (1997). TCF/LEF factors earn their wings. *Trends in Genetics* **13:**485-489.

Collado, M., Blasco, M. A. and Serrano, M. (2007). Cellular senescence in cancer and aging. *Cell* **130:**223-233.

Cristofano, A. D., Pesce, B., Cordon-Cardo, C. and Pandolfi, P. P. (1998). Pten is essential for embryonic development and tumour suppression. *Nature genetics* **19:**348-355.

Cufí, S., Vazquez-Martin, A., Oliveras-Ferraros, C., Martin-Castillo, B., Joven, J. and Menendez, J. A. (2010). Metformin against TGFβ-induced epithelial-to-mesenchymal transition (EMT): from cancer stem cells to aging-associated fibrosis. *Cell cycle (Georgetown, Tex.)* **9:**4461.

Cully, M., You, H., Levine, A. J. and Mak, T. W. (2006). Beyond PTEN mutations: the PI3K pathway as an integrator of multiple inputs during tumorigenesis. *Nature Reviews Cancer* **6:**184-192.

Dalerba, P., Dylla, S. J., Park, I. K., Liu, R., Wang, X., Cho, R. W., Hoey, T. *et al.* (2007). Phenotypic characterization of human colorectal cancer stem cells. *Proceedings of the National Academy of Sciences* **104:**10158-10163.

Daly , C. (2013). The roles of the Apc proteins in homeostasis and tumourigenesis. Thesis PhD, Cardiff University.

Das, P. M. and Singal, R. (2004). DNA methylation and cancer. *Journal of clinical oncology* **22:**4632-4642.

Davies, E. J. (2011). Modelling Intestinal Cancer Development and Progression in the Mouse. Thesis PhD, Cardiff University.

de Lau, W., Barker, N., Low, T. Y., Koo, B. K., Li, V. S. W., Teunissen, H., Kujala, P. *et al.* (2011). Lgr5 homologues associate with Wnt receptors and mediate R-spondin signalling. *Nature* **476:**293-297.

DEOME, K. B., FAULKIN, L. J., BERN, H. A. and BLAIR, P. B. (1959). Development of mammary tumors from hyperplastic alveolar nodules transplanted into gland-free mammary fat pads of female C3H mice. *Cancer Res* **19:**515-520.

Dhir, M., Montgomery, E. A., Glöckner, S. C., Schuebel, K. E., Hooker, C. M., Herman, J. G., Baylin, S. B. *et al.* (2008). Epigenetic regulation of WNT signaling pathway genes in inflammatory bowel disease (IBD) associated neoplasia. *Journal of Gastrointestinal Surgery* **12:**1745-1753.

Dihlmann, S. and von Knebel Doeberitz, M. (2005). Wnt/ -catenin-pathway as a molecular target for future anti-cancer therapeutics. *International Journal of Cancer* **113:**515-524.

Dillon, R. L., Brown, S. T., Ling, C., Shioda, T. and Muller, W. J. (2007). An EGR2/CITED1 transcription factor complex and the 14-3-3 sigma tumor suppressor are involved in regulating ErbB2 expression in a transgenic-Mouse model of human breast cancer. *Molecular and Cellular Biology* **27:**8648-8657.

Dontu, G., Abdallah, W. M., Foley, J. M., Jackson, K. W., Clarke, M. F., Kawamura, M. J. and Wicha, M. S. (2003). In vitro propagation and transcriptional profiling of human mammary stem/progenitor cells. *Genes Dev* **17:**1253-1270.

Ehrlich, M. (2002). DNA methylation in cancer: too much, but also too little. *Oncogene* **21:**5400-5413.

El Marjou, F., Janssen, K. P., Hung Junn Chang, B., Li, M., Hindie, V., Chan, L., Louvard, D. *et al.* (2004). Tissue specific and inducible Cre mediated recombination in the gut epithelium. *genesis* **39:**186-193.

Ernlund, A. W. (2011). Exploring Novel Properties of Adenomatous Polyposis Coli: Msi1-Knockout Mice Display Alterations in APC and Intestinal Cell Homeostasis; Topoisomerase IIa Binds to Truncated APC in Human Colon Cancer Cells. Thesis MA, University of Kansas.

Escobar, M., Nicolas, P., Sangar, F., Laurent-Chabalier, S., Clair, P., Joubert, D., Jay, P. *et al.* (2011). Intestinal epithelial stem cells do not protect their genome by asymmetric chromosome segregation. *Nature communications* **2:**258.

Farin, H. F., van Es, J. H. and Clevers, H. (2012). Redundant Sources of Wnt Regulate Intestinal Stem Cells and Promote Formation of Paneth Cells. *Gastroenterology*.

Fearon, E. R. and Vogelstein, B. (1990). A genetic model for colorectal tumorigenesis. *Cell* **61:**759-767.

Ferbeyre, G., de Stanchina, E., Querido, E., Baptiste, N., Prives, C. and Lowe, S. W. (2000). PML is induced by oncogenic ras and promotes premature senescence. *Genes & development* **14:**2015-2027.

Fletcher, A. G., Breward, C. J. W. and Jonathan Chapman, S. (2012). Mathematical modeling of monoclonal conversion in the colonic crypt. *Journal of theoretical biology* **300:**118-133.

Fodde, R., Edelmann, W., Yang, K., van Leeuwen, C., Carlson, C., Renault, B., Breukel, C. *et al.* (1994). A targeted chain-termination mutation in the mouse Apc gene results in multiple intestinal tumors. *Proceedings of the National Academy of Sciences* **91:**8969.

Frayling, I. M., Bodmer, W. F. and Tomlinson, I. P. M. (1997). Allele loss in colorectal cancer at the Cowden disease/juvenile polyposis locus on 10q. *Cancer genetics and cytogenetics* **97:**64-69.

Fre, S., Huyghe, M., Mourikis, P., Robine, S., Louvard, D. and Artavanis-Tsakonas, S. (2005). Notch signals control the fate of immature progenitor cells in the intestine. *Nature* **435:**964-968.

Gao YM, Zhong L, Zhang X, Hu XX and BZ., L. (2013). PML(NLS(-)) inhibits cell apoptosis and promotes proliferation in HL-60 cells. *Int J Med Sci* **10:**498-507.

Garabedian, E. M., Roberts, L. J. J., McNevin, M. S. and Gordon, J. I. (1997). Examining the role of Paneth cells in the small intestine by lineage ablation in transgenic mice. *Journal of Biological Chemistry* **272:**23729-23740.

George, R. J., Sturmoski, M. A., May, R., Sureban, S. M., Dieckgraefe, B. K., Anant, S. and Houchen, C. W. (2009). Loss of p21Waf1/Cip1/Sdi1 enhances intestinal stem cell survival following radiation injury. *Am J Physiol Gastrointest Liver Physiol* **296:**G245-254.

Giorgi, C., Ito, K., Lin, H. K., Santangelo, C., Wieckowski, M. R., Lebiedzinska, M., Bononi, A. *et al.* (2010). PML Regulates Apoptosis at Endoplasmic Reticulum by Modulating Calcium Release. *Science* **330:**1247-1247.

Goddard, A. D., Borrow, J., Freemont, P. S. and Solomon, E. (1991). Characterization of a zinc finger gene disrupted by the t (15; 17) in acute promyelocytic leukemia. *Science* **254:**1371-1374.

Goel, A., Arnold, C. N., Niedzwiecki, D., Carethers, J. M., Dowell, J. M., Wasserman, L., Compton, C. *et al.* (2004). Frequent inactivation of PTEN by promoter hypermethylation in microsatellite instability-high sporadic colorectal cancers. *Cancer research* **64:**3014-3021.

Gregorieff, A., Pinto, D., Begthel, H., Destrée, O., Kielman, M. and Clevers, H. (2005). Expression pattern of Wnt signaling components in the adult intestine. *Gastroenterology* **129:**626-638.

Groden, J., Thliveris, A., Samowitz, W., Carlson, M., Gelbert, L., Albertsen, H., Joslyn, G. *et al.* (1991). Identification and characterization of the familial adenomatous polyposis coli gene. *Cell* **66:**589-600.

Gryfe, R., Bapat, B., Gallinger, S., Swallow, C., Redston, M. and Couture, J. (1997). Molecular biology of colorectal cancer. *Current problems in cancer* **21:**233-299.

Guillemot, F., Nagy, A., Auerbach, A., Rossant, J. and Joyner, A. L. (1994). Essential role of Mash-2 in extraembryonic development.

Gurrieri, C., Capodieci, P., Bernardi, R., Scaglioni, P. P., Nafa, K., Rush, L. J., Verbel, D. A. *et al.* (2004). Loss of the tumor suppressor PML in human cancers of multiple histologic origins. *Journal of the National Cancer Institute* **96:**269.

Harada, N., Tamai, Y., Ishikawa, T., Sauer, B., Takaku, K., Oshima, M. and Taketo, M. M. (1999). Intestinal polyposis in mice with a dominant stable mutation of the β-catenin gene. *The EMBO Journal* **18:**5931-5942.

Haramis, A. P. G., Begthel, H., van den Born, M., van Es, J., Jonkheer, S., Offerhaus, G. J. A. and Clevers, H. (2004). De novo crypt formation and juvenile polyposis on BMP inhibition in mouse intestine. *Science* **303:**1684.

Hasebe, T., Fu, L., Miller, T. C., Zhang, Y., Shi, Y.-B. and Ishizuya-Oka, A. (2013). Thyroid hormone-induced cell-cell interactions are required for the development of adult intestinal stem cells. *Cell & Bioscience* **3:**18.

He, X. C., Yin, T., Grindley, J. C., Tian, Q., Sato, T., Tao, W. A., Dirisina, R. *et al.* (2007). PTEN-deficient intestinal stem cells initiate intestinal polyposis. *Nature genetics* **39:**189-198.

He, X. C., Zhang, J., Tong, W. G., Tawfik, O., Ross, J., Scoville, D. H., Tian, Q. *et al.* (2004). BMP signaling inhibits intestinal stem cell self-renewal through suppression of Wnt–β-catenin signaling. *Nature genetics* **36:**1117-1121.

Hewitson, P., Glasziou, P., Irwig, L., Towler, B. and Watson, E. (2007). Screening for colorectal cancer using the faecal occult blood test, Hemoccult. *Cochrane Database Syst Rev* **1**.

Hirsch, H. A., Iliopoulos, D., Tsichlis, P. N. and Struhl, K. (2009). Metformin selectively targets cancer stem cells, and acts together with chemotherapy to block tumor growth and prolong remission. *Cancer research* **69:**7507.

Ho, M. M., Ng, A. V., Lam, S. and Hung, J. Y. (2007). Side population in human lung cancer cell lines and tumors is enriched with stem-like cancer cells. *Cancer research* **67:**4827.

Ireland, H., Kemp, R., Houghton, C., Howard, L., Clarke, A. R., Sansom, O. J. and Winton, D. J. (2004). Inducible Cre-mediated control of gene expression in the murine gastrointestinal tract: effect of loss of β-catenin. *Gastroenterology* **126:**1236-1246.

Ito, K., Bernardi, R., Morotti, A., Matsuoka, S., Saglio, G., Ikeda, Y., Rosenblatt, J. *et al.* (2008). PML targeting eradicates quiescent leukaemia-initiating cells. *Nature* **453:**1072-1078.

Ito, K., Bernardi, R. and Pandolfi, P. P. (2009). A novel signaling network as a critical rheostat for the biology and maintenance of the normal stem cell and the cancer-initiating cell. *Current opinion in genetics & development* **19:**51-59.

Ito, K., Carracedo, A., Weiss, D., Arai, F., Ala, U., Avigan, D. E., Schafer, Z. T. *et al.* (2012). A PML-PPAR-[delta] pathway for fatty acid oxidation regulates hematopoietic stem cell maintenance. *Nature medicine* **18:**1350-1358.

Ito, K. and Ito, K. (2013). Newly identified roles of PML in stem cell biology. *Frontiers in Oncology* **3**.

Jarrett, C. R., Blancato, J., Cao, T., Bressette, D. S., Cepeda, M., Young, P. E., King, C. R. *et al.* (2001). Human APC2 localization and allelic imbalance. *Cancer research* **61:**7978.

Jubb, A. M., Chalasani, S., Frantz, G. D., Smits, R., Grabsch, H. I., Kavi, V., Maughan, N. J. *et al.* (2006). Achaete-scute like 2 (ascl2) is a target of Wnt signalling and is upregulated in intestinal neoplasia. *Oncogene* **25:**3445-3457.

Kaestner, K. H., Silberg, D. G., Traber, P. G. and Schütz, G. (1997). The mesenchymal winged helix transcription factor Fkh6 is required for the control of gastrointestinal proliferation and differentiation. *Genes & development* **11:**1583-1595.

Kayahara, T., Sawada, M., Takaishi, S., Fukui, H., Seno, H., Fukuzawa, H., Suzuki, K. *et al.* (2003). Candidate markers for stem and early progenitor cells, Musashi-1 and Hes1, are expressed in crypt base columnar cells of mouse small intestine. *FEBS letters* **535:**131-135.

Kim, K. A., Wagle, M., Tran, K., Zhan, X., Dixon, M. A., Liu, S., Gros, D. *et al.* (2008). R-Spondin family members regulate the Wnt pathway by a common mechanism. *Molecular biology of the cell* **19:**2588-2596.

Kim, T. H., Escudero, S. and Shivdasani, R. A. (2012). Intact function of Lgr5 receptor-expressing intestinal stem cells in the absence of Paneth cells. *Proceedings of the National Academy of Sciences*.

Kosinski, C., Stange, D. E., Xu, C., Chan, A. S., Ho, C., Yuen, S. T., Mifflin, R. C. *et al.* (2010). Indian Hedgehog Regulates Intestinal Stem Cell Fate Through Epithelial– Mesenchymal Interactions During Development. *Gastroenterology* **139:**893-903.

Kunttas-Tatli, E., Zhou, M.-N., Zimmerman, S., Molinar, O., Zhouzheng, F., Carter, K., Kapur, M. *et al.* (2012). Destruction Complex Function in the Wnt Signaling Pathway of Drosophila Requires Multiple Interactions Between Adenomatous Polyposis Coli 2 and Armadillo. *Genetics* **190:**1059-1075.

Kühn, R., Schwenk, F., Aguet, M. and Rajewsky, K. (1995). Inducible gene targeting in mice. *Science* **269:**1427-1429.

Lamlum, H., Papadopoulou, A., Ilyas, M., Rowan, A., Gillet, C., Hanby, A., Talbot, I. *et al.* (2000). APC mutations are sufficient for the growth of early colorectal adenomas. *Proceedings of the National Academy of Sciences* **97:**2225-2228.

Langlois, M.-J., Roy, S. A. B., Auclair, B. A., Jones, C., Boudreau, F., Carrier, J. C., Rivard, N. *et al.* (2009). Epithelial phosphatase and tensin homolog regulates intestinal architecture and secretory cell commitment and acts as a modifier gene in neoplasia. *The FASEB Journal* **23:**1835-1844.

Lapidot, T., Sirard, C., Vormoor, J., Murdoch, B., Hoang, T., Caceres-Cortes, J., Minden, M. *et al.* (1994). A cell initiating human acute myeloid leukaemia after transplantation into SCID mice.

Leedham, S. J., Rodenas-Cuadrado, P., Howarth, K., Lewis, A., Mallappa, S., Segditsas, S., Davis, H. *et al.* (2012). A basal gradient of Wnt and stem-cell number influences regional tumour distribution in human and mouse intestinal tracts. *Gut*.

Lessard, J. and Sauvageau, G. (2003). Bmi-1 determines the proliferative capacity of normal and leukaemic stem cells. *Nature* **423:**255-260.

Levina, V., Marrangoni, A. M., DeMarco, R., Gorelik, E. and Lokshin, A. E. (2008). Drug-selected human lung cancer stem cells: cytokine network, tumorigenic and metastatic properties. *PLoS One* **3:**e3077.

Li, Z., Dong, X., Wang, Z., Liu, W., Deng, N., Ding, Y., Tang, L. *et al.* (2005). Regulation of PTEN by Rho small GTPases. *Nature cell biology* **7:**399-404.

Liao, M. J., Zhang, C. C., Zhou, B., Zimonjic, D. B., Mani, S. A., Kaba, M., Gifford, A. *et al.* (2007). Enrichment of a population of mammary gland cells that form mammospheres and have in vivo repopulating activity. *Cancer Res* **67:**8131-8138.

Liaw, D., Marsh, D. J., Li, J., Dahia, P. L. M., Wang, S. I., Zheng, Z., Bose, S. *et al.* (1997). Germline mutations of the PTEN gene in Cowden disease, an inherited breast and thyroid cancer syndrome. *Nature genetics* **16:**64-67.

Loeffler, M., Birke, A., Winton, D. and Potten, C. (1993). Somatic mutation, monoclonality and stochastic models of stem cell organization in the intestinal crypt. *Journal of theoretical biology* **160:**471-491.

Logan, C. and Nusse, R. (2004). The Wnt signaling pathway in development and disease.

Lopez-Garcia, C., Klein, A. M., Simons, B. D. and Winton, D. J. (2010). Intestinal stem cell replacement follows a pattern of neutral drift. *Science* **330:**822-825.

Lovvorn Iii, H. N., Boyle, S., Shi, G., Shyr, Y., Wills, M. L., Perantoni, A. O. and de Caestecker, M. (2007). Wilms' tumorigenesis is altered by misexpression of the transcriptional co-activator, CITED1. *Journal of pediatric surgery* **42:**474-481.

Lunardi, A., Gaboli, M., Giorgio, M., Rivi, R., Bygrave, A., Antoniou, M., Drabek, D. *et al.* (2011). A role for PML in innate immunity. *Genes & cancer* **2:**10-19.

Madison, B. B., McKenna, L. B., Dolson, D., Epstein, D. J. and Kaestner, K. H. (2009). FoxF1 and FoxL1 link hedgehog signaling and the control of epithelial proliferation in the developing stomach and intestine. *Journal of Biological Chemistry* **284:**5936-5944.

Mandel, J. S., Bond, J. H., Church, T. R., Snover, D. C., Bradley, G. M., Schuman, L. M. and Ederer, F. (1993). Reducing mortality from colorectal cancer by screening for fecal occult blood. *New England Journal of Medicine* **328:**1365-1371.

Marsh, V., Winton, D. J., Williams, G. T., Dubois, N., Trumpp, A., Sansom, O. J. and Clarke, A. R. (2008). Epithelial Pten is dispensable for intestinal homeostasis but suppresses adenoma development and progression after Apc mutation. *Nature genetics* **40:**1436-1444.

Marshman, E., Booth, C. and Potten, C. S. (2002). The intestinal epithelial stem cell. *Bioessays* **24:**91-98.

Martin-Castillo, B., Vazquez-Martin, A., Oliveras-Ferraros, C. and Menendez, J. A. (2010). Metformin and cancer. *Cell Cycle* **9:**1057-1064.

Mashimo, H., Wu, D. C., Podolsky, D. K. and Fishman, M. C. (1996). Impaired defense of intestinal mucosa in mice lacking intestinal trefoil factor. *Science* **274:**262.

Matthews, J. R., Sansom, O. J. and Clarke, A. R. (2011). Absolute requirement for STAT3 function in small-intestine crypt stem cell survival. *Cell Death & Differentiation* **18:**1934-1943.

May, R., Riehl, T. E., Hunt, C., Sureban, S. M., Anant, S. and Houchen, C. W. (2007). Identification of a Novel Putative Gastrointestinal Stem Cell and Adenoma Stem Cell Marker, Doublecortin and CaM Kinase-Like-1, Following Radiation Injury and in Adenomatous Polyposis Coli/Multiple Intestinal Neoplasia Mice. *Stem cells* **26:**630-637.

Melnick, A. and Licht, J. D. (1999). Deconstructing a Disease: RAR・, Its Fusion Partners, and Their Roles in the Pathogenesis of Acute Promyelocytic Leukemia. *Blood* **93:**3167-3215.

Miyamoto, T., Hasuike, S., Jinno, Y., Soejima, H., Yun, K., Miura, K., Ishikawa, M. *et al.* (2002). The human ASCL2 gene escaping genomic imprinting and its expression pattern. *Journal of assisted reproduction and genetics* **19:**240-244.

Mokarram, P., Kumar, K., Brim, H., Naghibalhossaini, F., Saberi-firoozi, M., Nouraie, M., Green, R. *et al.* (2009). Distinct high-profile methylated genes in colorectal cancer. *PLoS One* **4:**e7012.

Molofsky, A. V., Pardal, R., Iwashita, T., Park, I.-K., Clarke, M. F. and Morrison, S. J. (2003). Bmi-1 dependence distinguishes neural stem cell self-renewal from progenitor proliferation. *Nature* **425:**962-967.

Montgomery, R. K., Carlone, D. L., Richmond, C. A., Farilla, L., Kranendonk, M. E. G., Henderson, D. E., Baffour-Awuah, N. Y. *et al.* (2011). Mouse telomerase reverse transcriptase (mTert) expression marks slowly cycling intestinal stem cells. *Proceedings of the National Academy of Sciences* **108:**179-184.

Moser, A. R., Luongo, C., Gould, K. A., McNeley, M. K., Shoemaker, A. R. and Dove, W. F. (1995). < i> ApcMin</i>: A mouse model for intestinal and mammary tumorigenesis. *European Journal of Cancer* **31:**1061-1064.

Moser, A. R., Pitot, H. C. and Dove, W. F. (1990). A dominant mutation that predisposes to multiple intestinal neoplasia in the mouse. *Science* **247:**322.

Muncan, V., Sansom, O. J., Tertoolen, L., Phesse, T. J., Begthel, H., Sancho, E., Cole, A. M. *et al.* (2006). Rapid loss of intestinal crypts upon conditional deletion of the Wnt/Tcf-4 target gene c-Myc. *Molecular and cellular biology* **26:**8418-8426.

Musteanu, M., Blaas, L., Mair, M., Schlederer, M., Bilban, M., Tauber, S., Esterbauer, H. *et al.* (2010). Stat3 Is a Negative Regulator of Intestinal Tumor Progression in< i> Apc</i>< sup> Min</sup> Mice. *Gastroenterology* **138:**1003-1011. e1005.

Muñoz, J., Stange, D. E., Schepers, A. G., van de Wetering, M., Koo, B. K., Itzkovitz, S., Volckmann, R. *et al.* (2012). The Lgr5 intestinal stem cell signature: robust expression of proposed quiescent '+ 4'cell markers. *The EMBO Journal*.

Méniel, V., Song, F., Phesse, T., Young, M., Poetz, O., Parry, L., Jenkins, J. R. *et al.* (2013). Cited1 deficiency suppresses intestinal tumorigenesis. *PLoS Genet* **9:**e1003638.

Nair, S. S., Chaubal, V. A., Shioda, T., Coser, K. R. and Mojamdar, M. (2001). Over-expression of MSG1 Transcriptional Co-activator Increases Melanin in B16 Melanoma Cells: A Possible Role for MSG1 in Melanogenesis. *Pigment Cell Research* **14:**206-209.

Nakagawa, H., Murata, Y., Koyama, K., Fujiyama, A., Miyoshi, Y., Monden, M., Akiyama, T. *et al.* (1998). Identification of a brain-specific APC homologue, APCL, and its interaction with β-catenin. *Cancer research* **58:**5176.

Nakanishi, Y., Seno, H., Fukuoka, A., Ueo, T., Yamaga, Y., Maruno, T., Nakanishi, N. *et al.* (2012). Dclk1 distinguishes between tumor and normal stem cells in the intestine. *Nature genetics*.

Nassif, N. T., Lobo, G. P., Wu, X., Henderson, C. J. A., Morrison, C. D., Eng, C., Jalaludin, B. *et al.* (2004). PTEN mutations are common in sporadic microsatellite stable colorectal cancer. *Oncogene* **23:**617-628.

Nissan, A., Zhang, J. M., Lin, Z., Haskel, Y., Freund, H. R. and Hanani, M. (1997). The contribution of inflammatory mediators and nitric oxide to lipopolysaccharide-induced intussusception in mice. *Journal of Surgical Research* **69:**205-207.

Okano, H., Imai, T. and Okabe, M. (2002). Musashi: a translational regulator of cell fate. *Journal of cell science* **115:**1355-1359.

Onuma, K., Ochiai, M., Orihashi, K., Takahashi, M., Imai, T., Nakagama, H. and Hippo, Y. (2013). Genetic reconstitution of tumorigenesis in primary intestinal cells. *Proceedings of the National Academy of Sciences*.

Oshima, M., Dinchuk, J. E., Kargman, S. L., Oshima, H., Hancock, B., Kwong, E., Trzaskos, J. M. *et al.* (1996). Suppression of intestinal polyposis in Apc [Delta] 716 knockout mice by inhibition of cyclooxygenase 2 (COX-2). *Cell* **87:**803-809.

O'Brien, C. A., Pollett, A., Gallinger, S. and Dick, J. E. (2006). A human colon cancer cell capable of initiating tumour growth in immunodeficient mice. *Nature* **445:**106-110.

Parry, L., Young, M., El Marjou, F. and Clarke, A. R. (2013). Evidence for A Crucial Role of Paneth Cells in Mediating the Intestinal Response to Injury. *Stem cells*.

Parsons, D. W., Wang, T. L., Samuels, Y., Bardelli, A., Cummins, J. M., DeLong, L., Silliman, N. *et al.* (2005). Colorectal cancer: mutations in a signalling pathway. *Nature* **436:**792-792.

Pearson, M., Carbone, R., Sebastiani, C., Cioce, M., Fagioli, M., Saito, S. i., Higashimoto, Y. *et al.* (2000). PML regulates p53 acetylation and premature senescence induced by oncogenic Ras. *Nature* **406:**207-210.

Pinto, D., Gregorieff, A., Begthel, H. and Clevers, H. (2003). Canonical Wnt signals are essential for homeostasis of the intestinal epithelium. *Genes & development* **17:**1709-1713.

Plateroti, M., Gauthier, K., Domon-Dell, C., Freund, J.-N., Samarut, J. and Chassande, O. (2001). Functional interference between thyroid hormone receptor α (TRα) and natural truncated TRΔα isoforms in the control of intestine development. *Molecular and cellular biology* **21:**4761-4772.

Plisov, S., Tsang, M., Shi, G., Boyle, S., Yoshino, K., Dunwoodie, S. L., Dawid, I. B. *et al.* (2005). Cited1 is a bifunctional transcriptional cofactor that regulates early nephronic patterning. *Journal of the American Society of Nephrology* **16:**1632-1644.

Polakis, P. (2000). Wnt signaling and cancer. *Genes & development* **14:**1837.

Polakis, P. (2007). The many ways of Wnt in cancer. *Current opinion in genetics & development* **17:**45-51.

Potten, C. S., Booth, C. and Pritchard, D. (1997). The intestinal epithelial stem cell: the mucosal governor. *International journal of experimental pathology* **78:**219-243.

Potten, C. S., Booth, C., Tudor, G. L., Booth, D., Brady, G., Hurley, P., Ashton, G. *et al.* (2003). Identification of a putative intestinal stem cell and early lineage marker; musashi-1. *Differentiation* **71:**28-41.

Potten, C. S., Hume, W. J., Reid, P. and Cairns, J. (1978). The segregation of DNA in epithelial stem cells. *Cell* **15:**899-906.

Potten, C. S., Kovacs, L. and Hamilton, E. (1974). Continuous labelling studies on mouse skin and intestine. *Cell proliferation* **7:**271-283.

Potten, C. S., Owen, G. and Booth, D. (2002). Intestinal stem cells protect their genome by selective segregation of template DNA strands. *Journal of cell science* **115:**2381-2388.

Powell, A. E., Wang, Y., Li, Y., Poulin, E. J., Means, A. L., Washington, M. K., Higginbotham, J. N. *et al.* (2012). The pan-ErbB negative regulator Lrig1 is an intestinal stem cell marker that functions as a tumor suppressor. *Cell* **149:**146-158.

Powell, S. M., Zilz, N., Beazer-Barclay, Y., Bryan, T. M., Hamilton, S. R., Thibodeau, S. N., Vogelstein, B. *et al.* (1992). APC mutations occur early during colorectal tumorigenesis. *Nature* **359:**235-237.

Quintana, E., Shackleton, M., Sabel, M. S., Fullen, D. R., Johnson, T. M. and Morrison, S. J. (2008). Efficient tumour formation by single human melanoma cells. *Nature* **456:**593-598.

Reed, K. R., Tunster, S. J., Young, M., Carrico, A., John, R. M. and Clarke, A. R. (2012). Entopic overexpression of Ascl2 does not accelerate tumourigenesis in ApcMin mice. *Gut* **61:**1435-1438.

Reya, T. and Clevers, H. (2005). Wnt signalling in stem cells and cancer. *Nature* **434:**843-850.

Reynolds, B. A. and Weiss, S. (1992). Generation of neurons and astrocytes from isolated cells of the adult mammalian central nervous system. *Science* **255:**1707-1710.

Rezza, A., Skah, S., Roche, C., Nadjar, J., Samarut, J. and Plateroti, M. (2010). The overexpression of the putative gut stem cell marker Musashi-1 induces tumorigenesis through Wnt and Notch activation. *J Cell Sci* **123:**3256-3265.

Rodriguez, T. A., Sparrow, D. B., Scott, A. N., Withington, S. L., Preis, J. I., Michalicek, J., Clements, M. *et al.* (2004). Cited1 is required in trophoblasts for placental development and for embryo growth and survival. *Mol Cell Biol* **24:**228-244.

Romagnolo, B., Berrebi, D., Saadi-Keddoucci, S., Porteu, A., Pichard, A., Peuchmaur, M., Vandewalle, A. *et al.* (1999). Intestinal dysplasia and adenoma in transgenic mice after overexpression of an activated β-catenin. *Cancer research* **59:**3875.

Roukos, D. H. (2010). Targeting gastric cancer with trastuzumab: new clinical practice and innovative developments to overcome resistance. *Annals of surgical oncology* **17:**14-17.

Sangiorgi, E. and Capecchi, M. R. (2008). Bmi1 is expressed in vivo in intestinal stem cells. *Nature genetics* **40:**915-920.

Sansom, O., Reed, K., Hayes, A., Ireland, H., Brinkmann, H., Newton, I., Batlle, E. *et al.* (2004a). Loss of Apc in vivo immediately perturbs Wnt signaling, differentiation, and migration. *Genes & development* **18:**1385.

Sansom, O. J., Meniel, V. S., Muncan, V., Phesse, T. J., Wilkins, J. A., Reed, K. R., Vass, J. K. *et al.* (2007). Myc deletion rescues Apc deficiency in the small intestine. *Nature* **446:**676-679.

Sansom, O. J., Reed, K. R., Hayes, A. J., Ireland, H., Brinkmann, H., Newton, I. P., Batlle, E. *et al.* (2004b). Loss of Apc in vivo immediately perturbs Wnt signaling, differentiation, and migration. *Genes & development* **18:**1385.

Saqui-Salces, M., Keeley, T. M., Grosse, A. S., Qiao, X. T., El-Zaatari, M., Gumucio, D. L., Samuelson, L. C. *et al.* (2011). Gastric tuft cells express DCLK1 and are expanded in hyperplasia. *Histochem Cell Biol* **136:**191-204.

Sato, T., van Es, J. H., Snippert, H. J., Stange, D. E., Vries, R. G., van den Born, M., Barker, N. *et al.* (2010). Paneth cells constitute the niche for Lgr5 stem cells in intestinal crypts. *Nature* **469:**415-418.

Sato, T., Vries, R. G., Snippert, H. J., Van De Wetering, M., Barker, N., Stange, D. E., Van Es, J. H. *et al.* (2009). Single Lgr5 stem cells build crypt villus structures in vitro without a mesenchymal niche. *Nature* **459:**262-265.

Schepers, A. G., Snippert, H. J., Stange, D. E., van den Born, M., van Es, J. H., van de Wetering, M. and Clevers, H. (2012). Lineage Tracing Reveals Lgr5+ Stem Cell Activity in Mouse Intestinal Adenomas. *Science*.

Schepers, A. G., Vries, R., van den Born, M., van de Wetering, M. and Clevers, H. (2011). Lgr5 intestinal stem cells have high telomerase activity and randomly segregate their chromosomes. *The EMBO Journal* **30:**1104-1109.

Schneikert, J., Chandra, S. H. V., Ruppert, J. G., Ray, S., Wenzel, E. M. and Behrens, J. (2013). Functional Comparison of Human Adenomatous Polyposis Coli (APC) and APC-Like in Targeting Beta-Catenin for Degradation. *PLoS One* **8:**e68072.

Schuebel, K. E., Chen, W., Cope, L., Glöckner, S. C., Suzuki, H., Yi, J.-M., Chan, T. A. *et al.* (2007). Comparing the DNA hypermethylome with gene mutations in human colorectal cancer. *PLoS genetics* **3:**e157.

Schuijers, J. and Clevers, H. (2012). Adult mammalian stem cells: the role of Wnt, Lgr5 and R-spondins. *The EMBO Journal* **31:**2685-2696.

Shao, J., Washington, M. K., Saxena, R. and Sheng, H. (2007). Heterozygous disruption of the PTEN promotes intestinal neoplasia in APCmin/+ mouse: roles of osteopontin. *Carcinogenesis* **28:**2476-2483.

She, Q.-B., Solit, D. B., Ye, Q., O'Reilly, K. E., Lobo, J. and Rosen, N. (2005). The BAD protein integrates survival signaling by EGFR/MAPK and PI3K/Akt kinase pathways in PTEN-deficient tumor cells. *Cancer cell* **8:**287-297.

Shibata, H., Toyama, K., Shioya, H., Ito, M., Hirota, M., Hasegawa, S., Matsumoto, H. *et al.* (1997). Rapid colorectal adenoma formation initiated by conditional targeting of the Apc gene. *Science* **278:**120.

Shioda, T., Fenner, M. H. and Isselbacher, K. J. (1996). msg1, a novel melanocyte-specific gene, encodes a nuclear protein and is associated with pigmentation. *Proceedings of the National Academy of Sciences* **93:**12298-12303.

Siddall, N. A., McLaughlin, E. A., Marriner, N. L. and Hime, G. R. (2006). The RNA-binding protein Musashi is required intrinsically to maintain stem cell identity. *Proc Natl Acad Sci U S A* **103:**8402-8407.

Singec, I., Knoth, R., Meyer, R. P., Maciaczyk, J., Volk, B., Nikkhah, G., Frotscher, M. *et al.* (2006). Defining the actual sensitivity and specificity of the neurosphere assay in stem cell biology. *Nat Methods* **3:**801-806.

Singh, S. K., Hawkins, C., Clarke, I. D., Squire, J. A., Bayani, J., Hide, T., Henkelman, R. M. *et al.* (2004). Identification of human brain tumour initiating cells. *Nature* **432:**396-401.

Smith, G. H. (2005). Label-retaining epithelial cells in mouse mammary gland divide asymmetrically and retain their template DNA strands. *Development* **132:**681-687.

Snippert, H. J., Van Der Flier, L. G., Sato, T., Van Es, J. H., Van Den Born, M., Kroon-Veenboer, C., Barker, N. *et al.* (2010). Intestinal crypt homeostasis results from neutral competition between symmetrically dividing Lgr5 stem cells. *Cell* **143:**134-144.

Snippert, H. J., van Es, J. H., van den Born, M., Begthel, H., Stange, D. E., Barker, N. and Clevers, H. (2009). Prominin-1/CD133 marks stem cells and early progenitors in mouse small intestine. *Gastroenterology* **136:**2187-2194. e2181.

Sobottka, S. B., Haase, M., Fitze, G., Hahn, M., Schackert, H. K. and Schackert, G. (2000). Frequent loss of heterozygosity at the 19p13. 3 locus without LKB1/STK11 mutations in human carcinoma metastases to the brain. *Journal of neuro-oncology* **49:**187-195.

Song, M. S., Salmena, L., Carracedo, A., Egia, A., Lo-Coco, F., Teruya-Feldstein, J. and Pandolfi, P. P. (2008). The deubiquitinylation and localization of PTEN are regulated by a HAUSP–PML network. *Nature* **455:**813-817.

Spears, E. and Neufeld, K. L. (2011). Novel double-negative feedback loop between adenomatous polyposis coli and Musashi1 in colon epithelia. *Journal of Biological Chemistry* **286:**4946-4950.

Staal, F. J. T., Weerkamp, F., Baert, M. R. M., van den Burg, C. M. M., van Noort, M., de Haas, E. F. E. and van Dongen, J. J. M. (2004). Wnt target genes identified by DNA microarrays in immature CD34+ thymocytes regulate proliferation and cell adhesion. *The Journal of Immunology* **172:**1099.

Steinbach, G., Lynch, P. M., Phillips, R. K. S., Wallace, M. H., Hawk, E., Gordon, G. B., Wakabayashi, N. *et al.* (2000). The effect of celecoxib, a cyclooxygenase-2 inhibitor, in familial adenomatous polyposis. *New England Journal of Medicine* **342:**1946-1952.

Stingl, J., Eirew, P., Ricketson, I., Shackleton, M., Vaillant, F., Choi, D., Li, H. I. *et al.* (2006). Purification and unique properties of mammary epithelial stem cells. *Nature* **439:**993-997.

Su, L. K., Kinzler, K. W., Vogelstein, B., Preisinger, A. C., Moser, A. R., Luongo, C., Gould, K. A. *et al.* (1992). Multiple intestinal neoplasia caused by a mutation in the murine homolog of the APC gene. *Science* **256:**668-670.

Suzuki, A., de la Pompa, J. L., Stambolic, V., Elia, A. J., Sasaki, T., Barrantes, I. d. B., Ho, A. *et al.* (1998). High cancer susceptibility and embryonic lethality associated with mutation of the< i> PTEN</i> tumor suppressor gene in mice. *Current Biology* **8:**1169-1178.

Suzuki, A., Yamaguchi, M. T., Ohteki, T., Sasaki, T., Kaisho, T., Kimura, Y., Yoshida, R. *et al.* (2001). T cell-specific loss of Pten leads to defects in central and peripheral tolerance. *Immunity* **14:**523-534.

Takeda, N., Jain, R., LeBoeuf, M. R., Wang, Q., Lu, M. M. and Epstein, J. A. (2011). Interconversion between intestinal stem cell populations in distinct niches. *Science* **334:**1420-1424.

Terris, B., Baldin, V., Dubois, S., Degott, C., Flejou, J.-F., Hénin, D. and Dejean, A. (1995). PML nuclear bodies are general targets for inflammation and cell proliferation. *Cancer research* **55:**1590-1597.

Tian, H., Biehs, B., Warming, S., Leong, K. G., Rangell, L., Klein, O. D. and de Sauvage, F. J. (2011). A reserve stem cell population in small intestine renders Lgr5-positive cells dispensable. *Nature*.

Trotman, L. C., Alimonti, A., Scaglioni, P. P., Koutcher, J. A., Cordon-Cardo, C. and Pandolfi, P. P. (2006). Identification of a tumour suppressor network opposing nuclear Akt function. *Nature* **441:**523-527.

van der Flier, L. G., Haegebarth, A., Stange, D. E., van de Wetering, M. and Clevers, H. (2009a). OLFM4 is a robust marker for stem cells in human intestine and marks a subset of colorectal cancer cells. *Gastroenterology* **137:**15-17.

van der Flier, L. G., van Gijn, M. E., Hatzis, P., Kujala, P., Haegebarth, A., Stange, D. E., Begthel, H. *et al.* (2009b). Transcription factor achaete scute-like 2 controls intestinal stem cell fate. *Cell* **136:**903-912.

Van der Meer, M., Baumans, V., Olivier, B., Kruitwagen, C., Van Dijk, J. E. and Van Zutphen, L. F. M. (2001). Behavioral and physiological effects of biotechnology procedures used for gene targeting in mice. *Physiology & behavior* **73:**719-730.

Van Es, J. H., De Geest, N., Van De Born, M., Clevers, H. and Hassan, B. A. (2010). Intestinal stem cells lacking the Math1 tumour suppressor are refractory to Notch inhibitors. *Nature communications* **1:**18.

Van Es, J. H., Kirkpatrick, C., Van de Wetering, M., Molenaar, M., Miles, A., Kuipers, J., Destree, O. *et al.* (1999). Identification of APC2, a homologue of the adenomatous polyposis coli tumour suppressor. *Current Biology* **9:**105-108, S101-S102.

Van Es, J. H., Van Gijn, M. E., Riccio, O., Van Den Born, M., Vooijs, M., Begthel, H., Cozijnsen, M. *et al.* (2005). Notch/γ-secretase inhibition turns proliferative cells in intestinal crypts and adenomas into goblet cells. *Nature* **435:**959-963.

Voskas, D., Ling, L. S. and Woodgett, J. R. (2010). Does GSK-3 provide a shortcut for PI3K activation of Wnt signalling? *F1000 biology reports* **2**.

Wang, D., Huang, B., Zhang, S., Yu, X., Wu, W. and Wang, X. (2013a). Structural basis for R-spondin recognition by LGR4/5/6 receptors. *Genes & development* **27:**1339-1344.

Wang, F., Scoville, D., He, X. C., Mahe, M., Box, A., Perry, J., Smith, N. R. *et al.* (2013b). Isolation and Characterization of Intestinal Stem Cells Based on Surface Marker Combinations and Colony-Formation Assay. *Gastroenterology*.

Wang, S. I., Puc, J., Li, J., Bruce, J. N., Cairns, P., Sidransky, D. and Parsons, R. (1997). Somatic mutations of PTEN in glioblastoma multiforme. *Cancer research* **57:**4183-4186.

Wang, Z. G., Ruggero, D., Ronchetti, S., Zhong, S., Gaboli, M., Rivi, R. and Pandolfi, P. P. (1998). PML is essential for multiple apoptotic pathways. *Nat Genet* **20:**266-272.

Wilkins, J. A. and Sansom, O. J. (2008). C-Myc is a critical mediator of the phenotypes of Apc loss in the intestine. *Cancer research* **68:**4963-4966.

Yahata, T., Shao, W., Endoh, H., Hur, J., Coser, K. R., Sun, H., Ueda, Y. *et al.* (2001). Selective coactivation of estrogen-dependent transcription by CITED1 CBP/p300-binding protein. *Genes & development* **15:**2598-2612.

Yan, K. S., Chia, L. A., Li, X., Ootani, A., Su, J., Lee, J. Y., Su, N. *et al.* (2012). The intestinal stem cell markers Bmi1 and Lgr5 identify two functionally distinct populations. *Proceedings of the National Academy of Sciences* **109:**466-471.

Yeatman, T. J. and Chambers, A. F. (2003). Osteopontin and colon cancer progression. *Clinical & experimental metastasis* **20:**85-90.

Young, M., Ordonez, L. and Clarke, A. R. (2013). What are the best routes to effectively model human colorectal cancer? *Molecular Oncology*.

Zhao, J., de Vera, J., Narushima, S., Beck, E. X., Palencia, S., Shinkawa, P., Kim, K. A. *et al.* (2007). R-spondin1, a novel intestinotrophic mitogen, ameliorates experimental colitis in mice. *Gastroenterology* **132:**1331-1343.

Zheng, B., Zhang, Z., Black, C. M., de Crombrugghe, B. and Denton, C. P. (2002). Ligand-dependent genetic recombination in fibroblasts: a potentially powerful technique for investigating gene function in fibrosis. *The American journal of pathology* **160:**1609-1617.

Zhou, J., Wulfkuhle, J., Zhang, H., Gu, P., Yang, Y., Deng, J., Margolick, J. B. *et al.* (2007). Activation of the PTEN/mTOR/STAT3 pathway in breast cancer stem-like cells is required for viability and maintenance. *Proceedings of the National Academy of Sciences* **104:**16158-16163.

Zhou, W. and Bao, S. (2013). PML-mediated signaling and its role in cancer stem cells. *Oncogene*.

Zhou, X. P., Gimm, O., Hampel, H., Niemann, T., Walker, M. J. and Eng, C. (2000). Epigenetic PTEN silencing in malignant melanomas without PTEN mutation. *American Journal of Pathology* **157:**1123.

Zhu, L., Gibson, P., Currle, D. S., Tong, Y., Richardson, R. J., Bayazitov, I. T., Poppleton, H. *et al.* (2008). Prominin 1 marks intestinal stem cells that are susceptible to neoplastic transformation. *Nature* **457:**603-607.

Ziskin, J. L., Dunlap, D., Yaylaoglu, M., Fodor, I. K., Forrest, W. F., Patel, R., Ge, N. *et al.* (2012). In situ validation of an intestinal stem cell signature in colorectal cancer. *Gut*.

Zysman, M. A., Chapman, W. B. and Bapat, B. (2002). Considerations When Analyzing the Methylation Status of< i> PTEN</i> Tumor Suppressor Gene. *The American journal of pathology* **160:**795-800.

Appendix 1: Publication List

Meniel V, Song F, Phesse T, **Young M**, Poetz O, Jenkins JR, Parry L, Williams G, Dunwoodie S, Watson A, Clarke AR. Cited1 Deficiency Suppresses Intestinal Tumorigenesis. *PLoS Genetics* 2013 9:e1003638.

Holik A, Krzystyniak J, **Young M**, Richardson K, Jarde T, Chambon P, Shorning B, Clarke AR, Brg1 is required for stem cell maintenance in the murine intestinal epithelium in a tissue-specific manner. *Stem Cells* 2013 1002/stem.1498

Young M, Ordonez L, Clarke AR. What are the best routes to effectively model human colorectal cancer? 2013, Molecular Oncology 7(2):178-89

Parry L, **Young M**, El Marjou F, Clarke AR. Evidence for A Crucial Role of Paneth Cells in Mediating the Intestinal Response to Injury, 2013, Stem Cells 31(4):776-85

Reed KR, Tunster SJ, **Young M**, Carrico A, John RM, Clarke AR. Entopic overexpression of Ascl2 does not accelerate tumourigenesis in ApcMin mice. 2012, Gut 61(10):1435-8

Young M, Clarke AR. Expanding the p53 toolkit: a new platform for rapid engineering of the p53 locus in vivo, 2011, Cell Cycle 15;10(14):2249-50

Papers in Preparation

Holik A, **Young M**, Krzystyniak J, Williams G, Metzger D, Shorning B, Clarke AR, Brg1 loss attenuates aberrant Wnt-signalling and prevents Wnt-dependent tumourigenesis in the murine small intestine. Submitted to "Gut"